

Design of Elastic Nanocomposite Materials from Polymers and Noble Metal Nanoparticles

Dissertation

zur Erlangung des akademischen Grades eines Doktors der
Naturwissenschaften (Dr. rer. nat.) an der Bayreuther
Graduiertenschule für Mathematik und Naturwissenschaften der
Universität Bayreuth

vorgelegt von

Holger Pletsch

Geboren in Frankfurt-Höchst

Bayreuth, 2014

Die vorliegende Arbeit wurde in der Zeit von 09/2011 bis 09/2012 in Marburg am Lehrstuhl Makromolekulare Chemie und von 10/2012 bis 12/2014 in Bayreuth am Lehrstuhl Makromolekulare Chemie 2 unter Betreuung von Frau Professor Dr. Seema Agarwal angefertigt.

Vollständiger Abdruck der von der Bayreuther Graduiertenschule für Mathematik und Naturwissenschaften (BayNAT) der Universität Bayreuth genehmigten Dissertation zur Erlangung des akademischen Grades eines Doktors der Naturwissenschaften (Dr. rer. nat.).

Dissertation eingereicht am: 18.11.2014

Zulassung durch das Leitungsgremium: 26.11.2014

Wissenschaftliches Kolloquium: 13.05.2015

Amtierender Direktor: Prof. Dr. Franz Xaver Schmidt

Prüfungsausschuss:

Prof. Dr. Seema Agarwal (Erstgutachterin)

Prof. Dr. Stephan Förster (Zweitgutachter)

Prof. Dr. Jürgen Senker (Vorsitz)

Dr. Munish Chanana

TABLE OF CONTENTS

Summary	1
Zusammenfassung	3
List of Abbreviations	5
1. Introduction	7
1.1 Noble Metal Nanoparticles	7
1.1.1 Anisotropic Morphologies	13
1.2 Noble Metal Nanoparticle/Polymer Nanocomposites	16
1.2.1 Synthesis of Polymer-Stabilized Nanoparticles	17
1.2.2 Applications	21
1.3 Cross-Linking of Polymer Chains	27
1.3.1 Chemical Cross-Linking	28
1.3.2 Reversible Cross-Linking	29
1.3.2.1 Physical Cross-Linking	29
1.3.2.2 Reversible Chemical Cross-Linking	33
1.4 Nanoparticles as Cross-Linkers and Reinforcing Agents	35
1.4.1 Non-Metallic Nanoparticles	36
1.4.2 Noble Metal Nanoparticles	38
1.5 References	42
2. Synopsis	63
2.1 Aim of the Thesis	63
2.2 Summary of Chapter 3: Design of Soft Materials from Liquid Triblock Co-Oligomers and Metal Nanoparticles	63
2.3 Summary of Chapter 4: Ultrasound-Mediated Synthesis for High-Molecular Weight Polystyrene-Grafted Silver Nanoparticles by Facile Ligand Exchange Reactions in Suspension	66
2.4 Summary of Chapter 5: Reversible Gold Nanorod Alignment in Mechano-Responsive Elastomers	69
2.5 Summary of Chapter 6: Mechanical Reinforcement of Polydentate Thioether Ligand by Silver Nanoparticles	72
2.6 Individual Contributions to Joint Publications	75
3. Design of Soft Materials from Liquid Triblock Co-Oligomers and Metal Nanoparticles	77
4. Ultrasound-Mediated Synthesis of High-Molecular Weight Polystyrene-Grafted Silver Nanoparticles by Facile Ligand Exchange Reactions in Suspension	99
5. Reversible Gold Nanorod Alignment in Mechano-Responsive Elastomers	123
6. Mechanical Reinforcement of Polydentate Thioether Ligand by Silver Nanoparticles	153
List of Publications	173
Conference participations	175
Acknowledgements	177

SUMMARY

The main theme of this thesis is the development of elastic nanocomposites from organic polymers and noble metal nanoparticles. The exploration of nanocomposites where noble metal nanoparticles serve as cross-linking sites and reinforcing agents is of special relevance. Employing spherical silver nanoparticles and rod-shaped gold nanoparticles, emphasis is placed on (1) the development of novel nanocomposite preparation routes, on (2) the engineering of elastic nanocomposites with unprecedented physical properties and on (3) the underlying mechanisms. The cumulative part of the thesis is divided into four interdependent chapters.

The cross-linking ability of spherical silver nanoparticles for the design of thermally processable elastic nanocomposites from viscous liquid oligomers is exhausted. In order to gain control over the resulting mechanical properties, a telechelic α,ω -dithiol-functionalized ABA block co-oligomer consisting of isoprene (A block) and styrene (B block) is employed. The mechanical properties are shown to be tunable as a function of the styrene content within the triblock co-oligomer as well as with the silver nanoparticle content. A broad range of tensile properties is covered with the presented sample set which is put into comparison with commercial elastomers and thermoplastic elastomers. In contrast to conventional block copolymer thermoplastic elastomers, microphase separation of the blocks is not required. Rather, very low polymerization degrees were sufficient in order to yield high tensile strengths and moduli in the cross-linked state. As a consequence of low polymerization degrees, viscosities at elevated temperatures are found to be remarkably small and independent from the block co-oligomer composition.

For the purpose of stabilizing noble metal nanoparticles with high molecular weight end-functionalized polymers, a novel preparation method is presented. It is shown that the limiting factor, namely the decreasing concentration of the end group with increasing molecular weight relative to the polymer tail, can be overcome by designing the grafting procedure independent of the length of the polymer tail. Therefore, a hetero-phase ligand exchange is presented in which ω -thiol polystyrene is grafted to *ex situ*-prepared spherical silver nanoparticles through diffusion-controlled phase transfer within an ultrasound-mediated emulsion. The reaction is claimed to become independent of molecular weight due to self-orientation of the terminal thiol groups towards the liquid-liquid interface with simultaneous accumulation of the polymer tail in the emulsion droplet bulk. As a result,

ω -thiol polystyrene with molecular weights up to 217200 g/mol can be successfully grafted to spherical silver nanoparticles with no signs of particle agglomeration. To put the results in context, a one-phase *in situ* preparation route is presented with significantly decreased tolerance towards high molecular weight polymers.

Mechano-responsive elastic nanocomposites are designed from gold nanorods and telechelic co-oligomers. The aim of this chapter is to master the orientational alignment of gold nanorods in the solid state by mechanical stimulus. Therefore, elastic films are prepared in which uniaxial mechanical elongation and relaxation regulate the alignment of gold nanorods within the stretching direction in a stepless and reversible fashion. *Ex situ*-prepared gold nanorods in aqueous dispersion are employed in a hetero-phase ligand exchange procedure in order to obtain thermally stable hydrophobic gold nanorods. These are either cross-linked with spherical silver nanoparticles or embedded into a thermoplastic elastomer matrix to yield elastic materials in which the gold nanorods are homogeneously dispersed. The impact of mechanical stimulation on the physical properties of these materials is demonstrated by means of absorption and scattering experiments.

Finally, spherical silver nanoparticles are presented as reinforcing agents for liquid, polydentate poly(propylene sulfide), yielding pseudo-solid elastic materials with an unfastened polymer-particle network microstructure. High molar mass, linear poly(propylene sulfide) is chosen as a ligand as it supplies a plethora of thioether units per chain, known for their ability to coordinate to noble metal nanoparticles. The resulting nanocomposites exhibit high colloidal stability, even under demanding conditions such as elevated temperatures and pressure. The polymer-particle interactions are investigated in detail by probing the polymer dynamics with dynamic rheology. Depending on the silver nanoparticle filling fraction, the G' - G'' crossover frequency significantly shifts to lower frequencies while segmental dynamics are not touched upon silver nanoparticle charging. Microscopically, a loose network in which polymer chains indirectly bridge the nanoparticles in the long-range is held responsible for reinforcement.

ZUSAMMENFASSUNG

Die vorliegende Doktorarbeit behandelt die Neuentwicklung von elastischen Nanokomposit-Materialien aus organischen Polymeren und Edelmetallnanopartikeln. Die Verwendung von Edelmetallnanopartikeln als Quervernetzer sowie als mechanische Verstärkungsstoffe stellt das Leitmotiv dieser Arbeit dar. Daher werden unter Verwendung von sphärischen Silbernanopartikeln als auch von Goldnanostäbchen vor allem (1) maßgeschneiderte Synthesemethoden zur gezielten Darstellung von Nanokomposit-Materialien, (2) die Entwicklung von elastischen Nanokompositen mit neuartigen physikalischen Eigenschaften und (3) deren zu Grunde liegenden mikroskopischen Strukturen diskutiert. Der kumulative Teil dieser Arbeit ist in vier ineinandergreifende Kapitel aufgeteilt.

Flüssige Oligomere werden thermisch reversibel durch sphärische Silbernanopartikel quervernetzt und in Hinblick auf ihre makroskopischen Materialeigenschaften untersucht. Die mechanischen Eigenschaften der elastischen Nanokomposite werden sowohl über die chemische Zusammensetzung der oligomeren Komponente, ein telecheles α,ω -dithiol-funktionalisiertes ABA Blockooligomer bestehend aus Isopren (Block A) und Styrol (Block B) als auch über den Anteil an Silbernanopartikeln angepasst. Mit dieser Methode kann ein breites und im Vergleich mit kommerziellen Elastomeren und thermoplastischen Elastomeren bisher nicht abgedecktes Spektrum an mechanischen Eigenschaften präsentiert werden. Im Gegensatz zu konventionellen thermoplastischen Elastomeren aus mikrophasen-separierten Blockcopolymeren werden hohe Zugfestigkeiten und Steifigkeiten schon mit sehr kleinen Polymerisationsgraden erreicht. Daher werden mit den hier vorgestellten Nanokomposit-Materialien stark verringerte Schmelzviskositäten beobachtet, die von der Blockooligomer-Zusammensetzung annähernd unabhängig sind.

Die Stabilisierung von Edelmetallnanopartikeln mit hochmolekularen, endgruppen-funktionalisierten Polymeren ist bisher an Mangel von geeigneten Synthesemethoden gescheitert. Daher wird eine „grafting to“-Synthesemethode vorgestellt, die von der Polymerkettenlänge unabhängig ist und daher auch für langkettige Polymere mit sehr niedriger Endgruppenkonzentration geeignet ist. *Ex situ* hergestellte sphärische Silbernanopartikel werden in einem Ultraschall-aktivierten Grenzflächen-Ligandenaustausch in Emulsion durch Phasentransfer an ω -Thiolpolystyrol gepfropft. Dieser diffusionskontrollierte Prozess ermöglicht die Verwendung von ω -Thiolpolystyrol

mit einem Molekulargewicht von bis zu 217200 g/mol, da die Endgruppen aufgrund erhöhter Hydrophilie an der Phasengrenzfläche angeordnet sind und somit eine von der Polymerkettenlänge unabhängige Wechselwirkung mit den Nanopartikeln eingehen können. Um das Potential dieser Methode einzuordnen, wird gezeigt, dass eine vergleichbare *in situ* Methode in homogener Lösung eine deutlich niedrigere Toleranz gegenüber endfunktionalisierten Polymeren mit hohen Molekulargewichten hat.

Mechano-responsive, elastische Nanokomposite werden aus Goldnanostäbchen und telechelen Oligomeren dargestellt. Ziel dieser Studie ist es, die räumliche Ausrichtung von Goldnanostäbchen in fester Phase durch mechanische Anregung zu kontrollieren. Daher werden elastische Filme präsentiert, in denen die räumliche Ausrichtung von Goldnanostäbchen durch mechanische Dehnung und Relaxation stufenlos und reversibel gesteuert werden kann. Thermisch stabile, hydrophobe Goldnanostäbchen werden zunächst durch Grenzflächen-Ligandenaustausch von *ex situ* hergestellten Goldnanostäbchen erhalten. Sowohl Quervernetzung mittels sphärischer Silbernanopartikel als auch das Einbetten in eine thermoplastisch elastomere Matrix ermöglicht im Folgeschritt die Herstellung von elastischen Materialien, in denen Goldnanostäbchen homogen dispergiert sind. Die Auswirkung mechanischer Anregung auf die physikalischen Eigenschaften dieser Materialien wird durch Absorptions- und Streuexperimente bestätigt.

Schließlich werden sphärische Silbernanopartikel als mechanische Verstärkungsstoffe für Polypropylensulfid, einem flüssigen, mehrzähligen („polydentaten“) Thioether, präsentiert. Dieser polymere Ligand in hochmolekularer, linearer Form gewährleistet auch unter anspruchsvollen Bedingungen wie erhöhter Temperatur und erhöhtem Druck dank einer außergewöhnlich großen Anzahl an Koordinationsstellen eine hohe Silbernanopartikelstabilität. Die Verstärkung des Polymers durch Silbernanopartikel wird durch ein lockeres Netzwerk ermöglicht, in dem Nanopartikel weiträumig durch Polymerketten verbunden sind. Um die Auswirkung der Silbernanopartikel auf die Kettendynamik zu verstehen, werden die elastomeren Materialien mittels dynamische Rheologie untersucht.

LIST OF ABBREVIATIONS

3-D	three-dimensional
AAS	atom absorption spectroscopy
AFM	atomic force microscopy
AgNP	silver nanoparticle
AR	aspect ratio
a.u.	arbitrary units
AuNP	gold nanoparticle
AuNR	gold nanorod
B	butadiene
<i>b</i>	block (copolymer)
<i>c</i>	concentration
<i>co</i>	copolymer
CTAB	cetyl trimethylammoniumbromide
<i>d</i>	diameter
DLS	dynamic light scattering
DMF	dimethylformamide
DNA	deoxyribonucleic acid
DSC	differential scanning calorimetry
<i>E</i>	E-modulus
e.g.	<i>exempli gratia</i>
EPDM	ethylene-propylene-diene monomer rubber
eq	equivalents
et al.	<i>et alii; et aliae</i>
eV	electron volt
FTS	frequency-temperature superposition
FWHM	full width half maximum
<i>g</i>	graft (copolymer)
G'	shear storage modulus
G''	shear loss modulus
GPC	gel permeation chromatography
Hz	hertz (unit)
I	isoprene
<i>I</i>	intensity (Raman)
ICP-MS	inductively coupled plasma – mass spectrometry
i.e.	<i>id est</i>
K	kelvin (unit)
L-LSPR	longitudinal localized surface plasmon resonance
LSP	localized surface plasmons
LSPR	localized surface plasmon resonance
LVE	linear viscoelasticity
MALLS	multi angle laser light scattering
MeOH	methanol
M_n	number average molar mass
M_w	weight average molar mass
<i>n</i>	degree of polymerization
NIPAM	<i>N</i> -isopropylacrylamide
(N)IR	(near) infrared

NMR	nuclear magnetic resonance
NP	nanoparticle
NR	nanorod
OD	orientational distribution
PDI	polydispersity index
PEG	poly(ethylene glycol)
PEO	poly(ethylene oxide)
PMMA	poly(methyl methacrylate)
ppm	parts per million
PPrS	poly(propylene sulfide)
PRA	plasmon resonance absorption
PS	polystyrene
PVA	poly(vinyl alcohol)
PVP	poly(vinyl pyrrolidone)
r	radius
R	gas constant
R	rest (chemical structure)
R_g	radius of gyration
S	styrene
S	orientational order parameter
SAXS	small angle x-ray scattering
SEM	scanning electron microscopy
SERS	surface-enhanced Raman scattering
SI	supporting information
SNP	silica nanoparticle
Superhydride®	lithium triethylborohydride (trade name)
T	temperature
$\tan(\delta)$	loss factor (rheology)
TEM	transmission electron microscopy
T_g	glass transition temperature
TGA	thermogravimetric analysis
THF	tetrahydrofuran
ThPS	ω -thiol polystyrene
TISIT	α, ω -dithiol poly(isoprene- <i>b</i> -styrene- <i>b</i> -isoprene)
TPE	thermoplastic elastomer
UPy	ureido-pyrimidone
UV	ultraviolet light
VIS	visible light
vol%	volume percent
wt%	weight percent
γ	surface tension
δ	chemical shift (NMR)
η^*	complex viscosity
λ	wavelength
A	interparticle distance
ϕ (f)	filling fraction
ω	angular frequency
ω_c	G' - G'' crossover frequency (rheology)

1. INTRODUCTION

The present thesis has a primary focus on elastic nanocomposite materials made from polymers and noble metal nanoparticles. In particular, materials where nanoparticles serve as cross-linking sites or reinforcing agents are explored. In the following, fundamentals and preliminary studies are discussed in order to put the research results into context.

In chapter 1.1 the chemical, physical and biological properties of noble metal nanoparticles are reviewed with the help of selected research highlights. In the light of noble metal nanoparticle preparation, fundamentals of colloid chemistry are discussed, followed by a sub-chapter on anisotropic noble metal nanoparticles. A dense discussion on noble metal nanoparticle/polymer nanocomposites is provided in chapter 1.2 with sub-chapters focusing on synthesis methods and applications. Chapter 1.3 covers fundamentals of cross-linked materials, including both chemical and reversible cross-linking approaches. Finally, chapter 1.4 reviews previous protocols in which non-metallic or noble metal nanoparticles are used as cross-linking sites or reinforcement agents in nanocomposites.

1.1 NOBLE METAL NANOPARTICLES

Colloidal metal particles with particle sizes below 100 nm (in the following: metal nanoparticles) have gained considerable scientific and commercial attention in recent years due to their unique size-dependent chemical, physical and biological properties. Approximately 10% of atoms are located at the surface in particles with diameters of 10 nm, whereupon particles with diameters of 5 nm already possess around 40% of their atoms at the surface.^{1,2} Surface atoms are less tightly bound compared to atoms in the bulk and therefore hold higher energies.³ Consequently, metal nanoparticles show significantly increased reactivity due to an enlarged surface area to volume ratio compared to the corresponding bulk state. This is exploited in heterogenic catalysis applications where molecule adsorption on solid surfaces is the critical stage. Catalytic activity enhancement was for example observed with decreasing particle diameters in gold nanoparticle (AuNP)-catalyzed CO oxidation reactions.⁴ Also, organic cross-coupling reactions such as SUZUKI⁵ or HECK⁶ types were successfully conducted using Palladium nanoparticles (PdNP). Yet, increased reactivity is not only a benefit, but makes metal nanoparticles prone to self-aggregation; therefore suitable electrostatic or steric stabilization by surfactants is required

to avoid coarsening of the particles. Electrostatic stabilization is based upon formation of a bilayer which induces repulsive forces at close range and in addition, provides amphiphilic character to the nanoparticles.⁷ Cetyl trimethylammoniumbromide (CTAB), an aqueous quaternary ammonium salt, is commonly used as a stabilization surfactant for AuNP⁸⁻¹⁰ as well as trisodium citrate for silver nanoparticles (AgNP)¹¹ and AuNP¹² in particular. Steric stabilization is attributed to the bulkiness of the attached surfactants and shall be discussed in chapter 1.2. Reports of naked noble metal nanoparticles are rare; yet stable aqueous AgNP suspensions without additional surfactants were obtained with the “solvation cage” being sufficient for stabilization.¹³

In addition to increased chemical reactivity, metal nanoparticles exhibit physical features which are absent in the bulk metal. The electronic states of conduction electrons are discrete rather than continuous in nanoparticles with the particle size-dependent KUBO gap between the valence band and the conducting band determining properties such as electrical conductivity and magnetic susceptibility.¹⁴ The threshold at which the system is rendered nonmetallic may be approached by decreasing cluster sizes and/or temperature. Quantum confined electrons exhibit a characteristic collective oscillation in the conduction band, commonly known as localized surface plasmons (LSP). Upon excitation with light of a certain frequency, the LSP will be in resonance with the incident light which is designated as the localized surface plasmon resonance (LSPR) mode (**Figure 1-1**).¹⁵

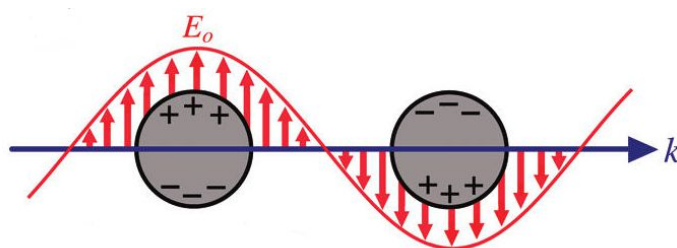


Figure 1-1. LSPR describes the collective oscillation of displaced free electrons in resonance with the electric field E_0 of light with the wave vector k . Reprinted from Ref. 16 with permission. Copyright American Chemical Society.

The interaction of light with LSPs is mathematically described by the MIE theory, according to which the extinction E of the incident light depends on the metal nanoparticle radius a , on the wavelength λ , on the dielectric constant of the surrounding medium ϵ_m , on the dielectric function of the metal nanoparticle ϵ and on the nanoparticle shape (**Equation 1-1**).¹⁷

$$E(\lambda) = \frac{24\pi N_A a^3 \varepsilon_m^{\frac{3}{2}}}{\lambda \ln(10)} \left[\frac{\varepsilon_i}{(\varepsilon_r + \chi \varepsilon_m)^2 + \varepsilon_i^2} \right] \quad (1 - 1)$$

with N_A being the areal density of the metal nanoparticle, ε_i and ε_r being the imaginary and real portion of the dielectric function of the metal nanoparticle and χ describing the aspect ratio of the nanoparticle (spheres equal a value of 2).¹⁸

The LSPR effect has been exploited in various applications. Based upon the impact of ε_m on the resonance frequency,¹⁹ molecule sensing techniques have emerged in which the introduction of an analyte causes changes in the wavelength of the resonance which can be detected by the absorption spectrum in light absorption and resonant Rayleigh scattering methods (**Figure 1-2**).^{20,21} In a different approach, the vicinity of a plasmonic nanostructure benefits from enhanced electromagnetic field intensities, giving rise to surface-enhanced Raman scattering (SERS).^{22,23} Scattering of molecules may be increased by factors of up to 10^{15} , depending on shape, size, aggregation state and metal type of the nearby nanoparticle.²⁴⁻²⁷ As a result, SERS provides strongly improved detection limits which may identify single molecule analytes.^{28,29}

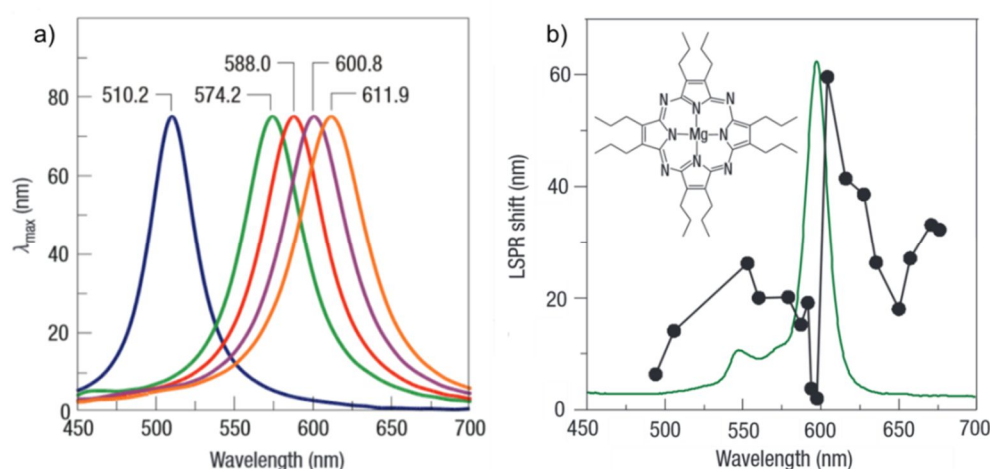


Figure 1-2. a) Resonance Rayleigh scattering spectra from AgNP in nitrogen, methanol, propan-1-ol, chloroform and benzene (from left to right) environment. Reprinted from Ref. 36 with permission. Copyright American Chemical Society. b) LSPR shift vs. LSPR wavelength for adsorption of [2,3,7,8,12,13,17,18-octakis(propyl)porphyrin]magnesium(II) (inset: chemical structure) on spherical AgNP. Solid green line: absorption spectrum of the adsorbate (arbitrary scaling). Solid black line with filled dots: plot of the AgNP LSPR shift vs. spectral position of Ag nanoparticles. The black dots represent the location of extinction maxima of bare Ag nanoparticles. Reprinted from Ref. 37 with permission. Copyright American Chemical Society.

Due to plasmon coupling of nanoparticles in close proximity, the SERS effect is most strongly observed using dense particle aggregates with small interparticle distances as substrates.^{30,31} With respect to this, many studies have been directed at generating permanent and small interparticle distances in a controlled fashion. Fixation of adjacent particles was amongst others put in to practice by connecting particles with adherent small molecules^{32,33} or by hard-template approaches.³⁴ Polymer-assisted nanoparticle assembly is discussed in chapter 1.2.2.

Excitation of metal nanoparticles with powerful light sources close to the LSPR results in local heat generation due to electron-electron scattering, also known as the photothermal effect.³⁵ Other physical properties of noble metal nanoparticles include fluorescence enhancement for the use in surface enhanced fluorescent microscopy³⁸ or as optical nanoantennas.³⁹ Superparamagnetism is observed for nanoparticles of ferromagnetic metals such as iron, cobalt or nickel.⁴⁰⁻⁴²

Metal nanoparticles strongly interact with biological systems at both the protein and the cellular level and are therefore predominantly used for antibacterial purposes and in drug delivery. Research on antibacterial activity is mainly affiliated with AgNP since biocidal effects of silver and silver ions on many species of bacteria have been known for a long time; but also iron nanoparticles (FeNP)⁴³ and copper nanoparticles (CuNP)⁴⁴ were investigated as promising candidates for biocides. AgNP are active against both gram-positive⁴⁵ and gram-negative⁴⁶ bacteria with the interaction being dependent on the particle shape.⁴⁷ Mechanistic studies revealed that both AgNP and Ag⁺ ions released from the particles contribute to the biocidal activity.⁴⁸ Both forms attach to the prevalent sulfur and phosphorus sites of the cell membrane in the first place after which the membrane morphology is altered so that its permeability is increased. After penetration, the Ag species interact with the DNA's sulfur and phosphor sites, causing cell death by affecting the respiratory chain and the cell division. In addition, Ag⁺ ions are accountable for DNA conglomeration and consequent loss of replication ability.⁴⁹ Due to its low toxicity against mammalian cells,⁵⁰ applications are amongst others directed at antibacterial coatings for the use in water purification,⁵¹ in paint⁵² or as wound dressing.⁵³

Because of their biocompatibility, AuNP are engaged in drug delivery and gene delivery applications, based upon the fact that cells naturally ingest gold nanoparticles.⁵⁴ Therefore, drugs and DNA adsorbed on AuNP as ligands may pass the cell membrane and afterwards

be released from the particle surface. Ligand modifications allow specific targeting, for example to cancer tissues.⁵⁵ The kinetics and saturation concentrations of AuNP uptake into mammalian cells follow a non-linear dependency on the particle sizes.⁵⁶ AuNP are furthermore used as contrast agents for biological labelling either *ex vivo* in clinical diagnostics or *in vivo*. Particularly, the visualization of antibody targets using antibody-attached AuNP is a major field of research interest. AuNP identification *via* transmission electron microscopy (TEM) is highly advantageous for this purpose due to the high electron density of Au; however this method is restricted to *ex vivo* applications.⁵⁷ Also, optical microscopy has been utilized to visualize human pancreatic carcinoma tissues and other diseases.⁵⁸ Endoscope-compatible microscopic methods for *in vivo* applications include optical coherence tomography and confocal microscopy.⁵⁹

The properties and applications mentioned above have a strong sensitivity towards metal nanoparticle sizes, size distributions and morphologies in common. Therefore, major research effort has been directed at bringing these parameters under control by suitable preparation methods. “Top down” preparation methods refer to those in which bulk metals are mechanically scaled down for example by using laser ablation techniques.^{60,61} However, these methods generally lack control over particle dimensions and shapes. Therefore, “bottom-up” approaches are widely used in which colloids are generated in the presence of surfactants by either reduction of metal salts or through thermal decomposition of organometallic compounds.^{62,63} This thesis exclusively focuses on reduction methods in which AgNO_3 , AgCO_2CF_3 and HAuCl_4 are used as precursors. A detailed description of noble metal nanoparticle synthesis with polymeric surfactants is given in chapter 1.2.1.

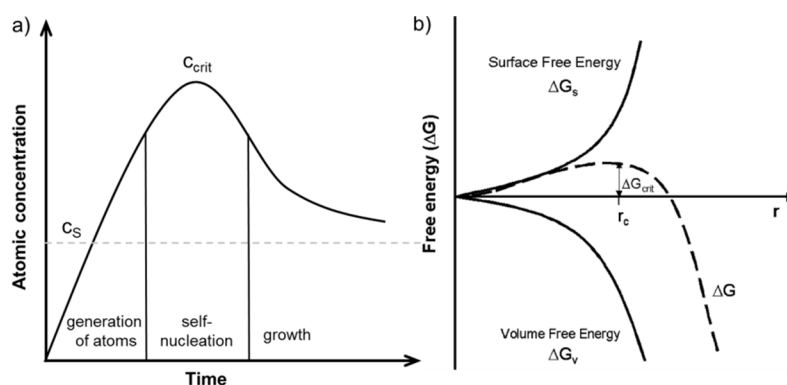


Figure 1-3. a) The classical LAMER model describes nanoparticle formation as a function of time and concentration of precursor atoms in a three-step process. b) As the formation of small nuclei is thermodynamically disfavored, condensation from the liquid phase takes place only in the supersaturated state above a critical nucleation concentration c_{crit} . Reprinted from Ref. 64 with permission. Copyright American Chemical Society.

Mechanistically, LAMER and DINEGAR described the surfactant-assisted bottom-up formation of colloids from solutions as a function of their concentration in three steps (**Figure 1-3a**).⁶⁵ Influence over particle sizes is mainly exerted by the surfactant type and concentration.⁶⁶ According to studies on the citrate-assisted nucleation of Ag, the surfactant interacts with solute Ag species through complexation and therefore affects nucleation already at early stages.⁶⁷ Moreover, small nanoparticle seeds can be used as nucleation centers to control nanoparticle growth up to the demanded size.⁶⁸ Because of temperature-dependent coarsening of colloids, also known as OSTWALD ripening, the particle size distributions become more homogeneous as a function of time.⁶⁹ Driven by the reduction of free surface energy, smaller particles redeposit on larger particles; therefore the average particle sizes are increased by the process. Control over particle size distributions may as well be exerted by centrifugation due to enrichment of heavy particles away from the center of rotation, by chromatographic methods, electrophoresis or by fractionated precipitation.^{70,71}

The behavior of metal nanoparticles at the interface of two non-miscible liquid phases is dependent on particle sizes, particle-particle interactions and on particle-liquid interactions according to **Equation 1-2**. The driving force for the self-assembly of metal nanoparticles or other colloids at liquid-liquid interfaces was identified to be reduction of total free energy.⁷²

$$\Delta E = - \frac{\pi r^2}{\gamma_{OW}} [\gamma_{OW} - (\gamma_{PW} - \gamma_{PO})]^2 \quad (1 - 2)$$

where ΔE represents the interfacial energy difference of an interface-attached particle, r the particle radius, γ_{PW} and γ_{PO} the tension between the particle and the respective phases and γ_{OW} the interfacial tension. The decrease of ΔE is close to the thermal energy kT if nanosized particles are used, whereupon larger particles contribute to a more effective reduction in energy. The interfacial tension determines the wettability of the particle surface and therefore, the contact angle. In all, nanoparticle assembly causes stabilization of oil-in-water or water-in-oil droplets; also known as PICKERING emulsion. Therein, the liquid with the inferior wetting ability becomes the dispersed phase.⁷³ Under ideal circumstances, assemblies in 90° angles will generate emulsions with the highest stability, whereupon contact angles below or higher than 90° would lead to a decrease in emulsion stability (**Figure 1-4**).

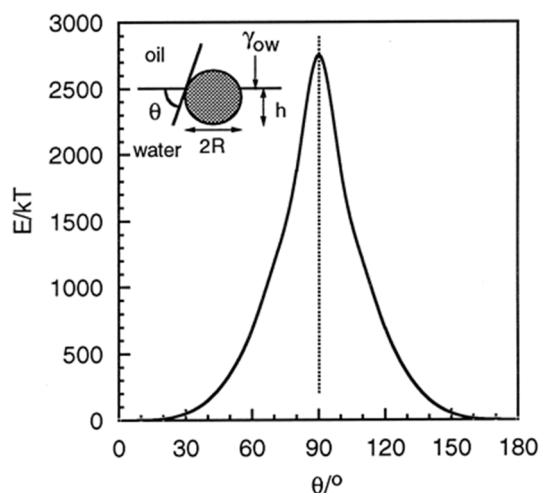


Figure 1-4. Interfacial energy difference E as a function of contact angle θ of a spherical silica particle with 10 nm radius at a planar toluene/water interface. Reprinted from Ref. 74 with permission. Copyright American Chemical Society.

1.1.1 ANISOTROPIC MORPHOLOGIES

Concerning preparation, handling and application of noble metal nanoparticles, spherical shapes have been best established among other possible morphologies. However, morphologies other than spheres are beneficial for various applications because physical properties, including but not limited to LSPR, are not only dependent on metal type, size and size distribution but also on the particle shape (**Figure 1-5**).

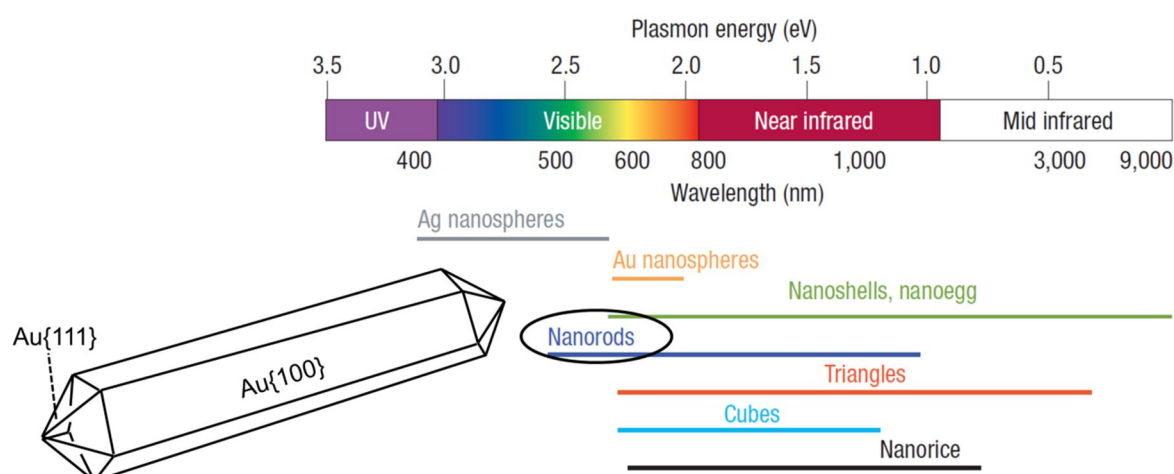


Figure 1-5. Nanoparticle shape-dependence of LSPR absorption ranges. Also shown (left): Crystal faces scheme of pentagonal faceted AuNR. The same structure applies for AgNR. Reprinted from Ref. 75 with permission. Copyright Nature Publishing Group.

In the following, only rod-like shapes of silver and gold nanoparticles (designated as AgNR and AuNR) shall be discussed with regards to synthesis, properties and applications. In ideal crystals, AgNR and AuNR exhibit $\{100\}$ faces along their longitudinal pentagonal cross-section and five $\{111\}$ faces at each end as face-centered cubic (fcc) lattices.

The $\{100\}$ faces have a low atomic density, whereupon the $\{111\}$ faces are closely packed. Therefore, bulky surfactants preferentially attach to the longitudinal planes on which high surfactant coverage leads to a decrease in reactivity.⁷⁶ Most commonly, CTAB or similar CTA⁺-based surfactants are used for this purpose as the sterics of the CTA⁺ headgroups match with the atom spacing of the $\{100\}$ faces. Nucleation from metal atoms in solution is inhibited at the stabilized longitudinal faces, but favored at the $\{111\}$ end faces. Based on the finding that control over the crystal growth direction can be exerted by CTA⁺-based surfactants (also named structure-directing agents), preparation of AgNR and AuNR as well as of other morphologies can be carried out using electrochemistry⁷⁷ or spherical seed particles as precursors.⁷⁸⁻⁸¹ In detail, the seed-mediated growth procedure is carried out by combining seeds, a metal precursor salt, a structure-directing agent and a weak reducing agent such as ascorbic acid. Dynamic bilayer formation of the CTA⁺ surfactant in a “zipping”-manner is considered the energetically most favored growth mechanism (**Figure 1-6a**).⁸² The resulting aspect ratio may vary as a function of the concentrations of the reagents relative to each other,⁸³ of the seed particle diameters,⁸⁴ of pH⁸⁵ and also of the structure-directing agent’s tail length⁸² and counter-ion.⁸⁶

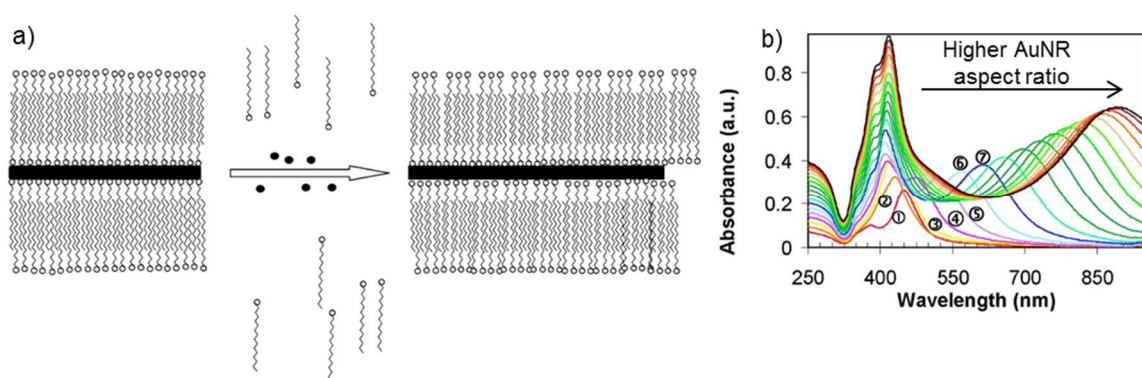


Figure 1-6. a) Scheme of AuNR growth by “zipping” mechanism and CTA⁺ bilayer formation at the longitudinal faces. Reprinted from Ref. 82 with permission. Copyright American Chemical Society. b) UV/Vis spectra of AuNR during unidirectional growth. Each spectrum is separated by 1 min at a total reaction time of 17 min. Reprinted from Ref. 87 with permission. Copyright American Chemical Society.

Besides wet chemical methods for preparing anisotropic metal structures, electrodeposition of gold into nanoporous templates with distinct pore diameters has been reported.⁸⁸⁻⁹⁰ Using this procedure, particle dimensions are well-controlled; however template preparation and removal is laborious and costly.

A straight-forward method to monitor unidirectional particle growth is given by absorption analysis. Anisotropic AuNR and AgNR exhibit two LSPR peaks which correlate to the extinction of light along the short axis of the rods (transverse LSPR band at shorter wavelength) and the long axis of the rod (longitudinal LSPR band at higher wavelengths) in which the shift of the longitudinal portion is dependent on the aspect ratio (**Figure 1-6b**). Spectral absorption ranges from visible to near infrared (NIR) can be covered. This has amongst other applications been exploited in SERS setups^{34,91} and for photothermal applications *in vivo*. In short, the conversion of light into localized heat, caused by the photothermal effect, is a tool for the ablation of cancer cells.^{92,93} AuNR with longitudinal LSPR absorption peaks in the NIR spectral range are promising candidates as photothermal agents *in vivo* because NIR light penetrates deeply and non-destructively into tissue. It was also shown that the photothermal effect causes melting of the rods and subsequent fragmentation into spherical shapes.⁹⁴

Due to their anisotropic shape, metal nanorods may be aligned into an ordered structure with common spatial orientation similar to liquid crystalline phases. Solution-based self-assembly as a method for nanorod orientation has been induced by several means, for example by mixed surfactant scenarios. Hydrophobic interaction of rod end-attached polymer chains was triggered by selective solvents, yielding worm-like structures.^{95,96} A similar approach was reported by THOMAS et al. who used a CTAB/3-mercaptopropionic acid mixed ligand scenario for AuNR self-assembly.⁹⁷ The authors claim hydrogen bonding interaction to be the driving force for AuNR orientation. Further end-to-end assemblies, leading to LSPR intercoupling have been realized with α,ω -difunctional organic compounds.^{98,99} Side-to-side alignment was induced by Biotin-Streptavidin linkages in aqueous dispersion.¹⁰⁰ Different from solution-based self-assembly, template-based assembly in the solid state may as well be used for nanorod orientation.¹⁰¹ In a representative example, polypyrrole-stabilized AuNRs are synthesized inside aluminum oxide hard templates after which the template is sacrificed by dissolution, yielding nanorod assemblies with dimensions dictated by template dimensions.¹⁰² Vapor deposition has as

well been demonstrated to generate aligned nanorods.¹⁰³ Polymer-assisted orientational assembly is discussed in chapter 1.2.2.

1.2 NOBLE METAL NANOPARTICLE/POLYMER NANOCOMPOSITES

Noble metal nanoparticles with organic, polymeric stabilizing shells grafted on the metal surface belong to the class of nanocomposites. In contrast to electrostatic repulsion, polymers prevent nanoparticle aggregation due to their steric bulkiness. Further to the stabilizing effect, nanocomposites combine the above discussed properties of noble metal nanoparticles with polymer properties symbiotically.

In general, polymers may not only serve as a ligand such as discussed in detail in the following chapter 1.2.1. Another popular strategy to combine polymers and noble metal nanoparticles is to use the polymer as dispersion medium where pre-synthesized noble metal nanoparticles with other ligands are embedded in. These ligands may be of polymeric or non-polymeric nature. An early protocol to prepare such mixtures describes the addition of pre-formed alkanethiol-stabilized nanoparticles to styrene or methyl methacrylate monomer solution, followed by polymerization.¹⁰⁴ However, it is known that homogeneous dispersion of pre-formed noble metal nanoparticles into a preformed polymer matrix is favored if the stabilizing ligand and the matrix are compatible; i.e. of the same polymer type. CORBIERRE et al. demonstrated successful embedment of pre-formed AuNP in pre-formed polystyrene matrix by using ω -thiol polystyrene as a stabilizing ligand.¹⁰⁵ The same workgroup also found out that the particle dispersibility is improved if the molecular weights of ligand and matrix are comparable.¹⁰⁶ Also, the nanoparticle stability improves with increasing matrix molecular weight if ligand and matrix are of the same polymer type.¹⁰⁷ Embedment of pre-formed nanoparticles into a polymer matrix usually is done *via* solution-blending and subsequent co-precipitation. Based on high thermal colloidal stability, our group reported on a co-extrusion procedure.¹⁰⁸

Grafting of a polymeric stabilizing layer to a noble metal surface is somewhat more complex. Due to the high reactivity of metal nanoparticles, only attractive energetic forces between polymer and nanoparticle (also known as adsorption) guarantee nanoparticle stability; therefore the interaction is governed by a polymer-attached anchor group with a high affinity to the metal type used. The anchor may be either located in the repeating unit

or at the chain end which has an influence on the microstructure of the nanocomposite. Wrapping structures are obtained by grafting macromolecules having their anchor groups located in the repeating unit such as oligomeric^{109,110} or dendritic¹¹¹⁻¹¹³ thioethers and polymeric trithiocarbonates.¹¹⁴ Other stabilizing polymers with anchor groups within the repeating unit include polyacrylonitrile,¹¹⁵ polypyrrole,¹¹⁶ poly(vinyl pyrrolidone) (PVP),¹¹⁷ poly(allylamine),¹¹⁸ poly(vinyl alcohol) (PVA),¹¹⁹ poly(acrylic acid),¹²⁰ poly(ethylene imine)¹²¹ and poly(vinyl pyridine).¹²² Brush-like structures are obtained by using polymers having their anchor group(s) located at the chain end such as ω -amine polymers¹²³ or ω -thiol polymers.¹²⁴ In particular, thiol groups have been the subject of many studies due to their high affinity to noble metal nanoparticles such as AuNP and AgNP.¹²⁵ Upon coordination onto the particle surface, thiols are deprotonated to give thiolates,^{126,127} which develop equilibrium between chemisorption and desorption and undergo place exchanges on the particle surface.^{128,129} Having bonding energies of around 50 kcal/mol, thiol groups exhibit the highest affinity to gold surfaces among other anchor groups.¹³⁰ However, oxidation of thiolates is easy and yields disulfides which develop a weaker bonding to noble metal surfaces.¹³¹

1.2.1 SYNTHESIS OF POLYMER-STABILIZED NANOPARTICLES

“Grafting from” as well as “grafting to” methods are used to prepare polymer-stabilized noble metal nanoparticles in solution. In the former, nanoparticles are functionalized with initiating groups such as ATRP-active moieties¹³²⁻¹³⁷ or with monomeric groups such as 4-vinyl thiophenol as used in our group^{138,139} in the first step. These surface-attached groups undergo polymerization in the second step. In contrast, pre-formed polymers are used in “grafting to” methods in combination with either *ex situ*- or *in situ*-prepared noble metal nanoparticles. It is noteworthy that any nanoparticle shapes other than spheres may exclusively be grafted *to* polymers in *ex situ* fashion. This thesis focuses on the application of “grafting to” methods.

In situ “grafting to” methods include those where the formation of noble metal nanoparticles and stabilization by a pre-formed polymer takes place simultaneously. Generally, this method is straight-forward and well-established for many metal and polymer types; however it lacks in control with regards to nanoparticle sizes, size distributions and morphologies. Single-phase *in situ* protocols are based on the reduction

of a metal precursor salt in presence of a polymeric to-be stabilizing ligand in homogeneous solution (**Figure 1-7**). Early reports on single-phase *in situ*-prepared *polymer*-stabilized noble metal nanoparticles describe the reduction of precursor salts within block copolymer micelles by SCHROCK et al. using phosphine groups in the polymer backbone as anchor groups¹⁴⁰ and by ANTONIETTI et al. using thiol and phosphine groups in the side chain as anchor groups.^{141,142} The latter protocols are based on the use of tetrachloroaurate, gold(III)chloride, silver nitrate or silver perchlorate precursors. Those are either dissolved or suspended in toluene and subsequently reduced by hydrazine or sodium borohydride inside the corresponding block copolymer micelles. Metallic,¹⁴³ semiconducting¹⁴⁴ and bimetallic¹⁴⁵ nanoparticles have been implemented into block copolymer micelles along the lines of this method. Our group reported on *in situ*-prepared ω -thio polystyrene-stabilized AgNP and CuNP with average diameters of less than 3 nm.¹⁰³ THF-soluble silver trifluoroacetate was used as the AgNP precursor salt in combination with the reducing agent Superhydride® for this purpose. Moreover, dendrimers,¹⁴⁶ graft copolymers,¹⁴⁷ hydrogels,¹⁴⁸ (co)polymers from RAFT polymerization¹⁴⁹ and thiol-capped polymers from ring-opening cationic polymerization¹⁵⁰ were charged with AuNP using single-phase *in situ* protocols.

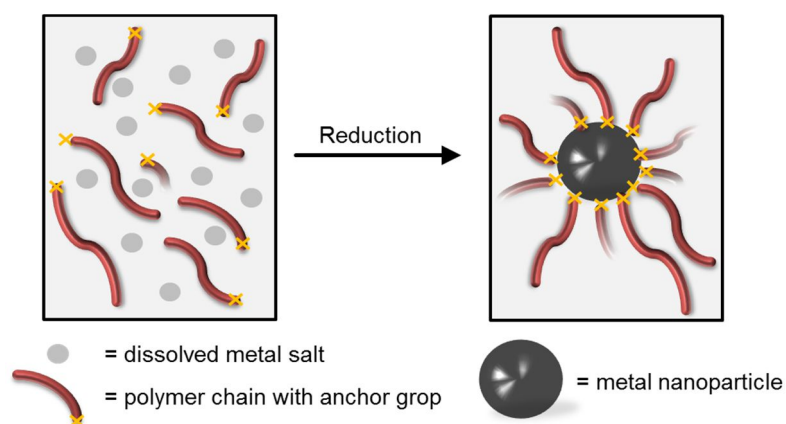


Figure 1-7. Simplified scheme of single-phase *in situ* reduction method for the preparation of polymer-stabilized noble metal nanoparticles.

BRUST et al. developed a hetero-phase *in situ* method in water/toluene for the purpose of using hydrophobic ligands and hydrophilic metal salt precursors.¹⁵¹ Water-to-toluene phase transfer of nanoparticles was conducted with assistance of the surfactant tetraoctylammonium bromide (TOAB). The corresponding preparation of AgNP was performed using AgNO_3 as a precursor.¹⁵²

In *ex situ* “grafting to” methods, pre-formed noble metal nanoparticles are combined with pre-formed polymers. These kinds of post-surface modifications allow preceding accurate preparation of noble metal nanoparticles with distinct sizes and morphologies using stabilizing ligands other than polymers. Subsequently, the particle surface may be modified by coating or exchanging of the surfactants. Layer-by-layer coating can be used to graft charged ligands such as polyelectrolytes to the particle. This type of surface modification has for example been employed for coating CTAB-stabilized AuNR with a polymeric layer.¹⁵³⁻¹⁵⁵ However, this technique is limited to charged polymers and does not remove the original surfactant. For these reasons, ligand exchange modifications in which ligands are replaced by those with a higher affinity to the metal surface are the most common way to graft polymers onto *ex situ* prepared nanoparticles. The success of ligand exchanges depend on the interplay between leaving ligand, exchanging ligand, solvents and other factors such as temperature and the presence of oxygen.¹⁵⁶ For instance, removal of CTAB surfactant which is commonly used for preparation and stabilization of AuNP and AuNR is somewhat more challenging compared to other common ligands due to tight CTAB adsorption on gold surfaces.

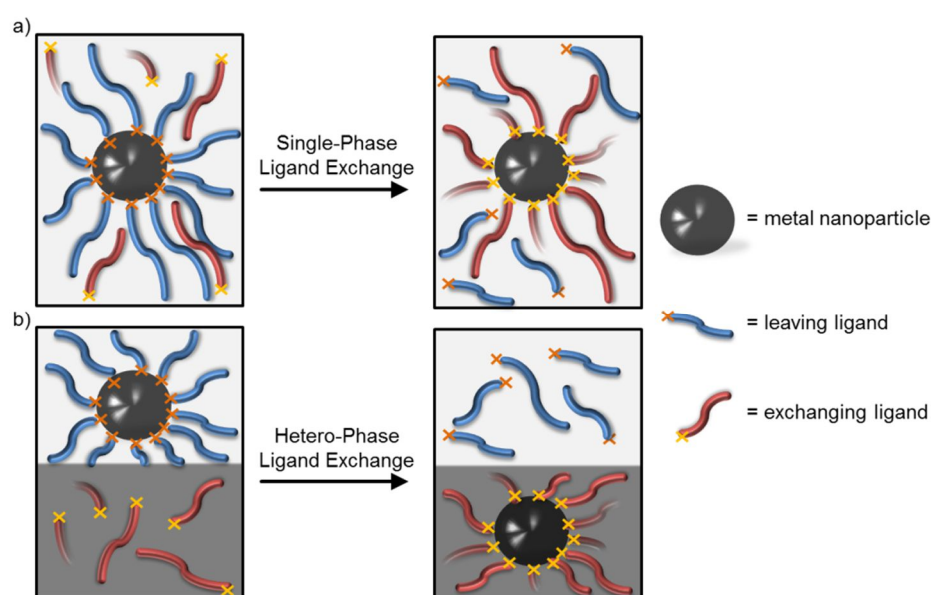


Figure 1-8. Simplified schemes of a) single-phase and b) hetero-phase (below) *ex situ* “grafting to” methods for the preparation of polymer-stabilized noble metal nanoparticles.

Depending on the polarity of the leaving and exchanging ligands, the reaction may either be carried out in single-phase using a single solvent (or miscible solvent mixture) or in hetero-phase using immiscible solvent mixtures (**Figure 1-8**). In the following, only those ligand exchanges are discussed where the leaving ligand is a hydrophilic type ligand such

as citrate, quaternary ammonium salt or water-soluble polymer and the exchanging ligand is a hydrophobic type ligand such as functionalized polymers. Nevertheless, hydrophobic ligands can also be replaced by either other hydrophobic¹⁵⁷⁻¹⁵⁹ or hydrophilic¹⁶⁰ ligands.

Single-phase ligand exchange has been for example carried out on AgNP and AuNP with different leaving ligands using a water/acetone mixture with ω -thio polystyrene being the exchanging ligand.¹⁶¹ Due to poor solubility of ω -thio polystyrene-stabilized nanoparticles in this solvent mixture, precipitation enabled isolation of the demanded product. A water/THF mixture was used for the single-phase ligand exchange of CTAB-stabilized AuNR with ω -thio polystyrene using ultrasound for activation.¹⁶² Upon isolation, incomplete conversion was observed which is ascribed to the differing reactivity of AuNR facets (see chapter 1.1.1). Complete CTAB removal from AuNR surface has been accomplished in more sophisticated approaches utilizing an ionic exchange resin¹⁶³ or by a two-step approach.¹⁶⁴ EHLERT et al. demonstrated complete replacement of oleic acid ligands on different inorganic nanoparticles by polymers with hydroxyl, amine or carboxylic acid end groups in single-phase.¹⁶⁵ The authors developed a quantitative precipitation method where phase-separation promotes the removal of oleic acid ligand. Exchanging 4-(*N,N*-dimethylamino)pyridine by ω -thio polystyrene on AuNP was performed within a specific solvent mixture, consisting of water/dichloromethane/ethanol 50:17:33 and acetic acid.¹⁶⁶

Hetero-phase ligand exchanges require the noble metal nanoparticles to phase transfer as the leaving ligand is exclusively soluble in one phase while the exchanging ligand is only soluble in the other phase.¹⁶⁷ The reaction takes place at the liquid-liquid interface of an incompatible solvent pair. Consequently, conversion can be easily monitored through color change of the phases - which is a tremendous advantage over single-phase ligand exchanges. The kinetics of such kind of conversion is exclusively influenced by diffusion of particles to the liquid-liquid interface and may thus be controlled by influencing the particle mobility and the interface area. Isolation of the desired product is provided by simple phase separation. However, hetero-phase ligand exchanges for the preparation of polymer-stabilized metal nanoparticles are largely unexplored. Yet, hetero-phase ligand exchanges are well-established for organic, *non-polymeric* exchanging ligands.¹⁶⁸⁻¹⁷² For example, KARG et al. performed rapid citrate-to-alkylamine exchange by transferring AuNP from water to a chloroform phase by vigorous stirring.¹⁷³ Moving of AuNP between different liquid phases *without* ligand exchange is described for AuNP stabilized by

amphiphilic polymers.¹⁷⁴⁻¹⁷⁶ The ability of nanoparticles to pass the liquid-liquid interface can also be controlled *via* external stimuli.¹⁷⁷

Previous attempts to graft hydrophobic polymers onto *ex situ*-prepared AuNP by hetero-phase ligand exchange faced multiple challenges: First, the repertory of suitable solvents is limited to immiscible pairs such as water/toluene, water/chloroform, water/hexane and water/diethylether. Second, the generation of an interphase consisting of AuNP-stabilized micelles was observed during citrate-to- ω -thio polystyrene exchange in water/toluene, yielding only partial ligand exchange.¹⁷⁸ In turn, citrate-to-poly(ethylene imine) ligand exchange in water/chloroform was reported successful.¹⁷⁹ Third, straight-forward, one-step hetero-phase ligand exchanges with CTAB as leaving ligand remain unreported. Merely, two-step¹⁸⁰ and three-step¹⁸¹ methods have been suggested recently to completely remove CTAB from gold surfaces. In the present thesis, novel hetero-phase ligand exchange methods are developed for the purpose of grafting ω -thio polymers on AgNP and AuNR where the leaving ligand is PVP or CTAB, respectively. It is shown that the hitherto existing challenges of micelle generation at the liquid-liquid interface as well as problematic CTAB removal from Au surfaces - both leading to incomplete ligand exchange - can be overcome using one-step methods.

1.2.2 APPLICATIONS

Providing sterical hindrance, polymers may protect noble metal nanoparticles from aggregation if grafted to the particle surface. Yet, nanocomposites from noble metal nanoparticles and polymer are more than that. Their combination opens interesting perspectives for the design of new materials where both components contribute to the resulting material properties.

Regardless whether polymers serve as ligands, as matrix or both as ligand and matrix, the three main purposes for combining noble metal nanoparticles and polymers are:

- (1) to make use of the facile nanoparticle properties in (solid state) applications
- (2) to control the assembly of nanoparticles and
- (3) to design responsive nanomaterials by engaging functional polymers.

In the following, relevant application highlights following these purposes are discussed separately, although many studies unite the aforesaid purposes.

Purpose 1:

Only those noble metal nanoparticles which are durable and also thermally and chemically stable can unfold their unique, above discussed properties in material applications. Special applications may also require biocompatibility or processability. Polymers can provide a basis for these demands. A tremendous focus has been placed on exploiting the physical - and in particular the optical - properties of noble metal nanoparticles in nanocomposite materials. In this context, solid SERS-active substrates have amongst others been designed from AgNP/PVA,¹⁸² AuNP/poly(dimethylsiloxane)¹⁸³ and AuNP/PEO-PS microbeads.¹⁸⁴ SERS performance in a broad temperature range from -60 °C to +65 °C was reported for AgNP/poly(*tert*-butylacrylate) nanocomposites.¹⁸⁵ The anisotropic photothermal effect of AuNR was exploited for selective melting of PEO nanofibers,¹⁸⁶ for laser light-induced patterning of AuNR/PVA films¹⁸⁷ and for the design of shape-memory materials.¹⁸⁸

Besides physical properties, the high chemical reactivity of noble metal nanoparticles is exhausted in combination with polymers in catalyst systems. In particular, PdNP and AuNP are of high interest for catalytic applications.¹⁸⁹ For example, AuNP-coated polystyrene microspheres from dispersion polymerization¹⁹⁰ and nanocomposites from AuNP and *N*-heterocyclic carbene-functionalized conducting polymers¹⁹¹ were used to catalyze the reduction of rhodamine B and of 4-nitrophenol, respectively. In our group, AuNP were immobilized in durable poly(*p*-xylylene) tubes and used as heterogeneous “tea-bag” catalysts for the alcoholysis and hydrolytic oxidation of dimethylphenylsilane.¹⁹² The reduction of 4-nitrophenol was also successfully catalyzed using AgNP in nanocomposites made with polystyrene-poly(acrylic acid) brush particles.¹⁹³

Antibacterial materials can be provided by blending AgNP into suitable polymeric matrices. For instance copolymers from acrylamide and cellulose¹⁹⁴ or poly(methyl methacrylate)¹⁹⁵ were loaded with AgNP and used as antibacterial materials. Food packaging or medical devices may amongst others be applications for such kind of materials.

Purpose 2:

Polymeric ligands are well-suited for gaining structural control over nanoparticle assemblies. Significant property changes are observed as a function of the interparticle distance and most notably, distinct plasmonic properties can be designed.¹⁹⁶ For instance, interparticle distances can be modified by changing the volume fraction of nanoparticles within the polymer matrix, such as demonstrated for PEG-stabilized AuNR in PMMA or PEO matrix.¹⁹⁷ Furthermore, controlled AuNP clustering with coordination numbers of up to 7 could be triggered by coating the particles with poly(ethylene oxide-*b*-propylene oxide-*b*-ethylene oxide). The authors reported substantial impact on the interaction with incident light as a function of the coordination number.¹⁹⁸ As a consequence from generating defined SERS hotspots within the interparticle gap, the SERS enhancement factors strongly scales with the particle coordination number (**Figure 1-9**).

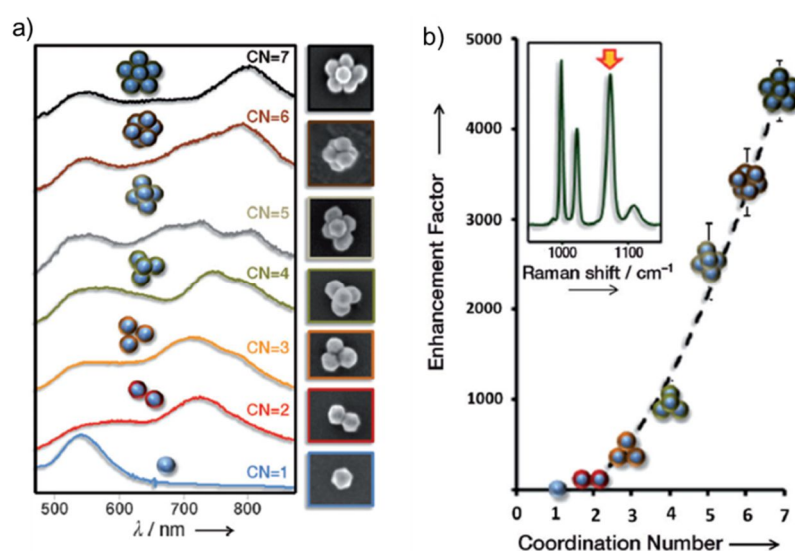


Figure 1-9. a) Dark-field single-particle optical spectroscopy as a function of the AuNP coordination number. Right: SEM pictures of the corresponding clusters. b) SERS enhancement as a function of the coordination number relative to the enhancement produced by a single particle. Inset: SERS spectrum of benzenethiol on the pentagonal bipyramid (coordination number 7). Reprinted from Ref. 198 with permission. Copyright John Wiley and Sons.

Gaining control over the alignment of anisotropic metal nanoparticles such as nanorods is one of the paramount research objectives for applications like sensing,^{199,200} wave guiding⁷⁵ and metamaterials.^{201,202} Solution-based self-assembly approaches are discussed in chapter 1.1.1.; however real applications require anisotropic metal nanoparticles in the *solid-state*. Therefore, polymer-assisted alignment of nanorods has been provided by several means.

Incorporation of metal nanorods in electrospun polymeric nanofibers is a well-established method where alignment is facilitated by strong shear forces (**Figure 1-10**).²⁰³⁻²⁰⁶ Macroscopic alignment of nanofibers and therefore, of the embedded nanorods could be achieved by oriented electrospinning with a rotating cylindrical collector.¹⁸⁶

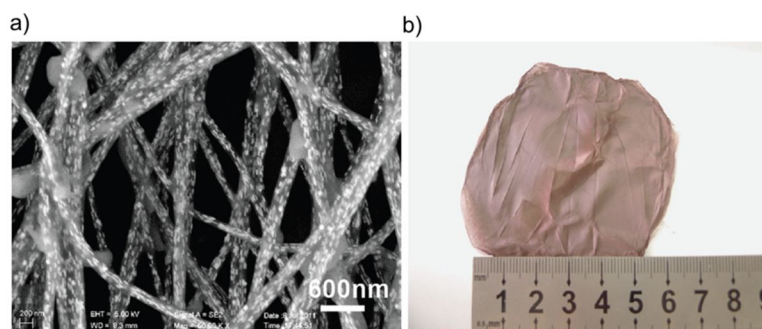


Figure 1-10. Alignment of AuNR inside electrospun PVA nanofibers. a) SEM image at 50,000-fold magnification. b) AuNR/PVA nanofiber mat with AuNR concentration of 200 nM. Reprinted from Ref. 206 with permission. Copyright John Wiley and Sons.

Selective sequestering of metal nanorods into microphase domains of block copolymers is guided by attractive interaction between the stabilizing nanorod ligand and one of the polymer blocks. In cylindrical or lamellar block copolymer morphologies, nanorods are confined as a function of their sizes: If the block domains are narrower than the nanorod length, the nanorods will be organized in end-to-end fashion. This is demonstrated for lamellar poly(styrene-*b*-methyl methacrylate) where PEO-coated AuNR undergo attractive interaction with the methyl methacrylate domain²⁰⁷ or for cylindrical poly(styrene-*b*-4-vinyl pyridine) where ω -thiol polystyrene-stabilized AuNR are compatible with the styrene domain.²⁰⁸ This concept is also assignable to macroscopic length scales by using lithographically defined, chemically nano-patterned surfaces. Electrostatic selectivity between mercaptopropene sulfonate-coated AuNR and the 2-vinyl pyridine domain on a polystyrene/poly(2-vinyl pyridine) nano-patterned surface was thus reported to yield either end-to-end or side-to-side AuNR assemblies as a function of the pattern width (**Figure 1-11**).²⁰⁹

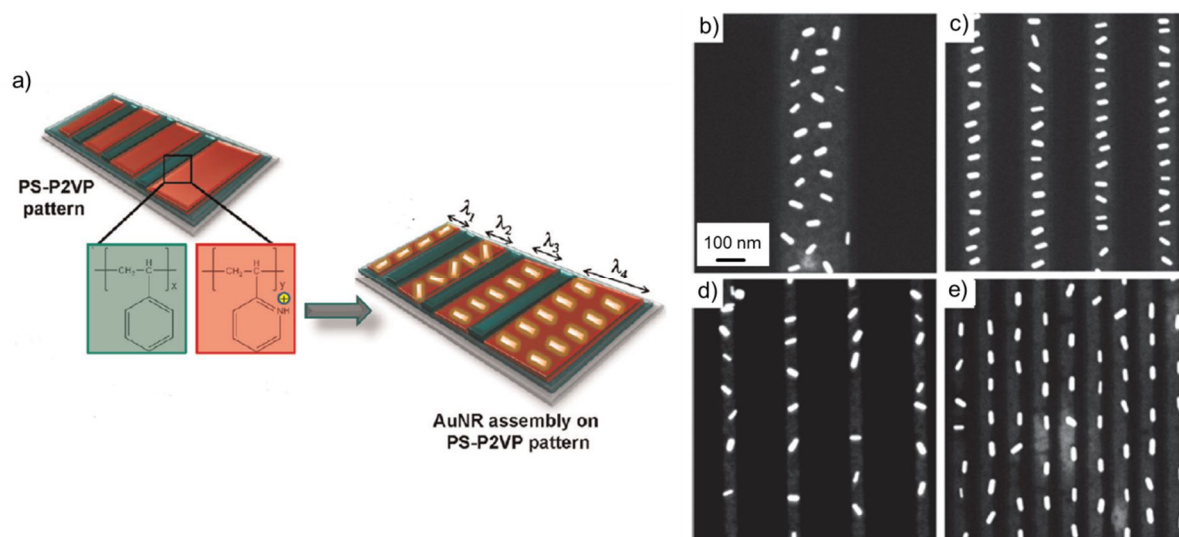


Figure 1-11. a) AuNR assembly within the poly(2-vinyl pyridine) pattern in polystyrene/poly(2-vinyl pyridine) lithographically nano-patterned surfaces. AuNR orientation is controlled by the width of the pattern: b) 250 nm; c) 100 nm; d) 50 nm; e) 30 nm. Reprinted from Ref. 209 with permission. Copyright American Chemical Society.

Macroscopic AuNR alignment in polymer films was provided *via* thermoplastic deformation of PVA films. Therefore, PVP-stabilized AuNR,²¹⁰ CTAB-stabilized AuNR^{211,212} or citrate-stabilized AgNR²¹³ were embedded in PVA matrix by solution-blending and casted on a glass substrate, followed by evaporation of the solvent. The resulting nanocomposites were melted and mechanically drawn. As a result from uniaxial mechanical force, the incorporated AuNR aligned along the stretching direction (**Figure 1-12**). Their orientation was conserved by cooling the film. Such nanocomposites have been further explored in view of macroscopic polarized light emission,²¹⁴ nonlinear light absorption as a function of the intensity of incident light²¹⁵ and quantification of the average orientation from light absorption data.²¹⁶ In general, nanorod alignment through thermoplastic deformation is a versatile method to generate macroscopic nematic arrangements; however controlled adjustment of the corresponding orientational order parameter S is not possible. Also, this method lacks reversibility of alignment back to a random orientational distribution. In the present thesis, it is shown that AuNR alignment can be controlled by uniaxial mechanical stimulation of elastic nanocomposites in a reversible and stepless fashion at room temperature.

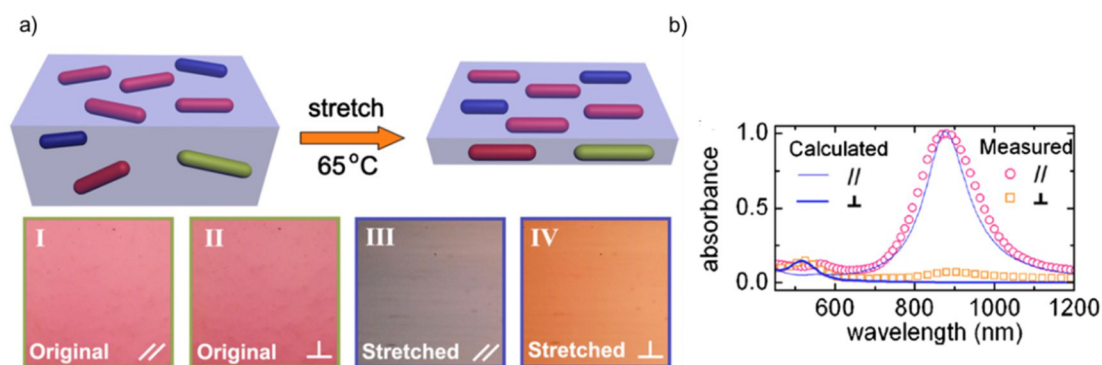


Figure 1-12. a) Above: Simplified illustration of AuNR alignment within PVA matrix through thermoplastic deformation. Below: Optical microscopy images under white light polarized parallel and perpendicular to the stretching direction. Dissimilar colors in the stretched state indicate dichroism due to AuNR alignment. b) The absorption behavior of the films is dependent on the polarization angle of incident light. Reprinted from Ref. 215 with permission. Copyright AIP Publishing LLC.

Purpose 3:

Combinations of functional polymers with noble metal nanoparticles yield responsive nanomaterials where external stimulation controls the nanoparticle activity. Reversible thermo-responsive changes in the optical properties of AuNR were for instance reported for AuNR-coated poly(NIPAM) microgels.²¹⁷ Collapse of the microgel at temperatures above the lower critical solution temperature of the polymer (ca. 32 °C) induced a 28 nm red shift of the longitudinal LSPR band due to changes in the nanorod density. The same effect was observed for a dispersion of thermo-responsive poly(ethylene oxide-*co*-propylene oxide)-coated AuNP in poly(ethylene oxide-*b*-propylene oxide-*b*-ethylene oxide) matrix.²¹⁸ Additionally, the authors demonstrate controlled and reversible particle aggregation as a function of temperature. The impact of the AuNR density on top of and within poly(NIPAM) spheres on the appearance of additional plasmon-coupled resonance modes was studied as a function of temperature by LANGE et al.²¹⁹

The thermo-responsive properties of poly(NIPAM) were further exploited for catalysis applications. AuNP/polyNIPAM²²⁰ and AuNP/poly(NIPAM-*b*-4-vinyl pyridine)²²¹ nanocomposites were employed to catalyze the reduction of ferricyanide ions by borohydride and the reduction of *p*-nitrophenol, respectively. The thermo-responsive phase transition behavior is used to control the diffusion of reagents through the polymer shell. Only in the swollen state below the LCST of poly(NIPAM), reagents pass the polymer layer to reach the catalytically active AuNP.

pH-responsive nanocomposites were made from AuNP and poly(vinylpyridine)²²²⁻²²⁴ where reversible nanoparticle aggregation was observed at pH values above 3-4 (**Figure 1-13**). Possible applications include controlled drug delivery and sensor performance.²²⁵

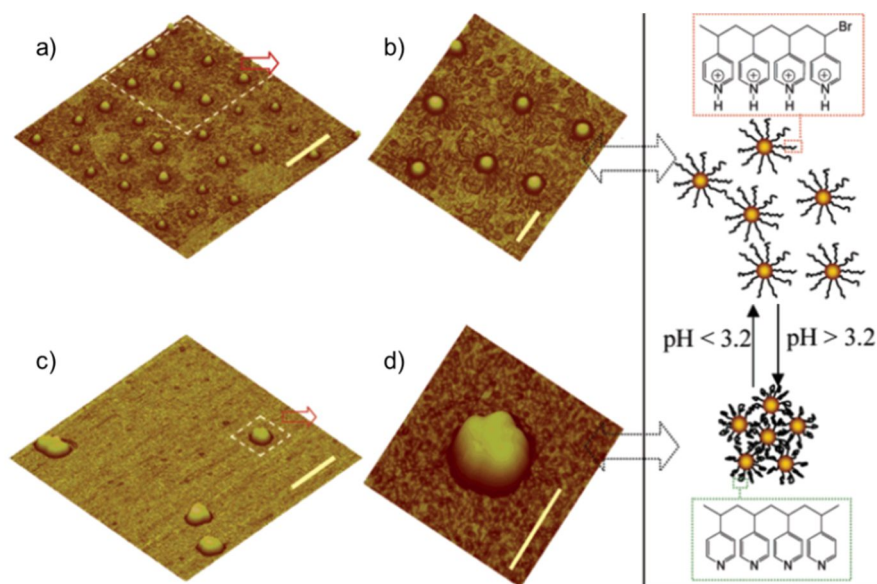


Figure 1-13. 3-D AFM images of poly(4-vinylpyridine)-coated AuNP below pH of 3.2 (a, b) and above pH of 3.2 (c, d). Reversible control of nanoparticle aggregation exerted *via* change of pH. Scale bar: 500 nm in panels a) and c); 200 nm in b) and d). Reprinted from Ref. 222 with permission. Copyright American Chemical Society.

Solvent-responsive polymeric materials such as hydrogels may as well be engaged as functional precursor for the preparation of nanomaterials. For instance, cross-linked polyacrylamide was charged with electrically conductive AuNP and applied onto an electrode surface. The polymeric network swells in good solvents and collapses in non-solvents, causing rearrangement of AuNP inside the network matrix. As a consequence, the electric resistivity of the nanocomposite was shown to decrease in the collapsed state and increase in the swollen state.²²⁶

1.3 CROSS-LINKING OF POLYMER CHAINS

Polymer chain dynamics may be probed at different time scales by for instance dynamic rheology,²²⁷ dielectric spectroscopy²²⁸ or Field-Cycling (FC) ¹H NMR spectroscopy.²²⁹⁻²³¹ The ROUSE model provides explanations for chain dynamics behavior at short time scales²³² whereas the tube reparation model by DE GENNES²³³ and DOI/EDWARDS²³⁴

describes the behavior at long time scales of entangled chains (**Figure 1-14**). At the longest time scales, terminal relaxation is approached, leading to liquid-like free diffusion of the polymer chains.²³⁵ Cross-linking can prevent terminal relaxation due to immobilization of chain segments.

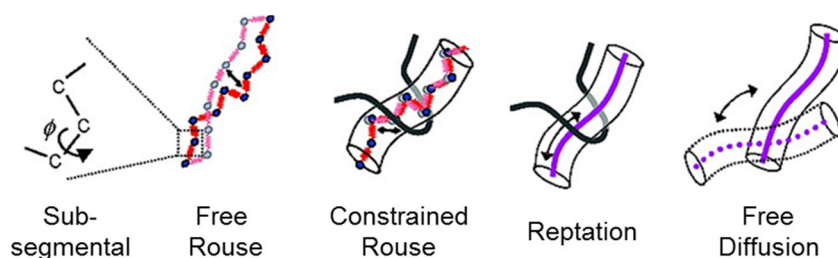


Figure 1-14. Schematic illustration of polymer dynamic theories at different time scales. Sub-segmental, free Rouse, constrained Rouse and reptation dynamics are probed at picosecond, nanosecond, microsecond and millisecond time scales, respectively. Free diffusion is probed at the longest time scales (milliseconds to days). Reprinted from Ref. 236 with permission.

1.3.1 CHEMICAL CROSS-LINKING

Apart from thermosetting plastics made from very dense networks and hydrogels made from cross-linked water-soluble polymers, rubbers are the most important class of chemically cross-linked materials. Rubbers are made up of non-rigid, amorphous polymers having glass transition temperatures (T_g) below usage temperature. Owing to cross-linking, plastic deformation is suppressed and strain-induced mechanical deformations are reversible in the linear viscoelastic (LVE) range.²³⁷ Under shear stimulation, rubbers reveal a “rubber plateau” at low shear frequencies where the storage modulus G' dominates the loss modulus G'' independent of the shear frequency over a large frequency range. The characteristic restoring force (also known as elasticity) may depend on many factors, most importantly including the single chain molecular weight,²³⁸ the cross-linking density,²³⁹ the regularity of cross-links²⁴⁰ and the type of cross-linking sites. Rubbers consist of chemical type cross-linking sites, most notably sulfur bridges from vulcanization with elemental sulfur or sulfur-containing reagents such as S_2Cl_2 .²⁴¹ Alternative common curing agents are peroxides²⁴² or curing triggered by irradiation.²⁴³ Conventional low T_g polymers for the preparation of rubbers include polydienes such as 1,4-*cis*-polyisoprene as the main integral part of natural rubber, 1,4-polybutadiene, polychloropren or polyisobutylene; yet many commercial elastomers, e.g. butyl rubber²³⁸ or nitrile rubber²⁴⁴ are based on copolymers.

Furthermore, silicone-based elastomers are among the most versatile and elastic materials with exceptional high thermal stability (both cold and heat).

Microscopically, the restoring force is described as an entropic effect in which elongation causes entropy decrease relative to the irregular network configuration in the relaxed state.²⁴⁵ Statistically, the restoring force, or retractive stress σ of an elastic network as a function of its extension ratio α is given by **Equation 1-3**.²⁴⁶

$$\sigma = \frac{\rho}{M_c} RT \left(\alpha - \frac{1}{\alpha^2} \right) \quad (1 - 3)$$

with ρ = density between cross-links; M_c = molecular weight between cross-links.

If subject to solvents, chemically cross-linked networks do not dissolve; yet they swell.²⁴⁷ The resulting volume changes can be associated with the cross-linking density.²⁴⁸

1.3.2 REVERSIBLE CROSS-LINKING

Contrary to chemical cross-linking, reversible cross-linking sites are cleavable under external stimulation. Besides that entanglements²⁴⁹ or crystallized domains²⁵⁰ may serve as inherent physical cross-linking, various other approaches have been developed to gain control over the cross-linking density. These are either based on physical interactions or on the reversibility of covalent bonds. Both classes will be discussed in the following with attention being given on thermoplastic elastomers (TPEs), the most notable example of reversibly cross-linked materials. TPEs behave elastomer-like at usage temperature and thermoplast-like at elevated temperatures and therefore, render high-throughput processing and recycling possible.

1.3.2.1 PHYSICAL CROSS-LINKING

Depending on the type and strength of the corresponding cross-link, physical cross-linking can eliminate terminal relaxation comparable to chemical cross-linking.²⁵¹ Conventionally, TPEs are prepared from microphase separated ABA block copolymers, consisting of incompatible hard (A) and soft (B) blocks such as poly(styrene-*b*-butadiene-*b*-styrene) (SBS) or poly(styrene-*b*-isoprene-*b*-styrene) (SIS) in which low A/B block length ratios

cause the hard blocks to disperse as domains in the soft matrix.²⁵² Generally, the phase behavior in block copolymers is subject to the total degree of polymerization N , the polymer architecture, the effective volume fraction ϕ or f (**Figure 1-15**) and the thermodynamic compatibility of the monomers. The latter is represented by the temperature-dependent enthalpic Flory-Huggins interaction parameter χ of the corresponding monomers.²⁵³ Transition from the ordered (microphase separated) state to the disordered, entropy-dominated state is only observed at low $N\chi$. Microphase-separated block copolymers exhibit separated T_g s of the corresponding homopolymers, whereupon T_g s coincide into one in disordered block copolymers.

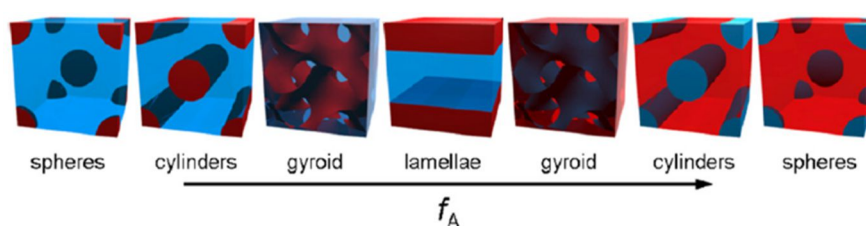


Figure 1-15. Schematic illustration of f -dependent morphologies in microphase separated AB block copolymers (A = red; B = blue). Reprinted from Ref. 254 with permission. Copyright Elsevier.

Microphase-separated hard block domains, dispersed in soft domains serve as immobile, rigid cross-linking sites in TPEs. Only at temperatures above their T_g the material will soften and may be processed. Apart from SBS and SIS, other block copolymer-based TPEs with different soft^{255,256} or hard segments²⁵⁷ have been prepared in order to make other applications accessible. Intensive research effort has been directed at increasing the softening thresholds by either using crystallized^{258,259} or high T_g ²⁶⁰ hard segments. Furthermore, alternately segmented polyurethanes made from polyaddition reaction of mostly diisocyanates, diesters and diols are widely used as TPEs.²⁶¹ Incompatibility of the resulting hard polyurethane and soft polyester segments triggers microphase separation.²⁶²

Further to microphase separation, several other reversible cross-linking concepts have been developed for generating TPEs and other materials. For example, thermo-reversible hydrogen bonding between hydrogen-bonding donors (D) such as amines and hydrogen-bonding acceptors (A) such as carbonyl groups has been exploited using amide,²⁶³ urazole,²⁶⁴ ureido-pyrimidone (UPy)^{265,266} or amide triazole-carboxylic acid²⁶⁷ moieties (**Figure 1-16a-b**). With this strategy, soft materials with self-healing ability were designed from supramolecular networks of non-polymeric hydrogen-bonding molecules (**Figure 1-16c**)²⁶⁸ and from linearly connected UPy units²⁶⁹ with the latter exhibiting additional shape memory upon mechanical stimulation (**Figure 1-16d**).

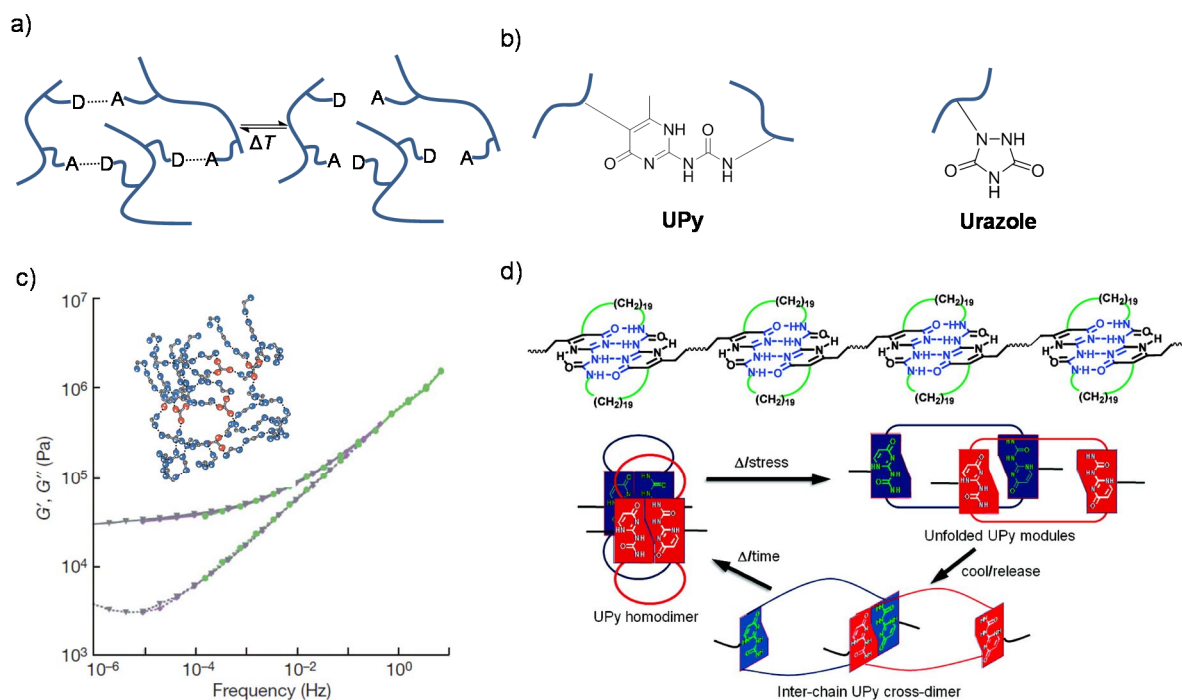


Figure 1-16. Hydrogen-bonding as reversible cross-linking method. a) Schematic concept of hydrogen-bonding-mediated reversible cross-linking. D = hydrogen-bonding donor. A = hydrogen-bonding acceptor. b) Chemical structures of the ureido-pyrimidone (UPy) and urazole moiety. c) G' and G'' master curves of hydrogen-bonded supramolecular network showing a clear rubber plateau at low shear frequencies. Inset: Schematic view of reversible network from ditopic (blue) and tritopic (red) molecules, connected *via* hydrogen-bonding. Reprinted from Ref. 268 with permission. Copyright Nature Publishing Group. d) Top: Linear polymer chain made from reversible UPy adducts. The resulting material shows self-healing and shape-memory abilities. Below: Shape memory upon mechanical stimulation is suggested to be due to UPy rearrangements. Reprinted from Ref. 269 with permission. Copyright American Chemical Society.

Polymers of low molecular weight with pyrenyl residues were used to generate self-healable elastomers *via* π - π -stacking interaction of the pyrenyl groups (Figure 1-17a).²⁷⁰ Moreover, mechanically robust supramolecular networks can be obtained by ligand-metal ion interaction or by ion-ion interaction. Attractive ligand-metal ion interaction is preferentially governed by multidentate ligands which were shown to serve as anchor groups if attached to polymer chains. Prominent materials on this field are made from telechelic 2,6-bis(1'-methylbenzimidazolyl)pyridine (*Mebip*) end-capped poly(*p*-xylylene)s in combination with Fe^{2+} , Zn^{2+} or La^{3+} ions²⁷¹ (Figure 1-17b) or from telechelic *Mebip* end-capped poly(ethylene-*co*-butylene) in combination with Zn^{2+} or La^{3+} ions²⁷² where trivalent ions act as cross-linking sites. The latter combination was reported to be able to self-heal under the influence of UV light (Figure 1-17c).

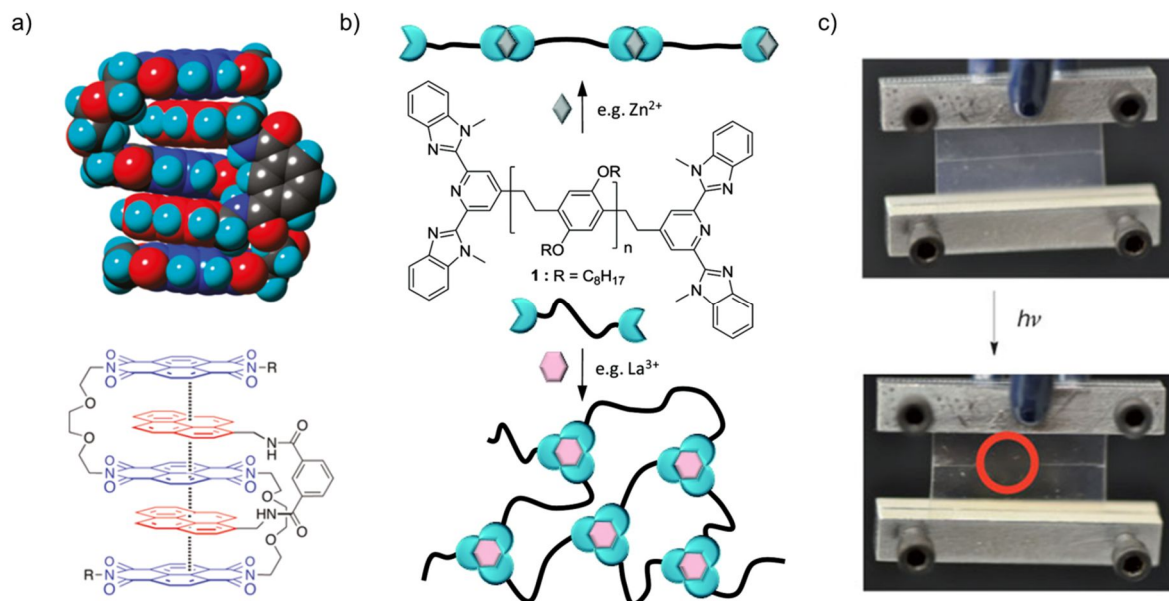


Figure 1-17. Supramolecular networks from π - π -stacking interaction and ligand-metal ion interaction. a) Polymer-attached pyrenyl end groups mediate π - π -stacking to generate a thermally healable elastic network. Reprinted from Ref. 270 with permission. Copyright American Chemical Society. b) Telechelic *Mebip* end-capped poly(*p*-xylylene) is cross-linked with trivalent metal ions. Reprinted from Ref. 271 with permission. Copyright American Chemical Society. c) Cross-linking of telechelic *Mebip* end-capped poly(ethylene-*co*-butylene) yields a UV-healable supramolecular material. Reprinted from Ref. 272 with permission.

Copyright Nature Publishing Group.

Materials in which ion-ion interaction is accountable for physical cross-linking are designated as ionomers.²⁷³ Using this concept, thermoplastic elastomers may be designed by doping polymers with low glass transition temperatures with a low amount (<10%) of anionic anchor groups, most notably sulfonic acids through sulfonation²⁷⁴ or carboxylic acids from acrylic acid copolymerization for example in carboxylated nitrile butadiene rubber (XNBR) (**Figure 1-18a**).²⁷⁵ Physical cross-linking is triggered by attractive intermolecular ionic forces of the corresponding salts, yielding ionic clusters (**Figure 1-18b**).²⁷⁶

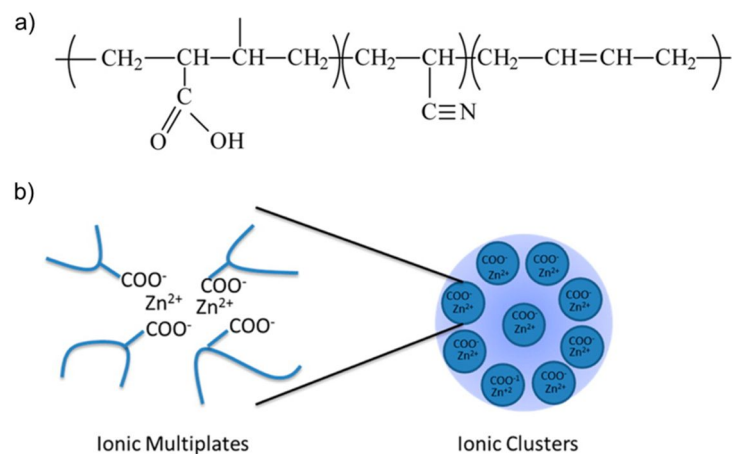


Figure 1-18. Ionomer carboxylated nitrile butadiene rubber (XNBR) is widely used as thermoplastic elastomer. a) Chemical structure of XNBR with a low fraction of carboxylic groups. b) Schematic illustration of ionic clusters as physical cross-linkers. Reprinted from Ref. 276 with permission. Copyright American Chemical Society.

1.3.2.2 REVERSIBLE CHEMICAL CROSS-LINKING

Certain classes of covalent bonds can be made reversible under the influence of temperature, light, changes in pH or with redox chemistry. Contrary to physical cross-linking, this dynamic covalent chemistry yields materials which are insoluble in solvents in the cross-linked state. Thermally reversible cross-links have for instance been put into practice using well-established DIELS-ALDER chemistry in which dienes and dienophiles react *via* [4+2]-cycloaddition and -reversion (**Figure 1-19a**).^{277,278} Suitable diene moieties are in *cis*-configuration; therefore cyclic dienes such as cyclopentadiene, furan or anthracene are preferentially used. Suitable dienophiles are characterized by their electron deficiency through conjugated electron-withdrawing groups as for example found in maleic anhydride, maleimide or methacrylate. DIELS-ALDER adducts with thermal healing ability at 120 °C were reported for both rigid polymeric networks²⁷⁹ as well as for linear architectures.²⁸⁰

In general, reshuffling of reversible covalent bonds is a widely utilized method for the design of healable materials. Besides DIELS-ALDER chemistry, catalyst-supplied transesterification,²⁸¹ catalyst-supplied olefin metathesis,²⁸² thermally induced siloxane equilibration,²⁸³ pH-controlled acylhydrazone cleavage²⁸⁴ and disulfide metathesis at

modest temperatures^{285,286} are selected examples that altogether demonstrate the potential of dynamic covalent chemistry.

Reversible cross-links which are sensitive to photochemistry are mainly associated with coumarin, but also with anthracene²⁸⁷ or cinnamate^{288,289} and their derivatives. [2+2]-cycloaddition of coumarin takes place if subject to UV light of wavelengths of $\lambda > 300$ nm while cycloreversion is performed with UV light of $\lambda < 280$ nm (**Figure 1-19b**),^{290,291} yet two-photon absorption has been demonstrated to enable cycloreversion from visible light.²⁹² For example, coumarin-mediated cross-linking of polyurethanes yielded elastomers with the ability to heal cracks under UV light.^{293,294}

Moreover, redox-active sites such as the redox couple thiol/disulfide were successfully utilized to generate reversibly cross-linked polymeric micelles for controlled drug release applications (**Figure 1-19c**).²⁹⁵ While oxygen was used as the oxidizing agent to convert thiol-containing cysteine to disulfides, back reaction was accomplished by adding a chemical reducing agent. A dual-responsive reversible cross-linking from photosensitive coumarin and redox-sensitive disulfide moieties has as well been used in drug delivery applications.²⁹⁶

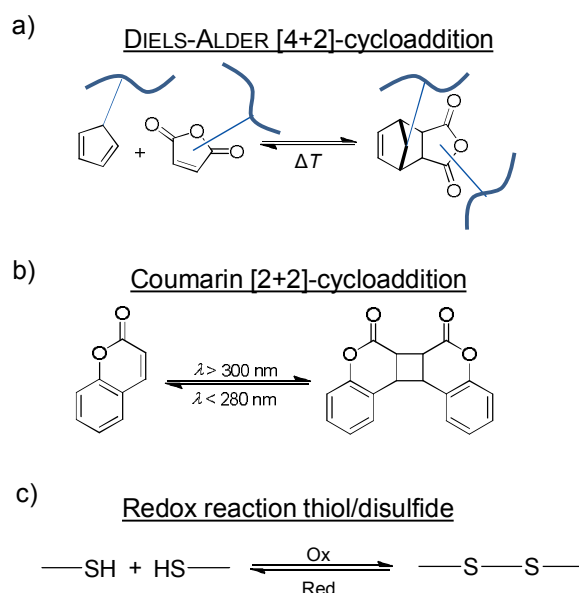


Figure 1-19. Schematic illustration of reversible covalent bonds. The reversibility may be driven by a) changes in temperature, b) impact of light or c) redox chemistry.

1.4 NANOPARTICLES AS CROSS-LINKERS AND REINFORCING AGENTS

Noble metal nanoparticles dispersed in polymer matrices are well known to contribute distinct physical, chemical and biological properties to nanocomposites as discussed in chapters 1.1 and 1.2. However, upon incorporation of noble metal nanoparticles into polymeric matrix, plasticizing or anti-plasticizing effects were reported. A thorough investigation of this phenomenon is provided by OH et al. who point out that interpenetrations of non-grafted matrix chain with polymer brushes emerging from the particle surface are responsible for particle-induced changes in chain dynamics (Figure 1-20).²⁹⁷ Energetic contributions to this effect are discussed in chapter 1.4.1.

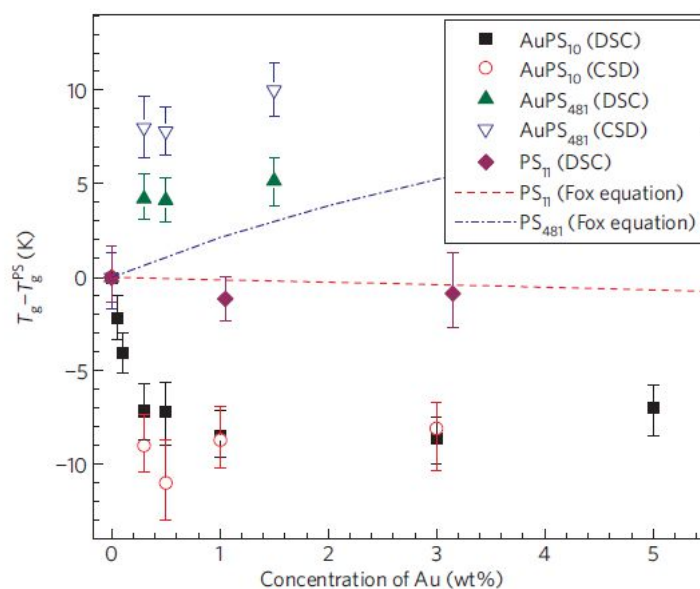


Figure 1-20. Impact of AuNP filling fraction on the glass transition temperature T_g in nanocomposites from polystyrene and ω -thiol polystyrene-stabilized AuNP as measured from DSC and capacitive scanning dilatometry (CSD). A strong dependency of the segmental dynamics on the polymerization degree P of the ω -thiol polystyrene ligand (the subscript in AuPS₁₀ and AuPS₄₈₁ refers to P) was observed. This was correlated to interpenetrations of matrix chains with the high P polymer brush emerging from the particle surface. The lines drawn through the data were computed using the Fox equation. Reprinted from Ref. 297 with permission. Copyright Nature Publishing Group.

More than that, a handful of recent studies show that metal nanoparticles can as well provide material properties by acting as reversible cross-linking sites for polymers. The resulting nanocomposites exhibit mechanical and viscoelastic properties which are strongly influenced by the energetic polymer-particle interaction on the one hand and on the topological polymer-particle architecture on the other hand. Particle-particle interactions

become significant as soon as the particle filling rate exceeds the percolation threshold. These relationships have extensively been studied on nanocomposites from polymers and *non-metallic* nanoparticles such as from silica, carbon black, starch, cellulose or polymers. Therefore, fundamental experiments and simulation studies are discussed with an eye on the reinforcement and cross-linking abilities of non-metallic nanoparticles first (chapter 1.4.1), followed by a close look on previous reports in which noble metal nanoparticles act as cross-linking sites in nanocomposites (chapter 1.4.2).

1.4.1 NON-METALLIC NANOPARTICLES

Nanoparticles dispersed in a polymeric matrix have long been known to contribute to mechanical reinforcement. Especially silica nanoparticles (SNP)²⁹⁸⁻³⁰² and carbon black³⁰³⁻³⁰⁷ are used as cheap and efficient filling materials both below and beyond the percolation threshold for all kinds of polymer classes ranging from thermoset elastomers to thermoplastics. At early research stages, the particle filling rate has been identified crucial for the microscopic nanocomposite structure and consequently, also for the macroscopic material properties. Once filled with carbon black at high filling rates, cross-linked elastomers for example exhibit outstanding mechanical properties, but also a significant dependence of the elastic modulus on the deformation, called the PAYNE effect.³⁰⁸ This is assigned to a continuous, agglomerated particle network inside the elastomer matrix which disrupts already at low deformations. The resulting energy dissipation during deformation is large relative to contributions from chain ends and internal friction.³⁰⁹ Similar particle networks have also been found using SNP as fillers.³¹⁰

Apart from these particle-particle interactions above the percolation threshold, energetic and topological polymer-particle interactions typically dictate changes of material properties in nanocomposites compared to the corresponding neat polymer and are controversially discussed. In terms of energy interaction, one has to distinguish between repulsive, neutral and attractive polymer-particle interactions. Computer simulations reveal that repulsive interactions cause the chain dynamics and diffusivity to accelerate whereas attractive interactions decelerate chain dynamics and diffusivity.³¹¹ However, it was experimentally shown with poly(methyl methacrylate), filled with hydroxyl-capped SNP, that attractive polymer-particle interactions do not slow down the macroscopic diffusion of polymer chains³¹² compared to a weakly interacting polymer-particle system (polystyrene

filled with phenyl-capped SNP).³¹³ Polymer chain segments in the particle vicinity were furthermore simulated to feature perturbed dynamics compared to those remote from the interface.^{314,315} Experimentally, a second glass transition peak was for example observed for various thermoplastic polymers in the vicinity of silica particles.^{316,317}

Topologically, the polymer-particle arrangement plays a key role in inducing mechanical reinforcement or cross-linking. Polymer-particle networks were first postulated by ZHANG et al. who observed a liquid-to-solid transition of linear, high molecular weight poly(ethylene oxide) if filled with SNP with filling fractions as low as 2 vol%.³¹⁸ Such networks were also designed from linear poly(dimethyl siloxane) and SNP.³¹⁹ Microscopically, the authors of both studies anticipated a scenario where different immobile SNP are bridged by polymer chains or chain segments (**Figure 1-21a**). SEN et al. substantiated this idea in computer simulations where –in comparison with other polymer-particle arrangement scenarios– bridging was found to be the main contributor to reinforcement up to the initiation of elasticity.³²⁰ In particular, bridging is favored if the interparticle distance Λ decreases³²¹ and the polymer molecular weight, i.e. the radius of gyration R_g , increases.³²² Based on these considerations, YANG et al. developed nanocomposite hydrogels in which SNP act as cross-linking sites for poly(acrylic acid),³²³ poly(acrylamide)³²⁴ and poly(acrylic acid)-g-poly(ethylene glycol).³²⁵

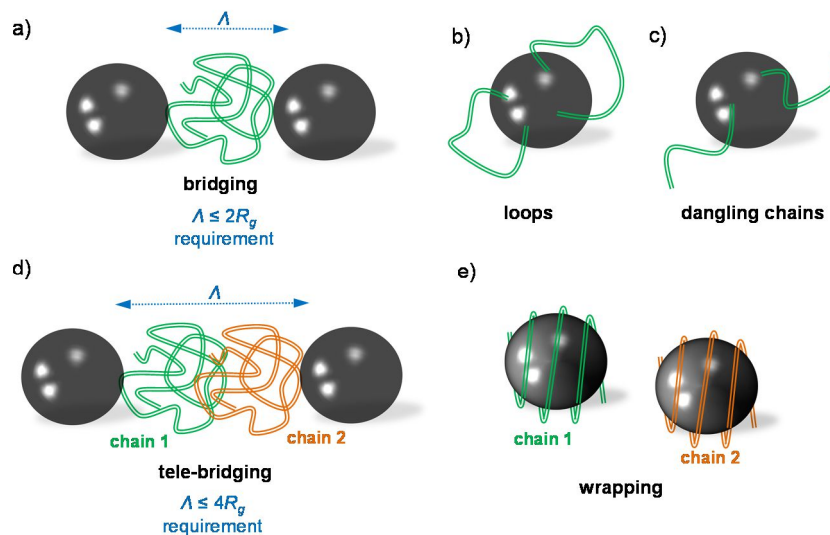


Figure 1-21. Simplified scheme of polymer-particle arrangements in nanocomposites. Grey spheres: nanoparticles. Lines: Polymer. a) Bridging of particles by polymer chains turns the particle into a cross-linking site and is therefore an elasticity-inducing scenario. b) Scenarios with polymer loops on the particle surface as well as with c) dangling chain ends may contribute to reinforcement. d) Tele-bridging is a long-range type interaction, generating a looser network compared to single-chain bridging (scenario a)). e) Wrapping comes into practice if disentangled chain segments three-dimensionally encase the particles.

Other topological polymer-particle arrangements include loops (also known as backbiting) where one polymer chain is twice attached to the particle surface (**Figure 1-21b**) such as prepared on SNP *via* “grafting from” synthesis³²⁶ as well as dangling chain ends where polymer chains emerge from the polymer surface like a brush (**Figure 1-21c**). Sen et al. concluded that these scenarios also cause reinforcement, yet to a much lesser extent.³²⁰ Furthermore, tele-bridging which is mediated *via* physical long-range interactions (**Figure 1-21d**) has been predicted in computational studies.³²⁷ Wrapping comes into effect if disentangled polymer chains encase the entire particle (**Figure 1-21e**) such as simulated for polyelectrolyte-particle systems.³²⁸

1.4.2 NOBLE METAL NANOPARTICLES

The potential of noble metal nanoparticles serving as cross-linking sites is hardly disclosed. Not more than four studies have been published up to now. In 2008, FARAH et al. described the generation of polymeric microspheres by using AgNP as cross-linkers (**Figure 1-22**).³²⁹ The authors developed a modified suspension polymerization where an aqueous suspension of citrate-stabilized AgNP with diameters of 30-80 nm was charged with a solution of 4-mercaptomehtylstyrene in toluene, followed by polymerization. The Ag-S bond was detected in X-ray photoelectron spectroscopy. Microspheres with diameters of 60-110 μm were yielded and used as SERS substrates.

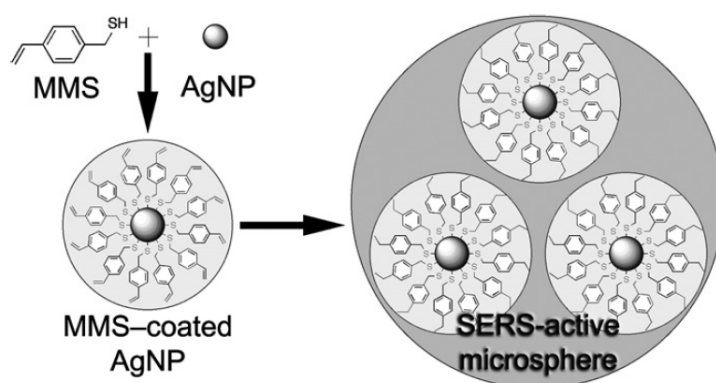


Figure 1-22. Concept illustration of AgNP-crosslinked polymeric microspheres. Reprinted from Ref. 329 with permission. Copyright Elsevier.

MORENO et al. used metal nanoparticles as cross-linking sites for the preparation of hydrogels. In detail, Thermoplastic PVA has been cross-linked with AuNP in a chemical post-surface modification reaction.³³⁰ Therefore, *ex situ*-prepared mercaptoundecanoic

acid-grafted AuNP underwent esterification with the hydroxyl side chains of PVA, yielding water-insoluble composite hydrogels (**Figure 1-23**). At AuNP filling fractions beyond 10 wt% the cross-linking density was found sufficient to form swellable hydrogels even at elevated temperatures.

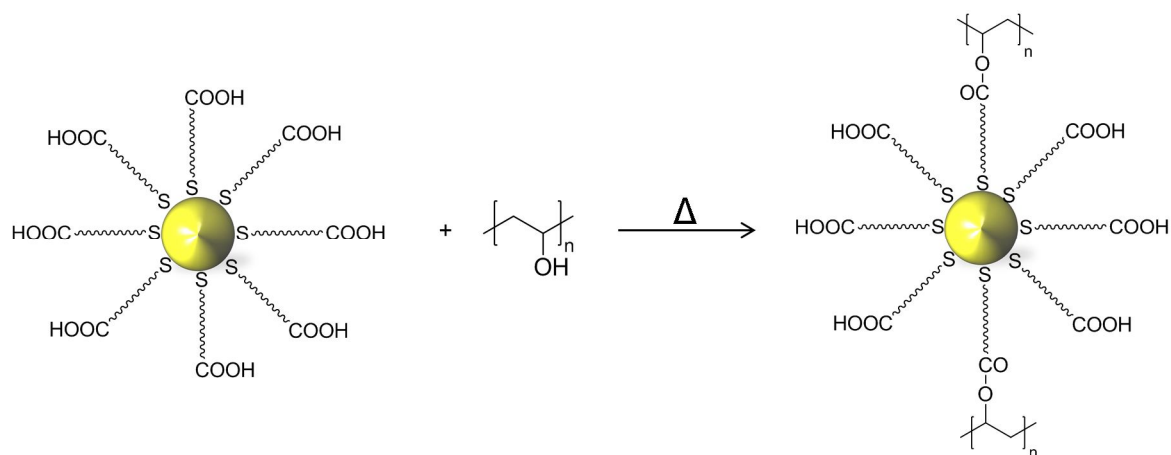


Figure 1-23. AuNP as cross-linkers for thermoplastic poly(vinyl alcohol) *via* post-surface modification to yield hydrogels.

Thermally processable elastomers with noble metal nanoparticles as reversible cross-linking sites have been developed recently in our group.³³¹ In this concept, a telechelic, liquid precursor α,ω -dithiol oligoisoprene interconnects AgNP. Thus, a three-dimensional network is created where AgNPs act as immobile cross-linking sites to yield a TPE-like material (**Figure 1-24**).

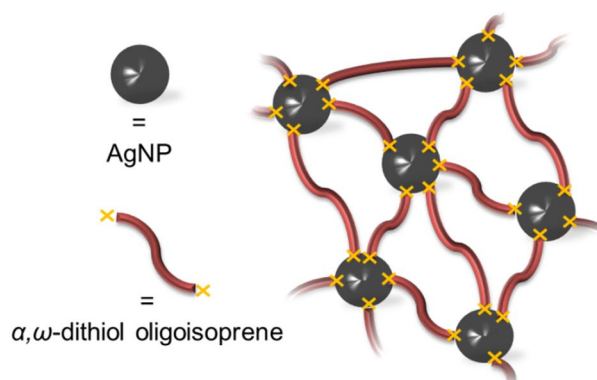


Figure 1-24. Schematic illustration of elastic network from liquid α,ω -dithiol oligoisoprene and AgNP where AgNP serve as cross-linking sites.

The generation of such an elastic network was performed *via* single-phase *in situ* “grafting to” reaction in which AgCO_2CF_3 was used as the precursor and Superhydride® as the reduction agent in homogeneous THF solution. The cross-linking density and therefore, the mechanical properties and viscoelasticity were found to be strongly dependent on the

polymer molecular weight and the AgNP filling fraction. Empirically, insufficient cross-linking densities were either caused by too low AgNP filling rates resulting in non-grafted or non-bridging (mono-grafted) polymer chains or by too high AgNP filling rates leading to particle aggregation and therefore, reduced specific particle surface areas. (**Figure 1-25a**). Using a suitable amount of AgNP, the liquid polymer is transferred to an insoluble, thermally processable, elastic material with distinct restoring force (**Figure 1-25b and c**).

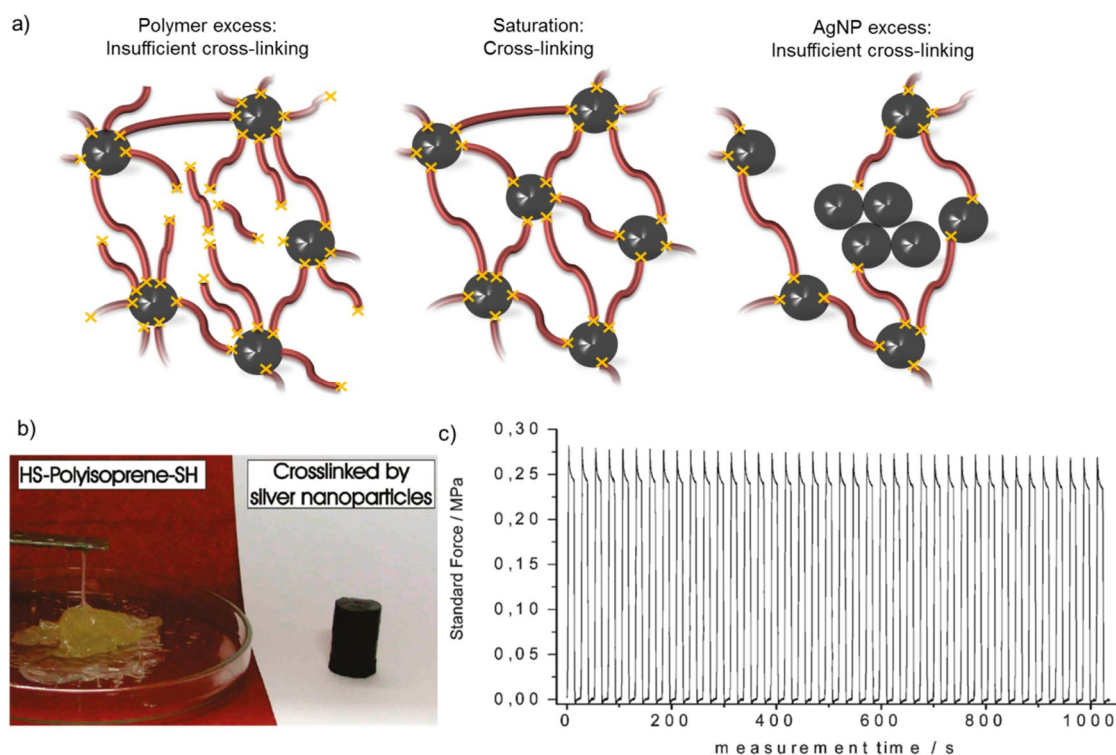


Figure 1-25. a) Cross-linking density in networks made from α,ω -dithiol oligoisoprene and AgNP as a function of the component ratio polymer/AgNP: Polymer excess favors the advent of non-grafted or mono-grafted polymer chains, whereas AgNP excess prevents cross-linking due to aggregation. b) Liquid α,ω -dithiol oligoisoprene is converted to an elastic solid if cross-linked with a balanced amount of AgNP. c) Cyclic stress-strain measurements (10 s strain, 10 s relaxation) of the nanocomposite network prove strong restoring force. Reprinted from Ref. 331 with permission. Copyright American Chemical Society.

In bulk, the resulting material adopts properties from pristine AgNP including LSPR, rendering a dark brown color as well as antibacterial activity, here shown against *Escherichia coli* bacteria. A qualitative description of the polymer-particle interactions is given by DSC measurements, showing increase of T_g upon AgNP addition; however the mechanism of temperature-induced softening is not yet understood.

Further to this study, AgNP have been employed as cross-linking sites for thiol-functionalized silicone oils to give elastic networks (**Figure 1-26**).³³² Equivalent to the networks made from α,ω -dithiol oligoisoprene and AgNP in our group, incorporation of AgNP has been provided by a single-phase *in situ* approach. Having low thermal stability, the materials were not thermally processed, but demonstrated self-healing behavior at room temperature instead. The authors proposed, but not substantiated a mechanism to explain self-healing based on previously reported thiolate exchanges on Au and AgNP surfaces.³³³

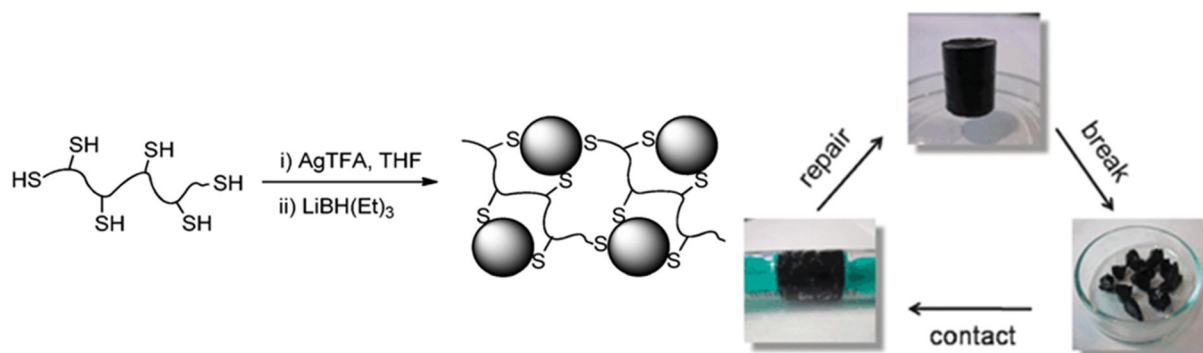


Figure 1-26. Thiol-functionalized silicone oils are cross-linked with spherical AgNP. The resulting material is shown to self-heal under pressure. Reprinted from Ref. 332 with permission. Copyright Royal Society of Chemistry.

1.5 REFERENCES

- [1] Rao, C. N. R.; Kulkarni, G. U.; Thomas, P. J.; Edwards, P. P. *Chem. Soc. Rev.* **2000**, *29*, 27-35.
- [2] Hanemann, T.; Szabó, D. V. *Materials* **2010**, *3*, 3468-3517.
- [3] Ruban, A.; Hammer, B.; Stoltze, P.; Skriver, H. L.; Nørskov, J. K. *J. Mol. Catal. A: Chem.* **1997**, *115*, 421-429.
- [4] Guzci, L.; Pető, G.; Beck, A.; Frey, K.; Geszti, O.; Molnár, Daróczi, C. *J. Am. Chem. Soc.* **2003**, *125*, 4332-4337.
- [5] Xiaoyong, Y. L.; Hong, M.; Collard, D. M.; El-Sayed, M. A. *Org. Lett.* **2000**, *2*, 2385-2388.
- [6] Ding, J. H.; Gin, D. L. *Chem. Mater.* **2000**, *12*, 22-24.
- [7] Kim, B.; Tripp, S. L.; Wei, A. *J. Am. Chem. Soc.* **2001**, *123*, 7955-7956.
- [8] Fink, J.; Kiely, C. J.; Bethell, D.; Schiffrin, D. J. *Chem. Mater.* **1998**, *10*, 922-926.
- [9] Sun, L.; Song, Y.; Wang, L.; Guo, C.; Sun, Y.; Liu, Z.; Li, Z. *J. Phys. Chem. C* **2008**, *112*, 1415-1422.
- [10] Yang, Y.; Matsubura, S.; Nogami, M.; Shi, J.; Huang, W. *Nanotechnology* **2006**, *17*, 2821-2827.
- [11] Henglein, A.; Giersig, M. *J. Phys. Chem. B* **1999**, *103*, 9533-9539.
- [12] Ji, X.; Song, X.; Li, J.; Bai, Y.; Yang, W.; Peng, X. *J. Am. Chem. Soc.* **2007**, *129*, 13939-13948.
- [13] Evanoff, D. D.; Chumanov, G. *J. Phys. Chem. B* **2004**, *108*, 13948-13956.
- [14] Volokitin, Y.; Sinzig, J.; de Jongh, L. J.; Schmid, G.; Vargaftik, M. N.; Moiseev, I. I. *Nature*, **1996**, *384*, 621-623.
- [15] Ghosh, S. K.; Nath, S.; Kundu, S.; Esumi, K.; Pal, T. *J. Phys. Chem. B* **2004**, *108*, 13963-13971.

- [16] Rycenga, M.; Cobley, C. M.; Zeng, J.; Li, W.; Moran, C. H.; Zhang, Q.; Qin, D.; Xia, Y. *Chem. Rev.* **2011**, *111*, 3669-3712.
- [17] Mie, G. *Ann. Phys.* **1908**, *25*, 377-445.
- [18] Haes, A. J.; Van Duyne, R. P. *Anal. Bioanal. Chem.* **2004**, *379*, 920-930.
- [19] Underwood, S.; Mulvaney, P. *Langmuir* **1994**, *10*, 3427-3430.
- [20] Mock, J. J.; Smith, D. R.; Schultz, S. *Nano Letters* **2003**, *3*, 485-491.
- [21] Grady, N. K.; Halas, N. J.; Nordlander, P. *Chem. Phys. Lett.* **2004**, *399*, 167-171.
- [22] Jeanmaire, D. L.; Vanduyne, R. P. *J. Electroanal. Chem.* **1977**, *84*, 1-20
- [23] Ru, E. C. L.; Etchegoin, P. G. *Chem. Phys. Lett.* **2006**, *423*, 63-66.
- [24] Shen, X. S.; Wang, G. Z.; Hong, X.; Zhu, W. *Phys. Chem. Chem. Phys.* **2009**, *11*, 7450-7454.
- [25] Sun, L.; Song, Y.; Wang, L.; Guo, C.; Sun, Y.; Liu, Z.; Li, Z. *J. Phys. Chem. C* **2008**, *112*, 1415-1422.
- [26] Ru, E. C. L.; Meyer, M.; Etchegoin, P. G. *J. Phys. Chem. B* **2006**, *110*, 1944-1948.
- [27] Emory, S. R.; Haskins, W. E.; Shuming, N. *J. Am. Chem. Soc.* **1998**, *120*, 8009-8010.
- [28] Dieringer, J. A.; Lettan, R. B.; Scheidt, K. A.; Van Duyne, R. P. *J. Am. Chem. Soc.* **2007**, *129*, 16249-16256.
- [29] Nie, S.; Emory, S. R. *Science* **1997**, *275*, 1102-1106.
- [30] Xu, H.; Bjerneld, E. J.; Käll, M.; Börjesson, L. *Phys. Rev. Lett.* **1999**, *83*, 4357-4360.
- [31] Michaelis, A. M.; Jiang, J.; Brus, L. *J. Phys. Chem. B* **2000**, *104*, 11965-11971.
- [32] Kumar, J.; Wei, X.; Barrow, S.; Funston, A. M.; Thomas, K. G.; Mulvaney, P. *Phys. Chem. Chem. Phys.*, **2013**, *15*, 4258-4264.
- [33] Sun, Z.; Ni, W.; Yang, Z.; Kou, X.; Li, L.; Wang, J. *Small* **2008**, *4*, 1287-1292.

- [34] Tebbe, M.; Cherepanov, P.; Skorb, E. V.; Poznyak, S. K.; de Abajo, J. G.; Fery, A.; Andreeva, D. V.; Puebla, R. A. A.; Pazos-Perez, N. *Part. Part. Syst. Charact.* **2014**, *31*, 1134-1140.
- [35] Maity, S.; Downen, L. N.; Bochinski, J. R.; Clarke, L. I. *Polymer* **2011**, *52*, 1674-1685.
- [36] McFarland, A.; Van Duyne, R. P. *Nano Letters* **2003**, *3*, 1057-1062.
- [37] Haes, A. J.; Zou, S.; Zhao, J.; Schatz, G. C.; Van Duyne, R. *J. Am. Chem. Soc.* **2006**, *128*, 10905-10914.
- [38] Guo, S.-H.; Tsai, S.-J.; Kan, H.-C.; Tsai, D.-H.; Zachariah, M. R.; Phaneuf, R. J. *Adv. Mater.* **2008**, *20*, 1424-1428.
- [39] Kühn, S.; Håkanson, U.; Rogobete, L.; Sandoghdar, V. *Phys. Rev. Lett.* **2006**, *97*, 017402.
- [40] Yoon, M.; Kim, Y. M.; Kim, Y.; Volkov, V.; Song, H. J.; Park, Y. J.; Vasilyak, S. L.; Park, I.-W. *J. Magn. Magn. Mater.* **2003**, *265*, 357-362.
- [41] Woods, S. I.; Kirtley, J. R.; Sun, S.; Koch, R. H. *Phys. Rev. Lett.* **2001**, *87*, 137205.
- [42] Fonseca, F. C.; Goya, G. F.; Jardim, R. F.; Muccillo, R.; Carreño, N. L. V.; Longo, E.; Leite, E. R. *Phys. Rev. B* **2002**, *66*, 104406.
- [43] Auffan, M.; Achouak, W.; Rose, J.; Roncato, M.-A.; Chanéac, C.; Waite, D. T.; Masion, A.; Woicik, J. C.; Wiesner, M. R.; Bottero, J.-Y. *Environ. Sci. Technol.* **2008**, *42*, 6730-6735.
- [44] Yoon, K.-Y.; Byeon, J. H.; Park, J.-H.; Hwang, J. *Sci. Total Environ.* **2007**, *373*, 572-575.
- [45] Panáček, A.; Kvítek, L.; Pucek, R.; Kolář, M.; Večeřová, R.; Pizúrová, N.; Sharma, V. K.; Nevěčná, T.; Zbořil, R. *J. Phys. Chem. B* **2006**, *110*, 16248-16253.
- [46] Sondi, I.; Salopek-Sondi, B. *J. Colloid Interface Sci.* **2004**, *275*, 177-182.
- [47] Pal, S.; Tak, K.; Song, J. M. *Appl. Environ. Microbiol.* **2007**, *73*, 1712-1720.

- [48] Morones, J. R.; Elechiguerra, J. L.; Camacho, A.; Holt, K.; Kouri, J. B.; Ramírez, J. T.; Yacaman, M. J. *Nanotechnology* **2005**, *16*, 2346-2353.
- [49] Feng, Q. L.; Wu, J.; Chen, G. Q.; Cui, F. Z.; Kim, T. N.; Kim, J. O. J. *Biomed. Mater. Res.* **2000**, *52*, 662-668.
- [50] Berger, T. J.; Spadaro, J. A.; Chapin, S. E., Becker, R. O. *Antimicrob. Agents Chemother.* **1976**, *9*, 357-358.
- [51] Jain, P.; Pradeep, T. *Biotechnol. Bioeng.* **2005**, *90*, 59-63.
- [52] Kumar, A.; Vemula, P. K.; Ajayan, P. M.; John, G. *Nature Mater.* **2008**, *7*, 236-241.
- [53] Kumar, P. T. S.; Abhilash, S.; Manzoor, K.; Nair, S. V.; Tamura, H.; Jayakumar, R. *Carbohydr. Polym.* **2010**, *80*, 761-767.
- [54] Liang, M.; Lin, I.-C.; Whittaker, M. R.; Minchin, R. F.; Monteiro, M. J.; Toth, I. *ACS Nano* **2010**, *4*, 403-413.
- [55] Rojo, J.; Díaz, V.; de la Fuente, J. M.; Segura, I.; Barrientos, A. G.; Riese, H. H.; Bernad, A.; Penadés, S. *ChemBioChem* **2004**, *5*, 291-297.
- [56] Chithrani, B. D.; Ghazani, A. A.; Chan, W. C. W. *Nano Letters* **2006**, *6*, 662-668.
- [57] Faulk, W. P.; Taylor, G. M. *Immunochemistry* **1971**, *8*, 1081-1083.
- [58] Eck, W.; Craig, G.; Sigdel, A.; Ritter, G.; Old, L. J.; Tang, L.; Brennan, M. F.; Allen, P. J.; Mason, M. D. *ACS Nano* **2008**, *2*, 2263-2272.
- [59] Sokolov, K.; Follen, M.; Aaron, J.; Pavlova, I.; Malpica, A.; Lotan, R.; Richards-Kortum, R. *Cancer Res.* **2003**, *63*, 1999-2004.
- [60] Kim, D.; Jang, D. *Appl. Surf. Sci.* **2007**, *253*, 8045-8049.
- [61] Mafuné, F.; Kohno, J.; Takeda, Y.; Kondow, T. *J. Phys. Chem. B* **2000**, *104*, 9111-9117.
- [62] Goyal, A.; Mohl, M.; Kumar, A.; Puskas, R.; Kukovecz, A.; Konya, Z.; Kiricsi, I.; Ajayan, P. M. *Compos. Sci. Technol.* **2011**, *71*, 129-133.
- [63] Samia, A. C. S.; Schlueter, J. A.; Jiang, J. S.; Bader, S. D.; Qin, C.-J.; Lin, X.-M. *Chem. Mater.* **2006**, *18*, 5203-5212.

- [64] Erdemir, D.; Lee, A. Y.; Myerson, A. S. *Acc. Chem. Res.* **2009**, *42*, 621-629.
- [65] LaMer, V. K.; Dinegar, R. H. *J. Am. Chem. Soc.* **1950**, *72*, 4847-4854.
- [66] Ji, X.; Song, X.; Li, J.; Bai, Y.; Yang, W.; Peng, X. *J. Am. Chem. Soc.* **2007**, *129*, 13939-13948.
- [67] Pillai, Z. S.; Kamat, P. V. *J. Phys. Chem. B* **2004**, *108*, 945-951.
- [68] Jana, N. R.; Gearheart, L.; Murphy, C. J. *Chem. Mater.* **2001**, *13*, 2313-2322.
- [69] Vorhees, P. W. *J. Stat. Phys.* **1985**, *38*, 231-252.
- [70] Kowalczyk, B.; Lagzi, I.; Grzybowski, B. A. *Curr. Opin. Colloid Interface Sci.* **2011**, *16*, 135-148.
- [71] Thai, T.; Zheng, Y.; Ng, S. H.; Ohshima, H.; Altissimo, M.; Bach, U. *Nanoscale* **2014**, *6*, 6515-6520.
- [72] Pieranski, P. *Phys. Rev. Lett.* **1980**, *45*, 569-572.
- [73] Pickering, S. U. *J. Chem. Soc. Trans.* **1907**, *91*, 2001-2021.
- [74] Binks, B. P.; Lumsdon, S. O. *Langmuir* **2000**, *16*, 8622-8631.
- [75] Lal, S.; Link, S.; Halas, N. J. *Nature Photon.* **2007**, *1*, 641-648.
- [76] Ni, C.; Hassan, P. A.; Kaler, E. W. *Langmuir* **2005**, *21*, 3334-3337.
- [77] Yu, Y.-Y.; Chang, S.-S.; Lee, C.-L.; Wang, C. R. C. *J. Phys. Chem. B* **1997**, *101*, 6661-6664.
- [78] Johnson, C. J.; Dujardin, E.; Davis, S. A.; Murphy, C. J.; Mann, S. *J. Mater. Chem.* **2002**, *12*, 1765-1770.
- [79] Murphy, C. J.; Jana, N. R. *Adv. Mater.* **2002**, *14*, 80-82.
- [80] Sun, Y.; Xia, Y. *Science*, **2002**, *298*, 2176-2179.
- [81] Vigderman, L.; Zubarev, E. R. *Chem. Mater.* **2013**, *25*, 1450-1457.
- [82] Gao, J.; Bender, C. M.; Murphy, C. J. *Langmuir* **2003**, *19*, 9065-9070.
- [83] Jana, N. R.; Gearheart, L.; Murphy, C. J. *J. Phys. Chem. B* **2001**, *105*, 4065-4067.

-
- [84] Gole, A.; Murphy, C. J. *Chem. Mater.* **2004**, *16*, 3633-3640.
- [85] Busbee, B. D.; Obare, S. O.; Murphy, C. J. *Adv. Mater.* **2003**, *15*, 414-416.
- [86] Millstone, J. E.; Wie, W.; Jones, M. R.; Yoo, H.; Mirkin, C. H. *Nano Lett.* **2008**, *8*, 2526-2529.
- [87] Pietrobon, B.; McEachran, M.; Kitaev, V. *ACS Nano* **2009**, *3*, 21-26.
- [88] Martin, C. R. *Science* **1994**, *266*, 1961-1966.
- [89] van der Zande, B. M. I.; Böhmer, M. R.; Fokkink, L. G. J.; Schönenberger, C. *J. Phys. Chem. B* **1997**, *101*, 852-854.
- [90] Sander, M. S.; Tan, L.-S. *Adv. Funct. Mater.* **2003**, *13*, 397.
- [91] Orendorff, C. J.; Gearheart, L.; Jana, N. R.; Murphy, C. J. *Phys. Chem. Chem. Phys.* **2006**, *8*, 165-170.
- [92] Huang, X.; El-Sayed, I. H.; Qian, W.; El-Sayed, M. A. *J. Am. Chem. Soc.* **2006**, *128*, 2115-2120.
- [93] Kim, E.; Yang, J.; Choi, J.; Suh, J.-S.; Huh, Y.-M.; Haam, S. *Nanotechnology* **2009**, *20*, 365602, 1-7.
- [94] Link, S.; Burda, C.; Mohamed, M. B.; Nikoobakht, B.; El-Sayed, M. A. *J. Phys. Chem. A* **1999**, *103*, 1165-1170.
- [95] Nie, Z.; Fava, D.; Rubinstein, M.; Kumacheva, E. *J. Am. Chem. Soc.* **2008**, *130*, 3683-3689.
- [96] Fava, D.; Nie, Z.; Winnik, M. A.; Kumacheva, E. *Adv. Mater.* **2008**, *20*, 4318-4322.
- [97] Thomas, K. G.; Barazzouk, S.; Ipe, B. I.; Joseph, S. T. S.; Kamat, P. V. *J. Phys. Chem. B* **2004**, *108*, 13066-13068.
- [98] Joseph, S. T. S.; Ipe, B. I.; Pramod, P.; Thomas, K. G. *J. Phys. Chem. B* **2006**, *110*, 150-157.
- [99] Pramod, P.; Thomas, K. G. *Adv. Mater.* **2008**, *20*, 4300-4305.
- [100] Gole, A.; Murphy, C. J. *Langmuir* **2005**, *21*, 10756-10762.

- [101] Atkinson, R.; Hendren, W. R.; Wurtz, G. A.; Dickson, W.; Zayats, A. V.; Evans, P.; Pollard, R. *J. Phys. Rev. B* **2006**, *73*, 235402.
- [102] Ciszek, J. W.; Huang, L.; Tsonchev, S.; Wang, Y.; Shull, K. R.; Ratner, M. A.; Schatz, G. C.; Mirkin, C. A. *ACS Nano* **2010**, *4*, 259-266.
- [103] Chaney, S. B.; Shanmukh, S.; Dluhy, R. A.; Zhao, Y.-P. *Appl. Phys. Lett.* **2005**, *87*, 031908.
- [104] Gonsalves, K. E.; Carlson, G.; Chen, X.; Gayen, S. K.; Perez, R.; Jose-Yacamán, M. *NanoStructured Materials* **1996**, *7*, 293-303.
- [105] Corbierre, M. K.; Cameron, N. S.; Sutton, M.; Mochrie, S. G. J.; Lurio, L. B.; Rühm, A.; Lennox, R. B. *J. Am. Chem. Soc.* **2001**, *123*, 10411-10412.
- [106] Corbierre, M. K.; Cameron, N. S.; Sutton, M.; Laaziri, K.; Lennox, R. B. *Langmuir* **2005**, *21*, 6063-6072.
- [107] Jia, X.; Listak, J.; Witherspoon, V.; Kalu, E. E.; Yang, X.; Bockstaller, M. R. *Langmuir* **2010**, *26*, 12190-12197.
- [108] Bokern, S.; Getze, J.; Agarwal, S.; Greiner, A.; *Polymer* **2011**, *52*, 912-920.
- [109] Peterle, T.; Leifert, A.; Timper, J.; Sologubenko, A.; Simon, U.; Mayor, M. *Chem. Comm.* **2008**, 3438-3440.
- [110] Peterle, T.; Ringler, P.; Mayor, M. *Adv. Funct. Mater.* **2009**, *19*, 3497-3506.
- [111] Hermes, J. P.; Sander, F.; Fluch, U.; Peterle, T.; Thompson, D.; Urbani, R.; Pfohl, T.; Mayor, M. *J. Am. Chem. Soc.* **2012**, *134*, 14674-14677.
- [112] Sander, F.; Fluch, U.; Hermes, J. P.; Mayor, M. *Small* **2014**, *10*, 349-359.
- [113] Hermes, J. P.; Sander, F.; Peterle, T.; Urbani, R.; Pfohl, T.; Thompson, D.; Mayor, M. *Chem. Eur. J.* **2011**, *17*, 13473-13481.
- [114] Ebeling, B.; Vana, P. *Macromolecules* **2013**, *46*, 4862-4871.
- [115] Zhang, Z.; Zhang, L.; Wang, S.; Chen, W.; Lei, Y. *Polymer* **2001**, *42*, 8315-8318.
- [116] Selvan, S. T.; Spatz, J. P.; Klok, H.-A.; Möller, M. *Adv. Mater.* **1998**, *10*, 132-134.

- [117] Huang, H. H.; Ni, X. P.; Loy, G. L.; Chew, C. H.; Tan, K. L.; Loh, F. C.; Deng, J. F.; Xu, G. Q. *Langmuir* **1996**, *12*, 909-912
- [118] Sardar, R.; Park, J.-W.; Shumaker-Parry, J. S. *Langmuir* **2007**, *23*, 11883-11889.
- [119] Porel, S.; Singh, S.; Radhakrishnan, T. P. *Chem. Comm.* **2005**, 2387-2389.
- [120] Jiang, L.; Wu, Z.; Wu, D.; Yang, W.; Jin, R. *Nanotechnology* **2007**, *18*, 185603.
- [121] Dai, J.; Bruening, M. L. *Nano Lett.* **2002**, *2*, 497-501.
- [122] Mendoza, C.; Pietsch, T.; Gutmann, J. S.; Jehnichen, D.; Gindy, N.; Fahmi, A. *Macromolecules* **2009**, *42*, 1203-1211.
- [123] Iwamoto, M.; Kuroda, K.; Zaporojtchenko, V.; Hayashi, S.; Faupel, F. *Eur. Phys. J. D* **2003**, *24*, 365-367.
- [124] Corbierre, M. K.; Cameron, N. S.; Lennox, R. B. *Langmuir* **2004**, *20*, 2867-2873.
- [125] Love, J. C.; Estroff, L. A.; Kriebel, J. K.; Nuzzo, R. G.; Whitesides, G. M. *Chem. Rev.* **2005**, *105*, 1103-1169.
- [126] Dubois, L. H.; Nuzzo, R. G. *Annu. Rev. Phys. Chem.* **1992**, *43*, 437-463.
- [127] Biebuyck, H. A.; Bain, C. D.; Whitesides, G. M. *Langmuir* **1994**, *10*, 1825-1831.
- [128] Schlenoff, J. B.; Li, M.; Ly, H. *J. Am. Chem. Soc.* **1995**, *117*, 12528-12536.
- [129] Hostelter, M. J.; Templeton, A. C.; Murray, R. W. *Langmuir* **1999**, *15*, 3782-3789.
- [130] Love, J. C.; Estroff, L. A.; Kriebel, J. K.; Nuzzo, R. G.; Whitesides, G. M. *Chem. Rev.* **2005**, *105*, 1103-1169.
- [131] Bain, C. D.; Biebuyck, H. A.; Whitesides, G. M. *Langmuir* **1989**, *5*, 723-727.
- [132] Shi, H.; Yuan, L.; Wu, Y.; Liu, S. *Biosens. Bioelectron.* **2011**, *26*, 3788-3793.
- [133] Li, D.; He, Q.; Cui, Y.; Wang, K.; Zhang, X.; Li, J. *Chem. Eur. J.* **2007**, *13*, 2224-2229.
- [134] Li, D.; Jones, G. L.; Dunlap, J. R.; Hua, F.; Zhao, B. *Langmuir* **2006**, *22*, 3344-3351.
- [135] Ohno, K.; Koh, K.-m.; Tsujii, Y.; Fukuda, T. *Macromolecules* **2002**, *35*, 8989-8993.

- [136] von Werne, T.; Patten, T. E. *J. Am. Chem. Soc.* **2001**, *123*, 7497-7505.
- [137] Mandal, T. K.; Fleming, M. S.; Walt, D. R. *Nano Lett.* **2002**, *2*, 3-7.
- [138] Krüger, C.; Agarwal, S.; Greiner, A. *J. Am. Chem. Soc.* **2008**, *130*, 2710-2711.
- [139] Bokern, S.; Gries, K.; Görtz, H.-H.; Warzelhan, V.; Agarwal, S.; Greiner, A. *Adv. Funct. Mater.* **2011**, *21*, 3753-3759.
- [140] Chan, Y. N. C.; Schrock, R. R.; Cohen, R. E. *Chem. Mater.* **1992**, *4*, 24-27.
- [141] Antonietti, M.; Wenz, E.; Bronstein, L.; Seregina, M. *Adv. Mater.* **1995**, *7*, 1000-1005.
- [142] Antonietti, M.; Förster, S.; Hartmann, J.; Oestreich, S. *Macromolecules* **1996**, *29*, 3800-3806.
- [143] Klingelhöfer, S.; Heitz, W.; Greiner, A.; Oestreich, S.; Förster, S.; Antonietti, M. *J. Am. Chem. Soc.* **1997**, *119*, 10116-10120.
- [144] Förster, S.; Antonietti, M. *Adv. Mater.* **1998**, *10*, 195-217.
- [145] Seregina, M. V.; Bronstein, L. M.; Platonova, O. A.; Chernyshov, D. M.; Valetsky, P. M.; Hartmann, J.; Wenz, E.; Antonietti, M. *Chem. Mater.* **1997**, *9*, 923-931.
- [146] Gröhn, F.; Bauer, B. J.; Akpalu, Y. A.; Jackson, C. L.; Amis, E. J. *Macromolecules* **2000**, *33*, 6042-6050.
- [147] Carrot, G.; Valmalette, J. C.; Plummer, C. J. G.; Scholz, S. M.; Dutta, J.; Hofmann, H.; Hilborn, J. G. *Colloid Polym. Sci.* **1998**, *276*, 853-859.
- [148] Kim, J.-H.; Lee, T. R. *Langmuir* **2007**, *23*, 6504-6509.
- [149] Lowe, A. B.; Sumerlin, B. S.; Donovan, M. S.; McCormick, C. L. *J. Am. Chem. Soc.* **2002**, *124*, 11562-11563.
- [150] Rusa, M.; Whitesell, J. K.; Fox, M. A. *Macromolecules* **2004**, *37*, 2766-2774.
- [151] Brust, M.; Walker, M.; Bethell, D.; Schiffrin, D. J.; Whyman, R. *J. Chem. Soc., Chem. Comm.* **1994**, 801-802.

-
- [152] Sarathy, K. V.; Raina, G.; Yadav, R. T.; Kulkarni, G. U.; Rao, C. N. R. *J. Phys. Chem. B* **1997**, *101*, 9876-9880.
- [153] Gole, A.; Murphy, C. J. *Chem. Mater.* **2005**, *17*, 1325-1330.
- [154] Alkilany, A. M.; Thompson, L. B.; Murphy, C. J. *ACS Appl. Mater. Interfaces* **2010**, *2*, 3417-3421.
- [155] Boev, V. I.; Pérez-Juste, J.; Pastoriza-Santos, I.; Silva, C. J. R.; Gomes, M. de J. M.; Liz-Marzán, L. M. *Langmuir* **2004**, *20*, 10268-10272.
- [156] Caragheorghopol, A.; Chechik, V. *Phys. Chem. Chem. Phys.* **2008**, *10*, 5029-5041.
- [157] Hostetler, M. J.; Templeton, A. C.; Murray, R. W. *Langmuir* **1999**, *15*, 3782-3789.
- [158] Azzam, T.; Bronstein, L.; Eisenberg, A. *Langmuir* **2008**, *24*, 6521-6529.
- [159] Zhang, T.; Ge, J.; Hu, Y.; Yin, Y. *Nano Lett.* **2007**, *7*, 3203-3207.
- [160] Gittins, D. I.; Caruso, F. *Angew. Chem. Int. Ed.* **2001**, *40*, 3001-3004.
- [161] Goulet, P. J. G.; Bourret, G. R.; Lennox, R. B. *Langmuir* **2012**, *28*, 2909-2913.
- [162] Nie, Z.; Fava, D.; Kumacheva, E.; Zou, S.; Walker, G. C.; Rubinstein, M. *Nature Mat.* **2007**, *6*, 609-614.
- [163] Dai, Q.; Coutts, J.; Zou, J. H.; Huo, Q.; *Chem. Comm.* **2008**, 2858-2860.
- [164] Thierry, B.; Ng, J.; Krieg, T.; Griesser, H. J. *Chem. Comm.* **2009**, 1724-1726.
- [165] Ehlert, S.; Taheri, S. M.; Pirner, D.; Drechsler, M.; Schmidt, H.-W.; Förster, S. *ACS Nano* **2014**, *6*, 6114-6122.
- [166] Rucareanu, S.; Maccarini, M.; Shepherd, J. L.; Lennox, R. B. *J. Mater. Chem.* **2008**, *18*, 5830-5834.
- [167] Sastry, M. *Curr. Sci.* **2003**, *12*, 1735-1745.
- [168] Mayya, K. S.; Caruso, F. *Langmuir* **2003**, *19*, 6987-6993.
- [169] Kumar, A.; Joshi, H.; Pasricha, R.; Mandale, A. B.; Sastry, M. *J. Colloid Interface Sci.* **2003**, *264*, 396-401.

- [170] Balasubramanian, R.; Xu, J.; Kim, B.; Sadtler, B.; Wei, A. J. *Dispersion Sci. Technol.* **2001**, *22*, 485-489.
- [171] Misra, T. M.; Chen, T.-S.; Liu, C.-Y. *J. Colloid Interface Sci.* **2006**, *297*, 584-588.
- [172] Sarathy, K. V.; Raina, G.; Yadav, R. T.; Kulkarni, G. U.; Rao, C. N. R. *J. Phys. Chem. B* **1997**, *101*, 9876-9880.
- [173] Karg, M.; Schelero, N.; Oppel, C.; Gradzielski, M.; Hellweg, T.; von Klitzing, R. *Chem. Eur. J.* **2011**, *17*, 4648-4654.
- [174] Sekiguchi, S.; Niikura, K.; Matsuo, Y.; Ijiro, K. *Langmuir* **2012**, *28*, 5503-5507.
- [175] Cheng, W.; Wang, E. *J. Phys. Chem. B* **2004**, *108*, 24-26.
- [176] Liu, J.; Alvarez, J.; Ong, W.; Román, E.; Kaifer, A. E. *J. Am. Chem. Soc.* **2001**, *123*, 11148-11154.
- [177] Stocco, A.; Chanana, M.; Su, G.; Cernoch, P.; Binks, B. P.; Wang, D. *Angew. Chem. Int. Ed.* **2012**, *51*, 9647-9651.
- [178] Tian, J.; Jin, J.; Zheng, F.; Zhao, H. *Langmuir* **2010**, *26*, 8762-8768.
- [179] Tang, Q.; Cheng, F.; Lou, X.-L.; Chen, Y. *J. Colloid Interface Sci.* **2009**, *337*, 485-491.
- [180] Dewi, M. R.; Laufersky, G.; Nann, T. *RSC Adv.* **2014**, *4*, 34217-34220.
- [181] Wijaya, A.; Hamad-Schifferli, K. *Langmuir* **2008**, *24*, 9966-9969.
- [182] Lin, W.-C.; Yang, M.-C. *Macromol. Rapid Commun.* **2005**, *26*, 1942-1947.
- [183] Giesfeldt, K. S.; Connatser, R. M.; De Jesús, M. A.; Dutta, P.; Sepaniak, M. J. J. *Raman Spectrosc.* **2005**, *36*, 1134 – 1142.
- [184] Farah, A. A.; Bravo-Vasquez, J. P.; Alvarez-Puebla, R. A.; Cho, J.-Y.; Fenniri, H. *Small* **2009**, *5*, 1283-1286.
- [185] Fateixa, S.; Girão, A. V.; Nogueira, H. I. S.; Trindade, T. *J. Mater. Chem.* **2011**, *21*, 15629-15636.

-
- [186] Maity, S.; Kozek, K. A.; Wu, W.-C.; Tracy, J. B.; Bochinski, J. R.; Clarke, L. I. *Part. Part. Syst. Charact.* **2013**, *30*, 193–202.
- [187] Zijlstra, P.; Chon, J. W. M.; Gu, M. *Nature* **2009**, *459*, 410–413.
- [188] Zhang, H.; Zhang, J.; Tong, X.; Ma, D.; Zhao, Y. *Macromol. Rapid Commun.* **2013**, *34*, 1575–1579.
- [189] Astruc, D.; Lu, F.; Aranzaes, J. R. *Angew. Chem. Int. Ed.* **2005**, *44*, 7852–7872.
- [190] Li, Y.; Pan, Y.; Zhu, L.; Wang, Z.; Su, D.; Xue, G. *Macromol. Rapid Commun.* **2011**, *32*, 1741–1747.
- [191] Song, S. G.; Satheeshkumar, C.; Park, J.; Ahn, J.; Premkumar, T.; Lee, Y.; Song, C. *Macromolecules* **2014**, *47*, 6566–6571.
- [192] Mitschang, F.; Schmalz, H.; Agarwal, S.; Greiner, A. *Angew. Chem. Int. Ed.* **2014**, *53*, 4972–4975.
- [193] Lu, Y.; Mei, Y.; Schrunner, M.; Ballauff, M.; Möller, M. W.; Brey, J. *J. Phys. Chem C* **2007**, *111*, 7676–7681.
- [194] Tankhiwale, R.; Bajpai, S. K. *Colloids Surf., B: Biointerfaces* **2009**, *69*, 164–168.
- [195] Lee, E. M.; Lee, H. W.; Park, J. H.; Han, Y. A.; Ji, B. C.; Oh, W.; Deng, Y.; Yeum, J. H. *Colloid Polym. Sci.* **2008**, *286*, 1379–1385.
- [196] Fan, J. A.; Wu, C.; Bao, K.; Bao, J.; Bardhan, R.; Halas, N. J.; Manoharan, V. N.; Nordlander, P.; Shvets, G.; Capasso, F. *Science* **2010**, *328*, 1135–1138.
- [197] Hore, M. J. A.; Composto, R. J. *ACS Nano* **2010**, *4*, 6941–6949.
- [198] Pazos-Perez, N.; Wagner, C. S.; Romo-Herrera, J. M.; Liz-Marzán, L. M.; de Abajo, F. J. G.; Wittemann, A.; Fery, A.; Alvarez-Puebla, R. A. *Angew. Chem. Int. Ed.* **2012**, *51*, 12688–12693.
- [199] Thai, T.; Zheng, Y.; Ng, S. H.; Mudie, S.; Altissimo, M.; Bach, U. *Angew. Chem. Int. Ed.* **2012**, *51*, 8732–8735.
- [200] Segev-Bar, M.; Haick, H. *ACS Nano* **2013**, *7*, 8366–8378.

- [201] Guerrero-Martínez, A.; Auguie, B.; Alonso-Gómez, J. L.; Džolić, Z.; Gómez-Graña, S.; Žinić, M.; Cid, M. M.; Liz-Marzán, L. M., *Angew. Chem. Int. Ed.* **2011**, *50*, 5499-5503.
- [202] Liu, Q.; Cui, Y.; Gardner, D.; Li, X.; He, S.; Smalyukh, I. I., *Nano Lett.* **2010**, *10*, 1347-1353.
- [203] Roskov, K. E.; Kozek, K. A.; Wu, W.-C.; Chhetri, R. K.; Oldenburg, A. L.; Spontak, R. J.; Tracy, J. B. *Langmuir* **2011**, *27*, 13965-13969.
- [204] Park, J. H.; Joo, Y. L. *Soft Matter* **2014**, *10*, 3494-3505.
- [205] Wang, P.; Zhang, L.; Xia, Y.; Tong, L.; Xu, X.; Ying, Y. *Nano Lett.* **2012**, *12*, 3145-3150.
- [206] Zhang, C.-L.; Lv, K.-P.; Cong, H.-P.; Yi, S.-H. *Small* **2012**, *8*, 648-653.
- [207] Deshmukh, R. D.; Liu, Y.; Composto, R. J. *Nano Lett.* **2007**, *7*, 3662-3668.
- [208] Li, W.; Zhang, P.; Dai, M.; He, J.; Babu, T.; Xu, Y.-L.; Deng, R.; Liang, R.; Lu, M.-H.; Nie, Z.; Zhu, J. *Macromolecules* **2013**, *46*, 2241-2248.
- [209] Nepal, D.; Onses, M. S.; Park, K.; Jespersen, M.; Thode, C. J.; Nealey, P. F.; Vaia, R. A. *ACS Nano* **2012**, *6*, 5693-5701.
- [210] van der Zande, B. M. I.; Pagès, L.; Hikmet, R. A. M.; van Blaaderen, A. *J. Phys. Chem. B* **1999**, *103*, 5761-5767.
- [211] Murphy, C. J.; Orendorff, C. J. *Adv. Mater.* **2005**, *17*, 2173-2177.
- [212] Pérez-Juste, J.; Rodríguez-González, B.; Mulvaney, P.; Liz-Marzán, L. M. *Adv. Funct. Mater.* **2005**, *15*, 1065-1071.
- [213] Wilson, O.; Wilson, G. J.; Mulvaney, P. *Adv. Mater.* **2002**, *14*, 1000-1004.
- [214] Liu, S.; Li, J.; Li, Z.-Y. *Adv. Optical Mater.* **2013**, *1*, 227-231.
- [215] Li, J.; Liu, S.; Liu, Y.; Zhou, F.; Li, Z.-Y. *Appl. Phys. Lett.* **2010**, *96*, 263103.
- [216] Stoenescu, S.; Truong, V.-V.; Packirisamy, M. *J. Appl. Phys.* **2014**, *115*, 114301.

-
- [217] Karg, M.; Pastoriza-Santos, I.; Pérez-Juste, J.; Hellweg, T.; Liz-Marzán, L. M. *Small* **2007**, *3*, 1222-1229.
- [218] Durand-Gasselin, C.; Sanson, N.; Lequeux, N. *Langmuir* **2011**, *27*, 12329-12335.
- [219] Lange, H.; Juárez, B. H.; Carl, A.; Richter, M.; Bastús, N. G.; Weller, H.; Thomsen, C.; von Klitzing, R.; Knorr, A. *Langmuir* **2012**, *28*, 8862-8866.
- [220] Carregal-Romero, S.; Buurma, N. J.; Pérez-Juste, J.; Liz-Marzán, L. M.; Hervés, P. *Chem. Mater.* **2010**, *22*, 3051-3059.
- [221] Wang, Y.; Wie, G.; Zhang, W.; Jiang, X.; Zheng, P.; Shi, L.; Dong, A. *J. Mol. Catal. A: Chem.* **2007**, *266*, 233-238.
- [222] Li, D.; He, Q.; Cui, Y.; Li, J. *Chem. Mater.* **2007**, *19*, 412-417.
- [223] Zhang, T.; Wu, Y.; Pan, X. Zheng, Z.; Ding, X.; Peng, Y. *Eur. Polym. J.* **2009**, *45*, 1625-1633.
- [224] Akamatsu, K.; Shimada, M.; Tsuruoka, T.; Nawafune, H.; Fujii, S.; Nakamura, Y. *Langmuir* **2010**, *26*, 1254-1259.
- [225] Riedinger, A., Leal, M. P.; Deka, S. R.; George, C.; Franchini, I. R.; Falqui, A.; Cingolani, R.; Pellegrino, T. *Nano Lett.* **2011**, *11*, 3136-3141.
- [226] Pardo-Yissar, V.; Gabai, R.; Shipway, A. N.; Bourenko, T.; Willner, I. *Adv. Mater.* **2001**, *13*, 1320-1323.
- [227] Watanabe, H. *Prog. Polym. Sci.* **1999**, *24*, 1253-1403.
- [228] Kremer, F. J. *Non-Cryst. Solids* **2002**, *305*, 1-9.
- [229] Herrmann, A.; Kresse, B.; Gmeiner, J.; Privalov, A. F.; Kruk, D.; Fujara, F.; Rössler, E. A. *Macromolecules* **2012**, *45*, 1408-1416.
- [230] Kruk, D.; Meier, R.; Rössler, E. A. *Phys. Rev. E* **2012**, *85*, 020201.
- [231] Hofmann, M.; Herrmann, A.; Elfadl, A. A.; Kruk, D.; Wohlfahrt, M.; Rössler, E. A. *Macromolecules* **2012**, *45*, 2390-2401.
- [232] Rouse, P. E. *J. Chem. Phys.* **1953**, *21*, 1272-1280.

- [233] de Gennes, P. G. *J. Chem. Phys.* **1971**, *55*, 572-579.
- [234] Doi, M.; Edwards, S. F. *J. Chem. Soc.; Faraday Trans. 2* **1987**, *74*, 1789-1801.
- [235] Nusser, K.; Schneider, G. J.; Richter, D. *Soft Matter* **2011**, *7*, 7988-7991.
- [236] Vaca Chávez, F.; Saalwächter, K. *Macromolecules* **2011**, *44*, 1549-1559.
- [237] James, H. M.; Guth, E. *J. Appl. Phys.* **1944**, *15*, 294.
- [238] Flory, P. J. *Ind. Eng. Chem.* **1946**, *38*, 417-436.
- [239] Plazek, D. J. *J. Polym. Sci.: Part A-2* **1966**, *4*, 745-763.
- [240] Squires, A. M.; Tajbakhsh, A. R.; Terentjev, E. M. *Macromolecules* **2004**, *37*, 1652-1659.
- [241] Okay, O.; Durmaz, S.; Erman, B. *Macromolecules* **2000**, *33*, 4822-4827.
- [242] Berry, J. P.; Watson, W. F. *J. Polym. Sci.* **1955**, *18*, 201-213.
- [243] Makuuchi, K.; Hagiwara, M. *J. Appl. Polym. Sci.* **1984**, *29*, 965-976.
- [244] Lawandy, S. N.; Halim, S. F. *J. Appl. Polym. Sci.* **2005**, *96*, 2440-2445.
- [245] Flory, P. J. *Trans. Faraday Soc.* **1961**, *57*, 829-838.
- [246] Flory, P. J.; Rabjohn, N.; Shaffer, M. C. *J. Polym. Sci.* **1949**, *4*, 225-245.
- [247] Back, A. L. *Ind. Eng. Chem.* **1947**, *39*, 1339-1343.
- [248] Flory, P. J.; Rehner Jr., J. *J. Chem. Phys.* **1943**, *11*, 521-526.
- [249] Flory, P. J. *Chem. Rev.* **1944**, *35*, 51-75.
- [250] van Krevelen, D. W.; te Nijenhuis, K. *Properties of Polymers*, 4th Ed. **2009**, Elsevier, Amsterdam, Netherlands, 400.
- [251] Seiffert, S.; Sprakel, J. *Chem. Soc. Rev.* **2012**, *41*, 909-930.
- [252] Holden, G.; Bishop, E. T.; Legge, N. R. *J. Polym. Sci.: Part C* **1969**, *26*, 37-57.
- [253] Bates, F. *Annu. Rev. Phys. Chem.* **1990**, *41*, 525-557.
- [254] Darling, S. B. *Prog. Polym. Sci.* **2007**, *32*, 1152-1204.

-
- [255] Cao, X.; Faust, R. *Macromolecules* **1999**, *32*, 5487-5494.
- [256] Dair, B. J.; Honeker, C. C.; Alward, D. B.; Avgeropoulos, A.; Hadjichristidis, N.; Fetters, L. J.; Capel, M.; Thomas, E. L. *Macromolecules* **1999**, *32*, 8145-8152.
- [257] Frick, E. M.; Zalusky, A. S.; Hillmyer, M. A. *Biomacromolecules* **2003**, *4*, 216-223.
- [258] Ban, H. T.; Kase, T.; Kawabe, M.; Miyazawa, A.; Ishihara, T.; Hagihara, H.; Tsunogae, Y.; Murata, M.; Shiono, T. *Macromolecules* **2006**, *39*, 171-176.
- [259] Morton, M.; Mikesell, S. L. *J. Macromol. Sci. Chem.* **1973**, *A7*, 1391-1397.
- [260] Karoly, G. *Block Copolymers* **1970**, 153-161.
- [261] Cooper, S. L.; Tobolsky, A. V. *J. Appl. Polym. Sci.* **1966**, *10*, 1837-1844.
- [262] Chu, B.; Gao, T.; Li, Y.; Wang, J.; Desper, C. R.; Byrne, C. A. *Macromolecules* **1992**, *25*, 5724-5729.
- [263] Chen, Y.; Kushner, A. M.; Williams, G. A.; Guan, Z. *Nat. Chem.* **2012**, *4*, 467-472.
- [264] Stadler, R.; de Lucca Freitas, L. *Colloid. Polym. Sci.* **1986**, *264*, 773-778.
- [265] Sijbesma, R. P.; Beijer, F. H.; Brunsveld, L.; Folmer, B. J. B.; Hirschberg, J. H. K.; Lange, R. M. F.; Lowe, J. K. L.; Meijer, E. W. *Science* **1997**, *278*, 1601-1604.
- [266] Söntjens, S. H. M.; Renken, R. A. E.; van Gemert, G. M. L.; Engels, T. A. P.; Bosman, A. W.; Janssen, H. M.; Govaert, L. E.; Baaijens, F. P. T. *Macromolecules* **2008**, *41*, 5703-5708.
- [267] Chino, K.; Ashiura, M. *Macromolecules* **2001**, *34*, 9201-9204.
- [268] Cordier, P.; Tournilhac, F.; Soulié-Ziakovic, C.; Leibler, L. *Nature* **2008**, *451*, 977-980.
- [269] Kushner, A. M.; Vossler, J. D.; Williams, G. A.; Guan, Z. *J. Am. Chem. Soc.* **2009**, *131*, 8766-8768.
- [270] Burattini, S.; Greenland, B. W.; Hayes, W.; Mackay, M. E.; Rowan, S. J.; Colquhoun, H. M. *Chem. Mater.* **2011**, *23*, 6-8.
- [271] Burnworth, M.; Rowan, S. J.; Weder, C. *Macromolecules* **2012**, *45*, 126-132.

- [272] Burnworth, M.; Tang, L.; Kumpfer, J. R.; Duncan, A. J.; Beyer, F. L.; Fiore, G. L.; Rowan, S. J.; Weder, C. *Nature* **2011**, *472*, 334-338.
- [273] Longworth, R.; Vaughan, D. J. *Nature* **1968**, *218*, 85-87.
- [274] Bagrodia, S.; Wilkes, G. L. Kennedy, J. P. *Polym. Eng. Sci.* **1986**, *26*, 662-672.
- [275] Ibarra, L.; Alzoriz, M. *J. Appl. Polym. Sci.* **2003**, *87*, 805-813.
- [276] Basu, D.; Das, A.; Stöckelhuber, K. W.; Jehnichen, D.; Formanek, P.; Sarlin, E.; Vuorinen, J.; Heinrich, G. *Macromolecules* **2014**, *47*, 3436-3450.
- [277] Murphy, E. B.; Bolanos, E.; Schaffner-Hamann, C.; Wudl, F.; Nutt, S. R.; Auad, M. L. *Macromolecules* **2008**, *41*, 5203-5209.
- [278] Chen, X.; Wudl, F.; Mal, A. K.; Shen, H.; Nutt, S. R. *Macromolecules* **2003**, *36*, 1802-1807.
- [279] Murphy, E. B.; Bolanos, E.; Schaffner-Hamann, C.; Wudl, F.; Nutt, S. R.; Auad, M. L. *Macromolecules* **2008**, *41*, 5203-5209.
- [280] Chen, X.; Dam, M. A.; Ono, K.; Mal, A.; Shen, H.; Nutt, S. R.; Sheran, K.; Wudl, F. *Science* **2002**, *295*, 1698-1702.
- [281] Montarnal, D.; Capelot, M.; Tournilhac, F.; Leibler, L. *Science* **2011**, *334*, 965-968.
- [282] Lu, Y.-X.; Guan, Z. *J. Am. Chem. Soc.* **2012**, *134*, 14226-14231.
- [283] Zhen, P.; McCarthy, T. J. *J. Am. Chem. Soc.* **2012**, *134*, 2024-2027.
- [284] Deng, G.; Tang, C.; Li, F.; Jiang, H.; Chen, Y. *Macromolecules* **2010**, *43*, 1191-1194.
- [285] Canadell, J.; Goossens, H.; Klumperman, B. *Macromolecules* **2011**, *44*, 2536-2541.
- [286] Rekondo, A.; Martin, R.; de Luzuriaga, A. R.; Cabañero, G.; Grande, H. J.; Odriozola, I. *Mater. Horiz.* **2014**, *1*, 237-240.
- [287] Jones, J. R.; Liotta, C. L.; Collard, D. M.; Schiraldi, D. A. *Macromolecules* **2000**, *33*, 1640-1645.

-
- [288] Ichimura, K.; Akita, Y.; Akiyama, H.; Kudo, K.; Hayashi, Y. *Macromolecules* **1997**, *30*, 903-911.
- [289] Gupta, P.; Trenor, S. R.; Long, T. E.; Wilkes, G. L. *Macromolecules* **2004**, *37*, 9211-9218.
- [290] Schenk, G. O.; von Wilucki, I.; Krauch, C. H. *Chem. Ber.* **1962**, *95*, 1409-1412.
- [291] Yonezawa, N.; Yoshida, T.; Hasegawa, M. *J. Chem. Soc. Perkin Trans. I* **1983**, 1083-1086.
- [292] Kim, H.-C.; Kreiling, S.; Greiner, A.; Hampp, N. *Chem. Phys. Lett.* **2003**, *372*, 899-903.
- [293] Ling, J.; Rong, M. Z.; Zhang, M. Q. *J. Mater. Chem.* **2011**, *21*, 18373.
- [294] Ling, J.; Rong, M. Z.; Zhang, M. Q. *Polymer* **2012**, *53*, 2691-2698.
- [295] Li, Y.; Xiao, K.; Luo, J.; Xiao, W.; Lee, J. S.; Gonik, A. M.; Kato, J.; Dong, T.; Lam, K. S. *Biomaterials* **2011**, *32*, 6633-6645.
- [296] Shao, Y.; Shi, C.; Xu, G.; Guo, D.; Luo, J. *ACS Appl. Mater. Interfaces* **2014**, *6*, 10381-10392.
- [297] Oh, H.; Green, P. F. *Nature Mater.* **2009**, *8*, 139-143.
- [298] Zou, H.; Wu, S.; Shen, J. *Chem Rev.* **2008**, *108*, 3893-3957.
- [299] Kontou, E.; Anthoulis, G. *J. Appl. Polym. Sci.* **2007**, *105*, 1723-1731.
- [300] Hong, R. Y.; Fu, H. P.; Zhang, Y. J.; Liu, L.; Wang, J.; Li, H. Z.; Zheng, Y. *J. Appl. Polym. Sci.* **2007**, *105*, 2176-2184.
- [301] Havet, G.; Isayev, A. I. *Rheol. Acta* **2003**, *42*, 47-55.
- [302] Bogoslovov, R. B.; Roland, C. M.; Ellis, A. R.; Randall, A. M.; Robertson, C. G. *Macromolecules* **2008**, *41*, 1289-1296.
- [303] Dutta, N. K.; Tripathy, D. K. *J. Appl. Polym. Sci.* **1992**, *44*, 1635-1648.
- [304] Fukahori, Y. *J. Appl. Polym. Sci.* **2005**, *95*, 60-67.
- [305] Katbab, A. A.; Nazockdast, H.; Bazgir, S. *J. Appl. Polym. Sci.* **2000**, *75*, 1127-1137.
-

- [306] Yurekli, K.; Krishnamoorti, R.; Tse, M. F.; Mcelrath, K. O.; Tsou, A. H.; Wang, H.-C. *J. Polym. Sci., Part B: Polym. Phys.* **2001**, *39*, 256-275.
- [307] Meier, J. G.; Klüppel, M. *Macromol. Mater. Eng.* **2008**, *293*, 12–38.
- [308] Payne, A. R. *J. Appl. Polym. Sci.* **1962**, *6*, 57-63.
- [309] Wang, J.; Hamed, G. R.; Umetsu, K.; Roland, C. M. *Rubber Chem. Technol.* **2005**, *78*, 76-83.
- [310] Yang, J.; Han, C.-R.; Duan, J.-F.; Xu, F.; Sun, R.-C. *J. Phys. Chem. C* **2013**, *117*, 8223-8230.
- [311] Desai, T.; Keblinski, P.; Kumar, S. K. *J. Chem. Phys.* **2005**, *122*, 134910.
- [312] Lin, C. C. ; Gam, S.; Meth, J. S.; Clarke, N.; Winey, K. I.; Composto, R. J. *Macromolecules* **2013**, *46*, 4502-4509.
- [313] Gam, S.; Meth, J. S.; Zane, S. G.; Chi, C.; Wood, B. A.; Seitz, M. E.; Winey, K. I.; Clarke, N.; Composto, R. J. *Macromolecules* **2011**, *44*, 3494-3501.
- [314] Smith, G. D.; Bedrov, D.; Li, L.; Bytner, O. *J. Chem. Phys.* **2002**, *117*, 9478-9489.
- [315] Starr, F. W.; Schröder, T. B.; Glotzer, S. C. *Macromolecules* **2002**, *35*, 4481-4492.
- [316] Tsagaropoulos, G.; Eisenberg, A. *Macromolecules* **1995**, *28*, 396-398.
- [317] Robertson, C. G.; Rackaitis, M. *Macromolecules* **2011**, *44*, 1177-1181.
- [318] Zhang, Q.; Archer, L. A. *Langmuir* **2002**, *18*, 10435-10442.
- [319] Şerbescu, A.; Saalwächter, K. *Polymer* **2009**, *50*, 5434-5442.
- [320] Sen, S.; Thomin, J. D.; Kumar, S. K.; Keblinski, P. *Macromolecules* **2007**, *40*, 4059-4067.
- [321] Jain, S.; Goossens, J. G. P.; Peters, G. W. M.; van Duin, M.; Lemstra, P. J. *Soft Matter* **2008**, *4*, 1848-1854.
- [322] Kim, S. Y.; Meyer, H. W.; Saalwächter, K.; Zukoski, C. F. *Macromolecules* **2012**, *45*, 4225-4237.
- [323] Yang, J.; Wang, X.-P.; Xie, X.-M. *Soft Matter* **2012**, *8*, 1058-1063.

- [324] Yang, J.; Deng, L.-H.; Han, C.-R.; Duan, J.-F.; Ma, M.-G.; Zhang, X.-M.; Xu, F.; Sun, R.-C. *Soft Matter* **2013**, *9*, 1220-1230.
- [325] Yang, J.; Gong, C.; Shi, F.-K.; Xie, X.-M. *J. Phys. Chem. B* **2012**, *116*, 12038-12047.
- [326] Rotzoll, R.; Vana, P. *J. Polym. Sci.: Part A: Polym. Chem.* **2008**, *46*, 7656-7666.
- [327] Hooper, J. B.; Schweizer, K. S. *Macromolecules* **2005**, *38*, 8858-8869.
- [328] Carnal, F.; Stoll, S. *J. Phys. Chem. B* **2011**, *115*, 12007-12018.
- [329] Farah, A. A.; Alvarez-Puebla, R. A.; Fenniri, H. *J. Colloid Interface Sci.* **2008**, *319*, 572-576.
- [330] Moreno, M.; Hernández, R.; López, D. *Eur. Polym. J.* **2010**, *46*, 2099-2104.
- [331] Bokern, S.; Mattheis, C.; Greiner, A.; Agarwal, S. *Macromolecules* **2011**, *44*, 5036-5042.
- [332] Martín, R.; Rekondo, A.; Echeberria, J.; Cabañero, Grande, H. J.; Odriozola, I. *Chem. Comm.* **2012**, *48*, 8255-8257.
- [333] Song, Y.; Huang, T., Murray, R. W. *J. Am. Chem. Soc.* **2003**, *125*, 11694-11701.

2. SYNOPSIS

2.1 AIM OF THE THESIS

The main theme of the present thesis is the exploration of elastic nanocomposites from noble metal nanoparticles and organic polymers in which the nanoparticles contribute to material properties by serving as reversible cross-linking sites or reinforcement agents. The paramount aim is to gain control over the relationships between microscopic structure and macroscopic properties in order to uncover the potential of this emerging class of nanomaterials.

In respect thereof, four cumulative chapters cover the improvement of mechanical properties in elastic polymer-particle networks where AgNPs act as cross-linking sites (chapter 3), the development of a “grafting to” method for the preparation of polymer-stabilized noble metal nanoparticles using high molecular weight end-functionalized polymers (chapter 4), the preparation of mechano-responsive elastic nanocomposites in which dispersed gold nanorods are reversibly aligned along the vector of uniaxial mechanical strain (chapter 5) and the use of AgNPs as reinforcing agent for linear, polydentate poly(propylene sulfide) (chapter 6).

The results are presented in the form of a cumulative thesis and are summarized in the following chapters 2.2. to 2.5. My individual contributions to each chapter are compiled in chapter 2.6.

2.2 SUMMARY OF CHAPTER 3:

DESIGN OF SOFT MATERIALS FROM LIQUID TRIBLOCK CO-OLIGOMERS AND METAL NANOPARTICLES

In the course of the pioneering study on the preparation of thermally processable elastomers using AgNP as cross-linking sites for telechelic α,ω -dithiol oligoisoprene, our group described the formation of a network with its cross-linking density being dependent on (1) the molecular weight of the oligomer and on (2) the component ratio

oligomer/AgNP.³³¹ Through modification of these two parameters the mechanical properties of the resulting material may be adjusted; however there is not much room for improvement and the tensile properties reported in this study were not competitive compared to commercial elastomers and TPEs. Therefore, the present study is dedicated to developing a novel approach for improving the mechanical properties of networks from AgNP and telechelic oligomers.

Replacement of the telechelic α,ω -oligoisoprene by a more versatile and stiff oligomeric compound was identified most promising in reaching this goal. For this reason, a novel block co-oligomer α,ω -dithiol poly(isoprene-*b*-styrene-*b*-isoprene) (in the following designated as TISIT standing for the sequence thiol-isoprene-styrene-isoprene-thiol) is employed. Once cross-linked with AgNP, a quasi-segmented microstructure is assumed in which hard segments (AgNP and styrene block) and soft segments (isoprene blocks) are alternating (**Figure 2-1**). It is hypothesized that the mechanical properties of the resulting elastomer may be tailored as a function of the ratio of hard and soft segments.

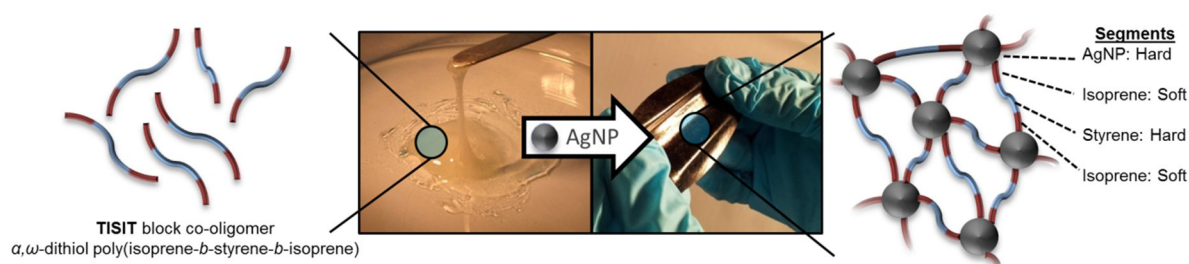


Figure 2-1. Cross-linking of TISIT block co-oligomers with AgNP provides soft, elastic materials with mechanical properties being dependent on the segment ratios.

Three TISIT block co-oligomers were synthesized *via* anionic polymerization with molar styrene contents of 28, 36 and 56%, having total molecular weights of 4600, 4800 and 4200 g/mol, respectively. These low molecular weights assured disordered microstructures with the single glass transition temperatures being dependent on the block length ratio. Cross-linking was carried out using a single-phase *in situ* “grafting to” method with different amounts of AgNP ranging from 0.59 to 11.0 molar equivalents with regards to one thiol group, yielding nanoparticles with average diameters of 1.9-3.5 nm, depending on the sample composition (**Figure 2-2a**). This sample set consisting of 9 TISIT_x@AgNP_y samples (with subscript x representing the percentage molar styrene content and subscript y the molar Ag equivalents) was characterized in detail in view of tensile and viscoelastic properties. A broad stiffness range of $E = 0.24$ -80.1 MPa is covered with ultimate

elongations ranging from 131-349% (**Figure 2-2b**). The latter property is mainly influenced from changes in the AgNP content and therefore, from the cross-linking density, whereupon high E-Moduli may only be realized with TISIT precursors of high styrene content. Compared to the α,ω -dithiol oligoisoprene reference system, holding E-Moduli of 0.20-1.12 MPa at ultimate elongations of 51% at most, a significant improvement can be achieved using TISIT precursors with high styrene contents.

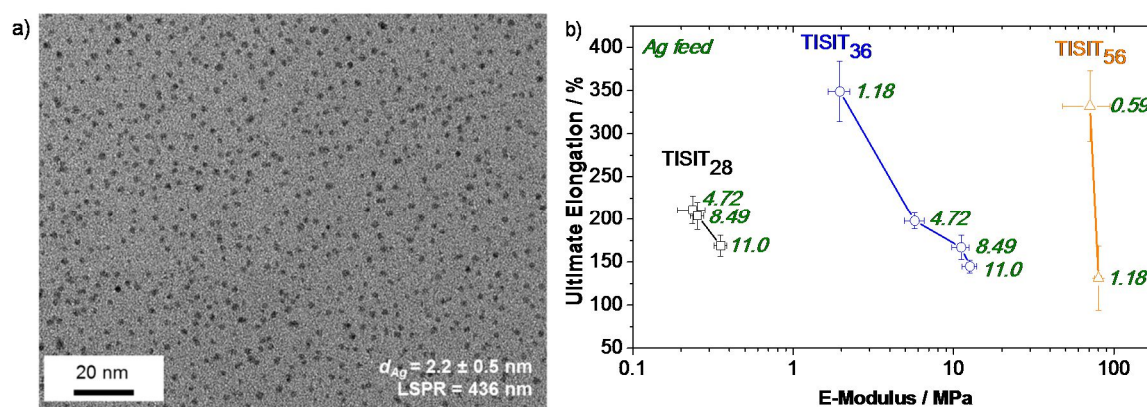


Figure 2-2. a) TEM micrograph of TISIT₂₈@AgNP_{4.72} sample after heat pressing at 110 °C and 300 bar for 90 s. AgNP are found well-dispersed with average particle diameters d_{Ag} of 2.2 ± 0.5 nm and a localized surface plasmon resonance (LSPR) maximum at 436 nm. b) E-moduli and ultimate elongation of TISIT@AgNP sample set showing strong dependency of E-Moduli on the styrene content.

In comparison with competing commercial elastomers and thermoplastic elastomers, TISIT-based quasi-segmented networks hold tensile strengths equally to natural rubber or unvulcanized blends from “ethylene propylene diene monomer” (EPDM) rubbers and polypropylene (PP). Concerning the material stiffness, TISIT@AgNP materials hold moduli at 100% elongation comparable to SBS TPEs and thermoset butadiene rubber, vulcanized with sulfur. In conclusion, a broad range of mechanical properties can be covered, filling a gap between existing materials (**Figure 2-3**).

As a consequence of very low TISIT polymerization degrees, the nanocomposites exhibit significantly decreased melt viscosities in comparison to conventional TPEs made from microphase-separated block copolymers. The viscoelastic properties at 20 °C are strongly dependent on changes in the styrene/isoprene block length ratio; while the flow behavior at 70 °C is mainly affected by the AgNP content.

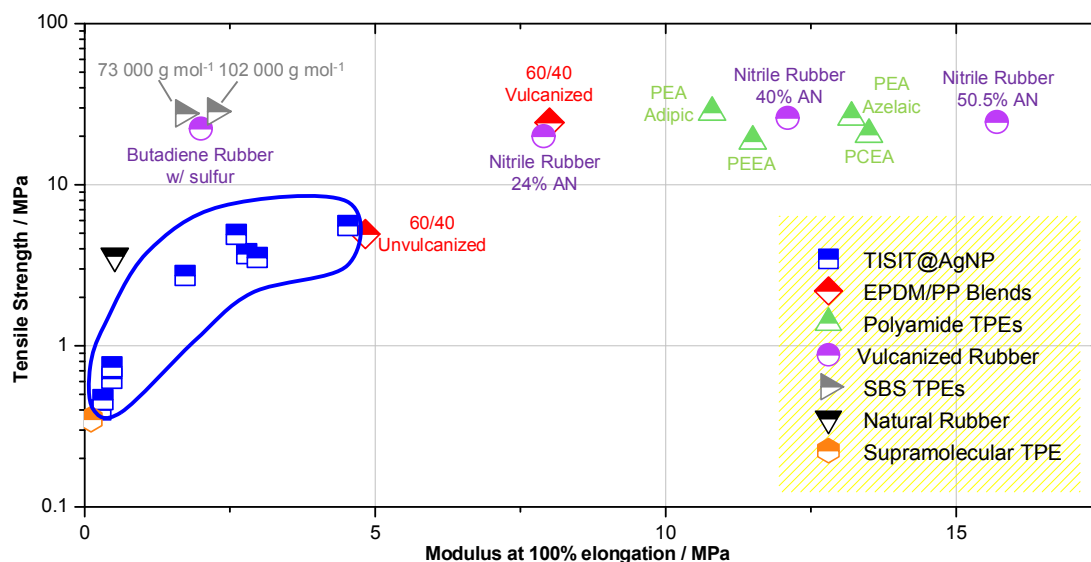


Figure 2-3. Tensile properties of TISIT@AgNP materials in comparison with commercial thermoset rubbers and TPEs. Holding tensile strengths comparable to natural rubber and unvulcanized EPDM/PP blends as well as moduli at 100% elongation comparable to SBS TPEs and sulfur-vulcanized butadiene rubber, TISIT@AgNP materials cover a broad range of mechanical properties and fill a gap between existing materials.

2.3 SUMMARY OF CHAPTER 4:

ULTRASOUND-MEDIATED SYNTHESIS FOR HIGH-MOLECULAR WEIGHT POLYSTYRENE-GRAFTED SILVER NANOPARTICLES BY FACILE LIGAND EXCHANGE REACTIONS IN SUSPENSION

Polymeric materials and in particular, elastomers exhibit highly sensitive mechanical behavior as a function of molecular weight. Up to now, this fundamental structure-property relationship has been hardly discussed in nanocomposite literature. In fact, previous protocols in which end-functionalized polymers are grafted to noble metal nanoparticles make use of very low molecular weights only. Therefore, the aim of this study is to develop a universal “grafting to” synthesis method using high molecular weight end-functionalized polymers as stabilizing ligands for noble metal nanoparticles. The challenge of this intent clearly lied in the decreasing concentration and therefore, in the decreasing availability of the coordinating end group relative to the polymer chain with increasing molecular weight. In order to overcome this challenge, a diffusion-controlled *ex situ*

method is presented where pre-formed ω -thiol polystyrene of different molecular weights are grafted to pre-formed AgNP by hetero-phase ligand exchange. Also, a kinetically controlled single-phase *in situ* “grafting to” method is investigated in order to put the results in context (**Figure 2-4**).

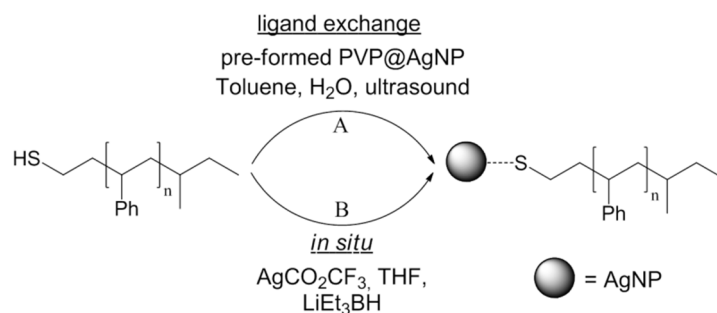


Figure 2-4. Synthetic methods to graft ω -thiol polystyrene onto AgNP. A: Ligand exchange in toluene/water hetero-phase system, using pre-formed aqueous AgNP with PVP as leaving ligand. B: *In situ* preparation in one phase using AgCO_2CF_3 as AgNP precursor.

ω -Thiol polystyrene, synthesized by anionic polymerization, with different molecular weights ranging from 21200 to 217200 g/mol were applied in the grafting reactions. Subsequent to grafting, transmission electron microscopy (TEM) and UV/Vis spectroscopy were used to evaluate whether AgNP are isolated (stabilized) or aggregated (not stabilized). Exceptional tolerance regarding high molecular weights, even up to 217200 g/mol is reported for this polymer-nanoparticle system by using the ligand exchange preparation method. During ligand exchange, AgNP did not transform in sizes and shape. However, low silver contents were identified as a precondition for successful grafting with such high molecular weights. In contrast, the *in situ* method performs well for 21200 g/mol ω -thiol polystyrene but fails to stabilize AgNP with any higher molecular weights, even with reduced silver content.

The liquid-liquid interface in ligand exchange preparations is considered as the key factor for high molecular weight tolerance. It is supposed that thiol end groups are more hydrophilic compared to the polymer tail which in turn causes end group self-orientation towards the aqueous phase. In contrast, the polymer tail remains in the toluene bulk (**Figure 2-5**). As ligand exchange takes place at the liquid-liquid interface only, the impact of the polymer molecular weight on the reaction is inferior. However, ligand exchange was not observed until ultrasound was utilized to generate a semi-stable PICKERING emulsion with toluene droplets being dispersed in the continuous aqueous phase.

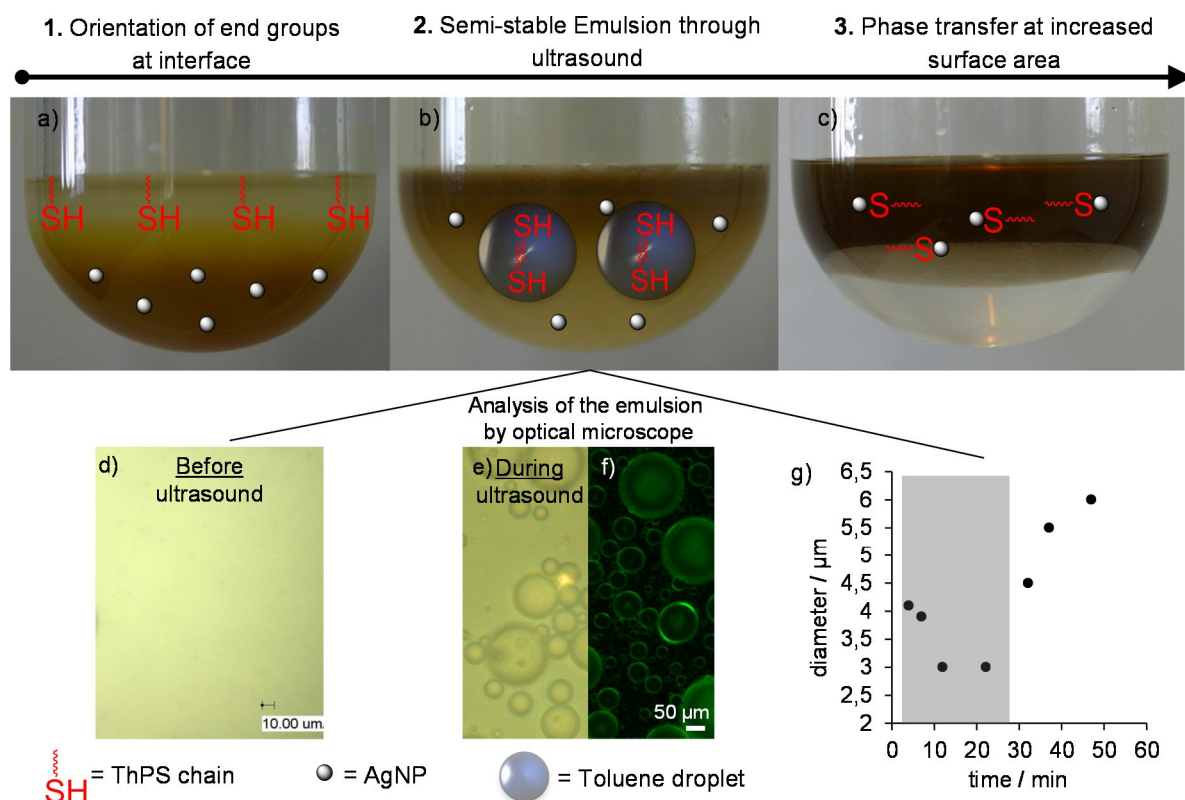


Figure 2-5. Illustration of the hetero-phase ligand exchange process. a)-c) AgNP are transferred from the aqueous phase to the upper hydrophobic toluene phase. Conversion can be monitored through LSPR color of AgNP. d)-e) Activation *via* ultrasound causes the phase mixture to emulsify, generating an enlarged interface area. f) Selective staining of the emulsion with rubrene reveals the toluene phase to be the dispersed phase in optical fluorescent microscopy. g) Plot of the emulsion droplet sizes as a function of time. The grey background represents the duration of ultrasound. Droplet sizes decrease down to 3.0 μm after 10 min of ultrasound activation. Disengaging ultrasound causes the emulsion to separate into two distinct phases with time.

In conclusion, hetero-phase ligand exchange allows grafting of very high molecular weight ω -thiol polystyrene onto AgNP through diffusion control. More than that, the exploration of such kind of surface modification methods is of major importance for the preparation of polymer-stabilized nanoparticles with morphologies other than spheres. For this reason, the herein described “grafting to” methods plays a key role for the chapter “Reversible Gold Nanorod Alignment in Mechano-Responsive Elastomers” in the course of this thesis.

2.4 SUMMARY OF CHAPTER 5: REVERSIBLE GOLD NANOROD ALIGNMENT IN MECHANO- RESPONSIVE ELASTOMERS

Combinations of polymers and nanoparticles with non-spherical, anisotropic morphologies are promising candidates for the design of nanocomposite materials with unprecedented physical properties. Gaining control over the orientational order of an ensemble of rod-like nanoparticles (nanorods) in the solid state is of special interest in this context as the macroscopic material thereby assumes anisotropy. In this study, AuNR are incorporated into an elastic environment where mechanical stimulation of the resulting nanocomposite triggers a change in the orientational order of the AuNR and therefore, a modification in the physical properties of the material. In detail, it was anticipated that uniaxial elongation of an elastic film causes the incorporated AuNR to align along the axis of elongation whereas random orientational AuNR distribution is maintained if the film is in the relaxed state (**Figure 2-6**). The key feature of such a system is the mechano-responsive control of physical properties in a stepless and reversible fashion. AuNR were chosen due to their momentousness in optical applications.

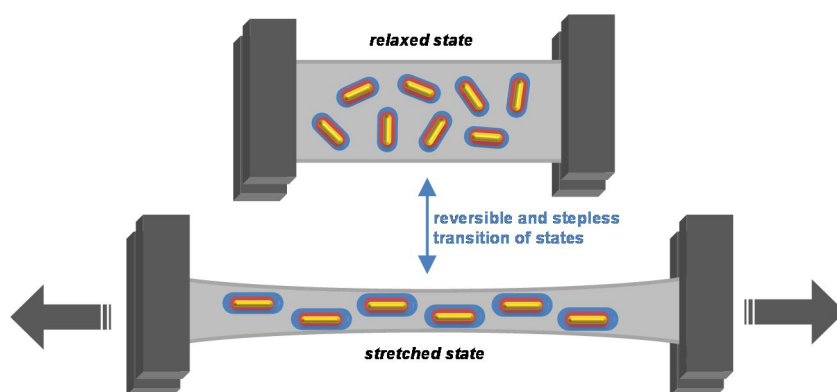


Figure 2-6. Well-dispersed AuNR within an elastic matrix are initially randomly oriented. Upon uniaxial elongation of a film, AuNR align along the axis of elongation. Due to inherent elastic restoring forces, alignment is reversible upon relaxation of the film. Therefore, it is anticipated that mechanical stimulation causes stepless and reversible transition between random and ordered AuNR orientation.

The first step of preparing mechano-responsive nanocomposites aims at converting CTAB-stabilized, aqueous AuNR with mean aspect ratios of 6.1 into hydrophobic and thermally

stable AuNR *via* exchange of the stabilizing ligand. TISIT as a hydrophobic, exchanging ligand was chosen due to its capability of generating elastic materials with outstanding mechanical properties as discussed in the chapter “Design of Soft Materials from Liquid Triblock Co-Oligomers and Metal Nanoparticles”. Complete CTAB-to-TISIT ligand exchange was performed in a hetero-phase toluene/water system such as successfully established in the chapter “Ultrasound-Mediated Synthesis for High-Molecular Weight Polystyrene-Grafted Silver Nanoparticles by Facile Ligand Exchange Reactions in Suspension”. Through auto-generation of a surfactant- and particle-stabilized emulsion (**Figure 2-7a**) and accumulation of thiol end groups at the increased liquid-liquid interface area (**Figure 2-7b**), AuNR were phase-transferred without changes in their sizes or shapes (**Figure 2-7c-d**). Isolation through precipitation and drying yielded materials with well-dispersed AuNR with a notable content of 1.9 wt% (**Figure 2-7e-f**).

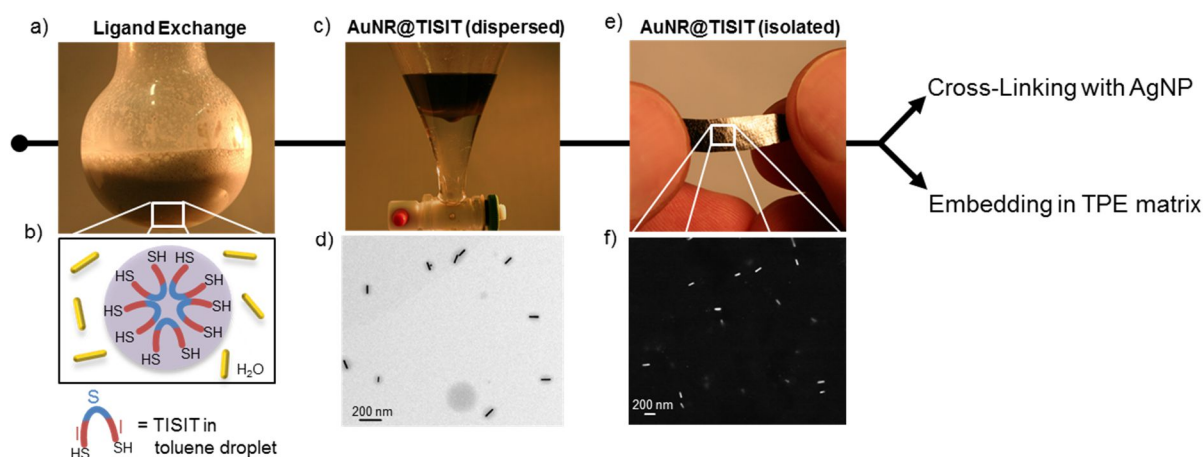


Figure 2-7. CTAB-to-TISIT Ligand exchange procedure. a) Surfactant- and particle-stabilized toluene/water emulsion provides increased liquid-liquid interface area, triggering accelerated AuNR phase transfer. b) Thiol end groups are preferentially oriented towards the water phase which supports the formation of intramolecular TISIT loops on the particle surface. c) Complete phase transfer is indicated by the color change of the respective phases. d) Complete CTAB-to-TISIT exchange yields core-shell arrangements in which TISIT serves as both the ligand and the dispersing medium. Here shown is a TEM micrograph of dispersed AuNR@TISIT, stained with RuO₄. e) Isolation *via* precipitation and drying of AuNR@TISIT yields a mechanically stable material in which AuNR are dispersed homogeneously as observed in f) SEM micrographs of the film surface. After ligand exchange, AuNR@TISIT was further cross-linked with spherical AgNP or embedded into a TPE matrix.

AuNR@TISIT could be cross-linked with spherical AgNP along the lines of the well-discussed single-phase *in situ* method (as used in the previous chapters) to yield thermally processable polymer-particle networks with mechano-responsiveness of the AuNR orientational alignment (proven by SAXS measurements). However, these networks were

optically too dense for optical characterization and the alignment performance was rather weak. Therefore, embedment of the isolated AuNR@TISIT materials into an optically transparent TPE matrix, Kraton FG1901x, assured dilution of AuNR and consequently, reduced optical density as well as improved mechanical properties. The impact of uniaxial mechanical elongation on the physical properties of Kraton FG1901x-embedded AuNR@TISIT was studied in detail using polarized UV-Vis spectroscopy, SEM imaging and SAXS.

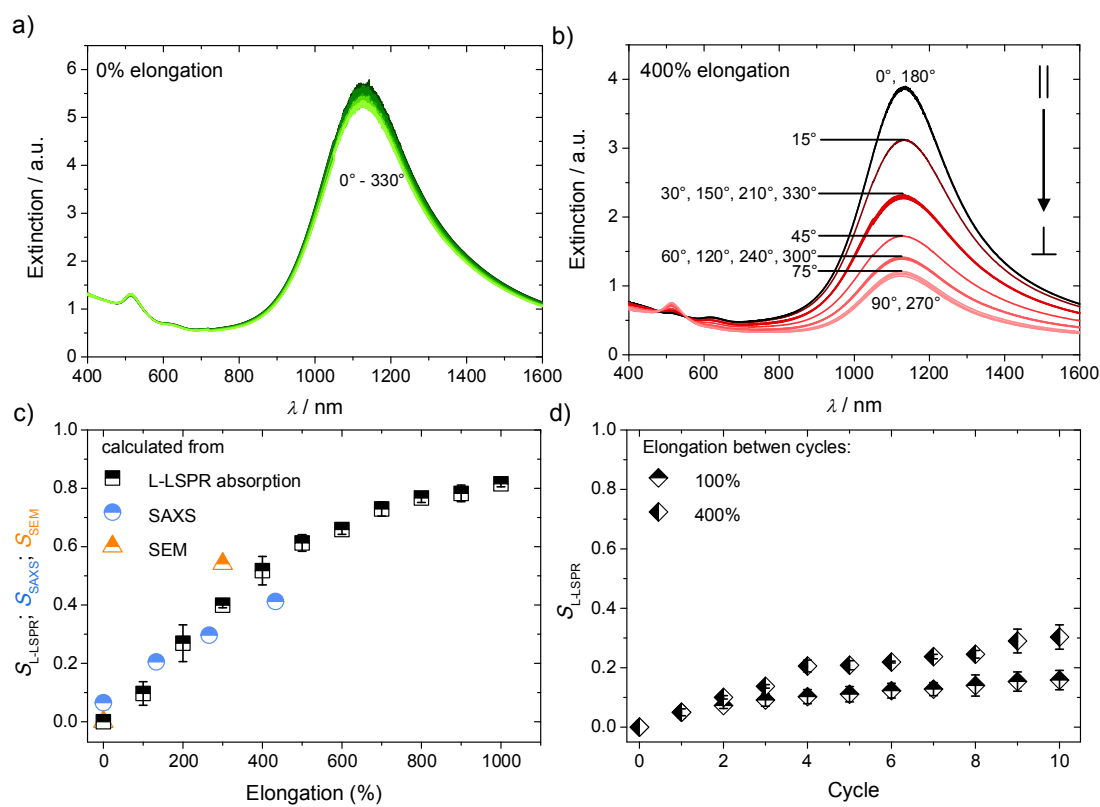


Figure 2-8. Change of physical properties as a function of mechanical stimulation of an elastic Kraton FG1901x film in which AuNR@TISIT is homogeneously embedded. a) Light absorption of relaxed films is independent of the polarization angle of incident light, indicating random orientational distribution of AuNR. b) Strong dependency of the LSPR responses on the polarization angle of incident light is observed upon stretching the film, indicating substantial alignment of AuNR along the axis of elongation. c) The orientational order parameter S (calculated either from SAXS, UV-Vis or SEM experiments) clearly scales as a function of the elongation. d) Distinct reversibility of AuNR alignment is observed upon relaxation of the film; however a slight memory effect is observed as well (here shown is the orientational order parameter S calculated from UV-Vis experiments as a function of 10 stretching cycles to either 100% or 400% elongation).

A close look was taken at the polarization-dependent absorption properties of the film. In the relaxed state, the LSPR response is independent from the polarization angle of incident

light (**Figure 2-8a**), indicating random orientational distribution within the matrix. In turn, substantial dependence of the polarization angle was observed in the stretched state (**Figure 2-8b**) where light polarized parallel to the stretching direction is absorbed more intensely than light polarized perpendicular to the stretching direction, indicating AuNR alignment along the axis of elongation. Moreover, it was shown with both UV-Vis spectroscopy and SAXS measurements that the degree of orientation (hence the orientational order parameter S) scales with the degree of elongation (**Figure 2-8c**). Distinct reversibility of AuNR alignment *via* film relaxation was observed, accompanied by a slight memory effect (**Figure 2-8d**) which could be reset by melting the film.

2.5 SUMMARY OF CHAPTER 6:

MECHANICAL REINFORCEMENT OF POLYDENTATE THIOETHER LIGAND BY SILVER NANOPARTICLES

While oligomeric and dendritic thioethers have been reported previously to stabilize gold and palladium nanoparticles, polymeric thioethers have never been used for this purpose. In fact, these polydentates are promising candidates as precursors for highly stable nanocomposites due to the virtually infinite availability of coordinating anchors per chain. In this study, linear poly(propylene sulfide) (PPrS) of high molecular weight is probed as a liquid ligand for AgNPs. Further to the fundamental outcome that PPrS protects AgNPs from agglomeration up to a particle filling fraction of $\phi = 0.30$ vol%, this study also revealed significant mechanical reinforcement of the liquid polymer up to the formation of an elastic material. The reinforcement mechanism is approached by a thorough investigation of viscoelastic properties from dynamic rheology measurements, followed by interpretation of the results in the light of established theories.

PPrS with $M_n = 44000$ g/mol is synthesized *via* ring-opening anionic polymerization of propylene sulfide with subsequent end-capping (**Figure 2-9a-c**). Afterwards, AgNPs are incorporated by *in situ* formation in solution, yielding materials with homogeneous particle distributions as seen in TEM micrographs (**Figure 2-9d**).

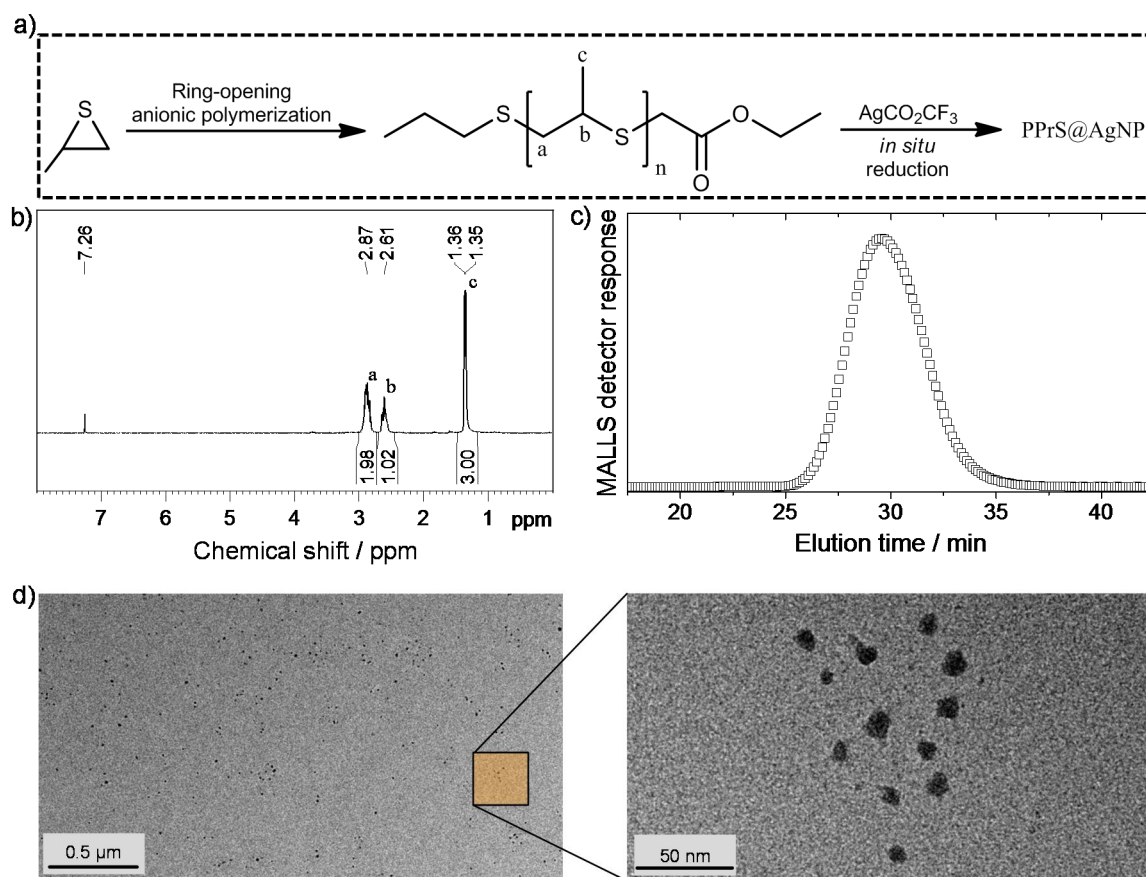


Figure 2-9. a) Preparation procedure for PPrS-stabilized AgNPs starting with the monomer propylene sulfide. Ring-opening anionic polymerization is initiated using an *S*-*n*-propyl thioacetate/NaOMe mixture and end-capped using ethyl bromoacetate. b) $^1\text{H-NMR}$ spectrum of PPrS, proving high chemical purity. c) GPC-MALLS elugram of PPrS from which $M_n = 44000$ g/mol is calculated. d) TEM micrograph (right side: magnification) of the nanocomposite with a particle filling fraction of 0.21 vol%.

Although G' and G'' master curves made from frequency-temperature superposition of frequency-dependent dynamic rheology measurements at different temperatures did not show a rubber plateau at lower frequencies, a significant retardation of chain dynamics was observed upon AgNP charging. In particular, the $G'-G''$ crossover frequencies ω_c are shifted to lower shear frequencies as a function of ϕ , reaching minimum for $\phi = 0.30$ vol% (**Figure 2-10a**). Despite being a liquid by definition, this sample exhibits form-stability over a time range of 100 h and above (**Figure 2-10b**) which is assumed to be a consequence of the strong ω_c shift.

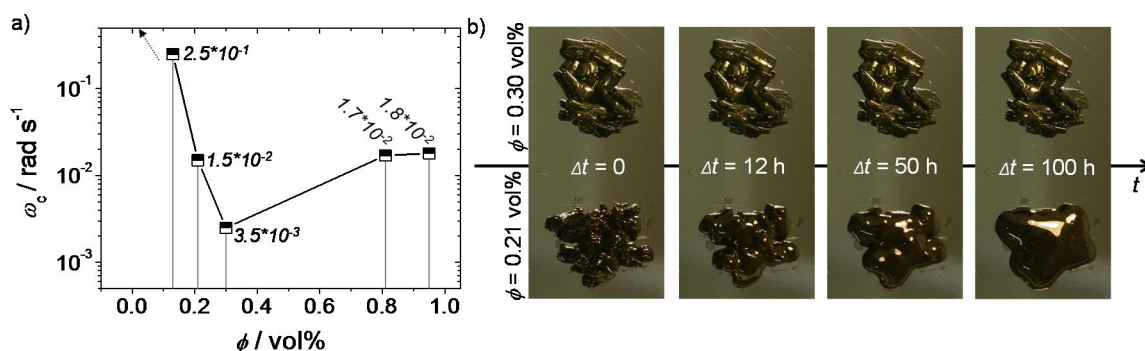


Figure 2-10. Viscoelastic properties of AgNP-reinforced PPrS. a) G' - G'' crossover frequencies ω_c as a function of the particle filling fraction ϕ . The most significant shift is observed for $\phi = 0.30$ vol%. b) Although AgNP-reinforced PPrS does not exhibit a rubber plateau at low shear frequencies, the nanocomposite with $\phi = 0.30$ vol% maintains form-stability over 100 h.

The interparticle distances Λ were calculated as a function of the polymer radius of gyration R_g , the particle filling fraction ϕ and the particle radius r_{AgNP} . It was shown that a loose polymer-particle network, in which polymer chains bridge the interparticle gap in a long-range manner, becomes plausible. In lieu of a dense network, AgNPs serve as additional topological constraints such as predicted previously in computer simulations under similar conditions. Owing to this, it is concluded that silver nanoparticles can be used as reinforcing agents for liquid polydentates already at low filling fractions, yielding elastic, pseudo-solid materials.

2.6 INDIVIDUAL CONTRIBUTIONS TO JOINT PUBLICATIONS

Chapter 3

This work is published in *Chem. Mater.* **2014**, *26*, 4805-4811 under the title

“Design of Soft Materials from Liquid Triblock Co-Oligomers and Metal Nanoparticles”

by Holger Pletsch, Max J. Schnepf and Seema Agarwal*.

I designed and performed all synthetic and analytic experiments and wrote the manuscript, except that Max J. Schnepf synthesized and analyzed the TISIT₂₈ part of the sample set and Seema Agarwal (corresponding author) was involved in designing the concept, scientific discussion as well as in correcting the manuscript.

Chapter 4

This work is published in *Small* **2014**, *10*, 201-208 under the title

“Ultrasound-Mediated Synthesis for High-Molecular Weight Polystyrene-Grafted Silver Nanoparticles by Facile Ligand Exchange Reactions in Suspension”

by Holger Pletsch, Ling Peng, Fabian Mitschang, Andreas Schaper, Michael Hellwig, David Nette, Andreas Seubert, Andreas Greiner* and Seema Agarwal*.

I designed and performed all synthetic and analytic experiments and wrote the manuscript, except that Ling Peng synthesized parts of the sample set as practical course student, Fabian Mitschang performed GPC characterization, Andreas Schaper and Michael Hellwig assisted in TEM characterization, David Nette and Andreas Seubert performed ICP-MS characterization and Andreas Greiner (corresponding author) as well as Seema Agarwal (corresponding author) were involved in designing the concept, scientific discussions and in correcting the manuscript.

Parts of this chapter are congruent with parts of my master thesis “Preparation of polymer-stabilized silver nanoparticles by interphase ligand exchange” which was published as part of the master program “Polymer Science” at the University of Bayreuth. The overlap

concerns synthesis and analytics of ω -thiol polystyrene with molecular weight of 21200 g/mol and the PVP-stabilized AgNP suspension as well as the investigation of suitable reaction parameters for ligand exchange.

Chapter 5

This work is *submitted* for publication under the title

“Reversible Gold Nanorod Alignment in Mechano-Responsive Elastomers”

by Holger Pletsch, Moritz Tebbe, Martin Dulle, Beate Förster, Andreas Fery, Stephan Förster, Andreas Greiner and Seema Agarwal*.

I designed and performed all synthetic and analytic experiments and assembled the manuscript except that Moritz Tebbe contributed in designing synthetic and analytic experiments, prepared and analyzed AuNR@CTAB suspensions, performed and analyzed parts of the absorption measurements and contributed in writing the manuscript and is therefore denoted as second author who contributed equally to this chapter, Martin Dulle performed and analyzed SAXS experiments, Beate Förster performed SEM experiments, Andreas Fery as well as Stephan Förster were involved in scientific discussions and in correcting the manuscript and Andreas Greiner as well as Seema Agarwal (corresponding author) were involved in designing the concept, scientific discussions and in correcting the manuscript.

Chapter 6

This work is *submitted* for publication under the title

“Mechanical Reinforcement of Polydentate Thioether Ligand by Silver Nanoparticles”

by Holger Pletsch, Andreas Greiner and Seema Agarwal*.

I designed and performed all synthetic and analytic experiments and wrote the manuscript, except that Andreas Greiner as well as Seema Agarwal (corresponding author) were involved in designing the concept, scientific discussions and in correcting the manuscript.

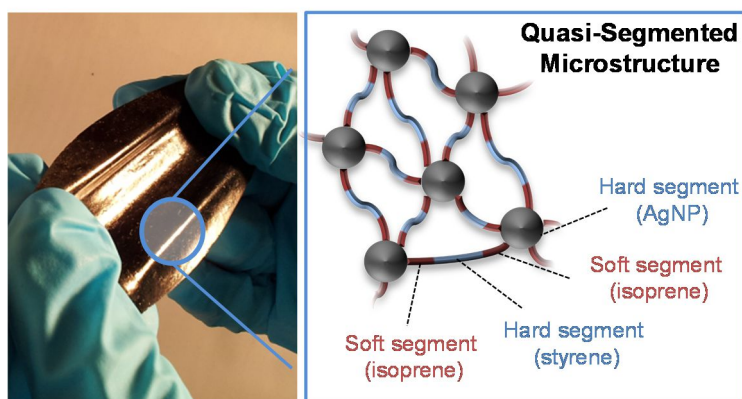
CHAPTER 3

DESIGN OF SOFT MATERIALS FROM LIQUID TRIBLOCK CO-OLIGOMERS AND METAL NANOPARTICLES

*Holger Pletsch, Max J. Schnepf and Seema Agarwal**

Faculty of Biology, Chemistry and Earth Sciences, Macromolecular Chemistry II and Bayreuth Center for Colloids and Interfaces, University of Bayreuth, Universitätsstraße 30, 95440 Bayreuth, Germany.

Fax: +49 921553393. E-mail: agarwal@uni-bayreuth.de



Published in *Chemistry of Materials* **2014**, 26, 4805-4811. Reprinted with permission.

Copyright American Chemical Society.

ABSTRACT

Thermally processable soft material networks with adjustable mechanical properties made from very low molar mass α,ω -dithiol functionalized ABA triblock co-oligomers (α,ω -dithiol oligo(isoprene-*b*-styrene-*b*-isoprene) (TISIT)) using AgNP as thermally reversible cross-linking points are highlighted in the present work. Liquid TISIT oligomers were synthesized by sequential anionic polymerization and subsequently cross-linked with AgNP. Low molar masses (4200-4800 g/mol) were engaged, assuring disordered microstructures and therefore, low viscosities at elevated temperatures. Smooth films with homogeneous nanoparticle distributions of the resulting quasi-segmented soft material networks (TISIT@AgNP) were made by heat pressing. The interplay of styrene and AgNP as the structure-supplying portions in TISIT@AgNP samples facilitates access to materials with tensile strengths up to 5.58 MPa, toughness up to 13.3 MN mm⁻² and tensile moduli up to 80.1 MPa at room temperature and strongly decreased elasticity and viscosity at elevated temperatures, even below the glass transition temperature of polystyrene.

KEYWORDS

Block co-oligomers, metal nanoparticles, cross-linking, elastomers, nanomaterials

INTRODUCTION

Physical interaction of polymer chains with low glass transition temperatures (T_g) in thermoplastic elastomers (TPE) yield non-covalent physical networks and provide material properties comparable to elastomers and melt-processability comparable to thermoplastics.¹ The thermoreversible nature of physical cross-links can be amongst others **(1)** phase separation in block copolymers with representative examples being poly(styrene-*b*-butadiene-*b*-styrene) (SBS), poly(styrene-*b*-isoprene-*b*-styrene) (SIS) or other triblock copolymers in which incompatibility between hard and soft blocks leads to microphase separation;² **(2)** reversible chemical bonding as demonstrated for example in chlorobutyl rubber and chlorinated poly(ethylene-*co*-propylene) (Cl-EPM) rubber using Diels-Alder chemistry;³ **(3)** hydrogen bonding which has been exploited in supramolecular assemblies from complementary hydrogen bonding groups like amidoethyl imidazolidone, di(amidoethyl) urea and diamidotetraethyl triurea, providing thermally processable glassy materials which showed rubber-like behavior only at temperatures well above room temperature (90 °C)⁴ as well as in segmented copolymeric TPEs where the hydrogen bonding-forming moiety was generating hard segments;⁵ **(4)** metal complexation where telechelic oligomers (poly(ethylene-*co*-butylene) with $M_n = 4000$ g/mol) having 2,6-bis(1'-methylbenzimidazolyl)pyridine end-groups were used as ligands for generating supramolecular networks *via* reversible ligand- Zn^{2+} bonding, providing optically healable materials⁶ or where segmented ABA triblock and AB multiblock copolymer systems or *N*-Pyrid-2-ylmethyl amide (MPY)-modified polyisoprene were cross-linked with Cu(I)⁷ and $ZnCl_2$,⁸ respectively; **(5)** electrostatic interactions as observed in ionomers in which ionic clustering act as physical cross-linking points.^{9,10}

Recently we showed a different concept of preparing processable elastic networks in which α,ω -thiol functionalized isoprene oligomers with very low glass transition temperatures (T_g) have been cross-linked with spherical silver nanoparticles (AgNP).^{11,12} The strong ligand-particle interactions of thiolate groups on the metal surface were exploited to form a stable, yet reversible bonding.^{15,16} This was different from the known silica-polymer composites wherein network structures are generated from bridging aggregated silica nanoparticles by much larger polymer molecules of molar mass between 45000-292000 g/mol and 90000 g/mol for poly(ethyleneoxide)¹³ and poly(dimethyl siloxane),¹⁴ respectively.

In the present work, soft material networks with adjustable glass transition points and mechanical properties are designed from very low molar mass α,ω -dithiol functionalized ABA triblock co-oligomers consisting of isoprene (A) and styrene (B) using AgNP as cross-linking points. The triblock co-oligomers in the article are designated as TISIT standing for thiol-isoprene-styrene-isoprene-thiol. The resulting soft materials (TISIT@AgNP) involve an alternating soft-hard arrangement of segments in which styrene and AgNP are giving mechanical strength as hard segments and isoprene acting as the flexible segment (**Figure 3-1**). Their mechanical properties may be designed by changing the corresponding segment ratios.

In order to provide block length-dependent microphase separation in commercial block copolymer TPEs such as SBS or SIS, high molecular weights are required.¹⁷ As a result, these materials generally suffer from high melt viscosities even at high temperatures which prevent effective processing. Replacement of non-compatible amorphous blocks by compatible blocks consisting of crystallizable hard segments was initially investigated to overcome this drawback.¹⁸ Verhoogt et al. addressed this problem by blending TPEs with low viscosity thermotropic liquid crystalline polymers.¹⁹ Our block co-oligomer-based approach uses TISIT precursors with molecular weights well below 5000 g/mol which should benefit thermic processing due to low viscosities. In early studies about block copolymer TPEs, Fedors already stated that “the most suitable molecular weight for a block copolymer would be the lowest value which provides a sufficiently high T_g ” in order to achieve low bulk viscosities.²⁰ Moreover, low polymerization degrees prevent microphase separation.²¹ Therefore, shear-induced phase coalescence phenomena should be outflanked which were for example reported for polystyrene/polybutadiene TPE blends.²² Based on these expectations we show for the first time quasi-segmented soft materials with investigations focused on synthesis, material properties and processability.

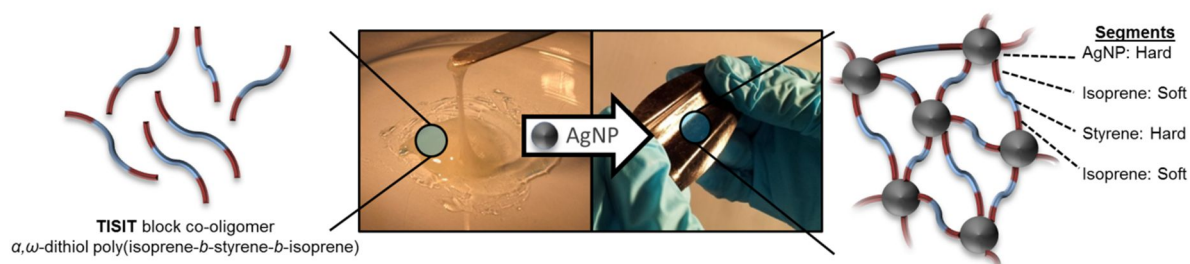


Figure 3-1. Cross-linking of liquid TISIT block co-oligomers with AgNP provides soft, elastic materials with mechanical properties being dependent on the segment ratios.

EXPERIMENTAL SECTION

Materials

Tetrahydrofuran (THF) and cyclohexane have been purified by consecutive drying over CaH₂ and potassium with subsequent distillation under nitrogen atmosphere. MeOH has been purified by distillation. Et₃N (Aldrich, >99%), 1,3-diisopropenylbenzene (97%, Aldrich), *N,N,N',N',N''*-pentamethyldiethylenetriamine (99%, Aldrich) and ethylene sulfide (98%, Aldrich) have been dried over CaH₂, distilled, degassed by freeze-pump-thaw (three cycles) and stored at 5 °C under argon. Styrene (Acros, 99%) has been dried over CaH₂, distilled, degassed by freeze-pump-thaw (three cycles) and used immediately. Isoprene (98%, Acros) has been dried over di-*n*-butylmagnesium (1 M in Heptan, Aldrich), distilled, degassed by freeze-pump-thaw (three cycles) and used immediately. Silver trifluoroacetate (98%, Acros) has been recrystallized from Et₂O. Lithium triethylborohydride (1.0 mol L⁻¹ in THF, Aldrich) and *tert*-butyllithium (1.6 M in pentane) have been used as received.

Methods

The number-average molecular weights (M_n) and the weight-average molecular weights (M_w) of TISIT were determined by gel permeation chromatography (GPC) in THF at 26 °C using an Agilent 1200 series system equipped with a PSS-SDV (10 μm) 50 × 8 mm² pre-column and three linear PSS-SDV (10 μm) 300 × 8 mm² columns at a flow rate of 0.8 mL min⁻¹ (sample concentration 2 mg mL⁻¹). A Wyatt Dawn Heleos multi angle laser light scattering (MALLS) detector was used to calculate the absolute molecular weight. dn/dc was determined with a PSS DnDc-2010 λ620 device.

A Mettler thermal analyzer 821 DSC was utilized for DSC scans. Temperature and enthalpy calibration was carried out with indium and zinc standards and tested with *n*-octan as a reference. 5 ± 2 mg of the samples were analyzed under nitrogen atmosphere (flow rate 80 mL min⁻¹) at a heating rate of 10 °C min⁻¹. The glass transition temperature (T_g) was taken as the inflection point of the observed shift in the baseline of the second heating cycle.

TEM measurements have been done in a Zeiss 922 OMEGA EFTEM at a voltage of 200 kV. Zero-loss filtered images were recorded using a bottom mounted Ultrascan 1000 (Gatan) CCD camera system. Gatan Digital Micrograph 3.9 for GMS 1.4 software was used for image acquisition. Samples have been prepared from solution by drop-casting on a

Quantifoil 300 mesh copper grid with carbon coating. For size calculation the software ImageJ (version 1.44p) of the National Institute of Health, USA, has been used. The mean particle diameters were calculated from at least 100 particles per sample.

Heat pressing was carried out using a Carver 2518 setup at 300 bar.

Tensile testing was carried out on a Zwick Roell Z0.5 device equipped with a Zwick Roell KAF-TC 1000 N load sensor at a strain rate of 200 mm min⁻¹ according to ISO 37 (DIN 53504) at 23 °C. Zwick Roell testXpert II V 3.0 software was used for acquisition. S3A shouldered test bars were stamped from homogeneous films made by heat-pressing for 90 s at 90 °C. Upon loading, a slack was observed which was deducted for ultimate elongation determination. The tensile strengths were identified at the stress maxima of the curves. E-Moduli were determined as the slope of the elastic region in the stress-strain-curve. Toughness of the samples were determined by calculating the area under the stress-strain-curve. All values represent the average of seven measurements and refer to the engineering curves.

Oscillatory tensile testing was carried out with S3A shouldered test bars on an Instron 5565 equipped with a 100 N load sensor at a strain rate of 20 mm min⁻¹ and at a temperature of 20 °C.

A Malvern Instruments Bohlin Gemini HR Nano device with a 2 cm stainless steel plate-plate setup in shear strain-controlled mode was used for dynamic rheology. Sample films made from heat-pressing were molded into discs with 2 cm diameter and 1.5 mm thickness. The linear viscoelastic (LVE) ranges of the samples were determined by carrying through strain sweeps with deformations between 0.01 and 10% and constant angular frequencies of 0.01, 0.1, 1.0 and 5.0 rad s⁻¹ at 20 °C and 70 °C. Constant dynamic rheology measurements were carried out at 0.1% strain, an angular frequency of 1.0 rad s⁻¹ and at temperatures of 20 and 70 °C. Frequency sweep experiments were carried out with constant temperatures between 20 °C and 70 °C in 5 °C steps, with constant strain of 0.1% and with an angular frequency range between 0.01 and 5.0 rad s⁻¹.

Preparation of TISIT₂₈

A flame-dried flask was charged with 20.0 mL (32.0 mmol) *tert*-butyllithium solution and cooled to -20 °C after which 4.44 mL (32.0 mmol) Et₃N was added. After 10 min, 2.72 mL (16.0 mmol) 1,3-diisopropenylbenzene were added dropwise at -20 °C with subsequent

stirring for 5 h. The initiator solution ($c = 0.59 \text{ mol L}^{-1}$) was used without further purification. 500 mL cyclohexane were degassed by Ar-bubbling, cooled to 0 °C and titrated with the initiator solution until a slightly yellow color was maintained constant. 15.0 mL (9.00 mmol) of the initiator solution were added after which 10.3 mL (90.0 mmol) styrene were added quickly. The solution was rapidly heated to 45 °C and stirred for 90 min. 27.0 mL (270 mmol) isoprene were added quickly and the solution was stirred for 18 h at 45 °C. After cooling to room temperature, 30.0 mL (144 mmol) *N,N,N',N',N''*-pentamethyldiethylenetriamine were added, stirred for 1 h, followed by addition of 1.13 mL (18.9 mmol) ethylene sulfide. After stirring for 2 h, the solution was concentrated and precipitated in degassed MeOH. The solvent was decanted under Ar atmosphere and the oligomer was dried in vacuo. $M_n = 4600$, $M_w = 5100$, PDI = 1.12 (calculated from GPC-MALLS). Block length ratio styrene:isoprene = 15:45, equals 28% molar styrene content (calculated from $^1\text{H-NMR}$ spectrum). The sample was designated as TISIT₂₈ with 28 representing the percentage molar styrene content. TISIT₃₆ and TISIT₅₆ were prepared by adjusting the molar monomer/initiator ratios. Please find an overview of the corresponding amounts used in the supporting information.

Preparation of TISIT₂₈@AgNP_{4.72}

4.27 g (0.930 mmol) TISIT₂₈ were dissolved in 30 mL THF and charged with 968 mg (4.38 mmol) AgCO₂CF₃. 26.3 mL of lithium triethylborohydride solution were added slowly at room temperature during vigorous stirring. After 30 min the reaction solution was precipitated in MeOH after which the supernatant was decanted and the residue dried in vacuo. A black elastomer was obtained. The sample was designated as TISIT₂₈@AgNP_{4.72} with 28 representing the percentage molar styrene content and 4.72 standing for the molar Ag feed. Other TISIT@AgNP materials were prepared by adjusting the TISIT:AgCO₂CF₃ ratio. Please find an overview of the corresponding amounts used in the supporting information.

RESULTS AND DISCUSSION

TISIT with 28%, 36% and 56% molar styrene content (the corresponding samples are designated as TISIT₂₈, TISIT₃₆ and TISIT₅₆ in the following) were synthesized by anionic polymerization with subsequent functionalization using ethylene sulfide. The molar styrene

contents and the 1,4-:3,4-oligoisoprene ratios were determined by comparison of characteristic oligostyrene signals ($\delta = 6.49\text{--}7.08$ ppm), 1,4-oligoisoprene signals ($\delta = 5.12\text{--}5.14$ ppm) and 3,4-oligoisoprene signals ($\delta = 4.70\text{--}4.76$ ppm) in $^1\text{H-NMR}$ analysis (**Figure 3-2**).²³ The 1,4-oligoisoprene contents varied in the range of 79-84% for all samples. Differences in total molecular weights were kept to a minimum in order to avoid influence on material properties. Absolute TISIT molecular weights (TISIT₂₈: 4600 g/mol; TISIT₃₆: 4800 g/mol; TISIT₅₆: 4200 g/mol) were determined by GPC with multi-angle laser light scattering (MALLS) detector. TISIT oligomers show single glass transition temperatures which indicate the absence of microphase separation due to low molecular weight. Depending on the block length ratios, the glass transition temperatures varied between -47 °C for TISIT₂₈ and $+1$ °C for TISIT₅₆ (**Table 3-1**).

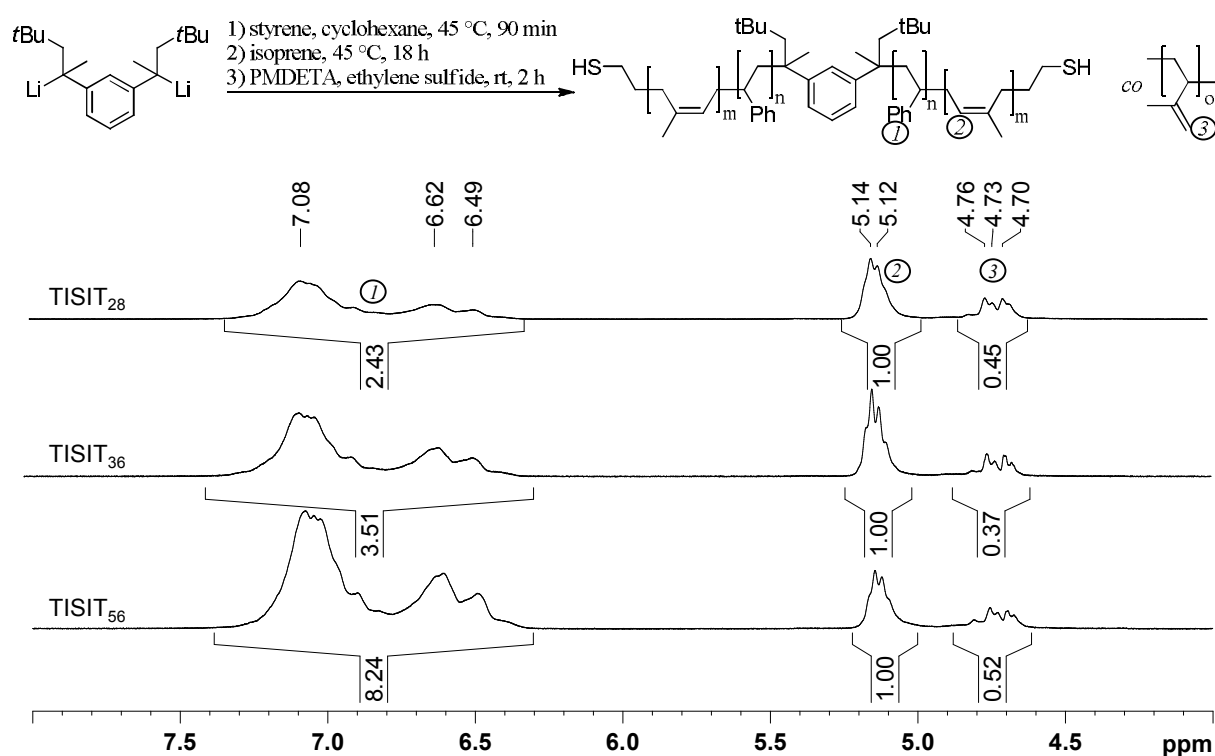


Figure 3-2. Preparation of TISIT is carried out via sequential anionic polymerization of styrene and isoprene using a difunctional lithium initiator, followed by end group functionalization with ethylene sulfide (above).

Detail views of TISIT $^1\text{H-NMR}$ spectra for calculation of the corresponding styrene amounts and 1,4-3,4-polyisoprene ratios (below): Polystyrene aromatic signals and 1,4-polyisoprene and 3,4-polyisoprene signals are identified at $\delta = 6.49\text{--}7.08$ ppm (1), $5.12\text{--}5.14$ ppm (2), and $4.70\text{--}4.76$ ppm (3), respectively. Please find the full view $^1\text{H-NMR}$ spectrum of TISIT₂₈ in the Supporting Information.

Cross-linking was carried out *via* the well-established *in situ* method using AgCO_2CF_3 as a precursor and lithium triethylborohydride as a reducing agent.²⁴ Different feed amounts of AgNP ranging from 0.59 up to 11.0 molar equivalents with respect to one thiol end group

were employed in order to transform TISIT precursors from viscous liquids into viscoelastic solids due to network formation. Determination of Ag contents utilizing TGA ash yield analysis confirmed quantitative conversions of the precursor salt to AgNP and are in good agreement with the expected values (**Table 3-1**). The resulting elastomers were designated as TISIT_x@AgNP_y with subscript x standing for the percentage molar styrene content and subscript y for the molar Ag feed. In order to probe interactions between AgNP and the styrene and isoprene blocks, control experiments were carried out in which a corresponding non-end-functionalized triblock co-oligomer ISI₃₆ was employed as a possible ligand for silver nanoparticle stabilization during *in situ* formation. As a result, immediate precipitation of coarse silver was observed which leads us to the conclusion that polymer-particle interactions are exclusively mediated *via* the terminal thiol groups.

Table 3-1. Ag Weight Content, Glass Transition Temperatures (T_g), and Average AgNP Diameters (d_{Ag}) of TISIT and TISIT@AgNP Elastomers

Sample	Ash yield Ag (wt.%) calculated / expected	T_g (°C) ^{a)}	d_{Ag} (nm) ^{b)}
TISIT ₂₈	-	-47	-
TISIT ₂₈ @AgNP _{1.18}	3.3 / 2.7	-35	2.5 ± 0.7
TISIT ₂₈ @AgNP _{4.72}	9.9 / 9.9	-34	2.3 ± 0.6
TISIT ₂₈ @AgNP _{8.49}	16.3 / 16.6	-33	2.8 ± 0.7
TISIT ₂₈ @AgNP _{11.0}	20.8 / 20.5	-32	3.0 ± 1.1
TISIT ₃₆	-	-42	-
TISIT ₃₆ @AgNP _{1.18}	2.4 / 2.6	-38	1.9 ± 0.5
TISIT ₃₆ @AgNP _{4.72}	9.4 / 9.6	-35	1.9 ± 0.4
TISIT ₃₆ @AgNP _{8.49}	15.3 / 16.0	-32	2.5 ± 0.6
TISIT ₃₆ @AgNP _{11.0}	19.3 / 19.8	-29	2.7 ± 0.7
TISIT ₅₆	-	+1	-
TISIT ₅₆ @AgNP _{0.59}	1.4 / 1.5	+14	2.4 ± 0.6
TISIT ₅₆ @AgNP _{1.18}	2.3 / 2.9	+20	2.5 ± 0.6
TISIT ₅₆ @AgNP _{4.72}	10.5 / 10.8	+32	3.1 ± 0.7
TISIT ₅₆ @AgNP _{8.49}	16.5 / 17.9	+35	3.5 ± 0.9

^{a)} T_g were determined by DSC.

^{b)} d_{Ag} were determined from TEM images by measuring at least 100 particles.

Heat pressing experiments were carried out to probe the sensitivity of nanoparticles in TISIT@AgNP elastomers against particle agglomeration at high temperatures and shear forces. Average particle diameters d_{Ag} and localized surface plasmon resonance (LSPR) absorption maxima were determined to understand possible particle transformations in the bulk. Within a pressing duration of 10 min at 130 °C and 300 bar pressure, nanoparticles were found to be heavily agglomerated. At given pressure, either reduced temperatures or shortening of the pressing durations were necessary to avoid particle coarsening. Then, good agreement of average particle diameters and LSPR maxima was observed with insignificant deviations compared to the control values. The by far best results were obtained with a short pressing duration of 90 s at high temperatures such as 90 or 110 °C (**Figure 3-3**). Under these conditions, films with smooth surfaces and homogeneous particle distributions were pressed. Particle agglomeration and therefore, continuous particle-particle networks are absent here. Processing at low temperatures such as 50 °C gave uneven films with inhomogeneous particle distributions, even at long pressing durations. TISIT₂₈@AgNP samples with low AgNP content (1.18 molar equivalents in feed and less) appeared as tar-like materials due to insufficient cross-linking and low glass transition points. In turn, TISIT₅₆@AgNP samples with high AgNP content (4.72 molar equivalents in feed and more) appeared as very brittle solids. Both types of materials are not considered in the following discussion. Regardless of the styrene content of the samples, AgNP diameters drifted to higher values with increasing Ag content and were found in a range between 1.9-3.5 nm (**Table 3-1**).

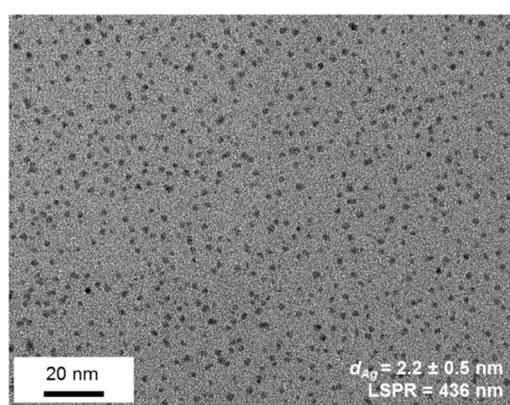


Figure 3-3. TEM image (scale bar 20 nm) of TISIT₂₈@AgNP_{4.72} sample after heat pressing at 110 °C and 300 bar for 90 s. Average particle diameters d_{Ag} and localized surface plasmon resonance (LSPR) absorption maximum from UV/Vis analysis do not differ from the non-processed control sample.

Significant increases in glass transition temperatures of up to 34 °C were observed upon addition of AgNP as the construction of a network enforces deceleration of the TISIT chain

segments. This effect has been reported for homo α,ω -dithiol oligoisoprene and homo ω -thiol polystyrene as well, yet to a lesser extent.^{11,25} Glass transition temperatures of TISIT₅₆@AgNP_{4.72} and TISIT₅₆@AgNP_{8.49} exceed room temperature which is why they appear as brittle materials.

The resulting materials revealed elastic behavior with characteristic restoring forces (**Figure 3-4a**) and a strong dependence of the mechanical properties on the styrene block length and the AgNP content (**Figure 3-4b**). Increasing styrene and AgNP contents significantly amplified E-Moduli of the novel soft materials and a broad stiffness range of more than three orders of magnitude from $E = 0.24$ -80.1 MPa is covered. In contrast, use of only homo α,ω -dithiol oligoisoprene exhibit very low E-Moduli and elongation at break between 0.20-1.12 MPa and 51%, respectively.¹¹ TISIT@AgNP ultimate elongations were predominantly influenced by the AgNP content rather than by the styrene amount and a range of 131-349% is covered. Higher AgNP contents yielded decreased ultimate elongation values. Therefore, we assume this property to be mainly followed from changes in cross-linking densities as modifications of styrene amounts do not affect the density of the network.

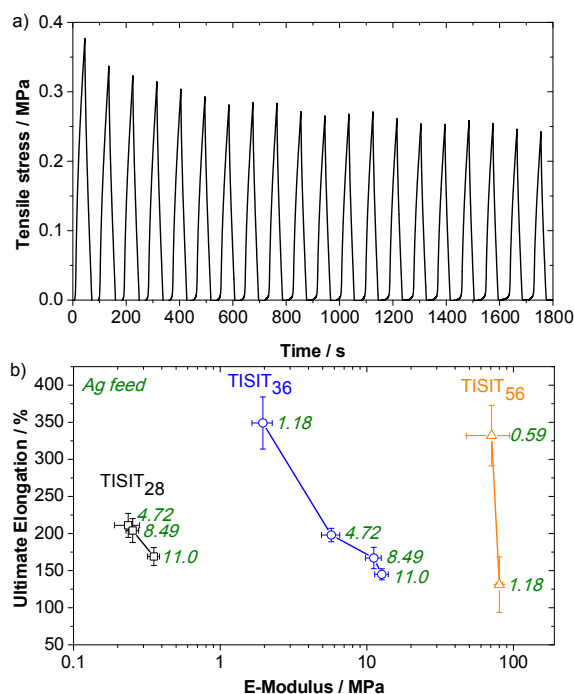


Figure 3-4. a) Oscillating tensile test of TISIT₂₈@AgNP_{4.72} at 100% maximum elongation (20 cycles, 20 mm min⁻¹ strain rate). Despite of partial irreversible plastic deformation, the material exhibit strong restoring forces. b) E-Moduli as a function of ultimate elongations of TISIT@AgNP samples. E-Moduli scale with both styrene amount and AgNP content whereas ultimate elongation is predominantly influenced by AgNP content.

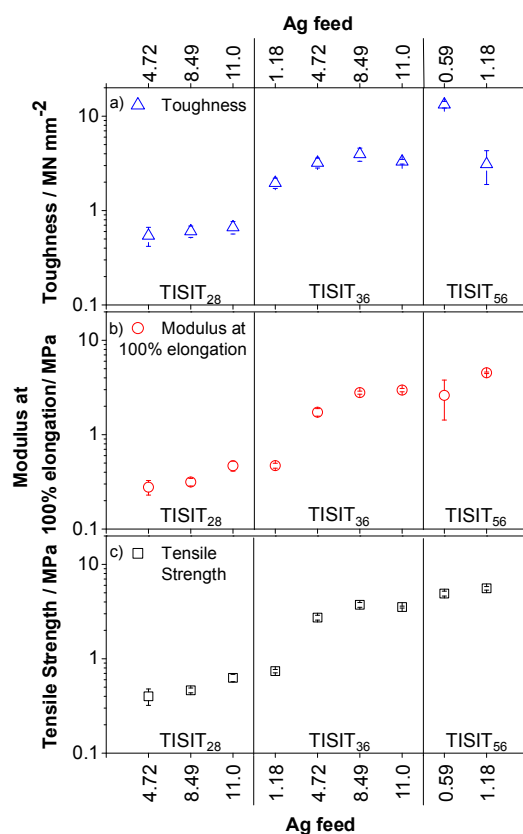


Figure 3-5. Plots of a) toughness, b) moduli at 100% elongation and c) tensile strengths as a function of styrene and AgNP content of TISIT@AgNP samples from tensile testing according to ISO 37. TISIT₃₆-based samples with high Ag contents and TISIT₅₆-based samples with low AgNP contents exhibit notably improved material properties compared to TISIT₂₈-based samples.

The mechanical properties of conventional SBS block copolymer TPEs are also affected by modifications in styrene content, yet in a different manner: E-Moduli were reported to increase as a function of styrene content, whereas ultimate elongations concurrently decreased.² This trade-off is circumvented in TISIT-based novel materials through balancing the tensile properties with a variable amount of AgNP. TISIT₃₆ and TISIT₅₆ are supposed to be the most suitable precursors for the preparation of stiff and yet stretchable materials due to their high toughness values (**Figure 3-5a**). The higher toughness in the entire sample set was found for TISIT₅₆@AgNP_{0.59}, holding a value of 13.3 ± 1.07 MN mm⁻². Generally, through increasing the styrene amounts, significantly less AgNP are required in order to yield equal or better mechanical properties. Moduli at 100% elongation vary in a range between 0.278 ± 0.049 MPa (TISIT₂₈@AgNP_{4.72}) to 4.53 ± 0.086 MPa (TISIT₅₆@AgNP_{1.18}), being comparable with vulcanized butadiene rubber holding a modulus of 2.0 MPa at 100% elongation²⁶ or SBS holding molecular weight-dependent moduli between 1.7-2.3 MPa at 100% elongation (**Figure 3-5b**).²

Tensile strengths of TISIT@AgNP samples are as well strongly influenced by both the styrene and the AgNP content (**Figure 3-5c**).

However, we emphasize that only the insertion of a hard styrene block is giving rise to higher tensile strength dimensions of up to 5.58 ± 0.24 MPa for the TISIT₅₆@AgNP_{1.18} sample. In comparison with other commercially available TPEs and elastomers, TISIT@AgNP materials are softer and cover different ranges of mechanical properties (**Figure 3-6**). Please find in the supporting information a summary of material properties of both reference materials discussed here and TISIT@AgNP elastomers, including Shore hardness values.

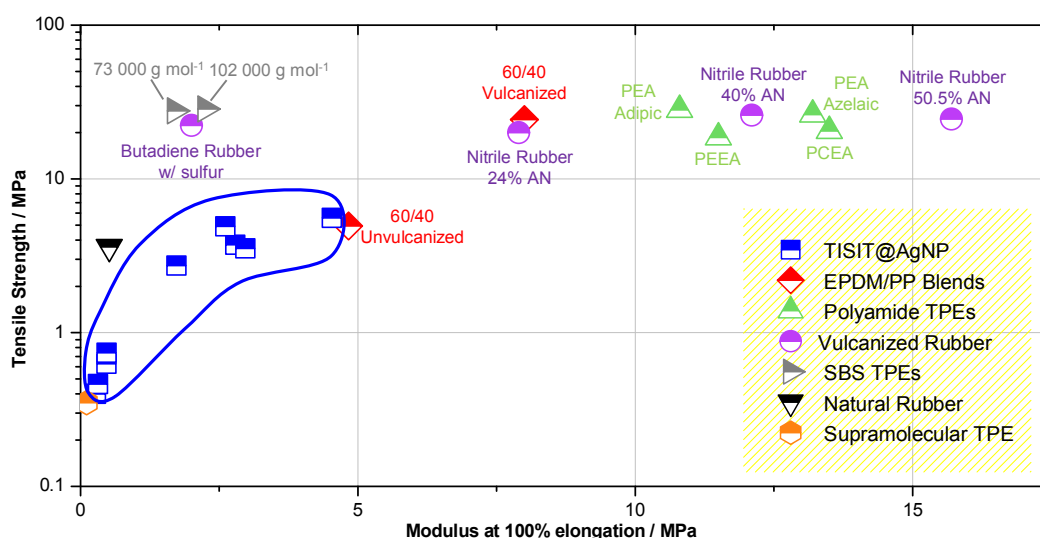


Figure 3-6. Ashby-plot of tensile strength as a function of modulus at 100% elongation. TISIT@AgNP materials (squares) cover a wide range of mechanical properties comparable to a soft rubber. Other rubbers and TPEs, including EPDM/PP blends (diamonds)²⁷, polyamides (up-pointing triangles)²⁸, natural rubber (down-pointing triangles)²⁹ vulcanized rubbers (circles),²⁶ hydrogen-bonded supramolecular networks (hexagon)⁴ and SBS (right-pointing triangles)² exhibit mechanical properties in ranges differing from TISIT@AgNP. Please find in the supporting information a summary of the mechanical properties of the reference materials shown here (Table 3-S2).

A dynamic rheology setup in frequency sweep mode was utilized to characterize the viscoelastic behavior of TISIT@AgNP samples at both room temperature and elevated temperatures. From time-temperature superposition, storage modulus G' and loss modulus G'' master curves were generated (**Figure 3-7a**). At low frequencies, TISIT@AgNP samples exhibit an obvious plateau with $G' > G''$, indicating eradication of the longer relaxation time processes and therefore, cross-linking. In isothermal and constant testing mode, the storage moduli G' were found to scale with AgNP as well as with the styrene content (**Figure 3-7b**).

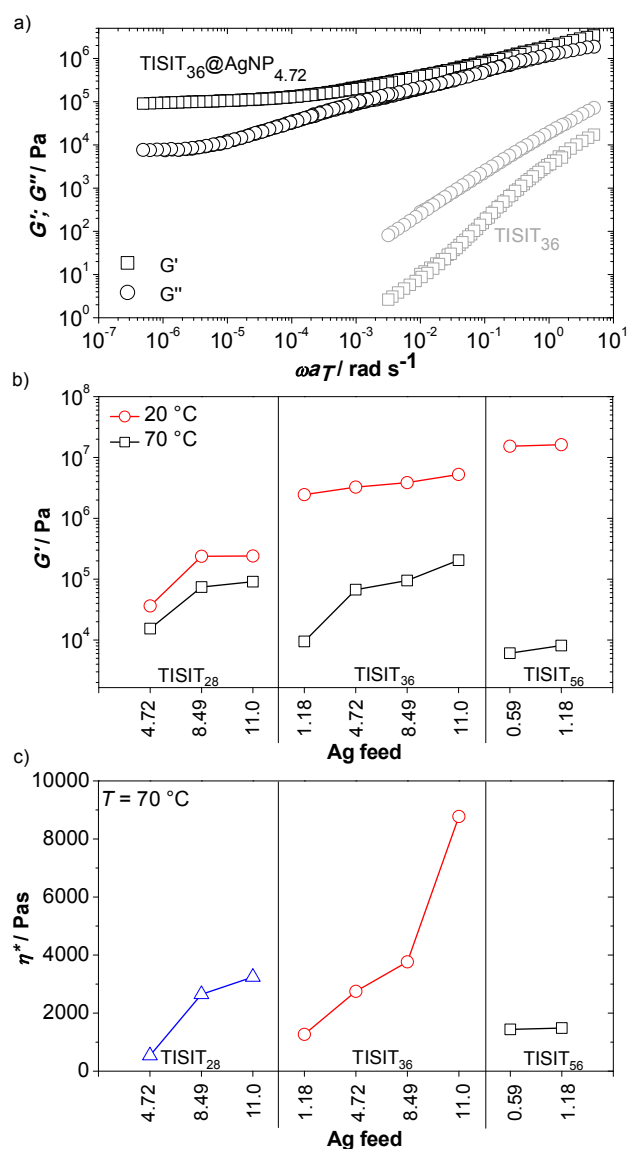


Figure 3-7. a) G' and G'' master curves from time-temperature superposition of TISIT₃₆@AgNP_{4.72} (20-70 °C in 5 °C steps with 20 °C being the reference temperature) with $G' > G''$ at low shear frequencies clearly indicates elimination of the terminal flow regime and thus, cross-linking. For comparison, G' and G'' master curves of liquid TISIT₃₆ (20-40 °C in 5 °C steps with 20 °C being the reference temperature) are also shown, being cropped as the lower G' detection limit of the rheometer is touched. b) G' as a function of temperature for TISIT@AgNP samples at a shear frequency of 1.0 Hz at 0.1% strain in isothermal and constant conditions. Circles: 20 °C; Squares: 70 °C. Temperature sensitivity of G' predominantly scales with styrene content, peaking for TISIT₅₆-based materials. c) Complex viscosities η^* at 70 °C, 5.0 Hz shear frequency and 0.1% strain are primarily affected by AgNP content.

Comparing G' at 20 °C and 70 °C, decline at elevated temperatures was observed throughout all samples, yet with different intensities. In detail, G' is decreased by averaged factors of 2.751, 373.8 and 2259 for TISIT₂₈, TISIT₃₆ and TISIT₅₆-based elastomers, respectively. The highest values at 20 °C and the lowest values at 70 °C in the entire sample set are both found for TISIT₅₆@AgNP materials. Therefore, we understand that the

rigidity of the three-dimensional quasi-segmented network structure is increased with both the styrene and the AgNP content whereas the cross-linking density is solely controlled by the AgNP content. This structure- property relationship is also reproduced by complex viscosity values at 70 °C which primarily are touched by the AgNP content rather than by the styrene content (**Figure 3-7c**). SBS block copolymers which are typically used as TPEs exhibit much higher complex viscosities of around 4000 Pas at $\omega = 5 \text{ s}^{-1}$ and $T = 200 \text{ °C}$ in the melt.³⁰ In all, TISIT₅₆-based samples exhibit ideal preconditions for processing at elevated temperatures, despite of being most rigid in terms of tensile moduli and elastic moduli at room temperature.

CONCLUSIONS

Low molar mass liquid TISIT oligomers with different styrene contents were used to prepare thermally processable quasi-segmented soft materials with AgNP as physical cross-linking points. Wide ranges of mechanical properties are covered depending on the styrene and AgNP content. TISIT@AgNP samples with higher styrene amounts required significantly less AgNP as cross-linkers in order to yield form-stable elastomers with equal or better mechanical properties compared to those with low styrene amounts. Nevertheless, the styrene portion should not solely be considered as a cheap substituent for AgNP since only the supplementation of a hard styrene block enables the preparation of materials with mechanical properties close to common rubbers and TPEs. The interplay of styrene and AgNP as the structure-supplying portions in TISIT@AgNP samples facilitates access to materials with high tensile strengths, tensile moduli and elastic moduli at room temperature and strongly decreased elasticity and viscosity at elevated temperatures. The by far best results were obtained using a TISIT precursor with a high styrene content of 56% as considerably improved mechanical and viscoelastic properties were found at very low AgNP contents, making this material versatile and cost-efficient. In comparison with other commercially available rubbers and TPEs, TISIT@AgNP materials are softer, occupying different mechanical property ranges than conventional TPEs such as SBS. Due to manifold inherent chemical, physical and biological features we envision a bright future for nanoparticle-induced cross-linking of soft oligomers and polymers. We furthermore believe that supplementary detailed studies about ligand-nanoparticle interactions as well as about different nanoparticle types and morphologies will further enhance the concept.

ACKNOWLEDGEMENTS

The authors are indebted to DFG for financial support as well as to R. Giesa from macromolecular chemistry 1 department of University of Bayreuth for conducting oscillatory tensile testing and further technical assistance.

SUPPORTING INFORMATION

Full ¹H-NMR spectrum of TISIT; Shore hardness 0 values of TISIT@AgNP samples; overview of the mechanical properties of TISIT@AgNP samples; overview of moduli at 100% elongation and tensile strengths of reference materials; overview of the experimental amounts used for preparation of TISIT samples; overview of the experimental amounts used for preparation of TISIT@AgNP samples. This material is available free of charge via the Internet at <http://pubs.acs.org>.

REFERENCES

- [1] Spontak, R. J.; Patel, N. P. *Curr. Opin. Colloid Interface Sci.* **2000**, *5*, 333.
- [2] Holden, G.; Bishop, E. T.; Legge, N. R. *J. Polym. Sci. C* **1969**, *26*, 37.
- [3] Kennedy, J. P.; Castner, K. F. *J. Polym. Sci. A: Polym. Chem. Ed.* **1979**, *17*, 2055.
- [4] Cordier, P.; Tournilhac, F.; Soulié-Ziakovic, C.; Leibler, L. *Nature* **2008**, *451*, 977.
- [5] Söntjens, S. H. M.; Renken, R. A. E.; van Gemert, G. M. L.; Engels, T. A. P.; Bosman, A. W.; Janssen, H. M.; Govaert, L. E.; Baaijens, F. P. T. *Macromolecules* **2008**, *41*, 5703.
- [6] Burnworth, M.; Tang, L.; Kumpfer, J. R.; Duncan, A. J.; Beyer, F. L.; Fiore, G. L.; Rowan, S. J.; Weder, C. *Nature* **2011**, *472*, 334.
- [7] Eisenbach, C. D.; Gödel, A.; Terskan-Reinold, M.; Schubert, U. S. *Macromol. Chem. Phys.* **1995**, *196*, 1077.
- [8] Moriguchi, N.; Tsugaru, T.; Amiya, S. *J. Mol. Struct.* **2001**, *562*, 205.

- [9] Agarwal, S.; Ren, L. *Macromolecules* **2009**, *42*, 1574.
- [10] Paeglis, A. U.; O'Shea, F. X. *Rubber Chem. Technol.* **1988**, *61*, 223.
- [11] Bokern, S.; Fan, Z.; Mattheis, C.; Greiner, A.; Agarwal, S. *Macromolecules* **2011**, *44*, 5036.
- [12] Martín, R.; Rekondo, A.; Echeberria, J.; Cabañero, G.; Grande, H. J.; Odriozola, I. *Chem. Commun.*, **2012**, *48*, 8255.
- [13] Zhang, Q.; Archer, L. A. *Langmuir* **2002**, *8*, 10435.
- [14] Şerbescu, A.; Saalwächter, K. *Polymer* **2009**, *50*, 5434.
- [15] Kankate, L.; Turchanin, A.; Götzhäuser, A. *Langmuir* **2009**, *25*, 10435.
- [16] Schlenoff, J. B.; Li, M.; Ly, H. *Am. Chem. Soc.* **1995**, *117*, 12528.
- [17] Khandpur, A. K.; Förster, S.; Bates, F. S.; Hamley, I. W.; Ryan, A. J.; Bras, W.; Almdal, K.; Mortensen, K. *Macromolecules* **1995**, *28*, 8796.
- [18] Falk, J. C.; Schlott, R. J. *Macromolecules* **1971**, *4*, 152.
- [19] Verhoogt, H.; Langelaan, H. C.; Van Dam, J.; Posthuma De Boer, A. *Polym. Eng. Sci.* **1993**, *33*, 754.
- [20] Fedors, R. F. *J. Polym. Sci.: Part C* **1969**, *26*, 189.
- [21] Leibler, L. *Macromolecules* **1980**, *13*, 1602.
- [22] Joseph, S.; Thomas, S. *Eur. Polym. J.* **2003**, *39*, 115.
- [23] Sato, H.; Tanaka, Y. *J. Polym. Sci.: Polym. Chem. Ed.* **1979**, *17*, 3551.
- [24] Yee, C. K.; Jordan, R.; Ulman, A.; White, H.; King, A.; Rafailovich, M.; Sokolov, J. *Langmuir* **1999**, *15*, 3486.
- [25] Bokern, S.; Getze, J.; Agarwal, S.; Greiner, A. *Polymer* **2011**, *52*, 912.
- [26] Bhattacharjee, S.; Bhowmick, A. K.; Avasthi, B. N. In *Elastomer Technology Handbook*; Cheremisinoff, N. P., Eds.; CRC Press: Boca Raton, **1993**, p. 539.

- [27] Rader, C. P. In *Handbook of Thermoplastic Elastomers*; Walker, B. M.; Rade, C. P., Eds.; Van Nostrand Reinhold: New York, **1988**, p. 86.
- [28] Nelb, R. G.; Chen, A. T. In *Thermoplastic Elastomers*; Holden, G.; Legge, N. R.; Quirk, R.; Schroeder, H. E., Eds.; Hanser Publishers: Munich, **1996**, p. 243.
- [29] Hundiwale, D. G.; Kapadi, U. R.; Desai, M. C.; Bidkar, S. H. *J. Appl. Polym. Sci.* **2002**, *85*, 995.
- [30] Arnold, K. R.; Meier, D. J. *J. Appl. Polym. Sci.* **1970**, *14*, 427.

SUPPORTING INFORMATION

FOR

DESIGN OF SOFT MATERIALS FROM LIQUID TRIBLOCK CO-OLIGOMERS AND METAL NANOPARTICLES

*Holger Pletsch, Max J. Schnepf and Seema Agarwal**

H. Pletsch, M. J. Schnepf, S. Agarwal

Universität Bayreuth, Macromolecular Chemistry II, Universitätsstraße 30, 95440 Bayreuth (Germany)

Fax: +49 921553393

E-mail: agarwal@uni-bayreuth.de

Keywords: block copolymers, silver nanoparticles, cross-linking, nanocomposites, elastomers

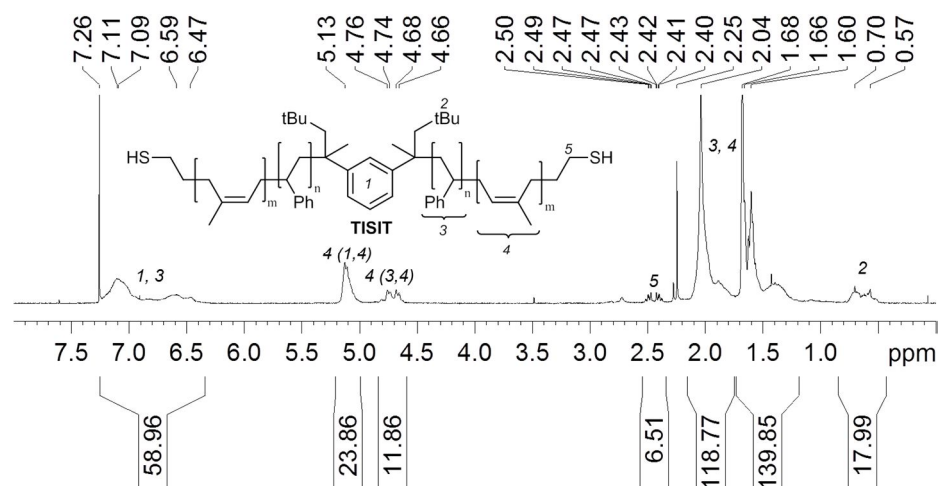


Figure 3-S1: $^1\text{H-NMR}$ spectrum of TISIT₂₈ proves successful thiol end group functionalization by comparing initiator signals at $\delta = 0.57\text{-}0.70$ ppm (2) with end group signals at $\delta = 2.41\text{-}2.50$ ppm (5).

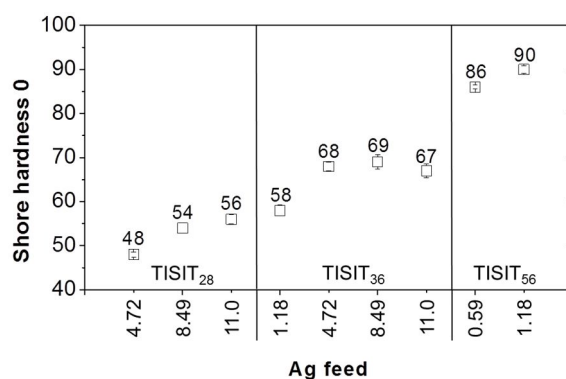


Figure 3-S2: Shore hardness 0 as a function of styrene and AgNP content of TISIT@AgNP samples from measurements according to ASTM D2240. TISIT precursors with higher styrene contents facilitate higher bulk hardness, yet different AgNP contents affect hardness as well.

Conclusions regarding hardness can be drawn from tensile properties as the resistance to penetration shows strong interdependence on the stiffness and strength of a material. In fact, measurement of shore hardness 0 of the TISIT@AgNP samples yields similar tendencies compared to tensile testing as hardness generally increases with styrene and AgNP content (**Figure 3-S2**). Stagnation of the increase is only observed with high AgNP contents in TISIT₃₆@AgNP samples which might be explained by aggregation of AgNP at high filling rates and subsequent loss of network density. This effect particularly concerns the TISIT₃₆@AgNP_{11.0} sample and was similarly observed for the corresponding tensile strength and toughness.

Hardness of the samples was tested on heat-pressed films using a calibrated Hildebrand shore hardness 0 durometer with a cone shaped indenter according to ASTM D2240 at 22 °C.

Table 3-S1. Overview of the mechanical properties of TISIT@AgNP samples.

Sample	E-Modulus	ultimate	toughness	modulus at	tensile	Shore 0
	/ MPa	elongation (%)	/ MN mm ⁻²	100% / MPa	strength / MPa	Hardness
TISIT ₂₈ @AgNP _{4.72}	0.236 ± 0.046	211 ± 16.2	0.541 ± 0.123	0.278 ± 0.049	0.400 ± 0.079	48 ± 0.58
TISIT ₂₈ @AgNP _{8.49}	0.253 ± 0.025	204 ± 16.1	0.603 ± 0.083	0.315 ± 0.029	0.463 ± 0.027	54 ± 1.15
TISIT ₂₈ @AgNP _{11.0}	0.353 ± 0.033	169 ± 12.1	0.665 ± 0.100	0.468 ± 0.057	0.628 ± 0.056	56 ± 1.00
TISIT ₃₆ @AgNP _{1.18}	1.954 ± 0.309	349 ± 35.1	1.96 ± 0.244	0.47 ± 0.028	0.74 ± 0.031	58 ± 1.26
TISIT ₃₆ @AgNP _{4.72}	5.725 ± 0.812	198 ± 9.08	3.21 ± 0.388	1.73 ± 0.159	2.73 ± 0.161	68 ± 1.00
TISIT ₃₆ @AgNP _{8.49}	11.15 ± 1.372	167 ± 14.4	3.96 ± 0.630	2.79 ± 0.107	3.73 ± 0.217	69 ± 1.63
TISIT ₃₆ @AgNP _{11.0}	12.65 ± 1.349	145 ± 7.44	3.30 ± 0.186	2.97 ± 0.121	3.53 ± 0.082	67 ± 1.58
TISIT ₅₆ @AgNP _{0.59}	70.98 ± 23.30	332.5 ± 40.8	13.310 ± 1.07	2.61 ± 1.18	4.912 ± 0.292	86 ± 0.45
TISIT ₅₆ @AgNP _{1.18}	80.11 ± 4.021	131 ± 37.4	3.10 ± 1.21	4.53 ± 0.086	5.581 ± 0.244	90 ± 0.89

Table 3-S2. Overview of moduli at 100% elongation and tensile strengths of reference materials.

Sample	modulus at	tensile	Reference
	100% / MPa	strength / MPa	
SBS – 73 000 g/mol	1.7	27.7	2
SBS – 102 000 g/mol	2.25	28.5	2
EPDM/PP (60/40) blends unvulcanized	4.83	4.94	23
EPDM/PP (60/40) blends vulcanized	8.00	24.31	23
Polyester amide (25% amide, adipic acid)	10.8	28.1	24
Polyester amide (35% amide, azlaic acid)	13.2	26.2	24
Polyether ester amide (31% amide, azelaic acid)	11.5	18.6	24
Polycarbonate ester amide (35% amide, adipic acid)	13.5	20.5	24
Vulcanized nitrile rubber (24% Acrylonitrile)	7.9	20	22
Vulcanized nitrile rubber (40% Acrylonitrile)	12.1	26	22
Vulcanized nitrile rubber (50.5% Acrylonitrile)	15.7	24.5	22
Butadiene rubber vulcanized with sulfur	2.00	22.3	22
Natural Rubber	0.518	3.610	25

Table 3-S3. Overview of the amounts used for preparation of TISIT samples.

Sample	Initiator solution ($c = 0.59 \text{ mol L}^{-1}$)	Styrene	Isoprene
TISIT ₂₈	15.0 mL (9.00 mmol)	10.3 mL (90.0 mmol)	27.0 mL (270 mmol)
TISIT ₃₆	15.0 mL (9.00 mmol)	10.3 mL (90.0 mmol)	18.0 mL (180 mmol)
TISIT ₅₆	15.0 mL (9.00 mmol)	10.3 mL (90.0 mmol)	9.00 mL (90.0 mmol)

Table 3-S4. Overview of the amounts used for preparation of TISIT@AgNP samples.

Sample	Polymer	AgCO ₂ CF ₃	lithium triethylborohydride ($c = 1 \text{ mol L}^{-1}$)
TISIT ₂₈ @AgNP _{1.18}	241 mg (52.4 μmol)	13.6 mg (62.0 μmol)	0.37 mL (0.37 mmol)
TISIT ₂₈ @AgNP _{4.72}	4.27 g (0.93 mmol)	968 mg (4.38 mmol)	26.3 mL (26.3 mmol)
TISIT ₂₈ @AgNP _{8.49}	703 mg (153 μmol)	287 mg (1.29 mmol)	7.80 mL (7.80 mmol)
TISIT ₂₈ @AgNP _{11.0}	621 mg (135 μmol)	328 mg (1.49 mmol)	8.91 mL (8.91 mmol)
TISIT ₃₆ @AgNP _{1.18}	1.39 g (289 μmol)	75.3 mg (341 μmol)	1.36 mL (1.36 mmol)
TISIT ₃₆ @AgNP _{4.72}	1.66 g (361 μmol)	377 mg (1.71 mmol)	6.80 mL (6.80 mmol)
TISIT ₃₆ @AgNP _{8.49}	1.76 g (366 μmol)	687 mg (3.11 mmol)	12.4 mL (12.4 mmol)
TISIT ₃₆ @AgNP _{11.0}	0.99 g (207 μmol)	503 mg (2.28 mmol)	9.10 mL (9.10 mmol)
TISIT ₅₆ @AgNP _{0.59}	1.11 g (266 μmol)	34.7 mg (157 μmol)	0.63 mL (0.63 mmol)
TISIT ₅₆ @AgNP _{1.18}	1.00 g (239 μmol)	62.3 mg (282 μmol)	1.13 mL (1.13 mmol)
TISIT ₅₆ @AgNP _{4.72}	1.03 g (246 μmol)	256 mg (1.16 mmol)	4.60 mL (4.60 mmol)
TISIT ₅₆ @AgNP _{8.49}	0.93 g (221 μmol)	415 mg (1.88 mmol)	7.52 mL (7.52 mmol)

CHAPTER 4

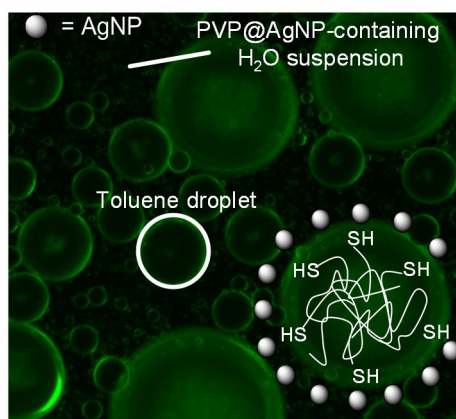
ULTRASOUND-MEDIATED SYNTHESIS OF HIGH-MOLECULAR WEIGHT POLYSTYRENE-GRAFTED SILVER NANOPARTICLES BY FACILE LIGAND EXCHANGE REACTIONS IN SUSPENSION

Holger Pletsch,¹ Ling Peng,¹ Fabian Mitschang,¹ Andreas Schaper,² Michael Hellwig,²
David Nette,³ Andreas Seubert,³ Andreas Greiner^{1*} and Seema Agarwal^{1*}

¹ Universität Bayreuth, Macromolecular Chemistry II and Bayreuth Center for Colloids and Interfaces. Universitätsstraße 30, 95440, Bayreuth, Germany. E-mail: greiner@uni-bayreuth.de; agarwal@uni-bayreuth.de

² Zentrum für Materialwissenschaften, Philipps-Universität Marburg, Hans-Meerwein-Straße, 35032, Marburg, Germany.

³ Fachbereich Chemie, Philipps-Universität Marburg, Hans-Meerwein-Straße, 35032, Marburg, Germany.



Published in *Small*, year **2014**, volume *10*, issue 1, pages 201-208. Reprinted with permission. Copyright John Wiley & Sons.

ABSTRACT

Ultrasound mediated facile ligand exchange method in suspension for the formation of polystyrene-grafted silver nanoparticles is reported. Amazingly, this method allows even grafting of very high molecular weight polystyrenes (up to 217200 g/mol) having a single terminal thiol group at the chain end. Detailed studies are carried out to gain insights in the role of molecular weight of the ligands and the mechanism of the ligand exchange reactions. Key factors are determined to be the droplet formation by ultrasonification and low silver content, which enhances the availability of the terminal thiol end group significantly. The extraordinary compatibility of the ligand exchange method in particular regarding high molecular weights is attributed to hydrophilic orientation of the terminal thiol groups at the liquid-liquid interphase. This is proved conclusively by using an *in situ* method as a reference approach in which agglomeration occurs at considerably lower molecular weights due to the absence of preferred end group orientation within the polymer coil. In homogeneous phase only the chain length is found to be the crucial factor in stabilization of silver nanoparticles.

KEYWORDS

Silver nanoparticles, ligand exchange, ultrasound, metal-polymer hybrid

INTRODUCTION

The design of hybrid materials is of major interest due to their capability of combining diverse physical, chemical, and mechanical properties. The use of metal nanoparticles as one component is particularly suitable for optical,^[1-4] catalytical^[5-7] or antibacterial^[8-10] applications. Deriving their distinct properties from the high surface to volume ratio, metal nanoparticles differ significantly from the bulk metal in terms of reactivity. The high tendency to aggregation and agglomeration arises from the elevated surface energy and can be overcome by functionalization with a surfactant which acts as a sterical and/or electronical protecting agent.^[11] Particle coarsening can occur through different mechanisms, most notably Ostwald ripening.^[12] This theory describes the diffusion of atoms from smaller to larger particles leading to a more homogeneous diameter distribution with elevated mean diameters. It has been found that the rate of particle coarsening in a polymeric matrix is highly dependent on molecular weight of the matrix and temperature.^[13]

Popular capping agents among soft metals like gold or silver are citrates^[14], quaternary ammonium salts,^[15] mercaptans^[16] or polymers.^[17] Using water-soluble polymers like poly(vinyl pyrrolidone) (PVP)^[18] or poly(vinyl alcohol) (PVA)^[19] stable aqueous suspensions can be established. Furthermore, numerous synthetic strategies have been developed to incorporate metal nanoparticles into a hydrophobic polymeric matrix by coordination through suitable end group or side chain functionalities. In “graft from” methods, the polymer shell is prepared by grafting monomers on the metal surface with subsequent initiation of the reaction.^[20-21] “Graft to” preparations imply the stabilization of metal nanoparticles by functionalized polymers.^[22] Thiol-functionalized polymers for the “graft to” approach on silver or gold nanoparticles were obtained by RAFT^[23] or anionic polymerization.^[24] Following the “graft to” approach utilizing anionic polymerizations, our group and others reported on straight-forward methods for the grafting of thiol-functionalized polystyrene (ThPS) on silver or gold nanoparticles. The ThPS was prepared by anionic polymerization of styrene followed by termination with ethylene sulfide. *In situ* or after work-up of ThPS silver or gold salts were added in the presence of reducing agents resulting in ThPS-grafted silver or gold nanoparticles which showed remarkable dispersion stability in solvents or polystyrene matrix.^[25-26]

An alternative method is the preparation by ligand exchange of pre-formed silver nanoparticles and pre-formed polystyrene. This method is based on the idea that surfactants can be interchanged by those with a higher affinity to the metal surface.^[27] Also, the substitution of polar surfactants with non-polar surfactants is possible, which opens up new vistas regarding the grafting of pre-formed aqueous metal nanoparticles with hydrophobic polymers like polystyrene. Amongst others, ligand exchange to ThPS has been carried out using a homogeneous acetone/water^[28] or a heterogeneous toluene/water^[29] system.

Regardless of the preparation route silver and gold nanoparticles grafted by ThPS showed remarkable colloidal stability against aggregation or coarsening of the nanoparticles. The stability is due to steric repulsion of the nanoparticles by the grafted polystyrene chains. Steric repulsion of grafted ligands stretched away from the nanoparticle surface plays, next to electrostatic repulsion of ligands, a key role for the stability of nanoparticles.^[30] We wondered whether the steric repulsion by the grafted polymer chains on nanoparticles scales with their length. Also, the interaction of polymer chains can result in bridging effects which were applied in a very elegant^[31] manner for nanoparticle arrangements^[31] but can also reduce the colloidal stability.^[32] It should not remain unmentioned here that polymer grafting does not only serve for modification of colloidal stability but can also result in sensing applications which were nicely reviewed for gold nanoparticles.^[33] These few examples demonstrate the role of polymer grafting. However, understanding the chain length of macromolecules grafted on the surface of metal nanoparticles would progress the full exploitation of polymer-nanoparticle conjugates significantly.

From the synthetic point of view grafting of polymers with a nanoparticle anchor group at the chain end, like ThPS, should be highly affected by the chain length of the polymer. Assuming that the chains become very long, the crucial question is: how reactive is the anchor group at the chain end? Typically, for grafting of nanoparticles by ThPS rather oligomers are used than polymers. Lennox et al. have used the longest chain length, to the best of our knowledge, with up to $M_n = 13.300$ for the “grafting to” method as well as for the ligand exchange method.^[34] In our experiments we observed grafting of silver nanoparticles by ThPS obtained by anionic polymerization even with ThPS of $M_n > 90.000$.^[26] With ThPS-grafted silver^[26] as well as gold nanoparticles^[35] we also have observed the presence of ungrafted ThPS, which significantly deteriorate the properties of grafted nanoparticles. The amount of ungrafted polymer is clearly influenced by the overall

concentration as observed by gel permeation chromatography (here with grafted poly(methacrylates))^[35] and could be also affected by the molecular weight of the ThPS grafts. First, the role of the molecular weight of the polymer grafts extending from the nanoparticle surface has to be understood in order to provide well-defined polymer grafted metal nanoparticles for property investigations. Second, it is a real challenge to learn at which threshold value the reactivity of a terminal thiol group is retarded by the chain length of the polymer. Third, the mechanism of ligand exchange reaction is not well understood and its potential has not been exploited. For these reasons we present a systematic study on the role of ThPS-grafted silver nanoparticles here. We gained surprising insights in the role of molecular weight of the ligands and the mechanism of the ligand exchange reactions, which opens completely new perspectives. In order to lift our results into context with related work, we have also investigated in comparative manner the *in situ* method for silver nanoparticle formation with ThPS.

RESULTS AND DISCUSSION

Silver nanoparticles grafted with polystyrene chains of different lengths were obtained by the ligand exchange route as well as by the *in situ* route (**Figure 4-1**). Anionic polymerization of styrene with subsequent termination using ethylene sulfide generated a mono-functionalized homopolymer bearing a thiol end group. Termination with MeOH yielded the unfunctionalized reference polymer. Grafting to the surface of silver nanoparticles was realized by the terminal thiol functionalities of the polystyrene chains. Six different molecular weights between 21200 g/mol and 217200 g/mol (M_n (number average molecular weight) determined by GPC) have been prepared and characterization was carried out using NMR and UV/Vis spectroscopy, as well as GPC, TGA and DSC. GPC analysis showed monomodal distributions, however in some cases a second peak with doubled molecular weight was found. This originated from dimerization of the polymer chains through disulfide bonds, which are easily formed from two thiols under the influence of oxygen. It could be shown that disulfide bonds cleave by stirring the polymer in THF solution and adding Superhydrid® under oxygen-free conditions. As a result, the intensity of the doubled molecular weight peak decreased to nearly zero.

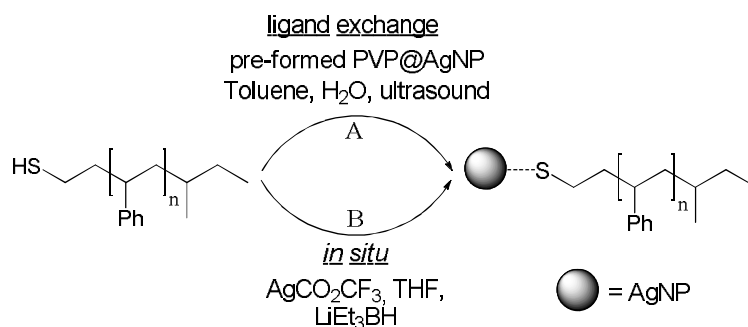


Figure 4-1. Overview of the synthetic approaches for grafting of ThPS on silver nanoparticles presented in this work. Route A is based on the heterogeneous combination of pre-formed polymer and pre-formed PVP-stabilized AgNP leading to a ligand exchange. The *in situ* formation of AgNP in homogenous solution is carried out using route B.

For the high molecular weight polymers, proof of functionalization could not be provided using methods like NMR, EDX, elemental analysis or XPS, since they are not sensitive enough for detecting a single thiol group. Therefore, the proof of functionalization was carried out by indirect means. It could be shown that ligand exchange of silver nanoparticles with unfunctionalized polystyrene was not possible, whereas ThPS was reacted with AgNP. Also, sulfur could be detected in EDX and elemental analysis, but not quantitatively evaluated. Raman measurements also yielded a qualitative proof of end group functionalization with C-S- and S-H-vibrations being visible in comparison to the non-functionalized polymer (please see Supporting Information).

Preparation of ThPS@AgNP conjugates by ligand exchange:

Ligand exchange was carried out in a two-phase reaction system with one phase consisting of hydrophobic thiol-terminated polystyrene, dissolved in a non-polar solvent. The second phase contained silver nanoparticles which were dispersed in aqueous media and stabilized with PVP. This stabilizing agent was chosen because of its ability to generate homogeneous particles with small diameters and a distinct plasmon resonance absorption (PRA) spectrum. PVP@AgNP was synthesized by reduction of silver nitrate with sodium borohydride in water, after which PVP was added as a stabilizer. The PRA band of PVP@AgNP was observed at 391 nm. The arithmetic mean particle diameter of 7.0 ± 1.9 nm of PVP@AgNP was determined using TEM. The concentration of the suspension was analyzed by ICP mass spectrometry and could be maximized to $2.05 \text{ mmol} \cdot \text{L}^{-1}$. The suspensions used for ligand exchange featured a concentration of $1.43 \text{ mmol} \cdot \text{L}^{-1}$ and was used as prepared.

The by far best results among different activation methods for the ligand exchange of pre-formed PVP@AgNP to ThPS@AgNP were achieved using 25 min of ultrasound activation and successive stirring at room temperature for at least 18 h. No conversion was observed without ultrasound activation and agglomeration of the nanoparticles occurred at higher temperatures. The progress of conversion could easily be followed by the color change of the aqueous and organic phase. The phase transfer was only possible with ThPS but not with pure PS which proved that the PS coordinates *via* the end group to AgNP. The conjugates are designated as PS_X@AgNP_Y with X standing for M_n of ThPS and Y representing the initial molar Ag ratio relative to one equivalent of ThPS. The time required for full conversion was noticeably depending on the molecular weight of the polymers and generally, a higher ratio of end group per repetition units resulted in faster transfers. In particular, 18 h of stirring were necessary for preparing ThPS₂₁₂₀₀@AgNP_{4.9}, whereas the preparation of ThPS₂₁₇₂₀₀@AgNP_{4.9} took 42 h. This is assigned to an increase of solution viscosity of the toluene phase with increasing molecular weight. Therefore, we suppose that the thiol end group mobility is decreased, leading to prolonged reaction times for the diffusion-controlled ligand exchange. The influence of the heat generated by ultrasound on the end group diffusion was neglected as the macroscopic temperature did not change more than 5 °C in the ultrasound time range. Not until the aqueous phase was discolored, the reaction was worked up by separation of the phases, followed by concentrating the toluene phase and precipitating it in methanol. The brown solid had to be dried thoroughly in order to remove toluene completely. No sign of polymer degradation during ultrasound impact could be observed in GPC analysis of the ThPS@AgNP conjugates in THF.

The ligand exchange should be driven by the availability of thiol groups at the interface of the liquid phases which generates a high compatibility for low end group concentrations. We suppose that the hydrophilic thiol end groups preferentially orientate towards the interphase, making itself available for coordination (**Figure 4-2a-c**). As an intermediate it is most likely that the nanoparticles are grafted with both ThPS and PVP at the interphase.

Furthermore, a high surface area of the interphase is presumed to boost the conversion due to a higher concentration of organized end groups. This scenario can be created by dispersing one phase into the other which explains the increase of reactivity when using ultrasound activation.^[36-37] During the preparation of ThPS₄₅₁₀₀@AgNP_{4.9} the emulsion properties were characterized by light microscopy.

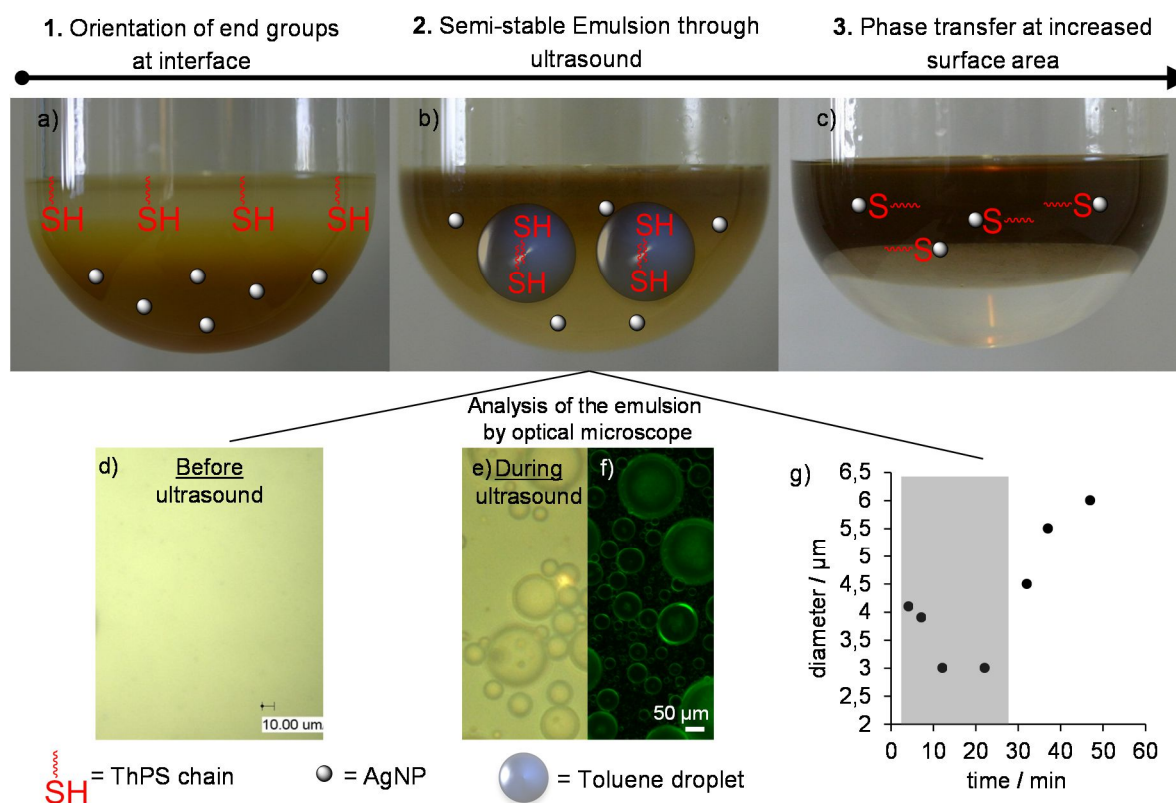


Figure 4-2. Illustration of the ligand exchange process during the preparation of ThPS₄₅₁₀₀@AgNP_{4.9}. a)-c):

As the ligand exchange proceeds, silver nanoparticles are transferred from the water phase to the upper toluene phase, which is indicated by the colour change. d) Reaction mixture is entirely segregated before ultrasound activation, no droplets can be observed by optical microscopy. e) After 10 min of ultrasound activation a semi-stable emulsion is generated, containing different-sized toluene droplets with an arithmetic mean diameter of $3.0 \pm 1.5 \mu\text{m}$; scale $10 \mu\text{m}$. f) Optical fluorescent microscopy reveals the toluene phase as the dispersed phase by using hydrophobic rubrene as a dye. g) Time dependent plot of arithmetic mean droplet diameters. Grey background indicates the duration of ultrasound activation ($t = 2 - 27 \text{ min}$). At $t = 2 \text{ min}$ (before ultrasound activation) and $t = 87 \text{ min}$ (60 min after ultrasound activation, not shown in graph) samples did not contain emulsion droplets, indicating entire segregation.

Upon ultrasound activation, a semi-stable Pickering emulsion is formed whose droplet sizes decrease with progressing time until a minimum limit of $3.0 \pm 1.5 \mu\text{m}$ is reached after 10 min. (**Figure 4-2g**). The droplet sizes are not significantly influenced by changing the ThPS molecular weight. The toluene phase was identified as the dispersed phase by coloration it with rubrene and subsequent fluorescent microscopic analysis of the emulsion (**Figure 4-2f**). Unlike the work of Zhao et al., the formation of colloidal particles with polystyrene as a core and AuNP as corona was not observed in this manner.^[29] This can be presumably explained by the differing initial ratios of components used in this preparation. After disengaging ultrasound, droplet sizes increase and droplet incidence decreases as segregation of the phases continues. A continuous Pickering emulsion has not been

observed^[38] and it took only short time for the emulsion to degenerate into two distinct phases again. With decreasing nanoparticle amount, the speed of phase segregation was increased. With a AgNP 4.9 excess feed, emulsion droplets could still be observed after 20 min of disengaging ultrasound, but not after 60 min. With a 0.9 feed, no emulsion droplets were found after 20 min of disengaging ultrasound. We also carried out a blank reaction without AgNP. Here it was not possible to generate an emulsion from ultrasound.

¹H-NMR spectra of ThPS and ThPS@AgNP in d7-DMF showed no difference regarding chemical shifts and integration values (**Figure 4-3**). This demonstrates the retention of ThPS under ultrasound conditions. Moreover, the ¹H-NMR spectrum of the conjugate does not show signals corresponding to PVP, indicating a quantitative ligand exchange. CHN analysis of the conjugates yielded a nitrogen content of 0% which is another proof for the complete PVP removal.

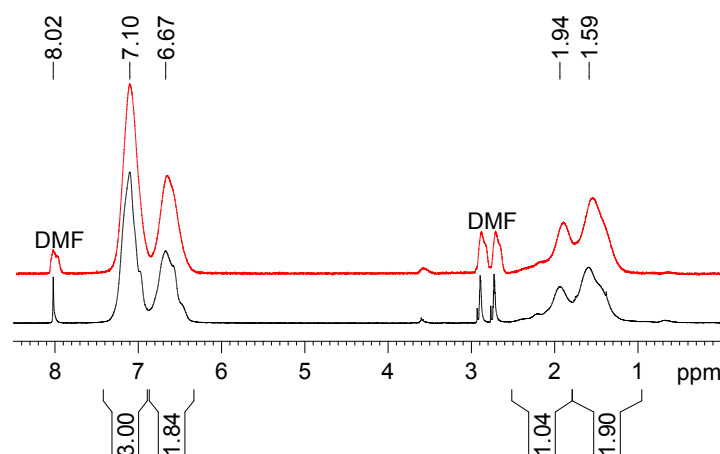


Figure 4-3. ¹H-NMR spectra of ThPS₄₅₁₀₀ (lower black trace) and ThPS₄₅₁₀₀@AgNP_{4.9} (upper red trace), redispersed in d7-DMF (30 g*L⁻¹), verifies the retention of ThPS after phase transfer reaction. Furthermore, no signals corresponding to PVP are visible. Integrals and peaks were assigned to the spectrum of ThPS₄₅₁₀₀.

The UV/Vis spectra of the ligand exchange products show a significant shift of the PRA band directed towards higher wavelengths compared to PVP@AgNP (**Figure 4-4**). The red shift can be attributed to the influence of the changed refractive index of the surroundings.^[39] Also, absorption of the aromatic moiety at 261 nm occurred. Both phenomena verify a successful ligand exchange. As expected, the ratio of absorption for ThPS (~261 nm) to AgNP (~410 nm) increases with growing chain lengths (**Figure 4-4**).

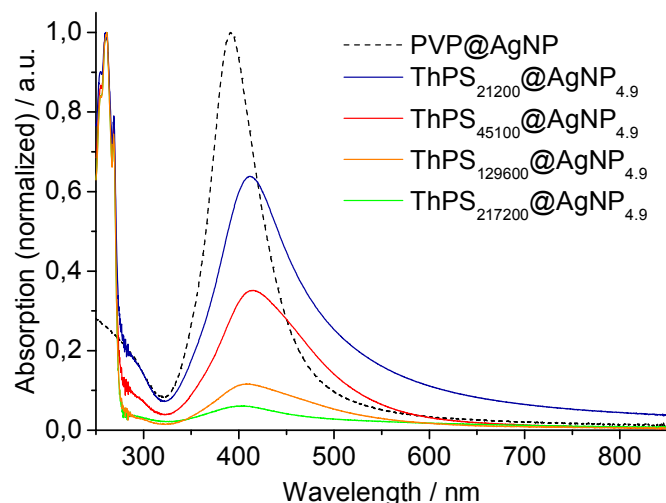


Figure 4-4. Absorption spectra of ThPS@AgNP prepared by ligand exchange; $c = 0.5 \text{ g}\cdot\text{L}^{-1}$. In comparison to PVP@AgNP (dotted black trace) PRA are shifted to higher wavelengths and aromatic absorption of ThPS appears. The absorption ratios Ag/ThPS are: 0.64, 0.35, 0.12 and 0.06 for ThPS₂₁₂₀₀@AgNP_{4.9}, ThPS₄₅₁₀₀@AgNP_{4.9}, ThPS₁₂₉₆₀₀@AgNP_{4.9} and ThPS₂₁₇₂₀₀@AgNP_{4.9}, respectively.

As already shown in recent publications, polymer-nanoparticle conjugates also consist of a certain amount of free polymer.^[26, 35] This is also shown here by GPC measurements with DMF as eluent using a diode array detector (**Figure 4-5**).

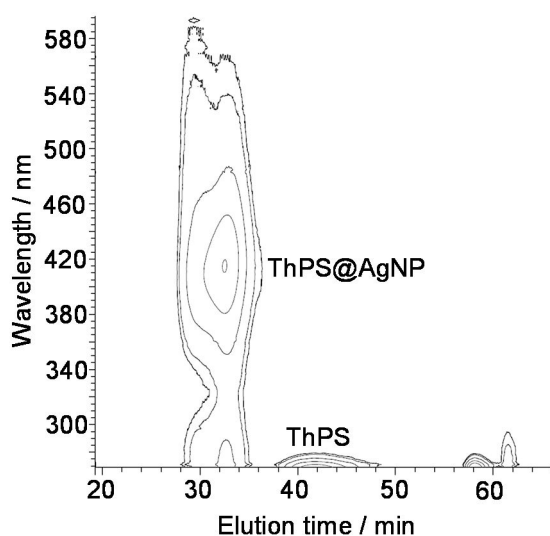


Figure 4-5. GPC of sample ThPS₂₁₂₀₀@AgNP_{4.9}. At an elution time of 34 min the conjugate occurs with absorption maxima at 410 nm and 261 nm, representing PRA of silver nanoparticles and polystyrene, respectively. Free polymer was detected at 43 min and toluene was identified at 59 min.

In order to compare results, an initial molar silver excess of 4.9 is used in this assay, gaining materials with a reasonably high silver yield. A tendency towards agglomeration with higher silver content can be derived from an increased absorption wavelength of the

PRA band. Samples ThPS₂₁₂₀₀@AgNP_{4.9} and ThPS₂₁₂₀₀@AgNP₁₂ are representative examples, featuring PRA wavelengths of 411 nm and 427 nm, respectively (**Table 4-1**). In fact, the initial 12-fold excess of silver could not be fully transported to the product during ligand exchange. A silver content of 2.15 wt% instead of 5.72 wt% was determined by AAS for ThPS₂₁₂₀₀@AgNP₁₂. Having both UV/Vis and AAS analysis in mind, high initial rates of silver are not suitable for this type of conversion.

Table 4-1. Characterization of ThPS@AgNP prepared by ligand exchange.

Sample ^{a)}	PRA [nm] ^{b)}	d_{Ag} [nm] ^{c)}	Ag content [wt.%] (expected) ^{d)}
ThPS ₂₁₂₀₀ @AgNP _{4.9}	411	7.4 ± 2.0	2.45 (2.42)
ThPS ₂₁₂₀₀ @AgNP ₁₂	427	$6.5 \pm 3.1^e)$	2.15 (5.72)
ThPS ₄₅₁₀₀ @AgNP _{4.9}	414	7.3 ± 2.6	0.96 (1.15)
ThPS ₄₅₁₀₀ @AgNP _{0.9}	409	7.9 ± 2.5	0.17 (0.20)
ThPS ₇₉₃₀₀ @AgNP _{4.9}	408	7.4 ± 3.3	0.30 (0.38)
ThPS ₁₂₉₆₀₀ @AgNP _{4.9}	410	8.1 ± 3.0	0.29 (0.41)
ThPS ₁₇₇₉₀₀ @AgNP _{4.9}	408	$10.1 \pm 3.0^e)$	0.29 (0.30)
ThPS ₂₁₇₂₀₀ @AgNP _{1.0}	407	$7.3 \pm 3.2^e)$	0.05 (0.05)
ThPS ₂₁₇₂₀₀ @AgNP _{4.9}	405	- ^{f)}	0.15 (0.24)

a) The initial molar ratio of ThPS/Ag is indicated in the sample names.

b) Absorption spectra were measured using a 0.5 g*L⁻¹ dispersion in THF.

c) Mean particle diameters d_{Ag} were determined by TEM.

d) The Ag content was experimentally verified by AAS analysis.

e) Slight agglomeration visible.

f) Strong agglomeration visible with mostly two or three particles involved; no determination of d_{Ag} possible.

When comparing ThPS@AgNP_{4.9} conjugates with different molecular weights, trends regarding the material properties can be construed (**Table 4-1**). As expected, a decrease of the relative silver content was found with increasing molecular weights. Experimental results match well with the expected silver content, calculated from the initial feed. Furthermore, PRA wavelengths virtually stay constant in a certain range between 408 and 414 nm. No red shift is visible at increasing molecular weights, indicating the absence of agglomerations. However, broadening of the curves with increasing chain lengths is not deniable and UV/Vis analysis of ThPS₂₁₇₂₀₀@AgNP_{4.9} turned out to be inaccurate due to the low silver content (**Figure 4-4**).

Therefore, TEM measurements have been carried out to evaluate the particle properties unambiguously (**Figure 4-6**). Compared to PVP@AgNP, particles do not transform in size and size distribution dramatically during ligand exchange, however TEM background noise increases drastically with molecular weight, making analysis more difficult. Molecular weights up to 129600 g/mol turned out to be suitable for ligand exchange experiments with an initial 4.9 molar excess of silver as the conjugates possess isolated particles only (**Figure 4-6b, d-g**). For ThPS₁₇₇₉₀₀@AgNP_{4.9}, slight agglomeration (**Figure 4-6h**) and for ThPS₂₁₇₂₀₀@AgNP_{4.9} (**Figure 4-6j**), strong agglomeration was observed, usually with two or three particles merging together. Enhanced stability of the nanoparticles was gained by decreasing the initial silver amount to 1.0 equivalent. This is especially apparent for ThPS₂₁₇₂₀₀. Only slight agglomeration was observed for ThPS₂₁₇₂₀₀@AgNP_{1.0} with mean diameters of 7.3 ± 3.2 nm which was confirmed by AAS measurement (**Table 4-1**) and by TEM analysis (**Figure 4-6i**).

DLS measurements have been carried out in toluene and it was found that the hydrodynamic radii scale with the silver content of samples with constant molecular weights (for detailed information please see the Supporting Information).

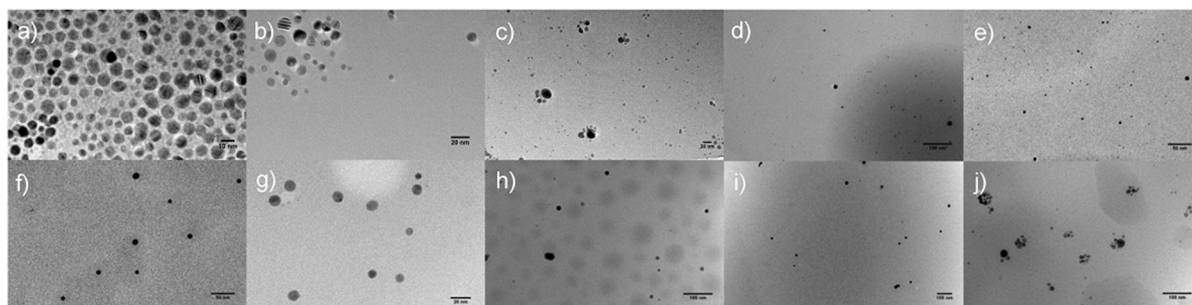


Figure 4-6. TEM images of PVP@AgNP and ThPS@AgNP samples prepared by ligand exchange. a) PVP@AgNP; scale 10 nm. b) ThPS₂₁₂₀₀@AgNP_{4.9}; scale 20 nm. c) ThPS₂₁₂₀₀@AgNP₁₂; scale 50 nm. Slight agglomeration is visible. d) ThPS₄₅₁₀₀@AgNP_{4.9}; scale 100 nm. e) ThPS₄₅₁₀₀@AgNP_{0.9}; scale 50 nm. f) ThPS₇₉₃₀₀@AgNP_{4.9}; scale 50 nm. g) ThPS₁₂₉₆₀₀@AgNP_{4.9}; scale 20 nm. h) ThPS₁₇₇₉₀₀@AgNP_{4.9}; scale 100 nm. Slight agglomeration is visible. i) ThPS₂₁₇₂₀₀@AgNP_{1.0}; scale 100 nm. Slight agglomeration is visible. j) ThPS₂₁₇₂₀₀@AgNP_{4.9}; scale 100 nm. Agglomeration of mainly two or three particles occurs. Sample a) has been prepared by dip coating a graphite-coated copper grid in dilute aqueous suspension. Samples b)-j) have been prepared by dip coating a graphite-coated copper grid in dilute THF dispersion.

Preparation of ThPS@AgNP conjugates by *in situ* method:

To put the results in context, an *in situ* method in homogeneous solution, which has been extensively studied before, was used to prepare correspondent ThPS@AgNP conjugates.^[31] Therefore, functionalized ThPS with identical molecular weights (as shown in **Table 4-1**) were employed. Silver trifluoroacetate was used as AgNP precursor and Superhydrid® as reduction agent. Purification was performed by precipitation in MeOH with subsequent filtration of the brown solid. For all samples, PRA maxima generally occurred at higher wavelengths (420-445 nm) compared to ThPS@AgNP prepared by ligand exchange. Regarding all samples except ThPS₂₁₂₀₀@AgNP_{4.9}, the existence of agglomerates could be confirmed by TEM analysis (**Figure 4-7**). Conclusively, agglomeration occurs at considerably lower molecular weights compared to ligand exchange. With ThPS₇₉₃₀₀@AgNP_{4.9} (**Figure 4-7c**) and ThPS₇₉₃₀₀@AgNP_{1.0} (**Figure 4-7d**), it could be shown that a decreased initial silver content did not lead to more isolated particles.

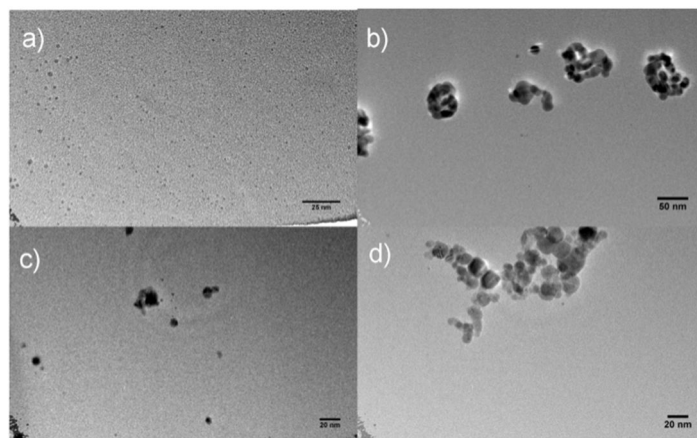


Figure 4-7. TEM images of ThPS@AgNP prepared by *in situ* reduction. a) ThPS₂₁₂₀₀@AgNP_{4.9}; scale 25 nm. Mean particle diameters: 2.2 ± 0.7 nm. b) ThPS₄₅₁₀₀@AgNP_{4.9}; scale 50 nm. Strong agglomeration occurs. c) ThPS₇₉₃₀₀@AgNP_{4.9}; scale 20 nm. Strong agglomeration occurs. d) ThPS₇₉₃₀₀@AgNP_{1.0}; scale 20 nm. Strong agglomeration occurs. All samples have been prepared by dip coating a graphite-coated copper grid in dilute THF dispersion.

CONCLUSIONS

ThPS@AgNP were prepared by ligand exchange and *in situ* methods, applying different molecular weights. Remarkably, using the ligand exchange approach, even high molecular weights up to 129600 g/mol provided conjugates with isolated and homogeneous

nanoparticles. Even ThPS with 217200 g/mol could be used for grafting to silver nanoparticles. Key factors were droplet formation by ultrasonification and low silver content, which enhances the availability of the terminal thiol end group significantly. In contrast, agglomeration-free silver nanoparticle formation with polystyrene grafts by the *in situ* route was possible only with significantly shorter polystyrene chains. The reduction of the silver content had no influence. Therefore, only the chain length is considered as the crucial factor for nanoparticle stability in the *in situ* route. We suggest that agglomeration occurs during the reduction step of silver only. If the rate of reduction is faster compared to the rate of coordination, stabilization of particles cannot be ensured. We anticipate that the rate of coordination decreases with increasing molecular weight due to the lower ratio of end groups to repetition unit per mole. Unlike the heterogeneous system used in the ligand exchange experiments, the homogeneous *in situ* solution does not provide the possibility of preferred end group orientation. Rather, end groups are in a random position within the dissolved polymer coil. Conclusively, the rate of coordination plays the decisive role in *in situ* preparations, preventing its application to high molecular weight polymers.

Ligand exchange, a diffusion-controlled approach, proved to be a more versatile method than the *in situ* method for the preparation of grafted nanoparticles because the onset of agglomeration has been observed at considerably higher molecular weights. The conversion was carried out using a pre-formed aqueous PVP-stabilized AgNP precursor suspension. The particle transportation to a hydrophobic toluene phase has been established with activation through ultrasound. Inert atmosphere is not necessary and functional groups are tolerated throughout. Also, scale-up is easily accessible, making this type of conversion a universal tool. The high compatibility of this method regarding low concentrations of coordinating thiol end groups is attributed to hydrophilic orientation of the end groups at the water-toluene interphase, which opens exciting new perspectives for further investigations, in particular with the great potential of ultrasound (for a review see Lit. 40). The huge length of polystyrene chains which can be grafted on the silver nanoparticle surface by ligand exchange opens several important but yet unanswered questions. What is the mechanism for agglomeration of nanoparticles when the grafts become extremely long? How many polystyrene chains can be grafted on a single silver nanoparticle with increasing chain length? Answers to these questions and the new perspectives by the interphase-driven ligand exchange are presently under investigation.

EXPERIMENTAL SECTION

Materials

Tetrahydrofuran (THF) has been purified by drying over Solvona® with subsequent distillation under argon atmosphere. Toluene and MeOH have been purified by distillation. Styrene (BASF) and ethylene sulfide (98%, ALDRICH) have been dried over CaH₂, distilled and stored at -20 °C under argon. Silver trifluoroacetate (98%, ACROS) has been recrystallized from Et₂O. *Sec*-butyl lithium (1.4 mol*L⁻¹ in cyclohexane, ALDRICH), silver nitrate (99%, ALDRICH), sodium borohydride (99%, ALDRICH), Superhydrid® (1.0 mol*L⁻¹ in THF, ALDRICH), rubrene (98%, ALDRICH) and PVP (BASF Kollidon 17PF®, M_w = 7000-11000) have been used as received. H₂O used for nanoparticle synthesis was taken from a pure water unit TKA micro.

Instrumentation

The number-average molecular weights (M_n) and the weight-average molecular weights (M_w) of the pure polymers were determined by gel permeation chromatography (GPC) using a Knauer system equipped with a PSS-SDV (10 μm) 50 × 8 mm² column and two columns with 600 × 8 mm² at 25 °C, a differential refractive index detector using THF as eluent at a flow rate of 0.5 mL*min⁻¹ and linear polystyrene as standard (obtained from Polymer Standard Service).

GPC of ThPS@AgNP were carried out using a Knauer system equipped with a 50 x 8 mm² pre-column, three linear 10 μm SDV columns with 300 x 8 mm² at 25 °C and a HP diode array detector (model 1040) measuring between 261 and 600 nm using DMF as a eluent with a flow rate of 0.5 ml*min⁻¹.

Proton nuclear magnetic resonance (¹H-NMR) spectra were recorded on a Bruker Avance 300 A (300.13 MHz) spectrometer using d7-DMF as solvent with a concentration of 30 g*L⁻¹.

Transmission electron microscopy (TEM) measurements have been done in a JEOL JEM 3010 with a LaB6-crystal cathode at a voltage of 300 kV. Images were recorded using a 4 megapixel CCD camera. Samples have been prepared from solution by dip-coating a Quantifoil 300 mesh copper grid with carbon coating. For size calculation the software

ImageJ (version 1.44p) of the National Institute of Health, USA, has been used. The mean particle diameter was calculated from at least 150 particles/sample.

A Perkin-Elmer Lambda 9 UV/Vis/NIR spectrophotometer was used for UV/Vis absorption spectroscopy. The concentration of the sample suspension was $0.5 \text{ g}\cdot\text{L}^{-1}$, the cuvette length was 1.0 cm.

For optical microscopy, a Keyence VH-Z500 digital microscope was used with a VHX-100 recording unit.

Silver contents of ThPS@AgNP conjugates were analyzed by digestion of the samples using nitric acid with subsequent analysis by atom absorption spectroscopy (AAS) on a Perkin-Elmer 5000 Atomic Absorption Spectrophotometer.

The silver concentration of the aqueous silver dispersion was analyzed by inductively coupled plasma mass spectrometry (ICP-MS) after a gravimetrically controlled 1:1000 dilution, using an Agilent 7500ce Inductively Coupled Plasma Mass Spectrometer device operating in the no gas mode. For quantification the isotope ^{107}Ag was used. The correctness of the results was checked by observation of the isotope ratio $^{107}\text{Ag}/^{109}\text{Ag}$. Calibration in the range of $1\text{-}100 \text{ ng}\cdot\text{g}^{-1}$ was carried out with gravimetrically prepared dilutions of the ICP multi-element standard solution VI from Merck (No. 110580).

A Bandelin Sonorex RK 102 H device was used for ultrasound generation with a frequency of 35 kHz.

Preparation of ThPS

A flame-dried flask was charged with 500 mL dry THF and cooled to $-78 \text{ }^\circ\text{C}$. *Sec*-butyl lithium ($1.4 \text{ mol}\cdot\text{L}^{-1}$ in cyclohexane) was added dropwise to remove eventual traces of water until a stable slight yellow color was established. $29.5 \text{ }\mu\text{L}$ ($41.3 \text{ }\mu\text{mol}$, 1.00 eq) *sec*-butyl lithium ($1.4 \text{ mol}\cdot\text{L}^{-1}$ in cyclohexane) were added, followed by 10.0 mL (87.3 mmol , 2112 eq) styrene. After 5 min the solution was allowed to warm to room temperature. $2.70 \text{ }\mu\text{L}$ ($45.4 \text{ }\mu\text{mol}$, 1.10 eq) ethylene sulfide were added to the remaining reaction mixture and the solution discolored. After concentration and precipitation in MeOH, the white precipitate was filtered, washed with MeOH and dried at $60 \text{ }^\circ\text{C}$ in vacuo (7.33 g, 81%). $M_n = 217200$, $M_w = 219600$, PDI = 1.01. Polymerization degree calculated from GPC: $P_n = 2085$. The polymer is designated as ThPS₂₁₇₂₀₀ with the subscript

representing M_n . ThPS with different molecular weights were prepared by changing the amount of *Sec*-butyl lithium.

Preparation of suspensions of PVP@AgNP: 77.6 mg (2.05 mmol) NaBH_4 were dissolved in 100 mL H_2O and stirred at 0 °C for 20 min. A solution of 49.0 mg (288 μmol) AgNO_3 in 20 mL H_2O was added at 0 °C very slowly. Immediately after the addition the suspension was allowed to warm to room temperature without further stirring. After 30 min a solution of 60.0 mg PVP in 20 mL H_2O was added slowly. The suspension was stirred for another 60 min. Mean particle diameter (TEM): 7.0 ± 1.9 nm. No agglomeration observed. $c = 2.05 \text{ mmol} \cdot \text{L}^{-1}$ (ICP-MS).

Preparation of ThPS@AgNP via ligand exchange reaction

60.0 mL of a freshly prepared PVP@AgNP suspension ($c = 1.43 \text{ mmol} \cdot \text{L}^{-1}$) were mixed with a solution of 788 mg (17.5 μmol) functionalized ThPS₄₅₁₀₀ in 60 mL toluene. After stirring for 15 min, the mixture was activated by ultrasound for 25 min at room temperature and subsequently, stirred for 18 h at room temperature. The toluene phase was separated, concentrated and precipitated in MeOH. The brown precipitate was filtered, washed with MeOH and dried at 60 °C *in vacuo* (611 mg, 77%). Applying the same procedure on unfunctionalized PS₄₅₁₀₀ no phase transfer could be observed. Mean particle diameter (TEM): 7.3 ± 2.6 nm. No agglomeration observed. The conjugate is designated as PS₄₅₁₀₀@AgNP_{4.9} with 45100 standing for M_n of ThPS and 4.9 representing the initial molar Ag ratio relative to one equivalent of ThPS. Conjugates with different ThPS:Ag ratios were prepared by changing the amount of ThPS.

In situ preparation of ThPS@AgNP

150 mg (7.08 μmol , 1.00 eq) functionalized ThPS₂₁₂₀₀ were dissolved in 30 mL dry THF and 7.70 mg (34.7 μmol , 4.90 eq) AgCO_2CF_3 were added. Under vigorous stirring, 283 μL (283 μmol , 40.0 eq) Superhydride® (1 $\text{mol} \cdot \text{L}^{-1}$ in THF) were added at room temperature. After 15 min, MeOH was added dropwise to remove excess Superhydrid® until no gas formation was observed. Precipitation in MeOH yielded a brown-grey solid which was filtered, washed with MeOH and dried at 60 °C *in vacuo* (146.5 mg, 93%). Applying the same procedure on unfunctionalized PS₂₁₂₀₀ no nanoparticles could be observed. Mean particle diameter (TEM): 2.2 ± 0.7 nm. No agglomeration observed. The conjugate is designated as ThPS₂₁₂₀₀@AgNP_{4.9}.

ACKNOWLEDGEMENTS

The authors are indebted to DFG for financial support, to I. Kuzu, C. Mischke, Y. Ulrich and H. Mallinger of the analytical department at Philipps-Universität Marburg for carrying out AAS measurements.

REFERENCES

- [1] X. Zheng, W. Xu, C. Corredor, S. Xu, J. An, B. Zhao, J. R. Lombardi, *J. Phys. Chem. C* **2007**, *111*, 14962.
- [2] S. Lal, S. Link, N. J. Halas, *Nature Photonics* **2007**, *1*, 641.
- [3] S. Link, M. A. El-Sayed, *J. Phys. Chem. B* **1999**, *103*, 8410.
- [4] D.D. Evanoff, G. Chumanov, *ChemPhysChem* **2005**, *6*, 1221.
- [5] M. M. Maye, Y. Lou, C. Zhong, *Langmuir* **2000**, *16*, 7520.
- [6] M. S. El-Deab, T. Ohsaka, *Electrochem. Commun.* **2002**, *4*, 288.
- [7] L. Pasquato, F. Rancan, P. Scrimin, F. Mancin, C. Frigeri, *Chem. Comm.* **2000**, 2253.
- [8] I. Sondi, B. Salopek-Sondi, *J. Colloid. and Interface Sci.* **2004**, *275*, 177.
- [9] S. Pal, Y. K. Tak, J. M. Song, *Appl. Environ. Microbiol.* **2007**, *73*, 1712.
- [10] P. Li, J. Li, C. Wu, Q. Wu, J. Li, *Nanotechnology* **2005**, *16*, 1912.
- [11] A. Y. Olenin, Y. A. Krutyakov, A. A. Kudrinskii, G. V. Lisichkin, *Colloid Journal* **2008**, *70*, 71.
- [12] P. W. Voorhees, *J. Statist. Phys.* **1985**, *38*, 231.
- [13] X. Jia, J. Listak, V. Witherspoon, E. E. Kalu, X. Yang, M. R. Bockstaller, *Langmuir* **2010**, *26*, 12190.
- [14] X. Ji, X. Song, Y. Bai, W. Yang, X. Peng, *J. Am. Chem. Soc.* **2007**, *129*, 13939.
- [15] L. Sun, Y. Song, C. Guo, Y. Sun, Z. Liu, Z. Li, *J. Phys. Chem. C* **2008**, *112*, 1415.

- [16] M. Brust, M. Walker, D. Bethell, D. J. Schiffrin, R. Whyman, *J. Chem. Soc., Chem. Commun.* **1994**, 7, 801.
- [17] C. H. Walker, J. V. S. John, P. Wisian-Neilson, *J. Am. Chem. Soc.* **2001**, 123, 3846.
- [18] H. H. Huang, X. P. Ni, G. L. Loy, C. H. Chew, K. L. Tan, f. C. Loh, J. F. Deng, G. Q. Xu, *Langmuir* **1996**, 12, 909.
- [19] T. Hasell, J. Yang, W. Wang, P. D. Brown, S. M. Howdle, *Mater. Lett.* **2007**, 61, 4906.
- [20] K. Gries, M. E. Helou, G. Witte, S. Agarwal, A. Greiner, *Polymer* **2012**, 53, 1632.
- [21] T. K. Mandal, M. S. Fleming, D. R. Walt, *Nano Lett.* **2002**, 2, 3.
- [22] M. K. Corbierre, N. S. Cameron, M. Sutton, S. G. J. Mochrie, L. B. Lurio, A. Rühm, R. B. Lennox, *J. Am. Chem. Soc.* **2001**, 123, 10411.
- [23] A. B. Lowe, B. S. Sumerlin, M. S. Donovan, C. L. McCormick, *J. Am. Chem. Soc.* **2002**, 124, 11562.
- [24] J. H. Youk, M. Park, J. Locklin, R. Advincula, J. Yang, J. Mays, *Langmuir* **2002**, 18, 2455.
- [25] M. K. Corbierre, N. S. Cameron, M. Sutton, K. Laaziri, R. B. Lennox, *Langmuir* **2005**, 21, 6063.
- [26] S. Bokern, J. Getze, S. Agarwal, A. Greiner, *Polymer* **2011**, 52, 912.
- [27] M. Sastry, *Curr. Sci.* **2003**, 85, 1735.
- [28] P. J. G. Goulet, G. R. Bourret, R. B. Lennox, *Langmuir* **2012**, 28, 2909.
- [29] J. Tian, J. Jien, F. Zheng, H. Zhao, *Langmuir* **2010**, 26, 8762.
- [30] B. A. Rozenberg, R. Tenne, *Prog. Polym. Sci.* **2008**, 33, 40.
- [31] Z. Nie, D. Fava, E. Kumacheva, S. Zou, G. C. Walker, M. Rubinstein, *Nature Materials* **2007**, 6, 609.
- [32] J. Duijneveldt, In *Colloid Science: Principles, Methods and Applications*, ed. T. Cosgrove, 2nd edn., Wiley-Blackwell: Hoboken, **2010**.

- [33] N. Uehara, *Anal. Sci.* **2010**, *26*, 1219.
- [34] M. K. Corbierre, N. S. Cameron, R. B. Lennox, *Langmuir* **2004**, *20*, 2867.
- [35] K. Gries, K. Bubel, M. Wohlfahrt, S. Agarwal, U. Koert, A. Greiner, *Macromol. Chem. Phys.* **2011**, *212*, 2551.
- [36] T. J. Mason, *Chem. Soc. Rev.* **1997**, *26*, 443.
- [37] N. A. Tsochatzidis, P. Guiraud, A. M. Wilhelm, H. Delmas, *Chem. Eng. Sci.* **2001**, *56*, 1831.
- [38] A. Böker, J. He, T. Emrick, T. P. Russell, *Soft Matter* **2007**, *3*, 1231.
- [39] S. Underwood, P. Mulvaney, *Langmuir* **1994**, *10*, 3427.
- [40] J. H. Bang, K. S. Suslick, *Adv. Mater* **2010**, 1039.

SUPPORTING INFORMATION

FOR

ULTRASOUND-MEDIATED SYNTHESIS OF HIGH-MOLECULAR WEIGHT POLYSTYRENE-GRAFTED SILVER NANOPARTICLES BY FACILE LIGAND EXCHANGE REACTIONS IN SUSPENSION

Holger Pletsch, Ling Peng, Fabian Mitschang, Andreas Schaper, Michael Hellwig, David Nette, Andreas Seubert, Andreas Greiner and Seema Agarwal**

H. Pletsch, L. Peng, F. Mitschang, Prof. A. Greiner, Prof. S. Agarwal

Universität Bayreuth, Macromolecular Chemistry II, Universitätsstraße 30, 95440 Bayreuth (Germany)

Fax: +49 921553393

E-mail: agarwal@uni-bayreuth.de; greiner@uni-bayreuth.de

Keywords: Silver nanoparticles, ligand exchange, ultrasound, metal-polymer hybrid

Raman analysis

Raman analysis was carried out in THF solution on a Labram HR 800 using a He/Ne laser emitting at 632.817 nm.

In comparison, the spectra of PS₂₁₂₀₀ and ThPS₂₁₂₀₀ reveal a significant difference at wavenumbers 734, 762 and 2572 cm⁻¹ which indicate a qualitative proof of functionalization (**Figure 4-S1**).

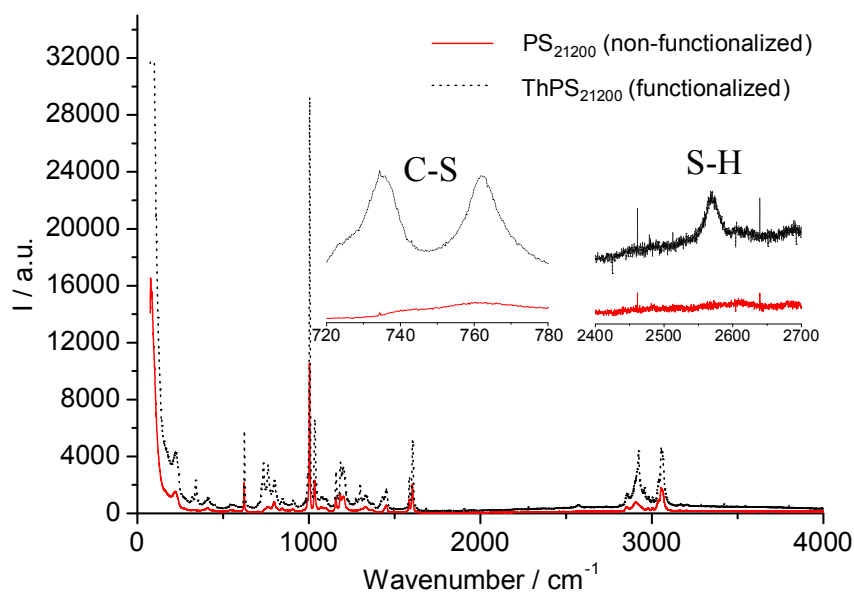


Figure 4-S1. Raman spectra of PS₂₁₂₀₀ and ThPS₂₁₂₀₀ with magnifications in the range between 720-780 cm⁻¹ and 2500-2650 cm⁻¹. Absorption at 734 cm⁻¹ and 762 cm⁻¹ represent C-S-vibrations. S-H-vibration occurs at 2572 cm⁻¹.

Fluorescent microscopy

37.1 mg ThPS₂₁₂₀₀ were dissolved in 6 mL toluene and 5 mg of rubrene dye were added. 6 mL of the freshly prepared aqueous AgNP suspension (corresponding to 85.7 μmol Ag content) were added. After stirring at room temperature for 15 min the mixture was activated by ultrasound for 10 min. Using a capillary, 5 drops of the emulsion were applied onto a glass slide which was instantly used in a Leica DMRX fluorescent microscope, equipped with an eby 100 UV light source. IrfanView-supported Leica DC 200 software was used to record images.

The images unambiguously show fluorescence in the dispersed phase only (**Figure 4-S2**). As a conclusion, the toluene phase is designated as the dispersed phase.

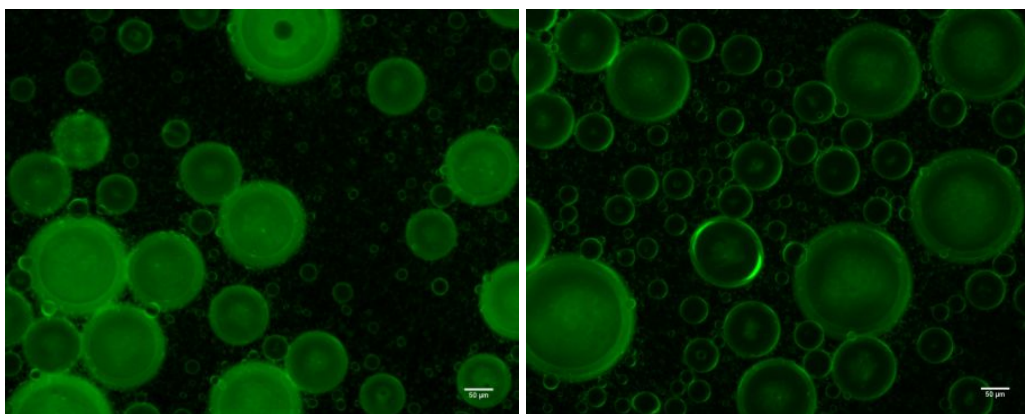


Figure 4-S2. Micrographs of the emulsion after 10 min of ultrasound. Fluorescence only occurs in the dispersed phase which indicates the toluene phase to be the dispersed phase. Scale is 50 μm for both images.

DLS measurements

Dynamic Light Scattering measurements (DLS) were carried out in toluene at 20 °C. We observed a change of the linearized number average weighted hydrodynamic radii with silver nanoparticle content at constant molecular weights. In particular, the radii are decreased with increasing silver content. This can be seen at the samples ThPS₂₁₂₀₀@AgNP_{4.9} versus ThPS₂₁₂₀₀@AgNP₁₂ with radii of 5.9 nm and 4.6 nm, respectively. The same trend is observable for ThPS₄₅₁₀₀@AgNP_{0.9} (9.5 nm) versus ThPS₄₅₁₀₀@AgNP_{4.9} (4.6 nm) and for ThPS₂₁₇₂₀₀@AgNP_{1.0} (9.5 nm) versus ThPS₂₁₇₂₀₀@AgNP_{4.9} (7.4 nm) (**Table 4-S1**). No conclusion can be drawn from comparing samples with constant silver content but different molecular weight. Measurements were performed on an ALV DLS/SLS-SP 5022F compact goniometer system with an ALV 5000/E cross correlator and a He–Ne laser ($\lambda = 632.8$ nm). The measurements were carried out in cylindrical scattering cells ($d = 10$ mm) at an angle of 90°. The CONTIN algorithm was applied to analyze the obtained correlation functions.

Table 4-S1: Linearized number average weighted hydrodynamic radii from DLS measurements in toluene at 20 °C for the pure ThPS polymers and the ligand exchange conjugate products.

Sample	Hydrodynamic radius/ nm
ThPS ₂₁₂₀₀	3.6
ThPS ₄₅₁₀₀	3.6
ThPS ₇₉₃₀₀	4.6
ThPS ₁₂₉₆₀₀	3.0
ThPS ₁₇₇₉₀₀	7.4
ThPS ₂₁₇₂₀₀	3.6
ThPS ₂₁₂₀₀ @AgNP _{4.9}	5.9
ThPS ₂₁₂₀₀ @AgNP ₁₂	4.6
ThPS ₄₅₁₀₀ @AgNP _{4.9}	4.6
ThPS ₄₅₁₀₀ @AgNP _{0.9}	9.5
ThPS ₇₉₃₀₀ @AgNP _{4.9}	7.5
ThPS ₁₂₉₆₀₀ @AgNP _{4.9}	19.4
ThPS ₁₇₇₉₀₀ @AgNP _{4.9}	12.0
ThPS ₂₁₇₂₀₀ @AgNP _{1.0}	9.5
ThPS ₂₁₇₂₀₀ @AgNP _{4.9}	7.4

CHAPTER 5

REVERSIBLE GOLD NANOROD ALIGNMENT IN MECHANO-RESPONSIVE ELASTOMERS

*Holger Pletsch,^{†1} Moritz Tebbe,^{†2} Martin Dulle,³ Beate Förster,⁴ Andreas Fery,²
Stephan Förster,³ Andreas Greiner¹ and Seema Agarwal^{1*}*

[†] These authors contributed equally to this work.

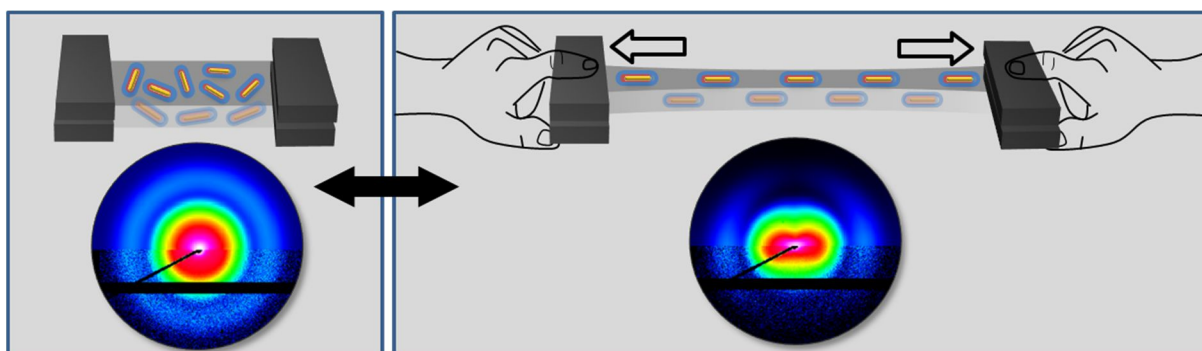
¹ Faculty of Biology, Chemistry and Earth Sciences, Macromolecular Chemistry II and Bayreuth Center for Colloids and Interfaces, University of Bayreuth, Universitätsstraße 30, 95440 Bayreuth, Germany.

Fax: +49 921553393. E-mail: agarwal@uni-bayreuth.de

² Faculty of Biology, Chemistry and Earth Sciences, Physical Chemistry II and Bayreuth Center for Colloids and Interfaces, University of Bayreuth, Universitätsstraße 30, 95440 Bayreuth, Germany.

³ Faculty of Biology, Chemistry and Earth Sciences, Physical Chemistry I and Bayreuth Center for Colloids and Interfaces, University of Bayreuth, Universitätsstraße 30, 95440 Bayreuth, Germany.

⁴ Bayreuther Institut für Materialforschung (BIMF), Universitätsstraße 30, 95440 Bayreuth (Germany).



Published in *Polymer*, year **2015**, volume *66*, pages 167-172. Reprinted with permission.

Copyright Elsevier.

ABSTRACT

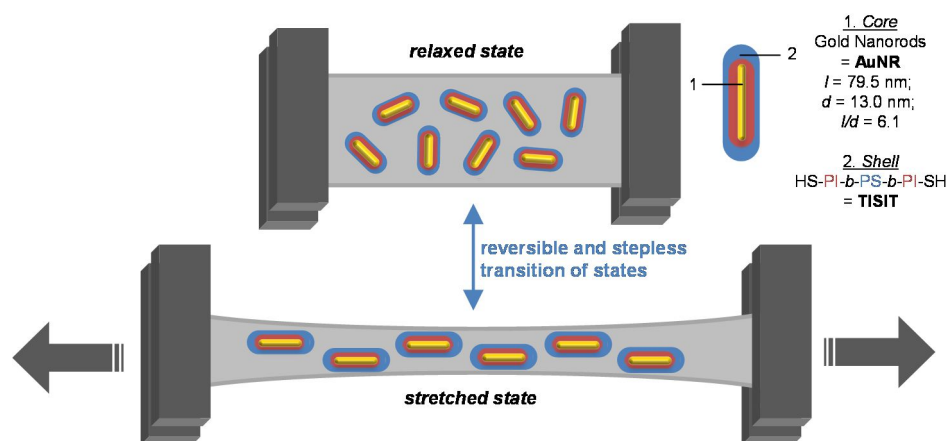
Inspired by an increasing demand for stimuli-controlled assembly of nanostructures, mechano-responsive nanocomposites are designed with tremendous scope in material applications. Providing switchable properties by means of mechanical stimulation, elastomer-incorporated gold nanorods (AuNR) are presented herein. Stepless and reversible control over the orientational AuNR alignment –and therefore over macroscopic anisotropy– is exerted by uniaxial film elongation. In context of optical applications, substantial impact on the plasmonic properties within adjustable spectral ranges is demonstrated. Mechano-responsive nanocomposites with high thermal colloidal stability are prepared via a facile hetero-phase ligand exchange procedure where complete coverage of the AuNR surface with hydrophobic ligands is achieved.

KEYWORDS

Nanocomposites, mechano-responsive, gold nanorods, anisotropy, ligand exchange

INTRODUCTION

Nanocomposites are amongst the most versatile materials gaining their unique properties from synergistic effects. Fabrication of continuous matrices with incorporated, homogeneously dispersed nano-sized functional particles is essential for bridging the gap between singular material properties and complex devices.^[1-4] Noble metal nanoparticles are in the center of research interest especially due to their inherent size- and shape-dependent physical and chemical properties. Most prominently, localized surface plasmon resonance (LSPR) modes are exploited in various emerging fields such as sensing,^[5-7] optical filters,^[8,9] wave guiding,^[10,11] and metamaterials.^[12,13] Most of these applications rely on precise spatial control and orientation of multi-dimensional, hierarchical nanoparticle assemblies. In this context, alignment of nanorods with polarization-dependent resonance modes is one of the recent paramount research objectives for the purpose of designing matter with high optical anisotropy efficiency.^[14-16] In contrast to self-assembly efforts in solution,^[17] real material applications require solid state alignment, which has amongst others been accomplished for noble metal nanorods by embedment in electrospun polymeric nanofibers,^[10,18,19] by selective incorporation in block copolymer microphase domains,^[20, 21] by co-alignment within liquid crystal phases^[22] or by thermoplastic deformation of nanocomposite films.^[2,14-16,23-27] However, those systems were ultimately fixed to one nanorod alignment constitution in which the alignment degree could not be altered by external stimuli. Yet the capability to change nanoparticle distances or orientation in a reversible and controllable fashion raises functionality to another level.^[7,28] Therefore, we incorporate gold nanorods (AuNR) into an elastic matrix, assuming that the orientational distribution of dispersed AuNR reversibly scales with mechanical stimulation during uniaxial elongation and relaxation (**Scheme 5-1**). As a consequence from nematic-like AuNR ordering, reversible macroscopic anisotropy for the use in strain sensor and mechano-responsive filter applications is expected. In context of optical applications, substantial impact on the plasmonic properties within adjustable spectral ranges is also demonstrated.



Scheme 5-1. Concept illustration of mechano-responsive nanocomposites. AuNR are homogeneously dispersed into an elastic film where uniaxial mechanical elongation induces stepless and reversible alignment of AuNR within the direction of elongation. Scheme is not true to scale.

RESULTS AND DISCUSSION

Cetyltrimethylammonium bromide (CTAB)-stabilized gold nanorods (AuNR) (in the following designated as AuNR@CTAB) in aqueous dispersion were prepared following a protocol by Vigdeman et al.,^[29] yielding rods with an aspect ratio (AR) of 6.1 nm (lengths $l = 79.5 \pm 9.3$ nm; diameters $d = 13.0 \pm 0.9$ nm; see also **Figure 5-S1**). UV-Vis-NIR characterization of as-prepared AuNRs reveals a longitudinal localized surface plasmon resonance (L-LSPR) within the NIR spectral range (peak maximum at 1039 nm) in good agreement with their determined ARs. Previous attempts to incorporate AuNR@CTAB into hydrophobic, elastic matrices with homogenous particle distribution were limited to elaborate physico-chemical routes where noxious CTAB was not removed from the particle surface but covered either with two layers of polyelectrolyte, followed by incorporation in PDMS matrix^[30] or with a silica shell and subsequent doping of ureasil,^[31] yielding materials with low AuNR filling fractions. Herein, a non-microphase-separated α,ω -dithiol functionalized ABA triblock co-oligomer ($M_n = 4800$ g/mol, PDI = 1.25) consisting of isoprene (A) and styrene (B) with a total molar styrene content of 36% (in the following designated as TISIT standing for the sequence thiol-isoprene-styrene-isoprene-thiol; characterization details provided in **Text S2** and **Figure 5-S2**) was used as the exchanging ligand for the preparation of thermally processable and CTAB-free AuNR nanocomposites *via* hetero-phase ligand exchange. TISIT is a promising liquid precursor for the preparation of thermally processable elastomers with high mechanical strength as

shown recently.^[32] Quantitative CTAB-to-TISIT replacement (proved by the non-existence of nitrogen in elementary analysis) in hetero-phase water-toluene system yielded a soft material, charged with 1.9 wt.% AuNR which is designated as AuNR@TISIT in the following. Key factors for complete ligand exchange were vigorous reduction of CTAB concentration below the critical micelle concentration of 1 mM followed by the generation of a particle- and surfactant-stabilized emulsion with droplet sizes of $3.5 \pm 1.4 \mu\text{m}$ through stirring (**Figure 5-1a-b**). Neither further emulsifiers and phase transfer agents were added nor ultrasound applied to induce phase transfer. According to similar hetero-phase ligand exchange studies, the reaction is promoted through orientation of thiol groups towards the liquid-liquid interface (**Figure 5-1c**).^[33] After complete phase transfer, KI is added to trigger phase separation (**Figure 5-1d**), allowing separation of the AuNR-loaded toluene phase. TEM micrographs of AuNR@TISIT dispersions prove that the particle sizes and shapes were not changed during ligand exchange and that isolated core-shell structures are obtained (**Figure 5-1e**). Comparison of UV-Vis-NIR extinction spectra of AuNR@TISIT dispersions with AuNR@CTAB reveal a red shift of about +48 nm for the L-LSPR band typical for changes in environmental refractive index and a slight peak broadening usually attributed to agglomeration (**Figure 5-1f**). However, SEM micrographs of the isolated and purified materials in the solid state, obtained by precipitation (**Figure 5-1g**), reveal efficient sterical protection against particle aggregation during phase transfer as 95% of AuNR are found to be well-dispersed (**Figure 5-1h**). Only 4% of AuNRs are aggregated in dimers and 1% in clusters of three or more particles (sample size $n = 655$), noteworthy in the context of very high filling fraction. TISIT not only serves as ligand but also as dispersing medium as it can be detected in the supernatant of centrifuged AuNR@TISIT dispersions (see also **Figure 5-S3**). The conversion of liquid TISIT into a mechanically stable material holding an E-modulus of $7.07 \pm 1.32 \text{ MPa}$, tensile strength of $0.60 \pm 0.01 \text{ MPa}$ and ultimate elongation of $320 \pm 11\%$ (please refer to **Figure 5-S4**) upon charging with AuNR is attributed to attractive oligomer-particle interaction forces such as demonstrated in simulation experiments.^[34]

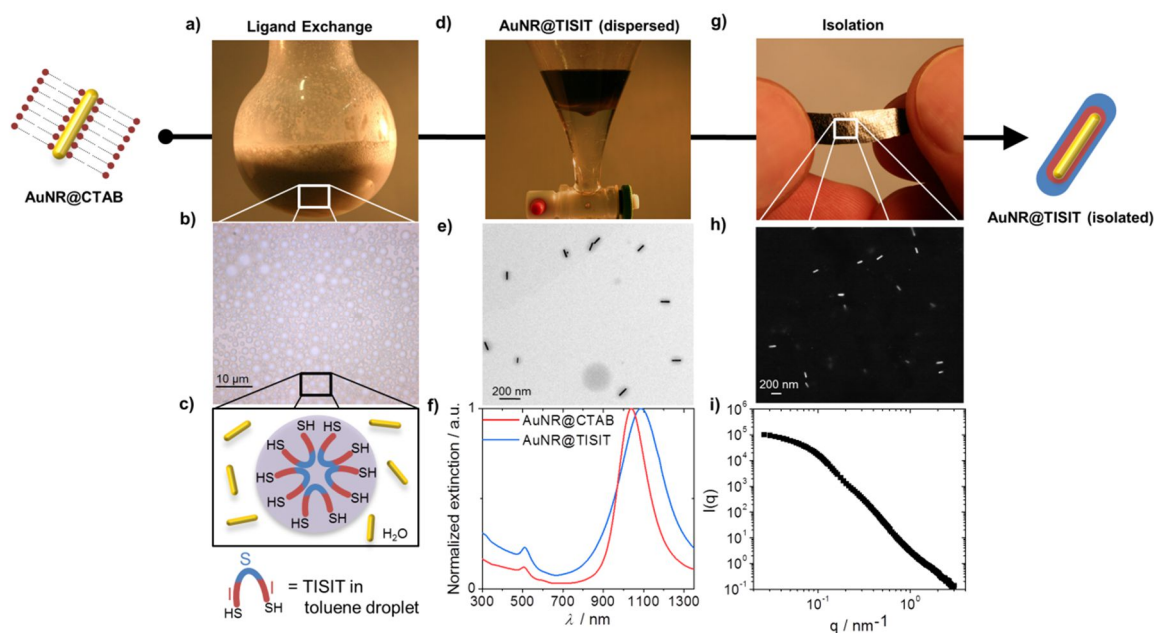


Figure 5-1. Preparation procedure of AuNR@TISIT. a) One-step CTAB-to-TISIT replacement is done via hetero-phase ligand exchange in emulsion. b) Optical micrograph of Pickering emulsion with droplet sizes of $3.5 \pm 1.4 \mu\text{m}$. c) Scheme of preferred thiol orientation towards the liquid-liquid interface within emulsion droplet. d) Complete AuNR transfer is indicated by discoloration of the aqueous phase. e) TEM micrograph of AuNR@TISIT from toluene dispersion shows isolated arrangements of AuNR cores and TISIT shells with preserved particle dimensions compared to AuNR@CTAB. f) Extinction spectra of AuNR@CTAB in aqueous dispersion and of AuNR@TISIT in THF dispersion. g) If isolated, AuNR@TISIT is a thermally processable soft material which is redispersible in apolar solvents. h) SEM micrograph of AuNR@TISIT in the solid state shows well-dispersed AuNR within the TISIT matrix (the micrograph shown here is modified in graphical appearance for enhanced contrast). i) 1D SAXS profile of AuNR@TISIT showing no aggregation of the particles.

Possible methods to introduce elasticity are (1) chemical cross-linking of the isoprene block for example in solution using S_2Cl_2 as cross-linking reagent to yield a thermoset elastomer, (2) physical cross-linking to yield a thermally reversible elastomer or (3) embedment into a thermoplastic elastomer matrix. Aiming at designing processable materials, (2) and (3) were performed. Physical cross-linking was done by *in situ* incorporation of silver nanoparticles (AgNPs) along the lines of a previous report on TISIT-AgNP materials,^[32] yielding a hybrid nanocomposite network from coexisting AuNRs (1.9 wt%) and small AgNPs (9.3 wt%). Reversible mechano-responsive alignment of AuNR is confirmed in SAXS experiments, however, the alignment performance is rather poor (please find details in the Supporting Information **Text 5-S1** and **Figure 5-S5**). Therefore, and for the purpose of decreasing the optical density, AuNR@TISIT was embedded into a thermoplastic elastic matrix. Co-precipitation with a five-fold weight

amount of highly resilient and optically transparent Kraton FG1901x yielded a material with high stretchability of more than 1000%, tensile strength of 20.7 ± 3.0 MPa, E-Modulus of 20.3 ± 2.4 MPa and reduced optical density. AuNR@TISIT are not selectively sequestered in one of the microphase-separated blocks within the matrix (see also **Figure S6** in the supporting information). We therefore assume compatibility of AuNR@TISIT with both rubber and the plastic phase of the matrix. Characterization of these nanocomposites was done using thin films made by hot pressing at 110°C and 300 bar. No variations in shape, size or aggregation behavior were observed upon processing.

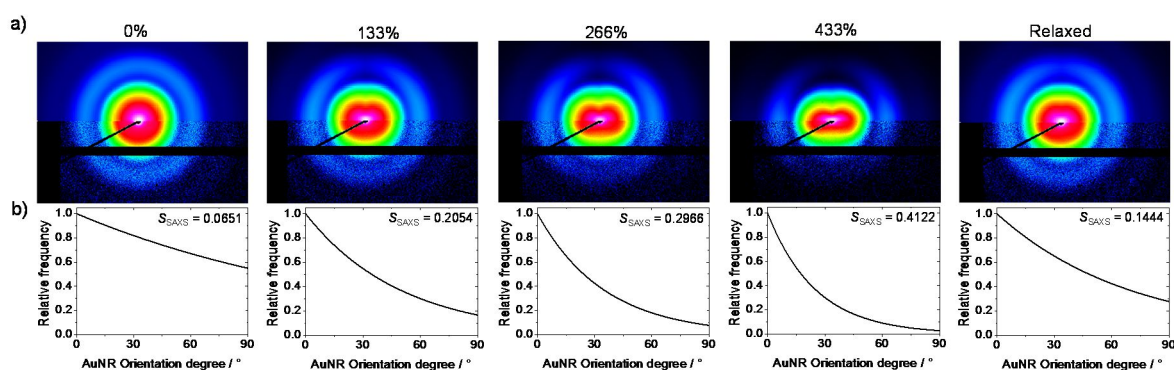


Figure 5-2. elongation-dependent SAXS measurements. a) 2D SAXS scattering patterns (upper half: calculated pattern; lower half: recorded pattern) at 0%, 133%, 266% and 433% elongation as well as for the relaxed sample after this elongation sequence. b) Corresponding ODs with the orientational order parameter S_{SAXS} .

Elongation-dependent SAXS measurements (the scattering response of neat Kraton FG1901x is insignificant compared to AuNR; see also **Figure 5-S7**) were performed in the sequence of 0%, 133%, 266%, 433% and 0% elongation and strongly substantiate the hypothesis that nematic-like AuNR alignment can be controlled as a function of mechanical stimulation in a stepless and reversible fashion since the corresponding orientational order parameter S_{SAXS} (calculated from the respective orientational distribution (OD) functions with 0 standing for random orientational distribution and 1 for perfect alignment) scales with increasing elongation and decreases upon film relaxation (**Figure 5-2**). It is noteworthy that minor pre-alignment was observed at 0% elongation for the freshly melt-processed sample which is attributed to the strong shear forces during hot pressing. In detail, S_{SAXS} was increased from 0.0651 at 0% elongation up to 0.4122 at 433% elongation. Upon relaxation, S_{SAXS} decreases to 0.1444, indicating a slight memory effect, i.e. the initial orientational distribution is not entirely restored which can be attributed to partial plastic deformation of the film and Mullin's effect which is very

common in filled and unfilled elastomers leading to a residual strain.^[35] Finding exact reason is beyond the scope of this work.

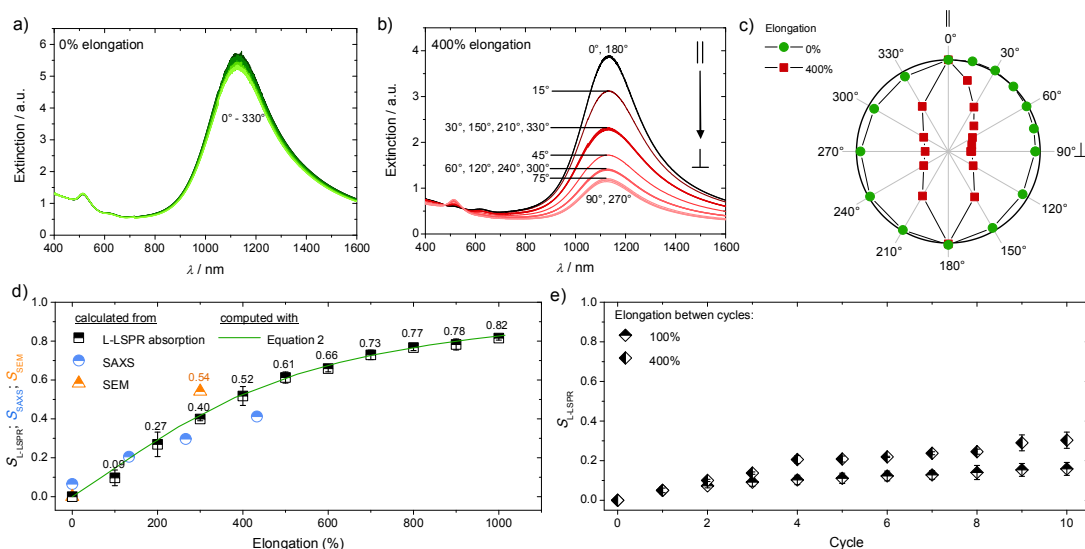


Figure 5-3: Mechano-responsive optical properties of AuNR@TISIT, embedded in Kraton FG1901x. The film stretching direction is defined as 0° . a) Light absorption is independent of the polarization angle of incident light at 0% elongation. b) When stretched to 400%, the polarization angle of incident light has tremendous impact on the absorption behavior of the film. c) This behavior is summarized in a dipole plot of the absorbance against the angle of the incident polarized light. The absorbance under the influence of 0° polarized light is defined as 1 in order to compensate changing film thicknesses during elongation. d) S_{L-LSPR} (average values from 3 measurements) scales as a function of elongation, reaching a maximum of 0.82 shortly before failure and matches well with the computed S from **Equation 2** (green line). S_{SAXS} and S_{SEM} are also shown for comparison. Please find the elongation-dependent extinction plots in the supplementary information **Figure S12**. e) S_{L-LSPR} (average values from 3 measurements) according to **Equation 1** in the relaxed state between stretching cycles.

In the non-stretched state, the extinction spectra from UV-Vis-NIR measurements are independent of the angle of polarization of the incident light, indicating a random distribution of well-dispersed AuNRs in the polymer matrix (**Figure 5-3a**). In contrast to that, substantial uniaxial AuNR orientation is observed in the stretched state under constant strain. Similar to previously reported non-reversible AuNR alignment through thermoplastic deformation in PVA nanocomposites,^[2,14,15] our reversible system is characterized by a significant dependency of the AuNR longitudinal plasmon resonance mode on incident polarization in the stretched state: Light polarized parallel to the stretching direction (0°) is more intensely absorbed whereas the absorption of the longitudinal mode is strongly reduced if subject to incident light polarized perpendicular to the stretching direction (90°) (**Figure 5-3b**). The polarization dependent behavior is

summarized in **Figure 5-3c** by plotting the normalized absorbance of the longitudinal plasmon resonance band against the angle of polarization of the incident light.

In the following we describe the reversible elongation-dependent optical properties of our nematic-like system. Along the lines of previous data evaluation,^[15] a relative orientational order parameter S_{L-LSPR} is calculated according to **Equation 5-1** where $Abs(\perp)_\varepsilon$ is the absorbance of the longitudinal plasmon resonance band subject to light polarized perpendicular to the stretching direction at a corresponding elongation ε and $B(\perp)_\varepsilon$ is the absorbance of the corresponding baseline.

$$S_{L-LSPR} = 1 - \frac{Abs(\perp)_\varepsilon - B(\perp)_\varepsilon}{Abs(\perp)_{\varepsilon=0} - B(\perp)_{\varepsilon=0}} \quad (5-1)$$

S_{L-LSPR} clearly scales with elongation in a range between 0 and 1000% elongation, ending in a flatter course while approaching ultimate elongation with a maximum of $S_{L-LSPR} = 0.82$ at 1000% elongation shortly before failure (**Figure 5-3d**). The observed trend is in approximate agreement with S_{SAXS} and also with the orientational order parameter S_{SEM} which is calculated by compiling the SEM micrographical orientational order of a set of AuNRs into an OD function both at 0% and 300% elongation (see also **Figure 5-S8** and **5-S9**). In comparison, AuNR alignment within nematic liquid crystal phases provides a maximum of $S = 0.474$ as reported recently.^[22]

The herein observed relationship between S and elongation can be compared to theoretical predictions for stretched nematic elastomers, assuming that the nematic mesogenic units correspond to AuNRs.^[36] The theory is based on the minimization of the nematic energy contribution due to the interaction of mesogenic units and on an elastic energy contribution arising from the stretching of the cross-linked polymer chains. It derives a relation between the elastic deformation λ and the nematic orientational order parameter S given by

$$\lambda^3 = \frac{\mu_1 + \mu_2(1-S)^{-1}}{\mu_1 + \mu_2(1+2S)^{-1}} \quad (5-2)$$

where μ_1 and μ_2 are dimensionless elastic moduli of the nematic system along and perpendicular to the director. The experimentally measured elongation ε can be related to the deformation λ obtained from **Equation 5-2** via $\varepsilon = \alpha(\lambda - 1) * 100\%$, where α is a coupling constant. It takes into account that in theory the nematic mesogens are strongly coupled to the polymer network via covalent bonds ($\alpha = 1$), whereas in our case the AuNRs are only weakly coupled to the network via steric or excluded volume interactions ($\alpha < 1$). The measured order parameters can be well described by $\mu_1 = \mu_2 = 1$ with a coupling

constant $\alpha = 0.07$ as shown by the solid line in **Figure 5-3d**. Thus the observed behavior can be well understood based on this model.

The reversibility of AuNR orientation based on intrinsic mechanical relaxation of the elastomer film was also probed *via* UV-Vis-NIR spectroscopy by irradiating a freshly hot pressed film with 90° polarized light as reference (cycle 0), followed by ten stretching cycles to either 100% or 400% elongation, each for a duration of 10 s. Between the stretching cycles, extinction spectra were measured at $\varepsilon = 0$, followed by calculation of S_{L-LSPR} according to **Equation 5-1**. Perfect AuNR alignment reversibility is assumed if S_{L-LSPR} match with the reference cycle 0. Our films exhibit considerable reversibility of AuNR alignment. However, similar to what can be seen in SAXS measurements, a slight memory effect is observed, scaling with increasing number of cycles and with increasing elongation between the cycles (**Figure 5-3e**). The memory effect can be reset by bringing the material into the melt; e.g. using the hot press.



Figure 5-4. Adjustment of spectral ranges as a function of AuNR aspect ratio. a) Extinction spectra of AuNR@CTAB with longitudinal plasmon resonances at 677 nm, 756 nm and 1039 nm corresponding to aspect ratios of 2.1, 3.0 and 6.1 for traces 1, 2 and 3, respectively. b) Polarized photo images of illuminated films made *via* CTAB-to-TISIT ligand exchange and embedment procedure. The films 1-3 consist of AuNR with different aspect ratios as indicated in the extinction spectra, having total Au contents of 0.08, 0.33 and 0.32 wt%, respectively. The polarizer was either set parallel or perpendicular to the stretching direction.

Materials with longitudinal plasmon resonance modes in other spectral ranges are obtained if AuNR@CTAB with different aspect ratios are provided to the herein discussed preparation procedure (see **Figures 5-S10** and **5-S11**). The considerable impact of light polarization on the visible color is summarized in **Figure 5-4** for AuNR aspect ratios of 2.1 and 3.0 in comparison with the above discussed 6.1, having longitudinal plasmon resonances at 677 nm, 756 nm and 1039 nm, respectively.

CONCLUSION

In conclusion, reversible and stepless stimuli-controlled assembly of nanostructures is facilitated *via* mechano-responsive nanocomposites made from elastomer-incorporated AuNRs. Key steps for the design of such a material are the compatibility between ligand and matrix through hydrophobization using TISIT and the employment of a highly resilient and thermally processable matrix. Nematic-like AuNR arrangements up to $S = 0.82$ are achieved at high uniaxial film elongation whereas film relaxation re-establishes random AuNR orientation. In comparison with previous attempts to align anisotropic nanoparticles into ordered superstructures with respect to their orientation, the herein presented mechanical driving force as well as distinct reversibility opens unique perspectives especially in context of strain sensor or reversible optical filter applications.

EXPERIMENTAL SECTION

Instrumentation

Ag and Au mass fractions were determined by TGA ash yield analysis with a Netzsch Libra TG209 F1 device.

TEM measurements have been done in a Zeiss 922 OMEGA EFTEM at a voltage of 200 kV. Zero-loss filtered images were recorded using a bottom mounted Ultrascan 1000 (Gatan) CCD camera system. Samples have been prepared from solution by drop-casting on a Quantifoil 300 mesh copper grid with carbon coating.

Stress-strain measurements were done using a Zwick Roell Z0.5 device with a Zwick Roell KAF-TC 1000 N load sensor at a strain rate of 200 mm min^{-1} at $23 \text{ }^\circ\text{C}$ on dumbbell-shaped specimen with diameters of 2 mm and thicknesses of 0.5 mm. A slack which was observed upon loading was subtracted manually subsequent to the measurement. Values represent the average of three measurements and refer to the engineering curves.

Films were obtained by hot-pressing using a Carver 2518 setup at 300 bar and $110 \text{ }^\circ\text{C}$ for 3 min.

Polarization angle-dependent extinction spectra of films (thickness: $400 \text{ }\mu\text{m}$) at 0% and 400% elongation were measured on an Agilent Cary 5000 spectrophotometer with an attached Cary Universal Measurement Accessory (UMA) with polarization angles ranging from $0\text{-}330^\circ$.

Elongation-dependent extinction spectra and extinction measurements between elongation cycles were performed using 90° incident light on a Jasco V-670 spectrophotometer equipped with a GPH-506 polarizer between the light source and the sample.

SAXS was measured using “Double Ganesha AIR” (SAXSLAB) equipped with a rotating anode x-ray source (copper, MicoMax 007HF, Rigaku Corporation) providing a micro-focused beam at $\lambda = 0.154$ nm and a position-sensitive detector (PILATUS 300K, Dectris). Liquid samples were measured in 1 mm glass capillaries (Hilgenberg, code 4007610) at different detector positions to cover a range of scattering vectors between 0.026-2 nm⁻¹. The scattering contribution of the solvent and the capillary were subtracted. Films (thickness: 500 μm; length: 2.5 cm; width: 5 mm) were measured in a tensile stage (TST 350 Linkam; maximum elongation: 433%) at a sample detector distance of 1.11 m covering a q-range between 0.045-2 nm⁻¹. The AuNR form factor was determined by fitting the data of the AuNR@CTAB dispersion with a model of a homogenous cylinder SASfit.^[37] The 2D data were fitted to an exponential function using *Scatter*^[38]. By changing the width of the OD the orientational order parameter S_{SAXS} was calculated from the best fitting OD according to $S_{SAXS} = \left\langle \frac{3 \cos^2 \theta - 1}{2} \right\rangle$.

SEM imaging of films was done on a Zeiss Ultra plus FE-SEM equipped with a Schottky field emission cathode and in lens, SE2, EsB and AsB detectors using an acceleration voltage of 7-10 kV. The samples were covered with a layer of platinum (1.3 nm thickness) prior to imaging using a Cressington HR208 sputter coater and a Cressington mtm20 thickness controller. A manually operated tensile stage was used to measure films (thickness: 500 μm) in the stretched state. The stretched samples were covered with a second 1.3 nm layer of platinum. The OD has the form of an exponential function and was fitted according to $S_{SEM} = \left\langle \frac{3 \cos^2 \theta - 1}{2} \right\rangle$.

Preparation of AuNR@TISIT

Concentration of the aqueous AuNR@CTAB suspension was done from 240 mL to 1 mL by centrifugation at 4000 rcf. The CTAB concentration was adjusted to 1 mM by consecutive washing cycles and a final washing step with 1 mM CTAB solution. 784 mg TISIT (163 μmol) were dissolved in 12 mL toluene and mixed with 12 mL of a freshly concentrated aqueous AuNR suspension. After stirring for 18 h, KI was added until the phase mixture demulgated, followed by phase separation and concentration of the toluene phase. After precipitation in MeOH, the supernatant was decanted and the residue was dried. 716 mg of a dark brown soft material were obtained. Au content: 1.9 wt.%

(determined by TGA ash yield analysis). N content: 0% (determined by elemental analysis). The preparation of AuNR@TISIT with AuNR of shorter aspect ratios was carried out accordingly by using the respective AuNR@CTAB suspension.

Embedding of AuNR@TISIT in Kraton FG1901x

203.0 mg AuNR@TISIT and 1.01 g Kraton FG1901x were dissolved in 10 mL THF, followed by precipitation in MeOH, decantation of the supernatant and drying of the residue.

*Please find more details on materials, preparation and analysis of TISIT and AuNR@CTAB in the Supporting Information **Text S1**.*

REFERENCES

- [1] J. Lee, S. Kim, J. Lee, D. Yang, B. C. Park, S. Ryu, I. Park, *Nanoscale* **2014**, *6*, 11932.
- [2] S. Liu, J. Li, Z.-Y. Li, *Adv. Opt. Mater.* **2013**, *1*, 227.
- [3] L. Vigderman, B. P. Khanal, E. R. Zubarev, *Adv. Mater.* **2012**, *24*, 4811.
- [4] P. Zijlstra, J. W. M. Chon, M. Gu, *Nature* **2009**, *459*, 410.
2005, *249*, 1870.
- [5] M. Alba, N. Pazos-Perez, B. Vaz, P. Formentin, M. Tebbe, M. A. Correa-Duarte, P. Granero, J. Ferré-Borrull, R. Alvarez, J. Pallares, A. Fery, A. R. de Lera, L. F. Marsal, R. A. Alvarez-Puebla, *Angew. Chem. Int. Ed.* **2013**, *52*, 6459.
- [6] M. Tebbe, P. Cherepanov, E. V. Skorb, S. K. Poznyak, J. G. de Abajo, A. Fery, D. V. Andreeva, R. A. A. Puebla, N. Pazos-Perez, *Part. Part. Syst. Charact.* **2014**, *31*, 1134.
- [7] M. Segev-Bar, H. Haick, *ACS Nano* **2013**, *7*, 8366.
- [8] T. Xu, Y.-K. Wu, X. Luo, L. J. Guo, *Nat. Commun.* 2010, *1*, DOI: 10.1038/ncomms1.

- [9] M. G. Millyard, F. M. Huang, R. White, E. Spigone, J. Kivioja, J. J. Baumberg, *Appl. Phys. Lett.* **2012**, *100*, 073101.
- [10] P. Wang, L. Zhang, Y. Xia, L. Tong, X. Xu, Y. Ying, *Nano Lett.* **2012**, *12*, 3145.
- [11] S. Lal, S. Link, N. J. Halas, *Nature Photon.* **2007**, *1*, 641.
- [12] A. Guerrero-Martínez, B. Auguie, J. L. Alonso-Gómez, Z. Džolić, S. Gómez-Graña, M. Žinić, M. M. Cid, L. M. Liz-Marzán, *Angew. Chem. Int. Ed.* **2011**, *50*, 5499.
- [13] Q. Liu, Y. Cui, D. Gardner, X. Li, S. He, I. I. Smalyukh, *Nano Lett.* **2010**, *10*, 1347.
- [14] J. Li, S. Liu, Y. Liu, F. Zhou, Z.-Y. Li, *Appl. Phys. Lett.* **2010**, *96*, 263103.
- [15] J. Pérez-Juste, B. Rodríguez-González, P. Mulvaney, L. M. Liz-Marzán, *Adv. Funct. Mater.* **2005**, *15*, 1065.
- [16] C. J. Murphy, C. J. Orendorff, *Adv. Mater.* **2005**, *17*, 2173.
- [17] Z. Nie, D. Fava, E. Kumacheva, S. Zou, G. C. Walker, M. Rubinstein, *Nature Mater.* **2007**, *6*, 609.
- [18] K. E. Roskov, K. A. Kozek, W.-C. Wu, R. K. Chhetri, A. L. Oldenburg, R. J. Spontak, J. B. Tracy, *Langmuir* **2011**, *27*, 13965.
- [19] C.-L. Zhang, K.-P. Lv, H.-P. Cong, S.-H. Yu, *Small* **2012**, *8*, 648.
- [20] R. D. Deshmukh, Y. Liu, R. J. Composto, *Nano Lett.* **2007**, *7*, 3662.
- [21] Thorkelsson, K.; Nelson, J. H.; Alivisatos, A. P.; Xu, T. *Nano Lett.* **2013**, *13*, 4908.
- [22] Q. Liu, M. G. Campbell, J. S. Evans, I. I. Smalyukh, *Adv. Mater.* **2014**, *26*, 7178.
- [23] B. M. I. van der Zande, L. Pagès, R. A. M. Hikmet, A. van Blaaderen, *J. Phys. Chem. B* **1999**, *103*, 5761.
- [24] S. Stoenescu, V.-V. Truong, M. Packirisamy, *J. Appl. Phys.* **2014**, *115*, 114301.
- [25] O. Wilson, G. J. Wilson, P. Mulvaney, *Adv. Mater.* **2002**, *14*, 1000.
- [26] Zhamg, H.; Zhang, J.; Tong, X.; Ma, D.; Zhao, Y. *Macromol. Rapid Commun.* **2013**, *34*, 1575.

- [27] Tao, J.; Lu, Y.; Chen, J.; Lu, D.; Chen, C.; Wang, P.; Ming, H. *Plasmonics* 2011, 6, 785.
- [28] Y. Kim, J. Zhu, B. Yeom, M. D. Prima, X. Su, J.-G. Kim, S. J. Yoo, C. Uher, N. A. Kotov, *Nature* **2013**, 500, 59.
- [29] L. Vigderman, E. R. Zubarev, *Chem. Mater.* **2013**, 25, 1450.
- [30] A. M. Alkilany, L. B. Thompson, C. J. Murphy, *ACS Appl. Mater. Interfaces* 2010, 2, 3417-3421.
- [31] V. I. Boev, J. Pérez-Juste, I. Pastoriza-Santos, C. J. R. Silva, M. d. J. M. Gomes, L. M. Liz-Marzán, *Langmuir* 2004, 20, 10268-10272.
- [32] H. Pletsch, M. J. Schnepf, S. Agarwal, *Chem. Mater.* **2014**, 26, 4805.
- [33] H. Pletsch, L. Peng, F. Mitschang, A. Schaper, M. Hellwig, D. Nette, A. Seubert, A. Greiner, S. Agarwal, *Small* **2014**, 10, 201.
- [34] T. Desai, P. Koblinski, S. K. Kumar, *J. Chem. Phys.* **2005**, 122, 134910.
- [35] A. Dorfmann, R.W. Ogden, *Int. J. Solids Str.* **2004**, 41, 1855.
- [36] E. Fried, S. Sellers, *J. Chem. Phys.* **2005**, 123, 044901.
- [37] G. Porod, IV. *Acta Physica Austriaca* **1948**, 2, 255.
- [38] S. Förster, L. Apostol, W. Bras, *J. Appl. Cryst.* **2010**, 43, 639.

ACKNOWLEDGEMENTS

This work was funded by German Research Foundation (DFG) and the European Research Council (ERC-2012-StG 306686 METAMECH). M.T. was supported by the EliteNetwork Bavaria in the frame of the Elite Study Program “Macromolecular Science” and funded via a grant for Ph.D. candidates according to Bavarian elite promotion law (BayEFG). We gratefully acknowledge M. Heider, M. Krekhova and T. Löbbling for technical assistance and N. Pazos-Pérez for fruitful discussion.

SUPPORTING INFORMATION

FOR

REVERSIBLE GOLD NANOROD ALIGNMENT IN MECHANO-RESPONSIVE ELASTOMERS

Holger Pletsch¹, Moritz Tebbe,² Martin Dulle,³ Beate Förster,⁴ Andreas Fery,² Stephan Förster,³ Andreas Greiner¹ and Seema Agarwal¹

¹ Faculty of Biology, Chemistry and Earth Sciences, Macromolecular Chemistry II and Bayreuth Center for Colloids and Interfaces, University of Bayreuth, Universitätsstraße 30, 95440 Bayreuth, Germany.

Fax: +49 921553393. E-mail: agarwal@uni-bayreuth.de

² Faculty of Biology, Chemistry and Earth Sciences, Physical Chemistry II and Bayreuth Center for Colloids and Interfaces, University of Bayreuth, Universitätsstraße 30, 95440 Bayreuth, Germany.

³ Faculty of Biology, Chemistry and Earth Sciences, Physical Chemistry I and Bayreuth Center for Colloids and Interfaces, University of Bayreuth, Universitätsstraße 30, 95440 Bayreuth, Germany.

⁴ Bayreuther Institut für Materialforschung (BIMF), Universitätsstraße 30, 95440 Bayreuth (Germany).

Keywords: Nanocomposites, mechano-responsive, gold nanorods, anisotropy, ligand exchange

Text 5-S1: Experimental Section

Instrumentation: The number-average molecular weights (M_n) and the weight-average molecular weights (M_w) of TISIT was determined by gel permeation chromatography (GPC) in THF at 26 °C using a Agilent 1200 series system equipped with a PSS-SDV (10 μ m) 50 \times 8 mm² pre-column and three linear PSS-SDV (10 μ m) 300 \times 8 mm² columns at a flow rate of 0.8 mL/min (sample concentration 2 mg/mL). A Wyatt Dawn Heleos multi angle laser light scattering (MALLS) detector was used to calculate the absolute molecular weight. dn/dc was determined with a PSS DnDc-2010 λ 620 device.

¹H-NMR (300.13 MHz) spectra were recorded on a Bruker Avance 300 A spectrometer using CDCl₃ as solvent with a concentration of 100 g/L. The solvent signal was used for calibration.

A Mettler thermal analyzer 821 DSC was utilized for DSC scans. Temperature and enthalpy calibration was carried out with indium and zinc standards and tested with *n*-octan as a reference. 5 \pm 2 mg of the samples were analyzed under nitrogen atmosphere (flow rate 80 mL/min) at a heating rate of 10 °C/min. The glass transition temperature (T_g) was taken as the inflection point of the observed shift in the baseline of the second heating cycle.

For optical microscopy, a Keyence VH-Z500 digital microscope was used with a VHX-100 recording unit.

Elemental analysis was carried out using a CHN(S) analysator by Elementar.

Materials: Tetrahydrofuran (THF) and cyclohexane have been purified by consecutive drying over CaH₂ and potassium with subsequent distillation under nitrogen atmosphere. MeOH has been purified by distillation. Et₃N (Aldrich, >99%), 1,3-diisopropenylbenzene (97%, Aldrich), *N,N,N',N',N''*-pentamethyldiethylenetriamine (99%, Aldrich) and ethylene sulfide (98%, Aldrich) have been dried over CaH₂, distilled, degassed by freeze-pump-thaw (three cycles) and stored at 5 °C under argon. Isoprene (98%, Acros) has been consecutively dried over CaH₂ and di-*n*-butylmagnesium (1 M in Heptan, Aldrich), distilled, degassed (by freeze-pump-thaw, three cycles) and used immediately. Styrene has been dried over CaH₂, distilled, degassed (by freeze-pump-thaw, three cycles) and used immediately. *Tert*-butyllithium (Sigma-Aldrich, 1.6 M in pentane), sodium borohydride (NaBH₄, \geq 99.99%, Sigma-Aldrich), gold(III) chloride trihydrate (HAuCl₄·3H₂O, \geq 99.9%, Sigma-Aldrich), silver(I) nitrate (AgNO₃, \geq 99.9%, Sigma-Aldrich), ascorbic acid (99 %, Sigma Aldrich) and hexadecyltrimethylammonium bromide (CTAB, 99%, Merck) were used as received.

Preparation procedure of TISIT: 20.0 mL (32.0 mmol) *tert*-butyllithium solution were cooled to -20 °C and charged with 4.44 mL (32.0 mmol) Et₃N after which 2.72 mL (16.0 mmol) 1,3-diisopropenylbenzene was added dropwise at -20 °C with subsequent stirring for 5 h. This initiator solution was used without further purification. 500 mL cyclohexane were degassed and titrated with the initiator solution at 0 °C until a slight color stayed constant. After addition of 15.0 mL (9.00 mmol) of the initiator solution, 10.3 mL (90.0 mmol) styrene were injected quickly. The solution was heated to 45 °C and stirred for 90 min. 18.0 mL (180 mmol) isoprene were added quickly, followed by stirring for 18 h at 45 °C. 30.0 mL (144 mmol) *N,N,N',N',N''*-pentamethyldiethylenetriamine were added at room temperature, stirred for 1 h, after which 1.13 mL (18.9 mmol) ethylene sulfide were added. The solution was stirred for 2 h, concentrated and precipitated in degassed MeOH. The supernatant was decanted under Ar atmosphere and TISIT was dried *in vacuo*. $M_n = 4800$, $M_w = 6000$, PDI = 1.25 (calculated from GPC-MALLS). Block length ratio styrene:isoprene = 21:37, equals 36% molar styrene content (calculated from ¹H-NMR). $T_g = -42$ °C (calculated from DSC).

Preparation of AuNR@CTAB: According to a protocol recently published by Vigdermann et al.²⁶ seeds were prepared by mixing 10 mL of a 0.2 M aqueous CTAB solution with 10 mL of a 0.5 mM aqueous HAuCl₄ x H₂O solution, prepared by the addition of 50 μL of a 0.1 M HAuCl₄ x H₂O solution to 10 mL water. Subsequently, 120 μL of a freshly prepared 0.2 M NaBH₄ solution was quickly added under vigorous stirring at 1200 rpm. After 2 min of stirring the solution was allowed to age undisturbed for 30 min. GNR growth was performed in 1 L of a 0.1 M CTAB solution containing 0.5 mM HAuCl₄ at 32 °C. The gold concentration was adjusted by adding 5 mL of a 0.1 M aqueous HAuCl₄ stock solution. AgNO₃ concentration was adjusted to a final concentration of 0.4 mM by adding 4 mL of a 0.1 M aqueous AgNO₃ solution followed by the addition of 50 ml of an aqueous 0.1 M hydroquinone solution. The solution was stirred until colorless (3 min). GNR growth was induced by the addition of 15 mL of the as prepared seed solution. Growth was performed at 32 °C over night. Please find experimental details for the preparation of AuNR with shorter aspect ratios in the Supporting Information.

Preparation procedure of hybrid nanocomposite AuNR@TISIT + AgNP: 1.21 mg (244 μmol) AuNR@TISIT were dissolved in 30 mL THF and charged with 269 mg (1.22 μmol) AgCO₂CF₃ (98%, Acros, recrystallized from Et₂O), followed by slow addition of 4.88 mL (4.88 mmol) lithium triethylborohydride (Sigma-Aldrich, 1 mol L⁻¹ in THF). After stirring for 30 min the solution was precipitated in MeOH, after which the supernatant was

decanted and the residue dried to constant weight. 1.09 g of a dark brown elastomer was obtained. Au content: 1.9 wt.%; Ag content: 9.3 wt.% (determined by TGA ash yield analysis).

Preparation procedure of CTAB@AuNR with AR of 2.1 and 3.0: Following a modified procedure published by Nikoobakht and El-Sayed (B. Nikoobakht, M. A. El-Sayed, *Chem. Mater.* **2003**, *15*, 1957), seeds were prepared by adding 25 μL of an aqueous 0.1 M HAuCl_4 stock solution to 10 mL of an aqueous 0.1 M CTAB solution. The mixture was stirred at 1200 rpm and reduction was performed by quick addition of 600 μL of a freshly prepared 0.01 M NaBH_4 solution at RT. After 2 min stirring was stopped and seeds were aged undisturbed for 30 min. For nanorod growth 1 L (AR 3.0) or 500 mL (AR 2.1) of a 0.1 M CTAB solution in water were prepared at 32 $^\circ\text{C}$ to ensure CTAB solubility. Subsequently, 2.5 mL (AR 3.0) or 1.25 μL (AR 2.1) of aqueous 0.1 M HAuCl_4 solution were added to yield a 0.25 mM HAuCl_4 solution followed by the addition of 8 mL or 4 mL of an aqueous 5 mM AgNO_3 solution resulting in a final concentration of 0.04 mM AgNO_3 . The pH was adjusted to 3-4 by adding 3.25 mL of a 0.1 M aqueous HBr solution. Finally, 3.75 mL of a 0.1 M aqueous ascorbic acid solution was added going along with a change in color from yellow to colorless. With the addition of 7 mL (AR 3.0) or 0.6 mL (AR 2.1) seeds the growths of nanorods was initiated. The solution was kept at 32 $^\circ\text{C}$ undisturbed overnight.

Characterization of AuNR@CTAB

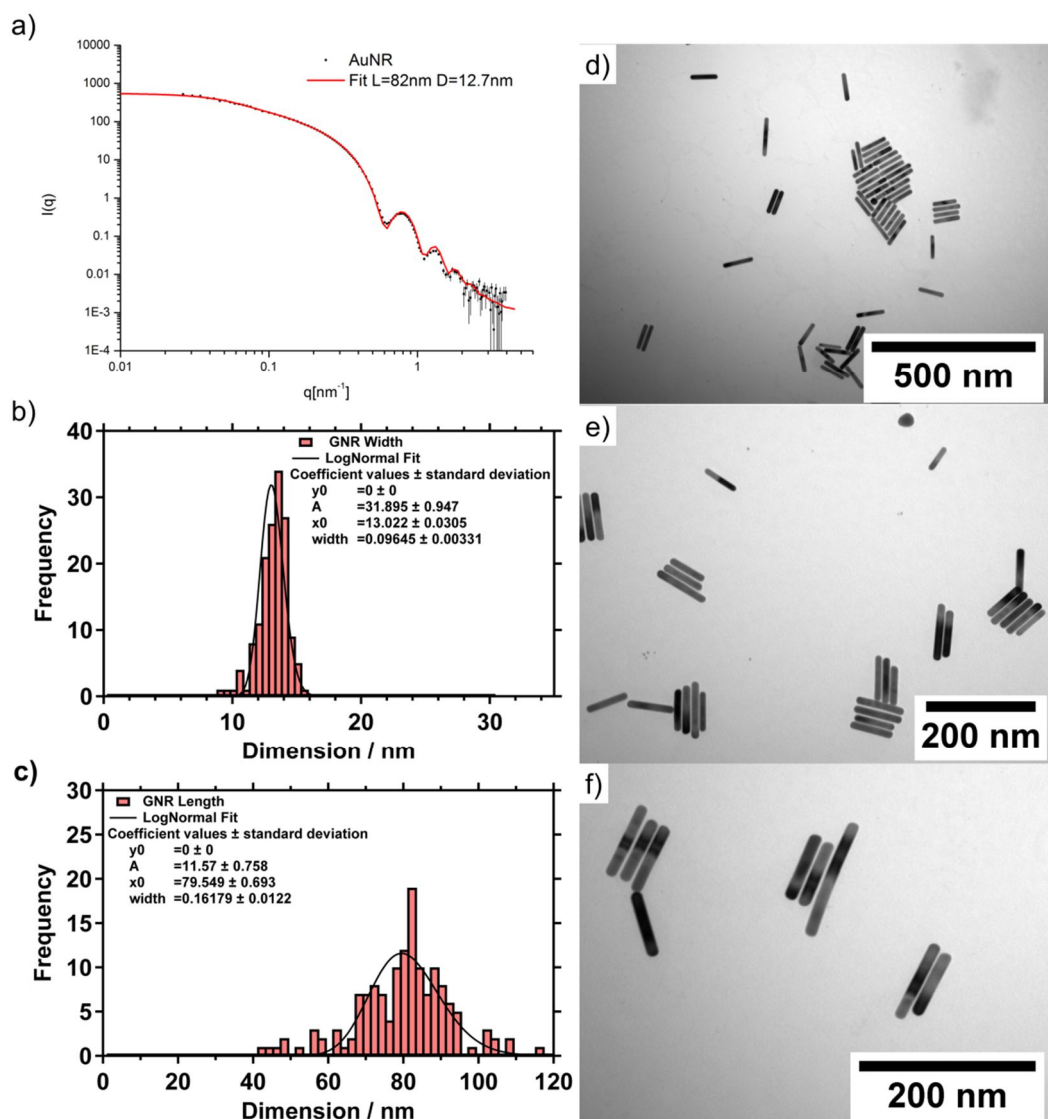


Figure 5-S1: Characterization of AuNR@CTAB in aqueous dispersion. a) SAXS measurements exhibit scattering responses characteristic for non-aggregated, well-stabilized AuNR. b) Frequency distribution of AuNR widths, derived from TEM images. c) Frequency distribution of AuNR lengths, derived from TEM images. d)-f) Representative TEM images of AuNR@CTAB.

Characterization of TISIT

TISIT with a molecular weight of 4800 g/mol (determined by GPC-MALLS), a molar styrene content of 36% (determined by $^1\text{H-NMR}$ by comparing characteristic oligostyrene signals at $\delta = 6.51\text{--}7.14$ ppm with oligoisoprene signals at $\delta = 4.72\text{--}5.17$ ppm) and a 1,4-:3,4-oligoisoprene ratio of 84:16 (determined by $^1\text{H-NMR}$ by comparing the respective signals at $\delta = 5.17$ ppm and $\delta = 4.72\text{--}4.79$ ppm) is prepared *via* sequential anionic polymerization of styrene and isoprene, starting with an difunctional lithium initiator. Thiol end groups are obtained by subsequent ring-opening of ethylene sulfide by the living ABA block co-oligomer. **Figure 5-S2** includes a summary of the preparation route as well as the $^1\text{H-NMR}$ spectrum and the GPC elugram.

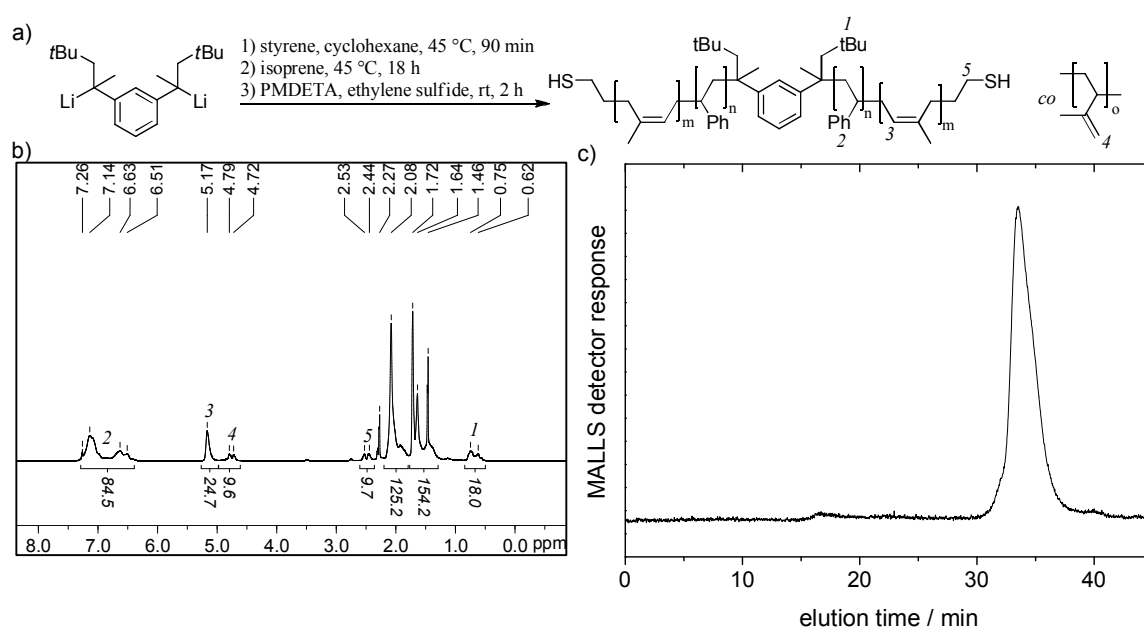


Figure 5-S2. Preparation and Characterization of TISIT. a) TISIT is prepared by anionic polymerization of styrene and isoprene with subsequent end-capping using ethylene sulfide. b) $^1\text{H-NMR}$ spectrum of TISIT. The molar styrene content of 36% was calculated from comparing the signals the characteristic signals for oliostyrene at $\delta = 6.51\text{--}7.14$ ppm with oligoisoprene signals at $\delta = 4.72\text{--}5.17$ ppm. The 1,4-:3,4-oligoisoprene ratio of 84:16 was calculated from comparing the respective signals at $\delta = 5.17$ ppm and $\delta = 4.72\text{--}4.79$ ppm. c) GPC-MALLS elugram of TISIT showing monomodal molecular weight distribution. A molecular weight of $M_n = 4800$ g/mol was calculated (PDI = 1.25).

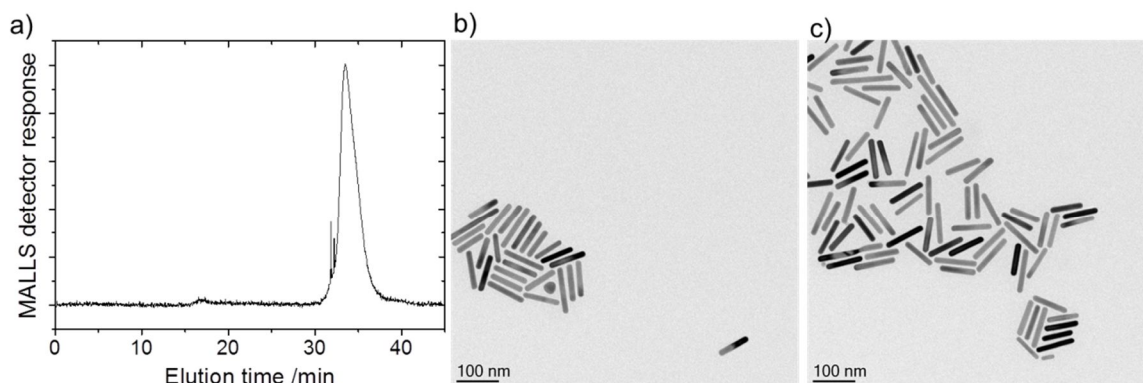
Characterization of AuNR@TISIT

Figure 5-S3. Separation of grafted and unbound TISIT in AuNR@TISIT dispersion. A diluted dispersion was centrifuged at 14,000 rpm for 60 min after which the supernatant was characterized by GPC and the residue by TEM. a) GPC-MALLS trace of the supernatant shows a signal for TISIT which proves the presence of unbound TISIT chains in AuNR@TISIT materials. b) As a consequence from centrifugation, AuNR agglomerate to clusters, but remain sterically protected against flocculation.

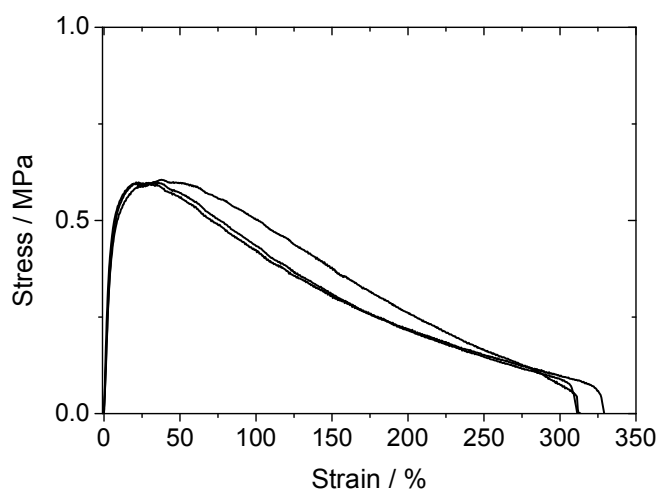


Figure 5-S4. Stress-Strain curves of AuNR@TISIT. E-Modulus = 7.1 ± 1.3 MPa.
Tensile strength = 0.60 ± 0.01 MPa.

Physically cross-linked hybrid nanocomposite network

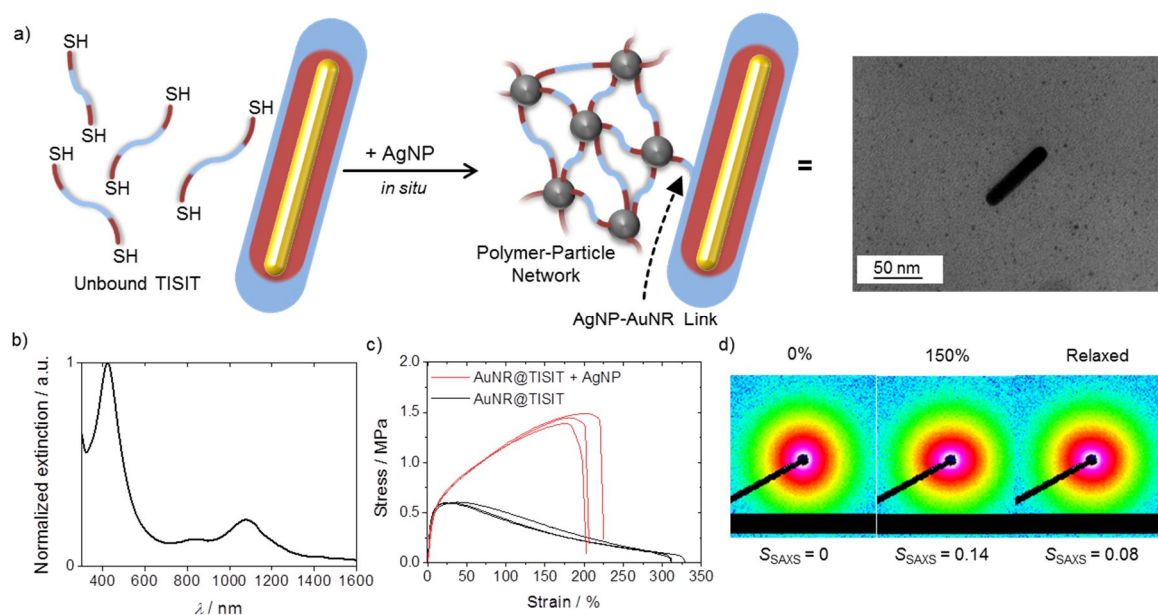


Figure 5-S5. a) Unbound TISIT telecheles within AuNR@TISIT nanocomposite are cross-linked using small AgNP with diameters of $d_{\text{AgNP}} = 2.6 \pm 0.4$ nm as cross-linking sites. AgNP are prepared *in situ* by reduction of AgCO_2CF_3 with lithium triethylborohydride in homogeneous THF solution. Scheme is not true to scale.

TEM images of this hybrid nanocomposite prove the coexistence of AgNP and AuNR. b) Extinction spectrum of AgNP-charged AuNR@TISIT, redispersed in THF for a duration of 2 d, shows plasmon resonance modes of both AgNP at $\lambda = 423$ nm and AuNR at $\lambda = 1077$ nm. c) Engineering stress-strain curves reveal a considerable improvement of mechanical properties as a consequence from cross-linking with E-Moduli increasing from 7.1 ± 1.3 MPa to 8.0 ± 1.2 MPa and tensile strengths increasing from 0.60 ± 0.01 MPa to 1.45 ± 0.06 MPa. d) SAXS measurements of a film at 0% and 150% elongation as well as in the relaxed state after elongation. In the stretched state, AuNR tend to align along the axis of elongation.

Relaxation of the same film causes the AuNR to return to a less ordered orientation.

Cross-linking of AuNR@TISIT with small, spherical silver nanoparticles yielded a hybrid nanocomposite network from coexisting AuNRs (1.9 wt%) and small AgNPs (9.3 wt%) with diameters of $d_{\text{AgNP}} = 2.6 \pm 0.4$ nm (**Figure 5-S5a**). Mechanistically, AgNP occupy the unbound thiol end groups of the TISIT matrix. Possible dangling chain ends emerging from the AuNR surface may supply a link between the two particle types. As a result, a soft material of low solubility is obtained, having characteristic plasmon resonance modes of both spherical AgNP at 438 nm and AuNR (**Figure 5-S5b**) at 1149 nm as well as considerably improved tensile properties (**Figure 5-S5c**). SAXS measurements show characteristic signals corresponding to both AgNP and to AuNR with the latter being randomly distributed with respect to their orientation (**Figure 5-S5d**). Through stretching the film to 150% elongation, the SAXS scattering patterns reveal that AuNR tend to align

into the direction of stretching with the orientational order parameter S_{SAXS} (calculated from the corresponding orientational distribution (OD) functions with 0 standing for random orientational distribution and 1 for perfect alignment) being increased from 0 to 0.14. The orientation is partially reversible as S_{SAXS} reduces down to 0.08 upon relaxation of the elastic film.

Characterization of AuNR@TISIT, embedded in Kraton FG1901x

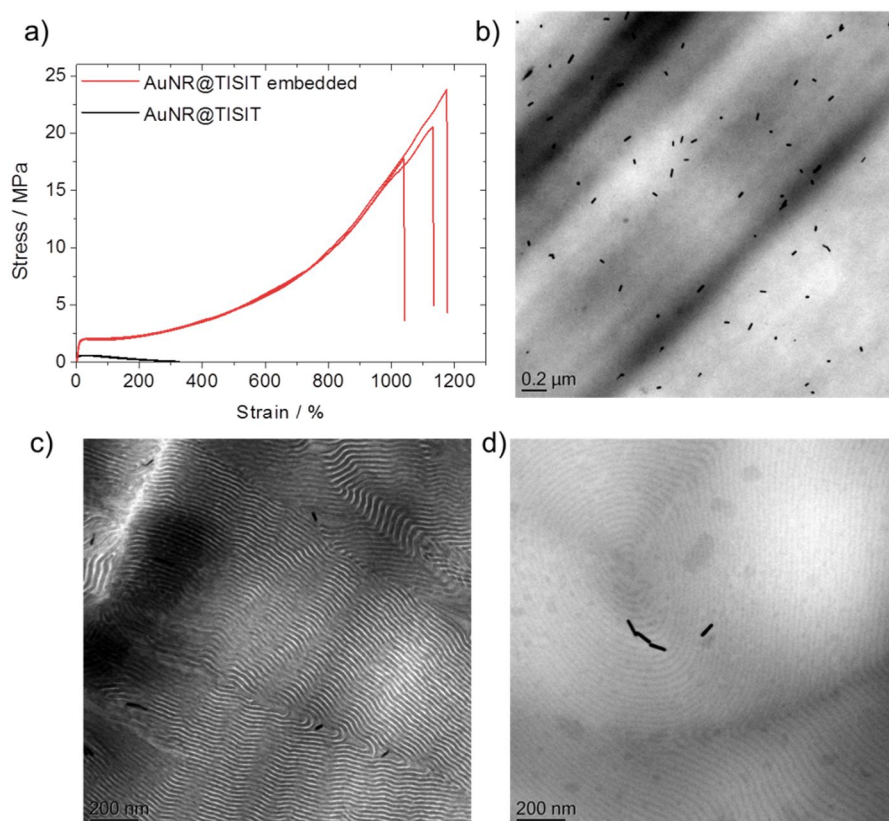


Figure 5-S6: Embedding of AuNR@TISIT in Kraton FG1901x by co-precipitation from THF. a) Stress-strain curve of neat and embedded AuNR@TISIT. E-Modulus increases from 7.1 ± 1.3 MPa to 20.3 ± 2.4 MPa. Tensile strengths increase from 0.60 ± 0.01 MPa to 20.7 ± 3.0 MPa. b) TEM micrographs of cryo-cut, freshly hot pressed films of Kraton FG1901x-embedded AuNR@TISIT, showing homogenous distribution of isolated particles. c-d) TEM micrographs of cryo-cut, RuO₄-stained Kraton FG1901x-embedded AuNR@TISIT film made by solvent evaporation from THF reveal that AuNR are not selectively dispersed in one of the matrix microphases.

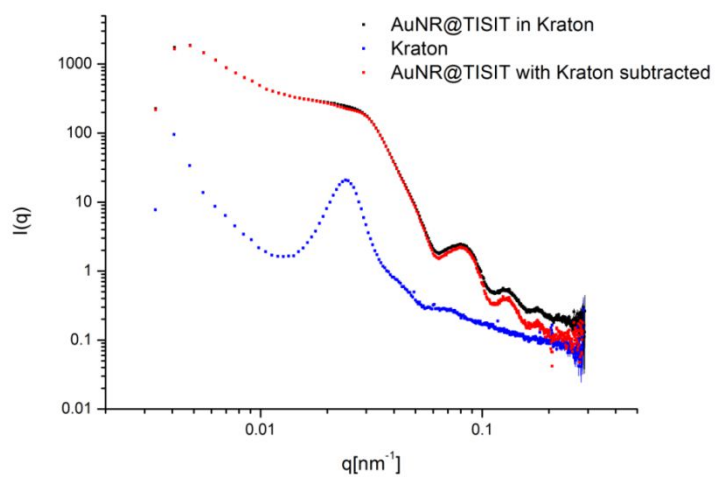


Figure 5-S7. SAXS response is dominated by AuNR. Kraton FG1901x only adds very little signal to the scattering curve and is therefore not included in fitting and calculation of the orientational distribution functions.

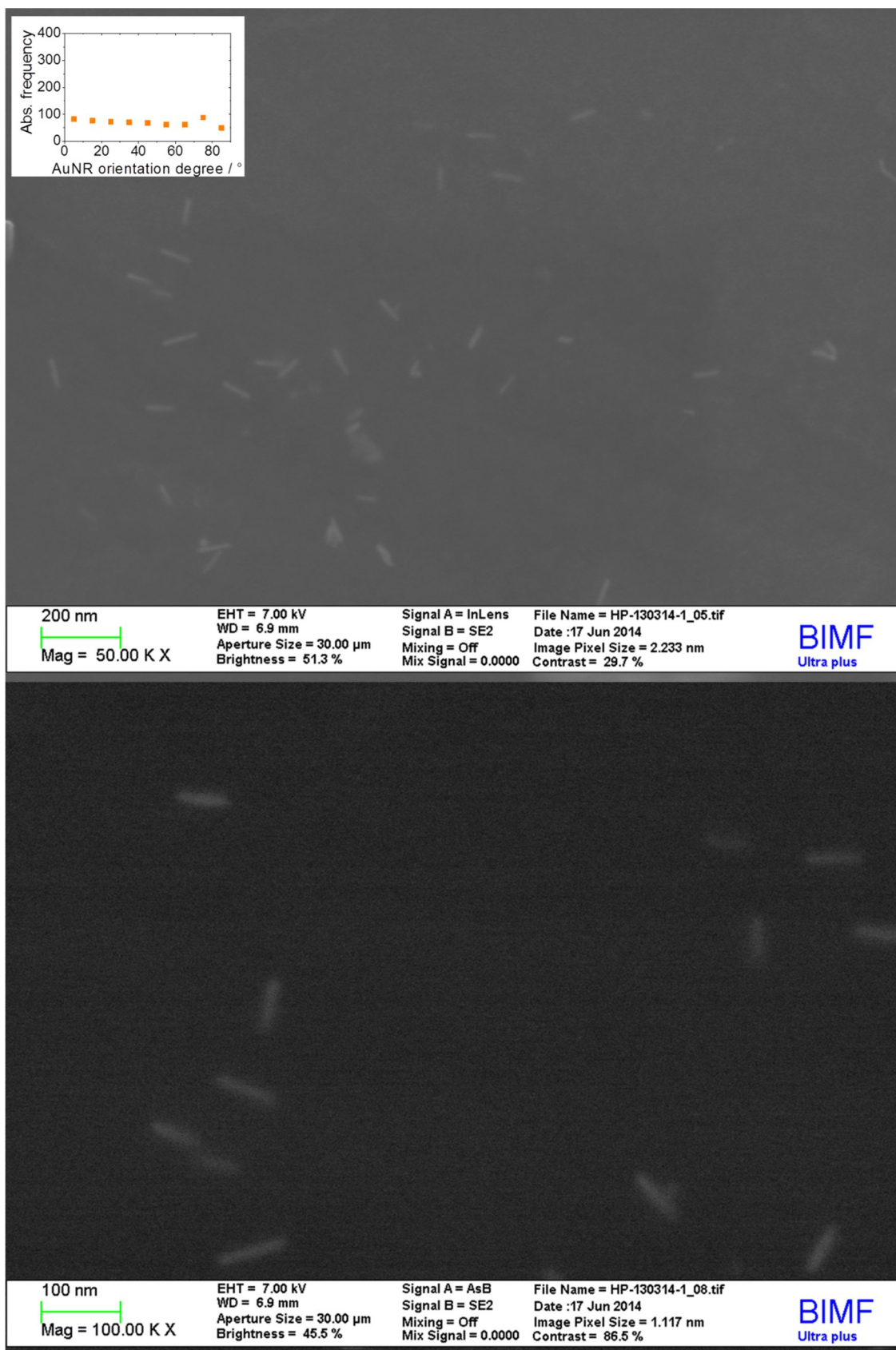


Figure 5-S8: SEM micrographs of AuNR@TISIT embedded in Kraton FG1901x at 0% elongation, including the corresponding OD function.

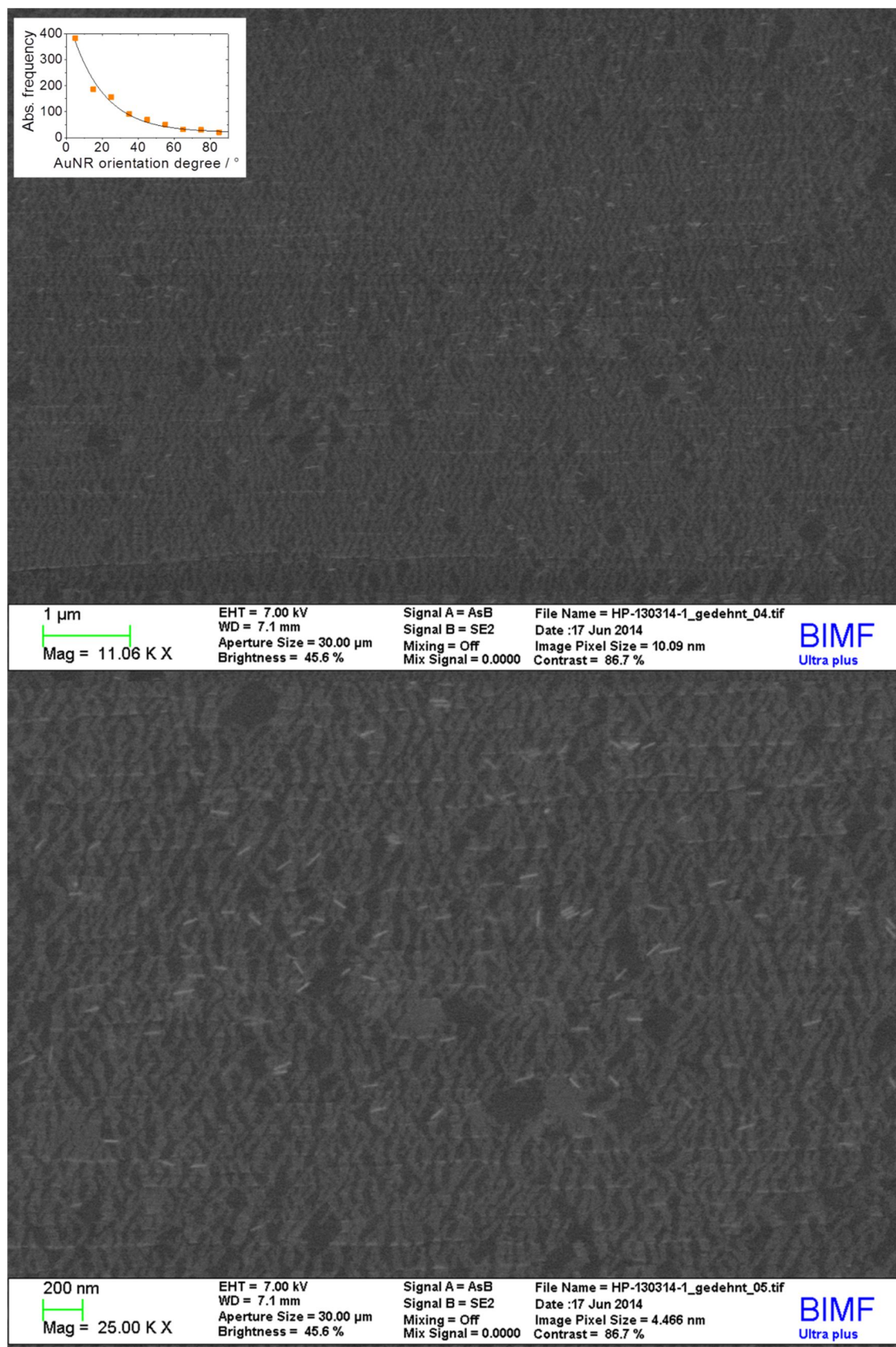


Figure 5-S9: SEM micrographs of AuNR@TISIT embedded in Kraton FG1901x during elongation to 300%, including the corresponding OD function.

TEM characterization of AuNR@CTAB with AR = 2.1 and 3.0.

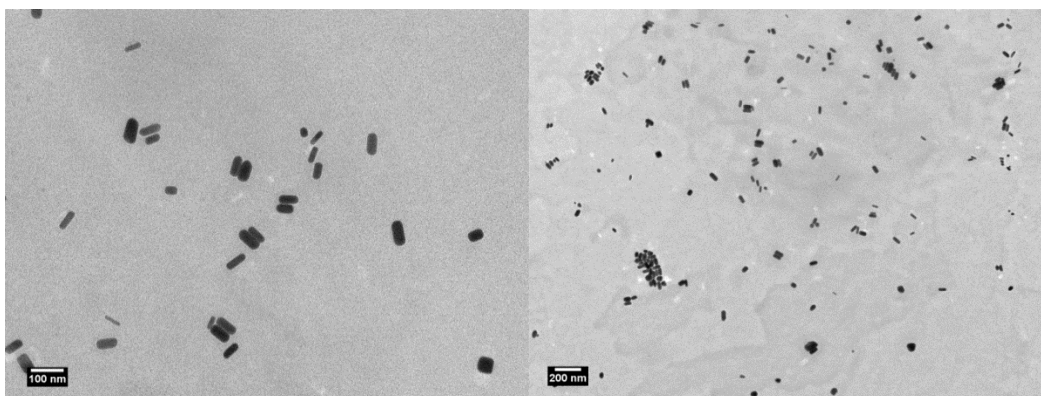


Figure 5-S10: TEM micrographs of AuNR@CTAB with AR = 2.1.

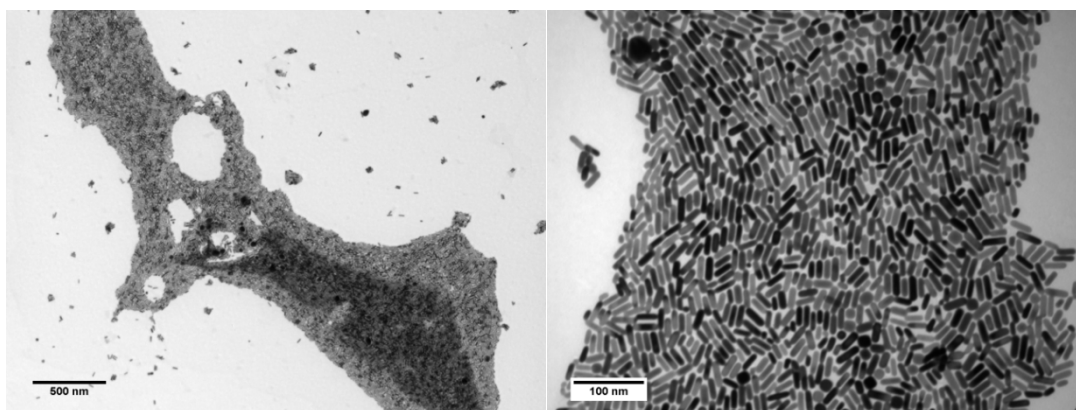


Figure 5-S11: TEM micrographs of AuNR@CTAB with AR = 3.0.

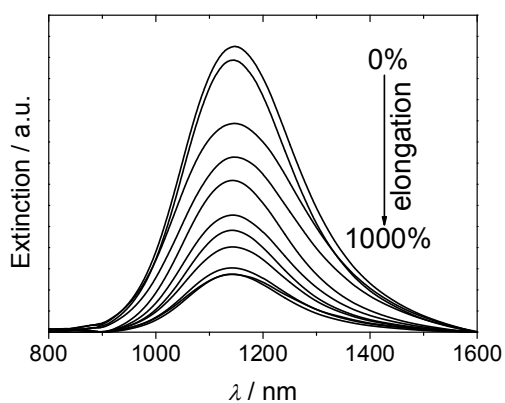


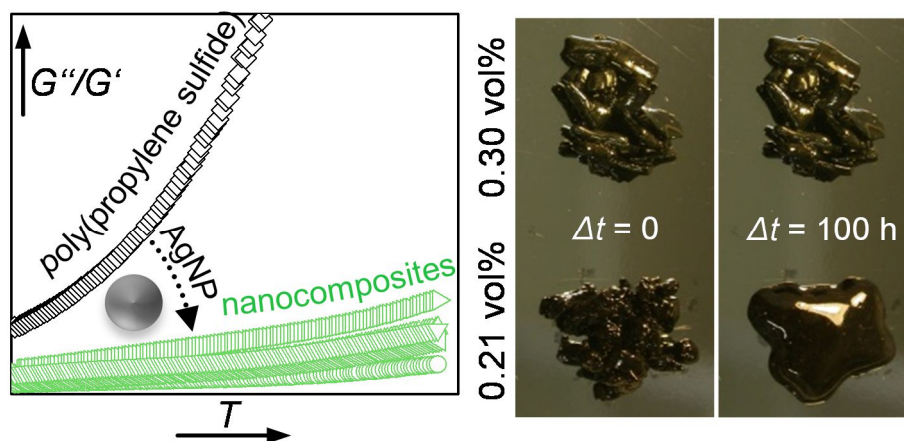
Figure 5-S12. Extinction plots of AuNR@CTAB, embedded in Kraton FG1901x as a function of elongation. This experiment was performed three times (here shown exemplarily: one out of three experiments) and the averaged data was used to calculate S_{L-LSPR} (cf. Figure 3d) according to **Equation 1**.

CHAPTER 6

MECHANICAL REINFORCEMENT OF POLYDENTATE THIOETHER LIGAND BY SILVER NANOPARTICLES

*Holger Pletsch, Andreas Greiner and Seema Agarwal**

Faculty of Biology, Chemistry and Earth Sciences, Macromolecular Chemistry II and Bayreuth Center for Colloids and Interfaces, University of Bayreuth, Universitätsstraße 30, 95440 Bayreuth, Germany. Fax: (+) 49921553393. E-mail: agarwal@uni-bayreuth.de



Published in *Nanoscale*, year 2015, volume 7, pages 1977-1983. Reprinted with permission. Copyright Royal Society of Chemistry.

ABSTRACT

Linear polydentate poly(propylene sulfide) (PPrS) is introduced as a liquid thioether ligand for silver nanoparticles, providing colloidal stability against aggregation also under demanding conditions. Very low amounts (0.30 vol%) of AgNPs lead to significant mechanical reinforcement of PPrS, yielding viscoelastic properties of an unfastened network with solid-like elastic responses at mechanical stimulation. The materials are made by ring-opening anionic polymerization of propylene sulfide to yield high molar mass PPrS with a total of 593 thioether functionalities per chain, followed by a simple *in situ* “grafting to” method to homogeneously incorporate AgNPs into the polymer matrix. From investigations on the chain dynamics using dynamic rheology it is concluded that well-dispersed AgNP impose additional topological constraints on the polymer chains. Calculations of the statistical interparticle distances support a tele-bridging polymer-particle arrangement.

KEYWORDS

Poly(propylene sulfide), Silver Nanoparticles, Reinforcement, Chain Dynamics

INTRODUCTION

Polymer-grafted metal nanoparticles have been subject to a plethora of studies, including but not limited to those with a focus on nanomaterials,^[1-5] on interaction with biological systems^[6-8] and on plasmonic applications.^[9-12] Most decisive considerations for the design of such symbiotic nanocomposites not only include the right choice of polymer type, but also of a suitable anchor group as well as its position and quantity in the polymer chain. Despite of being the “gold standard” anchor group for noble metal nanoparticles such as Ag or Au for good reasons, thiols can also be a handicap if used as anchor groups in polymers. First, thiols may only be structurally located at the termini of polymer main or side chains and second, their considerable sensitivity towards photodegradation by UV light^[13,14] and oxidation^[15] impedes real-world applications. Thioether groups overcome these drawbacks and have been identified suitable for stabilizing noble metal nanoparticles both in experiment^[16,17] and in simulation.^[18] While oligomeric^[19,20] and dendritic^[21,22] thioether ligands were shown to wrap around noble metal nanoparticles, herein our aim is to use linear, high molar mass polydentate thioethers in order to design a polymer-particle network microstructure in which metal nanoparticles act as structural reinforcing sites. Therefore, we present for the first time poly(propylene sulfide) (PPrS) as a liquid polydentate thioether ligand for silver nanoparticles (AgNP).

Although metal nanoparticles are well known for their capacity to contribute to chemical, physical and also biological properties in nanocomposite materials, their potential as cross-linking and reinforcing agents is still largely unexplored. Only recently, thermally processable elastomers have been designed from polymer-particle networks in which bidentate (telechelic) α,ω -dithiol oligomers were grafted to AgNP.^[23, 24] In this context, Zhang et al. pioneered in suggesting a polymer-particle network microstructure from linear, polydentate poly(ethylene oxide) with high molar masses (ranging from 45 000 to 292 000 g mol⁻¹) and silica nanoparticles.^[25] However, the authors reported that homogeneous dispersions of silica particles in the polymer matrix well below the percolation threshold were subject to thermal instability, leading to particle flocculation and therefore, to a reduced specific surface area. Improved colloidal stability of silica nanoparticle-polymer networks was provided *via* covalent polymer-particle bonding, for instance induced by additional silane coupling agents as shown for the preparation of hydrogel networks.^[26] It is further known that by exceeding the percolation threshold, liquid polymers such as non-cross-linked 1,4-polybutadiene^[27] and poly(dimethyl

siloxane)^[28] undergo reinforcement if charged with silica nanoparticles at high filling rates, leading to continuous particle-particle networks. In the present work we will show that already low AgNP filling rates below the percolation threshold are sufficient to trigger significant reinforcement of PPrS, accompanied by high colloidal stability.

RESULTS

Linear PPrS with high purity (**Figure 6-1a**) was obtained as a viscous, colorless liquid *via* ring-opening anionic polymerization of propylene sulfide along the lines of a previously published procedure.^[29] Subsequent end-capping using ethyl bromoacetate successfully suppressed formation of thiol end groups as seen in the Raman spectrum (**Figure 6-1b**).^[13]

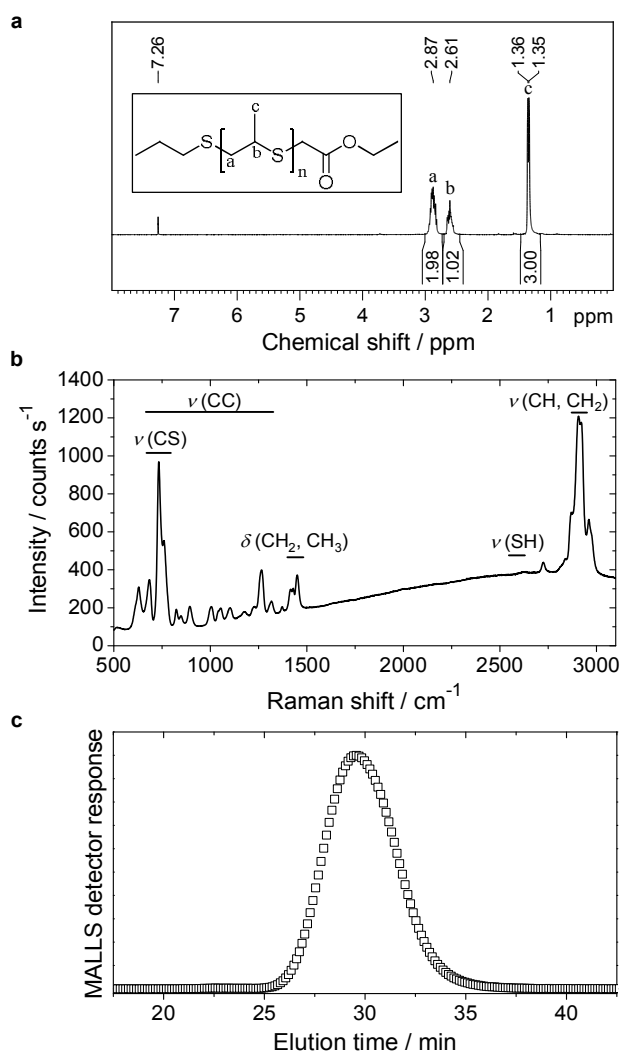


Figure 6-1. Characterization of PPrS. a) ¹H-NMR spectrum of PPrS showing characteristic signals of the repeating unit. The absence of monomer, initiator or solvent signals indicate a high purity of PPrS. Inset: Structure of PPrS used herein with $n = 593$. b) Raman spectrum of PPrS. Signals corresponding to S-H vibrations are absent. c) GPC elution chromatogram of PPrS from multi angle laser light scattering (MALLS) detector at 90°. The signal maximum is identified at 29.5 min which corresponds to $M_n = 44000$ g/mol.

A total of 593 thioether units per polymer chain is calculated from $M_n = 44000 \text{ g mol}^{-1}$, determined by GPC with multi angle laser light scattering detector (MALLS) (**Figure 6-1c**).

Grafting of PPrS as a polydentate ligand to AgNP was performed using an *in situ* method in which different feed amounts of THF-soluble AgCO_2CF_3 were employed as the AgNP precursor and Superhydride® as the reducing agent to yield AgNP filling rates ϕ ranging from 0.13 to 0.95 vol%. The resulting materials are designated as for example PPrS@AgNP_{0.13} with subscript 0.13 representing ϕ in vol% (**Table 6-1**).

Table 6-1. PPrS made from ring-opening anionic polymerization of propylene sulfide is charged with varying amounts of AgNP to yield PPrS@AgNPs. Significantly altered material properties are observed as a function of the AgNP filling fraction ϕ .

AgNP filling fraction ϕ [vol%]	d_{AgNP} [nm] ^{a)}	T_g [K] ^{b)}	Material Appearance
0	-	235	Viscous Liquid
0.13	14.4 ± 3.6	235	Very Soft Material
0.21	14.3 ± 4.0	234	Soft Material
0.30	14.9 ± 4.6	233	Soft Material
0.81	aggregation	234	Very Soft Material
0.95	aggregation	233	Very Soft Material

^{a)} The average AgNP diameters d_{Ag} were calculated from TEM micrographs by measuring at least 150 particles for each sample; ^{b)} Obtained from DSC measurements.

According to TEM investigations, AgNPs are successfully stabilized by PPrS up to a filling rate of $\phi = 0.30$ vol%, being well-dispersed with no signs of particle aggregation (**Figure 6-2**). The presence of a regular AgNP superlattice is not observed which leads us to the conclusion that the nanocomposite is a mixture of AgNP-grafted PPrS and excess non-grafted PPrS chains. Localized surface plasmon resonance responses characteristic for AgNP were observed in absorption spectroscopy (please find details in the supporting information; Figure 6-S1). The colloidal stability of PPrS@AgNP was maintained even under demanding conditions such as during hot pressing at 353 K and 300 bar pressure or during long-term exposure to high temperatures (7 h at 343 K) as TEM micrographs did not unfold changes in particle sizes and morphology. The high particle stability is assumed to be due to a virtually ubiquitous presence of anchor groups. Please find information about further experiments on thermal stability in the supporting information (Figure 6-S2).

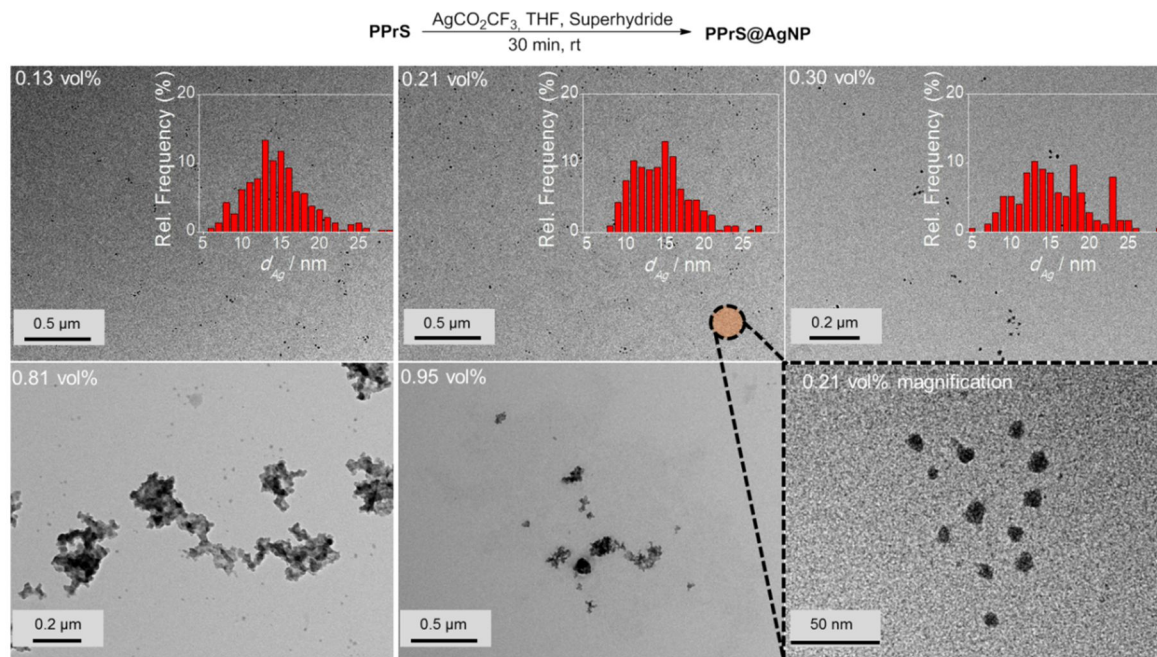


Figure 6-2. Above: *in situ* preparation procedure of PPrS@AgNP. Below: representative TEM micrographs of PPrS@AgNPs, redispersed in THF. Nanoparticles are well-dispersed and stable against aggregation. Only at $\phi \geq 0.81$ vol%, particle aggregation reduces the specific AgNP surface area. Insets: Corresponding diameter distributions for the samples with isolated particles. Bottom right image: Magnification image of PPrS@AgNP_{0.21}.

In particular, samples PPrS@AgNP_{0.21} and PPrS@AgNP_{0.30} appear as soft materials with high extensibility, showing ultimate elongations of $906 \pm 77\%$ and $1011 \pm 142\%$, respectively, in linear uniaxial tensile testing (**Figure 6-3**). With tensile strengths of 106 ± 10 Pa for PPrS@AgNP_{0.21} compared to 212 ± 18 Pa for PPrS@AgNP_{0.30} we observed a strong impact of the AgNP filling rate on the material properties.

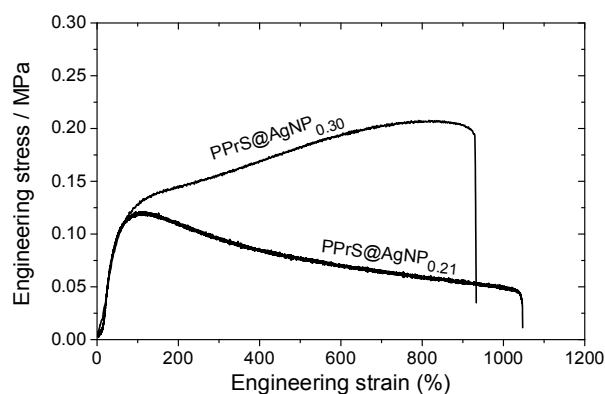


Figure 6-3. Linear uniaxial tensile testing. Representative engineering stress-strain curves of PPrS@AgNP_{0.30} (upper curve) and PPrS@AgNP_{0.21} (lower curve) from linear uniaxial tensile testing.

Improved tensile strength and flow suppression is obtained with increasing ϕ .

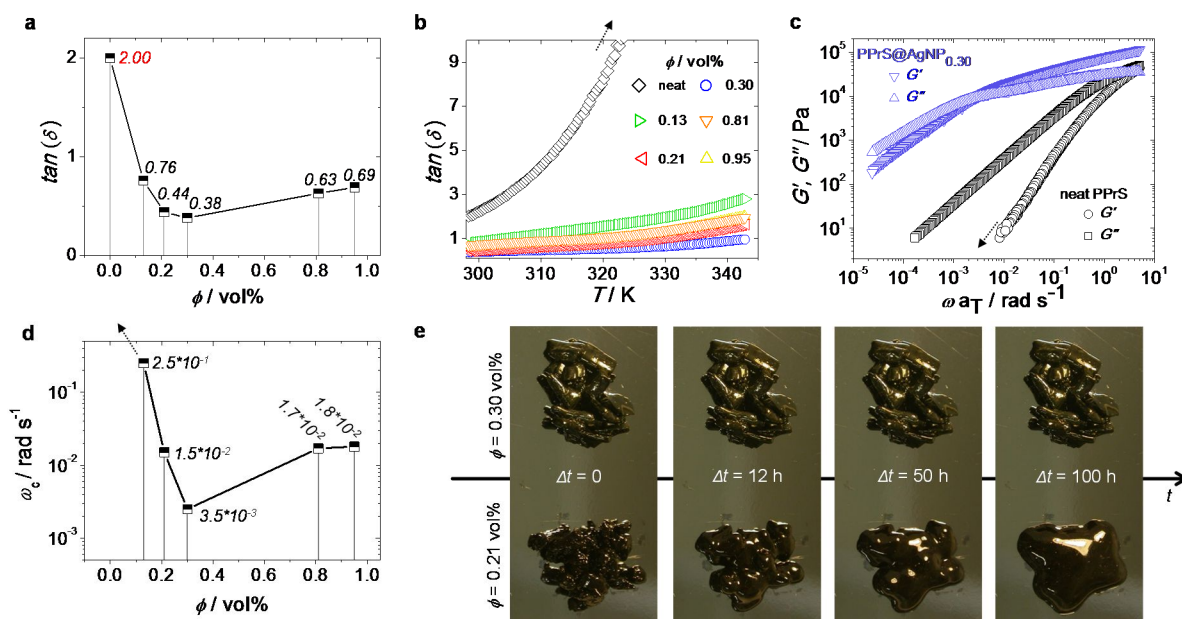


Figure 6-4. ϕ - and T -dependent viscoelastic behavior. a) Plot of the loss factors $\tan(\delta)$ as a function of ϕ at $T = 298$ K and $\omega = 1$ rad s $^{-1}$ for both neat PPrS and PPrS@AgNP samples (italic typed values represent the exact loss factor of the corresponding sample). Elasticity increased significantly after AgNP addition, reaching extreme value at $\phi = 0.30$ vol%. Standard deviations are below 1% for all samples and therefore, not cited. b) Loss factors $\tan(\delta)$ of neat PPrS and PPrS@AgNP samples as a function of temperature (heating rate $\Delta T = 0.5$ K min $^{-1}$; $\omega = 1.0$ rad s $^{-1}$). The softening degree according to the slopes is damped down for PPrS@AgNP samples in comparison to neat PPrS. c) G' and G'' master curves of neat PPrS and PPrS@AgNP $_{0.30}$ from frequency-temperature superposition (FTS). For clarity, master curves of the other samples are not shown here, but can be found in the supporting information (Figure 6-S3). The G' trace of neat PPrS is cropped as the rheometer detection limit is reached. d) G' - G'' crossover frequency ω_c as a function of ϕ (italic typed values represent the exact crossover frequency of the corresponding sample). The trend shown here is comparable to the loss factors depicted in part a) of this figure with PPrS@AgNP $_{0.30}$ exhibiting the most increased relaxation times within the sample set. e) Demonstration of flow behavior at $T = 293$ K without external stimuli. PPrS@AgNP $_{0.21}$ exhibits liquid flow up to formation of a droplet, whereupon PPrS@AgNP $_{0.30}$ remains form-stable in the same time range.

The degree of reinforcement is quantified using dynamic rheology at both 298 K and at elevated temperatures. Measurements at constant conditions ($T = 298$ K, angular frequency $\omega = 1.0$ rad s $^{-1}$) were performed, followed by determination of the loss factors $\tan(\delta) = G''/G'$ (shear loss modulus/shear storage modulus) as a function of ϕ (Figure 6-4a) in order to quantify the impact of AgNP on the viscoelastic properties. Through grafting with AgNP, the loss factors are heavily decreased, yet ϕ was found to be a variable of major importance. A minimum of $\tan(\delta) = 0.38 \pm 0.003$ is identified for $\phi = 0.30$ vol% which represents the most effective reinforcement scenario as here the elastic portions preponderate to a large extent. In context, reinforcement of non-cross-

linked liquid polymers has also been accomplished by using carbon black^[30] and spherical silica nanoparticles;^[25,31] yet much higher filling rates were employed in these works. At filling rates of $\phi = 0.81$ and 0.95 vol%, AgNP aggregation impairs polymer-particle interactions leading to slight increase in $\tan(\delta)$. Temperature-dependent measurements at constant $\omega = 1.0 \text{ rad s}^{-1}$ show stepless softening for all samples, resulting in less elastic behavior at elevated temperatures (**Figure 6-4b**). The degree of softening can be derived from the slopes of the temperature-dependent loss factor curves with steep ascending slopes representing a high affinity towards temperature-induced softening. By addition of AgNP, slopes are significantly damped down; therefore softening of PPrS@AgNP is suppressed in comparison to the neat polymer.

In the following, we probe the chain dynamics of our samples in order to approach the origin for reinforcement. From DSC measurements it is known that the segmental chain dynamics are not affected by AgNP addition (cf. **Table 6-1**). Insight into the frequency-dependent viscoelastic behavior was provided *via* assumption of frequency-temperature superposition (FTS) for frequency sweep experiments in a dynamic rheology setup at $T = 298\text{-}343 \text{ K}$ in $\Delta T = 5 \text{ K}$ steps, yielding G' and G'' master curves (those of neat PPrS and PPrS@AgNP_{0.30} are presented in **Figure 6-4c**; please find those of the other samples in the supporting information; Figure 6-S3). We find liquid-like viscoelastic properties for the nanocomposites with $G'' > G'$ at low frequencies; however we also observe clear alterations concerning the terminal relaxation time as a function of ϕ . Most notably, the PPrS@AgNP $G'-G''$ crossover frequencies ω_c significantly shift to lower frequencies compared to neat PPrS. Following the same trend as observed during evaluation of $\tan(\delta)$ from constant measurement conditions (cf. **Figure 6-4a**), PPrS@AgNP_{0.30} is affected most intensively within this sample set with ω_c being shifted more than three orders of magnitude down to $3.5 \cdot 10^{-3} \text{ rad s}^{-1}$ compared to neat PPrS holding $\omega_c > 5 \text{ rad s}^{-1}$ (**Figure 6-4d**). Though longer relaxation time processes are not completely eliminated, the strong shift of ω_c causes PPrS@AgNP_{0.30} to maintain form-stability over five days (**Figure 6-4e**) and is therefore regarded as a pseudo-solid.

DISCUSSION

A relaxation enhancement caused by decelerated polymer dynamics at low shear frequencies and simultaneous retention of segmental dynamics as observed for the nanocomposites with respect to the neat system herein (cf. **Figure 6-4c**) is evidence for

additional topological constraints imposed by well-dispersed nanoparticles which have been simulated previously under similar conditions.^[32] It is a challenge to disclose the actual topological polymer-particle arrangement within the nanocomposite. One possible approach is to calculate the statistical averaged interparticle distance Λ by assuming a homogenous particle packing on a cubic lattice along the lines of previous considerations on other polymer-particle systems.^[25,33] Assuming attractive energetic polymer-particle interaction such as simulated for similar systems^[18] and therefore, a closed polymer ligand shell around the particle core, we first calculate the polymer shell thickness according to **Equation 6-1**.

$$R_g = \frac{4\pi}{3} \frac{(r_{AgNP} + \delta_P)^3 - r_{AgNP}^3}{4\pi r_{AgNP}^2} \quad (6-1)$$

where R_g = radius of gyration (PPrS); r_{AgNP} = AgNP radius.

Taking the polymer shell thickness into consideration, the effective particle volume fraction ϕ_{eff} is then calculated from **Equation 6-2**.

$$\phi_{eff} = \phi \left(1 + 3 \frac{\delta_P}{r_{AgNP}} \right) \quad (6-2)$$

Finally, the AgNP interparticle distances Λ are calculated according to **Equation 6-3**.

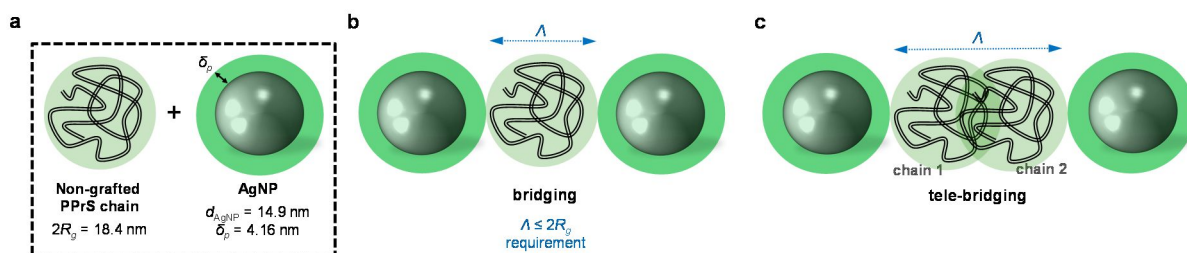
$$\frac{\Lambda}{r_{AgNP}} = \sqrt[3]{\frac{\phi_{Cub}}{\phi_{eff}}} - 1 \quad (6-3)$$

where $\phi_{Cub} = 0.638$ is the maximum packing fraction of particles on a cubic lattice.

In a non-dynamic approach where chain diffusion and particle-induced chain conformation changes such as contraction though attractive polymer-particle interactions are neglected, conclusions can be drawn on the dominating topological polymer-particle arrangement as a function of the interparticle gap size:

(1) If Λ approached 0, a superlattice layout without interjacent non-grafted polymer chains would be the consequence. (2) A scenario where one non-grafted polymer chain is confined by two particles is referred to as bridging (**Scheme 6-1b**) and has been identified accountable for inducing a polymer-particle network and therefore, mechanical reinforcement in previous simulation experiments.^[34,35] Bridging only comes into effect if the interparticle distance Λ is small relative to the polymer dimensions; i.e. $\Lambda \leq 2R_g$. (3) For larger interparticle distances, exceeding $2R_g$, long range polymer-particle-interactions through physical polymer-polymer junctions (entanglements) between at least two polymer chains come into effect (**Scheme 6-1c**). This scenario is also referred to as “tele-bridging” and has been predicted in computer simulations.^[36]

For PPrS@AgNP with $\phi = 0.30, 0.21, 0.13$, polymer shell thicknesses $\delta_p = 4.16, 4.14, 4.15$ nm are estimated from $R_g = 9.2$ nm (determined by GPC with multi angle laser light scattering detector) and $r_{AgNP} = 7.45, 7.15, 7.20$ nm, yielding $\Lambda = 24.6, 27.2, 33.7$ nm, respectively. Thus, Λ approaches $2R_g$ with increasing ϕ ; still $\Lambda > 2R_g$ holds for the non-aggregated nanocomposites. In turn, our PPrS@AgNP materials do not meet the $\Lambda \leq 2R_g$ requirement for bridging nanoparticles over a single polymer chain. However, $\Lambda \leq 4R_g$ applies for our nanocomposites, guaranteeing overlap of two (or more) different polymer chains in between the interparticle gap. Consequently, a tele-bridging scenario becomes plausible for our system. The resulting topological constraints and therefore, the levels of confinement densify with decreasing Λ (i.e. with increasing ϕ) and trap the chains' primitive paths, yielding rather unfastened than permanent networks which explain our experimental results well. We believe that in particular field cycling $^1\text{H-NMR}$ spectroscopy^[37] may provide a promising spectroscopic insight into such particle-and entanglement-mediated networks in future studies.



Scheme 6-1. Simplified illustration of possible topological polymer-particle interaction scenarios for PPrS@AgNP. a) Scheme is true to scale for PPrS@AgNP_{0.30} in which PPrS is regarded as a random coil with a diameter of $2R_g$. AgNPs have average diameters d_{AgNP} of 14.9 nm and a polymer shell thicknesses δ_p of 4.16 nm. b) Direct interparticle bridging comes into effect if the interparticle distance Λ is small relative to $2R_g$. c) Indirect interparticle bridging or “tele-bridging” is a long-range type of bridging where physical interactions (entanglements) between at least two polymer chains indirectly link multiple particles.

CONCLUSION

We conclude that for the first time AgNP could be used as a reinforcing agent for polydentate PPrS already at very low filling rates. AgNP were incorporated by a simple *in situ* method, yielding nanocomposites with high colloidal stability against aggregation also at elevated temperatures. PPrS of high molar mass was converted from a viscous liquid to a soft material having viscoelastic properties of an unfastened network which makes the materials respond elastic at mechanical stimulation but liquid-like on larger time scales.

Yet, solid-like long-term suppression of flow is approached for PPrS@AgNP_{0.30} due to a significant shift of the G' - G'' crossover frequency ω_c . The observed decelerated dynamics at low shear frequencies provide strong evidence for AgNP-imposed additional topological constraints. Calculations on polymer-particle dimensions substantiate a scenario where the chain's primitive paths are loosely trapped by AgNP; thus generating a long-range entanglement-mediated polymer-particle network. In all, we believe that due to various metal type-dependent chemical, physical or biological features, the exploitation of metal nanoparticles as reinforcing agent will rapidly gain momentum for a wide variety of liquid and also cross-linked polymers.

EXPERIMENTAL SECTION

Materials

Tetrahydrofuran has been purified by consecutive drying over CaH₂ and potassium with subsequent distillation under nitrogen atmosphere. MeOH has been purified by distillation. Propylene sulfide (Acros, 98%) has been dried over CaH₂, distilled and stored at 5 °C under argon. Silver trifluoroacetate (98%, Acros) has been purified by recrystallization from Et₂O. Superhydride® (1.0 mol L⁻¹ in THF, Aldrich), S-*n*-propyl thioacetate (Alfa Aesar, 98%), tri-*n*-butyl phosphine (Acros, 95%), NaOMe (Fluka, >97%) and ethyl bromoacetate (Aldrich, 98%) have been used as received.

Instrumentation

The number-average molecular weights (M_n) and the number-average radius of gyration R_g of the neat polymer were determined by gel permeation chromatography (GPC) in THF at 26 °C using a Agilent 1200 series system equipped with a PSS-SDV (10 μm) 50 × 8 mm² pre-column, three linear PSS-SDV (10 μm) 300 × 8 mm² columns at a flow rate of 0.8 mL min⁻¹ (sample concentration 2 mg mL⁻¹) and a Wyatt Dawn Heleos multi angle laser light scattering (MALLS) detector. dn/dc was determined with a PSS DnDc-2010 λ620 device. dn/dc of PPrS was 0.168 mL g⁻¹.

A confocal microscope (LabRAM Division, HORIBA Jobin Yvon) equipped with a Olympus 10x, NA = 0.25 lens, a linear-polarized HeNe laser (633 nm) and a Peltier-cooled CCD camera (-70°C, Synapse) detector situated behind an 1800 grooves/mm grating spectrometer was used for Raman measurements. Spectra were accumulated from 10 measurements at three positions more than 300 μm apart from each other.

A Mettler thermal analyzer 821 DSC was utilized for DSC scans. Temperature and enthalpy calibration was carried out with indium and zinc standards and tested with *n*-octane as a reference. 5 ± 2 mg of the samples were analyzed under nitrogen atmosphere (flow rate 80 mL/min) at a heating rate of 10 K min^{-1} . The glass transition temperature (T_g) was taken as the inflection point of the observed shift in the baseline of the second heating cycle.

$^1\text{H-NMR}$ (300.13 MHz) spectrum was recorded on a Bruker Avance 300 A spectrometer using CDCl_3 as solvent with a concentration of 100 g L^{-1} . The signals were calibrated to the solvent signal. TEM measurements have been done in a Zeiss 922 OMEGA EFTEM at a voltage of 200 kV. Zero-loss filtered images were recorded using a bottom mounted Ultrascan 1000 (Gatan) CCD camera system. Gatan Digital Micrograph 3.9 for GMS 1.4 software was used for image acquisition. Samples have been prepared from solution by drop-casting on a Quantifoil 300 mesh copper grid with carbon coating. For AgNP mean diameter determination, ImageJ (version 1.44p) of the National Institute of Health, USA, has been used.

A Malvern Instruments Bohlin Gemini HR Nano device with a 2 cm stainless steel plate-plate setup in shear strain-controlled mode was used for dynamic rheology. Solid samples were molded into discs with 2 cm diameter. Liquid samples were distributed between the plates without previous molding. The plate-plate gap was kept constant at 1 mm throughout all measurements. The linear viscoelastic (LVE) ranges of the samples were determined by carrying through strain sweeps with deformations between 0.01 and 10% and constant angular frequencies of 0.01, 0.1, 1.0 and 5.0 Hz at 298 and 343 K. Constant dynamic rheology was carried out at 1.0% strain, at a frequency of 1.0 Hz and at a temperature of 298 K. Temperature-ramp experiments were carried out between 298 and 343 K with a constant strain of 1.0%, a constant frequency of 1.0 Hz and a constant heating rate of 0.5 K min^{-1} . Frequency sweep experiments were carried out with constant temperatures between 298 and 343 K in 5 K steps, with constant strain of 1.0% and with a frequency range between 0.01 and 5.0 Hz. The master curve was generated by frequency-temperature superposition (FTS) with the frequency curve measured at 298 K being the reference temperature.

Linear uniaxial tensile testing was carried out on a Zwick Roell Z0.5 device equipped with a Zwick Roell KAF-TC 1 kN load sensor at a strain rate of 200 mm min^{-1} . Zwick Roell

testXpert II V 3.0 software was used for acquisition. The dog bone specimens were pressed with a hand-operated Ray-Ran cutting press from homogenous films with a thickness of 1 mm (PPrS@AgNP_{0.30} made by heat-pressing and PPrS@AgNP_{0.21} made by cold-pressing). The exact thicknesses of the specimens were determined by a Mitutoyo micrometer screw. Grip-to-grip separation was 10 mm and the bar width was 2 mm. Upon loading, a slack was observed which was deducted in elongation at break determination. The tensile strengths were identified at the stress maxima of the curves. Values represent the average of seven measurements and refer to the engineering curves.

Preparation of PPrS

A previously reported procedure²⁹ was modified to synthesize PPrS. 1.37 mL of an S-*n*-propyl thioacetate stock solution in THF ($c = 165 \text{ mmol L}^{-1}$) and 0.16 mL (631 μmol) tri-*n*-butyl phosphine were added into 100 mL THF with subsequent degassing *via* Ar-bubbling. 0.27 mL of a degassed NaOMe solution in MeOH ($c = 0.5 \text{ mol L}^{-1}$) were added and stirred for 15 min. 12.0 mL (153 mmol) degassed propylene sulfide were added quickly. After stirring for 70 min at room temperature 0.56 mL (5.04 mmol) degassed ethyl bromoacetate were added and stirred for 2 h at room temperature. After precipitation in MeOH the supernatant was decanted and the polymer was dried *in vacuo*. A transparent, colorless viscous liquid was obtained.

$M_n = 44000$, $M_w = 64200$, $R_g = 9.2 \text{ nm}$. Polymerization degree calculated from GPC-MALLS: 593.

Preparation of PPrS@AgNP_{0.21}: 1.153 g (58.8 μmol) PPrS were dissolved in 30 mL THF and charged with 49.0 mg (222 μmol) AgCO₂CF₃. 0.9 mL of a Superhydrid® solution in THF ($c = 1 \text{ mol L}^{-1}$) were added slowly at room temperature during vigorous stirring. After 30 min the reaction solution was precipitated in MeOH after which the supernatant was decanted and the residue dried *in vacuo*. A black, tar-like material was obtained.

Other PPrS@AgNP were prepared by adjusting the PPrS : AgCO₂CF₃ ratio. The sample is designated as PPrS@AgNP_{0.21} with 0.21 standing for the AgNP filling fraction ϕ in vol%.

SUPPORTING INFORMATION

Supporting Information is available from the Wiley Online Library or from the author.

ACKNOWLEDGEMENT

The authors are indebted to DFG for financial support and to M. Böhm, R. Dersch, M. Müller, R. Giesa and P. Ohlendorf for technical support. We gratefully thank C. Kuttner and A. Fery at physical chemistry 2 department of University of Bayreuth for performing and analyzing Raman measurements. Especially, we give credit to M. Hofmann and E. Rößler at experimental physics 2 department of University of Bayreuth for supporting with technical expertise.

REFERENCES

- [1] R. Shenhar, T.B. Norsten, V. M. Rotello, *Adv. Mater.* **2005**, *17*, 657.
- [2] B. C. Sih, M. O. Wolf, *Chem. Comm.* **2005**, 3375.
- [3] S. Bokern, J. Getze, S. Agarwal, A. Greiner, *Polymer* **2011**, *52*, 912.
- [4] J. Shan, M. Nuopponen, H. Jiang, T. Viitala, E. Kauppinen, K. Kontturi, H. Tenhu, *Macromolecules* **2005**, *38*, 2918.
- [5] P. Schexnailder, G. Schmidt, *Colloid. Polym. Sci.* **2009**, *287*, 1.
- [6] J. Rojo, V. Díaz, J. M. de la Fuente, I. Segura, A. G. Barrientos, H. H. Riese, A. Bernad, S. Penadés, *ChemBioChem* **2004**, *5*, 291.
- [7] M. Liang, I.-C. Lin, M. R. Whittaker, R. F. Minchin, M. J. Monteiro, I. Toth, *ACS Nano* **2010**, *4*, 403.
- [8] C. Ayomonier, U. Schlotterbeck, L. Antonietti, P. Zacharias, R. Thomann, J. C. Tiller, S. Mecking, *Chem. Comm.* **2002**, 3018.
- [9] S. Gupta, M. Agrawal, M. Conrad, N. A. Hutter, P. Olk, F. Simon, L. M. Eng, M. Stamm, R. Jordan, *Adv. Funct. Mater.* **2010**, *20*, 1756.
- [10] W.-C. Lin, M.-C. Yang, *Macromol. Rapid Commun.* **2005**, *26*, 1942.
- [11] S.-W. Baek, J. Noh, C.-H. Lee, B. S. Kim, M.-K. Seo, J.-Y. Lee, *Sci. Rep.* **2013**, *3*, 3.

- [12] M. B. Müller, C. Kuttner, T. König, V. Tsukruk, S. Förster, M. Karg, A. Fery, *ACS Nano* **2014**, *8*, 9410.
- [13] C. Kuttner, P. C. Maier, C. Kunert, H. Schlaad, A. Fery, *Langmuir* **2013**, *29*, 16119.
- [14] N. ten Brummelhuis, C. Diehl, H. Schlaad, *Macromolecules* **2008**, *41*, 9946.
- [15] N. Hisano, H. Iwata, Y. Teramura, H. Chen, Y. Ikada, *J. Polym. Sci., Part A: Polym. Chem.* **2011**, *49*, 671.
- [16] I. Hussain, S. Graham, Z. Wang, B. Tan, D. C. Sherrington, S. P. Rannard, A. I. Cooper, M. Brust, *J. Am. Chem. Soc.* **2005**, *127*, 16398.
- [17] M. Ganesan, R. G. Freemantle, S. O. Obare, *Chem. Mater.* **2007**, *19*, 3464.
- [18] D. Thompson, J. P. Hermes, A. J. Quinn, M. Mayor, *ACS Nano* **2012**, *6*, 3007.
- [19] J. P. Hermes, F. Sander, T. Peterle, C. Cioffi, P. Ringler, T. Pfohl, M. Mayor, *Small* **2011**, *7*, 920.
- [20] T. Peterle, A. Leifert, J. Timper, A. Sologubenko, U. Simon, M. Mayor, *Chem. Comm.* **2008**, 3438.
- [21] J. P. Hermes, F. Sander, T. Peterle, R. Urbani, T. Pfohl, D. Thompson, M. Mayor, *Chem. Eur. J.* **2011**, *17*, 13473.
- [22] J. P. Hermes, F. Sander, U. Fluch, T. Peterle, D. Thompson, R. Urbani, T. Pfohl, M. Mayor, *J. Am. Chem. Soc.* **2012**, *134*, 14674.
- [23] S. Bokern, Z. Fan, C. Mattheis, A. Greiner, S. Agarwal, *Macromolecules* **2011**, *44*, 5036.
- [24] H. Pletsch, M. J. Schnepf, S. Agarwal, *Chem. Mater.* **2014**, *26*, 4805.
- [25] Q. Zhang, L. A. Archer, *Langmuir* **2002**, *18*, 10435.
- [26] J. Yang, C.-R. Han, J.-F. Duan, F. Xu, R.-C. Sun, *J. Phys. Chem. C* **2013**, *117*, 8223.
- [27] Z. Zhu, T. Thompson, S.-Q. Wang, E. D. von Meerwall, A. Halasa, *Macromolecules* **2005**, *38*, 8816.

- [28] A. Şerbescu, K. Saalwächter, *Polymer* **2009**, *50*, 5434.
- [29] L. Wang, G. Kilcher, N. Tirelli, *Macromol. Chem. Phys.* **2009**, *210*, 447.
- [30] K. Yurekli, R. Krishnamoorti, M. F. Tse, K. O. Mcelrath, A. H. Tsou, H.-C. Wang, *J. Polym. Sci., Part B: Polym. Phys.* **2001**, *39*, 256.
- [31] G. P. Baeza, A.-C. Genix, C. Degrandcourt, L. Petitjean, J. Gummel, R. Schweins, M. Couty, J. Oberdisse, *J. Macromolecules* **2013**, *46*, 6621.
- [32] R. A. Riggleman, G. Toepperwein, G. J. Papakonstantopoulos, J.-L. Barrat, J. J. de Pablo, *J. Chem Phys.* **2009**, *130*, 244903.
- [33] S. Jain, J. G. P. Goossens, G. W. M. Peters, M. van Duin, P. J. Lemstra, *Soft Matter* **2008**, *4*, 1848.
- [34] M. Surve, V. Pryamitsyn, V. Ganesan, *Langmuir* **2006**, *22*, 969.
- [35] S. Sen, J. D. Thomin, S. K. Kumar, P. Koblinski, *Macromolecules* **2007**, *40*, 4059.
- [36] J. B. Hooper, K. S. Schweizer, *Macromolecules* **2005**, *38*, 8858.
- [37] M. Hofmann, A. Herrmann, A. A. Elfadl, D. Kruk, M. Wohlfahrt, E. A. Rössler, *Macromolecules* **2012**, *45*, 2390.

SUPPORTING INFORMATION

FOR

MECHANICAL REINFORCEMENT OF POLYDENTATE THIOETHER LIGAND BY SILVER NANOPARTICLES

*Holger Pletsch, Andreas Greiner and Seema Agarwal**

Universität Bayreuth, Macromolecular Chemistry II, Universitätsstraße 30, 95440 Bayreuth (Germany)

Fax: +49 921553393

E-mail: agarwal@uni-bayreuth.de

Keywords: Poly(propylene sulfide), Silver Nanoparticles, Reinforcement, Chain Dynamics

UV/Vis measurements

PPrS@AgNP materials exhibit distinct plasmonic properties. In **Figure 6-S1**, PPrS@AgNP_{0.21} is shown as an example, having a maximum LSPR absorption at 440 nm.

The measurements were conducted in THF solution (0.5 g/L) on a Jasco V-670 spectrophotometer in a wavelength range of 350-700 nm with a scan speed of 400 nm min⁻¹.

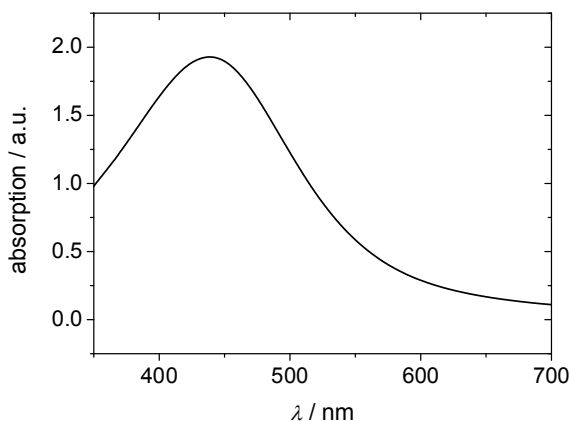


Figure 6-S1. Absorption spectrum of PPrS@AgNP_{0.21}. The maximum LSPR band is identified at 440 nm.

Thermal stability

We probed the temperature stability of PPrS@AgNP by heating rheology specimen discs to 343 K for 7 h. After cooling to 298 K, a frequency sweep data set was collected and compared with a previously collected control data set. As a result, no significant changes in the G' and G'' traces were observed, indicating full retention of the viscoelastic properties (**Figure 6-S2**).

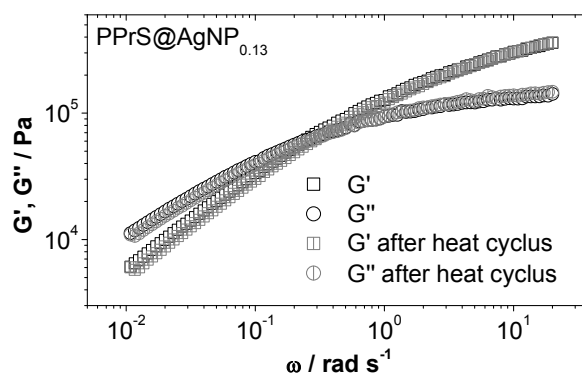


Figure 6-S2. G' and G'' traces of PPrS@AgNP_{0.13} in frequency sweep mode as representative examples for the full retention of viscoelastic properties after heat treatment. Measuring temperature was 298 K both before and after heat treatment at 343 K for 7 h.

G' and G'' Master curves from FTS

Further to the G' and G'' master curves of neat PPrS and PPrS@AgNP_{0.30} from FTS shown in **Figure 6-4c**, **Figure 6-S3** includes master curves of the remaining nanocomposites.

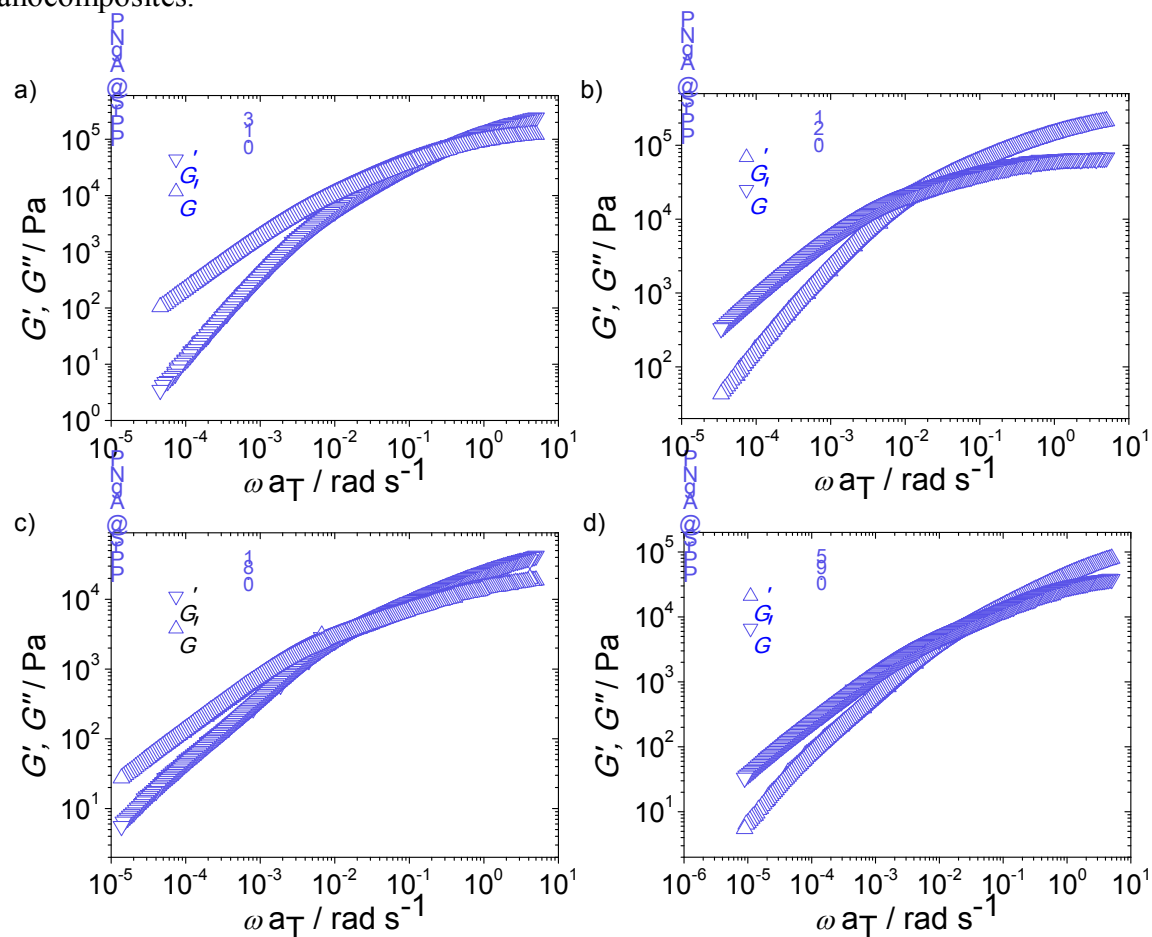


Figure 6-S3. G' and G'' master curves from FTS of a) PPrS@AgNP_{0.13}, b) PPrS@AgNP_{0.21}, c) PPrS@AgNP_{0.81} and d) PPrS@AgNP_{0.95}.

LIST OF PUBLICATIONS

1. Pletsch, H.; Peng, L.; Mitschang, F.; Schaper, A.; Hellwig, M.; Nette, D.; Seubert, A.; Greiner, A.; Agarwal, S.; *Small* **2014**, *10*, 201-208.
2. Pletsch, H.; Schnepf, M. J.; Agarwal, S. *Chem. Mater.* **2014**, *26*, 4805-4811.
3. Pletsch, H.; Greiner, A.; Agarwal, S. *submitted*.
4. Pletsch, H.; Tebbe, M.; Dulle, M.; Förster, B.; Fery, A.; Förster, S.; Greiner, A.; Agarwal, S. *submitted*.

CONFERENCE PARTICIPATIONS

1. **Poster and oral presentation**

Pletsch, H.; Agarwal, S.; Greiner, A.

Systematic Study on Grafting of Thio-Functionalized Polystyrene on Silver Nanoparticles as a Function of Molecular Weight

Makromolekulares Kolloquium, Freiburg, Germany, 23.02.2013.

2. **Oral presentation**

Pletsch, H; Agarwal, S.; Greiner, A.

Could interphase chemistry push the frontiers of polymer-grafted nanoparticles?

9th IUPAC NMS conference, Shanghai, China, 21.10.2013.

3. **Oral presentation**

Pletsch, H.; Agarwal, S.

Metal Nanoparticles as Physical Cross-Linkers: A New Type of Thermally Processable Rubbers

MACRO conference 2014, Chiang Mai, Thailand, 10.07.2014.

ACKNOWLEDGEMENTS

First I offer my cordial gratitude to my supervisor, Prof. Dr. Seema Agarwal, who kindly placed the responsibility of this fascinating, diverse and highly topical research area on me. I also thank her for supporting my wish to perform a dual graduation by completing my master degree simultaneously to the doctoral degree. Moreover, I want to express my sincere appreciation for recommending me as a representative of the workgroup during fair trades in Japan and Germany as well as during scientific conferences in Germany, China and Thailand.

Likewise, I give Prof. Dr. Andreas Greiner credit for the reasons mentioned above. I particularly appreciate his strong commitment for the success of my research goals as well as his visionary considerations on the overall development of the present thesis as a “second Doktorvater”.

I acknowledge [REDACTED] and [REDACTED] for being my BayNat mentors and for giving me significant inspiration concerning my scientific projects.

I thank Deutsche Forschungsgemeinschaft (DFG) and the University of Bayreuth Graduate School for financial support.

Many thanks are addressed at [REDACTED], at [REDACTED] and [REDACTED] [REDACTED] for making administrative issues much easier.

Important scientific discussions within the workgroup were held with [REDACTED],

[REDACTED]

[REDACTED] I thank you for your help!

In this context, special thanks are dedicated to my external collaborators

[REDACTED]

[REDACTED] and [REDACTED]

I received vital technical support from [REDACTED]

[REDACTED]

[REDACTED]

[REDACTED]

I am grateful for supervising the above-average students [REDACTED]
[REDACTED]. Your contribution to this thesis is fundamental!

The time-consuming burden of proof-reading of the present thesis was kindly carried by [REDACTED]
[REDACTED].

I am thankful for the great working atmosphere within the entire workgroup. Special thanks go out to my laboratory partners [REDACTED]
[REDACTED].

I was lucky to be accompanied by my close friends [REDACTED]
[REDACTED] in the recent years. I will never forget the precious time with you.

Finally, I want to express my deepest appreciation for the everlasting and tremendous support of my family, [REDACTED] as well as of my beloved fiancée [REDACTED]

(EIDESSTATTLICHE) VERSICHERUNGEN UND ERKLÄRUNGEN

(§ 8 S. 2 Nr. 6 PromO)

Hiermit erkläre ich mich damit einverstanden, dass die elektronische Fassung meiner Dissertation unter Wahrung meiner Urheberrechte und des Datenschutzes einer gesonderten Überprüfung hinsichtlich der eigenständigen Anfertigung der Dissertation unterzogen werden kann.

(§ 8 S. 2 Nr. 8 PromO)

Hiermit erkläre ich eidesstattlich, dass ich die Dissertation selbstständig verfasst und keine anderen als die von mir angegebenen Quellen und Hilfsmittel benutzt habe.

(§ 8 S. 2 Nr. 9 PromO)

Ich habe die Dissertation nicht bereits zur Erlangung eines akademischen Grades anderweitig eingereicht und habe auch nicht bereits diese oder eine gleichartige Doktorprüfung endgültig nicht bestanden.

(§ 8 S. 2 Nr. 10 PromO)

Hiermit erkläre ich, dass ich keine Hilfe von gewerblichen Promotionsberatern bzw. -vermittlern in Anspruch genommen habe und auch künftig nicht nehmen werde.

Ort, Datum, Unterschrift
